

**Experimental and Numerical  
Investigation of Droplet Formation and  
Material Interactions Under Different  
Conditions**

**Khaled Abdulrazak Al-Badani**

**A thesis submitted in partial fulfilment of the requirement of  
the Liverpool John Moores University for the degree of  
Doctor of Philosophy**

**September 2019**

## ACKNOWLEDGEMENTS

I would like to express my sincere gratitude and special thanks to my supervisors, Prof. James Ren, Dr Lisa Li and Dr Dave Allanson, who have provided guidance, advice and encouragement during this research study.

Several Academics also helped my development in particular Dr Glynn Rothwell. Many other secretarial and technical members of staff have facilitated the realisation of this thesis and I express my gratitude to all of them. I would like to thank Mr Mr. Clive Eyre, Mr. Anthony Dunmore, Mr. Steve Gotts for their invaluable technical support with material testing, sample manufacturing process and sensor and data logging design.

I would like to take this opportunity to thank my group mates, Dr. Shudong Li, Dr. Andrew Norbury, Dr. Hongyi Zhao, Mr Cong Tang, Mr Tammam Kaid, for their friendship and sharing their experience. I am also grateful for the help from my friends, who gave me help in many ways and shared a great time in my studies and life at Liverpool John Moores University.

I am grateful for LJMU for providing the support and facilities for the research;

It is with infinite gratitude that I dedicate this work to my beloved parents, Abdulrazak Mohammed Al Badani and Zahra Ali Mulhi, who both believed in my ability to be successful in the academic and professional life. You are both gone but your belief in me, and my brothers, has made me the hard worker humble person I am today. Finally, of course, my wife, my inspiration, my world: Wejdan. Without here patience and constant encouragement and un-conditioning love, none of this work would ever been possible.

## ABSTRACT

This work focused on developing a framework of numerical models for simulating the formation of droplet under different situations. The formation of a pendant droplet was studied through an integrated experimental, numerical and theoretical procedures, establishing the key factors influencing the dynamics of a pendant droplet and examining key material parameters such as the density, viscosity, wetting coefficient and surface tension. A numerical model was developed using the volume of fluid (VOF) solver in ANSYS FLUENT and validated using qualitative and quantitative approaches (e.g. droplet shape, length, volume, separation time). The numerical data was correlated with an analytical solution based on pressure and velocity data from a mathematical approach and experimental; works on model materials with different properties. The program has been used to establish a range of models relevant to industrial processes, including droplet for semifluid material systems, formation of satellite droplets, merging of droplets from two inlets at an angle, multiphase liquid in micro channels and generating droplets smaller than the nozzles diameter through using a code to control the flowrate and cycles. The data from the numerical models is also coded into Matlab to automatically plot the contour and calculate the volume of the droplet. Some cases in the modelling of merging of liquid in welding of thin tubes, effect of contact angles on liquid dripping and use of numerical modelling in microchannel design, are also evaluated and key results are presented.

The interaction between liquid droplet with a homogenous material and a matrix with an embedded thin stiffer layer is studied in comparison to a similar loading situation with rigid indenters of different shapes. A particular focus has been on the effect of material properties (Negative Poisson's ratio and layer depth) on the enhancement of the indentation resistance and material deformation. The FE results are correlated with an analytical solution for homogenous materials and results from a mathematical approach for embedded systems in an elastic half-space. The influence of auxeticity (i.e. negative Poisson's ratio) on the indentation stiffness ratio between systems with an inserted layer against a homogenous matrix (no reinforcement) is established. The deformation of the embedded system under different conditions (indenter size, thickness and embedment depth of the embedded layer) is presented and key mechanisms of the Poisson's ratio effect are highlighted.

## Nomenclature

Symbol	Description	Unit
a	Acceleration	m/s <sup>2</sup>
A	Area	m <sup>2</sup>
$\beta$	Bond Number.	
$\gamma$	Boundary/surface tension	
CFD	Computational Fluid Dynamics	
$\theta$	Contact angle.	°
$\rho$	Density	kg/m <sup>3</sup>
d	Diameter	mm
de	Diameter of a droplet at the equator	mm
$\Delta\rho$	Difference in density	kg/m <sup>3</sup>
$\sigma$	Difference in density the multiphase fluids	kg/m <sup>3</sup>
i	Discrete elements	
j	Discrete elements	
ds	Distance diameter from the arbitrarily plane	mm
$\mu$	Dynamic viscosity	Pa s
EM	Eulerian model	
FE	Finite Element Analysis	
F	Force	N
P/ $\Delta$	Force-displacement ratio	
$g$	Gravitational acceleration	m/s <sup>2</sup>
IS	Indentation Stiffness	Mpa
$\Delta$	Indenter Displacement	mm
L	The radius of curvature of the droplet	mm
LM	Lagrangian model	
P	load on the indenter	N
m	Mass	kg
NOE	Number of Elements	
NOD	Number of Nodes	
$\nu$	Poisson's ratio of the matrix	
p	Pressure due to droplet curvature	Pa
R	Principal radii of curvatures	mm
R'	Principal radii of curvatures	mm
R <sub>0</sub>	Radii of curvature for a droplet	mm
r	Radius	mm
b	radius of the cylindrical indenter	mm
S	Ratio of droplet diameters	
H	Ratio of droplet equator to	

	the curvature at the origin	
RF	Reference Point	
SPH	Smoothed Particle Hydrodynamics	
$E_m$	Stiffness of Matrix	Mpa
$\gamma^{lv}$	The liquid surface free energy	J
$\pi$	The ratio of a circle's circumference to its diameter	
$\gamma^{sv}$	The solid surface free energy	J
$\gamma^{sl}$	The solid/liquid interfacial free energy	J
s	Velocity of sphere	m/s
V	Volume	$m^3$
VOF	Volume of Fluids	
$\dot{V}$	Volumetric flow rate	$m^3/s$
E	Young's Modulus of the matrix	Pa

# Contents

Acknowledgements.....	i
Abstract.....	ii
Nomenclature.....	iii
Contents.....	v
List of Figures .....	vii

## CHAPTER ONE INTRODUCTION

1.1 Introduction	2
1.2 Aims and objectives	6
1.3 Outline of the thesis	7

## CHAPTER TWO BACKGROUNDS AND LITERATURE REVIEW

2.1 Introduction	10
2.2 Key parameters controlling the fluid and semifluid behaviours	11
2.3 Viscosity and effect of viscosity on fluids and droplets	18
2.4 Different form of droplets and key stages of droplet formation process	20
2.5 The dynamics of droplet formation, and different analysis approaches	23
2.6 Main factors affecting the shape and size of a droplet and analysing approaches.	25
2.7 Wetting between liquid and different surfaces and testing methods.	28
2.8 Droplet formation in different processes and Numerical modelling of drop formation.	34
2.9 Smooth particle hydrodynamics modelling methods and applications	41
2.10 Droplet formation and materials development	44

## CHAPTER THREE EXPERIMENTALS, NUMERICAL MODELLING AND DATA ANALYSIS PROGRAMS

3.1 Introduction	48
3.2 Testing and material preparation	51
3.2.1 Pendent droplet apparatus.	51
3.2.2 Material systems	52
3.2.3 Testing procedure for obtaining material properties for pendant droplet test and modelling.	53
3.3. Facilities and process for studying the bead formation in welding processes and surface finishes.	55
3.4 Numerical Modelling and other data analysis programs	63

## CHAPTER FOUR NUMERICAL AND EXPERIMENTAL STUDIES OF DROPLET FORMATION OF DIFFERERT MATERIAL SYSTEMS UNDER VARIOUS CONDITIONS

4.1 Introduction and main research works	68
4.2 Numerical modelling of droplet: model development and analysis	71
4.2.1 Mesh sensitivity study	72
4.2.2 Theoretical validation of the initial numerical model	73
4.3 Experimental tests and data	74
4.4 Experimental, qualitative and quantitative analysis of numerical and experimental droplet test	76
4.4.1 Experimental work with Glycerine-Water solution and comparison with numerical models	76

4.4.2 Quantitative analysis of the droplet dimension and shape and effect of material properties	77
4.4.3 Droplet simulation of semi fluidic materials and surface tension estimation	79
4.5 Formation of different types of droplet dynamics	80
4.6 Modelling of small volumes of liquid and their interaction with different types of materials	
4.7 Discussion	
4.8 Summary	78

## CHAPTER FIVE NUMERICAL STUDIES OF THE INTERACTION BETWEEN SOLID INDENTER/LIQUID DROPLETS WITH DIFFERENT FORMS OF SUBSTRATES AND EFFECTS OF MATERIAL PROPERTIES

5.1 Introduction and main research works	131
5.2 Indentation of soft materials with flat ended and spherical indenters	135
5.3 Indentation resistance of soft elastic materials with embedded shell with a Spherical indenter	139
5.4 Numerical modelling investigation of interaction between liquid droplet and different forms of material systems	141
5.4.1 FE model	141
5.4.2 Droplet modelling with Smoothed Particle Hydrodynamics method (SPH)	141
5.4.3 Boundary conditions	143
5.4.4 Effect of linear and nonlinear solver approaches	143
5.4.5 Effect of meshing schemes	144
5.5 Effect of impact velocity and the matrix properties	146
5.6 Discussion	148
5.7 Summary	152

## CHAPTER SIX DISCUSSIONS AND FUTURE WORKS

7.1 Summary and conclusions	169
7.2 Recommendations for further works	171
References	172
List of publications and external reports	183

# List of Figures

## Chapter 1

**Figure 1.1** Typical cases of droplets in different situation relevant to industrial processes.

**Figure 1.2** Schematics to show the interaction between a rigid indenter (a) and liquid droplet with a surface with an embedded thin layer.

## Chapter 2

**Figure 2.1** Figure 2.1 Different types of liquid loading condition conations used to characterise the surface tension.

**Figure 2.2** Schematic change of the force measured during the process of a ring tensiometer experiment.

**Figure 2.3** Schematic of a pendant drop below a needle.

**Figure 2.4** Schematic to show a general parallel flow, the gradient of the flow velocity is proportional to the shear stress.

**Figure 2.5** Main stages in a single droplet.

**Figure 2.6** Geometry and notation of symbols of a pendant-drop profile.

**Figure 2.7** Wetting process for fluids. Drop (A) shows a fluid with very little wetting. Drop (C, S) shows a fluid with more wetting.

**Figure 2.8** Definition and measurement of contact angle of a droplet on a solid surface.

**Figure 2.9** Factor affects the fluid behaviour in contact with different types of surfaces.

**Figure 2.10** Evolution in time of the computed velocity field in a drop of 85% glycerine in water growing out of a capillary when  $R_{50}$ .16 cm and  $Q$  525.0 ml /min.

**Figure 2.11** FE modelling of droplet formation in a welding process.

**Figure 2.12** Typical design of drop generator (a) and the effect of nozzle size on the size of the droplets.

**Figure 2.13** Typical examples shows droplet formation in 3D printing.

**Figure 2.14** Schematic diagram showing the principle of the droplet formation by the technology of drop-on-demand (DOD) and continuous inkprinting.

**Figure 2.15** (c ) Simulation results for  $\alpha = 25^\circ$  at  $Q_c = 2.0 \mu\text{l}/\text{min}$  and  $Q_d = 0.2 \mu\text{l}/\text{min}$ . (a) Surface plot showing the generation of one droplet pair (b) Graph showing variation of pressure at points A and B over the droplet generation time period.

## Chapter 3

**Figure 3.1** Experimental arrangement used to visualize droplet formation.

**Figure 3.2** Typical captured image of a pendant droplet.

**Figure 3.3** Apparatus used to calculate the viscosity of Glycerine-Water solution with various concentration levels.

**Figure 3.4** Typical facilities used in welding tests and evaluation of the metal melting bead formation.

**Figure 3.5** Welding apparatus designed to hold the TIG and CDE torches (a) and typical tube closure (b).

**Figure 3.6** Bill of Material for the Welding Apparatus designed.

**Figure 3.7** Tungsten electrode used for the TIG welding experiment and stainless steel tubes.

**Figure 3.8** Struers Prontopress machine used to prepare welded nuggets for analysing the shape of the weldment and flow feature of the liquid during the welding process.

**Figure 3.9** ContourGT-K 3D Optical Microscope used to measure the surface roughness.

## Chapter 4

**Figure 4.1** Numerical properties and boundary conditions for the CFD model of the multiphase flow.

**Figure 4.2** Typical simulation results showing of the droplet growth and detachment process using FLUENT. The air is blue in colour and the water is red in colour based on the EM model).

**Figure 4.3** Typical different mesh densities/scheme used in the mesh sensitivity and convergence study.

**Figure 4.4** Typical example of droplet contour plots at different time stages showing the effect of mesh density on interface shapes obtained using FLUENT.

**Figure 4.5** Typical pressure contour of a tapered nozzle and data showing the effect of mesh density on the convergence of the pressure at the stagnation/nozzle exit.

**Figure 4.6** Typical velocity contour and effect of mesh density on the convergence of the velocity at stagnation/nozzle exit.

**Figure 4.7** Typical data on a single PC showing that the time taken for each study is increasing nonlinearly when the density of mesh is increased. The data is representative (i.e. the ratio) to other cases when a more powerful computer system is used.

**Figure 4.8** Diagram of the nozzle used in the analytical analysis and the numerical contour. The velocity data at a typical preselected point (coordinates (0.1, 0.099, 5.01) is extracted to be compared with analytical calculation.

**Figure 4.9(a)** Apparatuses used to measure the properties of Glycerine-Water solution with various concentration levels of Glycerine.

**Figure 4.9 (b)** Diagram showing the principle and procedure of the vertical falling drop ball viscosity experiment measurement.

**Figure 4.9 (c)** Measured data showing the effect of Glycerine concentration on the density of the Glycerine-Water mixture solution.

**Figure 4.10** Effect of temperatures on the viscosity of pure Glycerine oil.

**Figure 4.11** Typical results comparing between experimental and numerically predicted droplet shapes at different stages (a plastic syringe with a tapered nozzle)

**Figure 4.12(a)** Experimental arrangement used to visualize droplet formation.

**Figure 4.12 (b)** Typical images showing the growth of the droplet with controlled increasing liquid volume. (Straight tube,  $D=1.6\text{mm}$ ).

**Figure 4.12** Typical images showing the growth of the pendant droplet with increasing liquid volume. (Straight tube stainless tube).

**Figure 4.13** Definition of the key parameters of a droplet for quantitative analysis. (a)The effect of increasing the viscosity of the liquid on the droplet length. (b) The effect of volumetric flowrate on the separation time of droplet.

**Figure 4.15** The effect of changing the nozzle exist size and the volumetric flow rate on the dynamics behaviour of the droplet.

**Figure 4.16** Interface shape comparison between FLUENT results and published data with CFX and Flow 3D. (all based on 50% Glycerine data)

**Figure 4.17** Comparison between FLUENT predicted droplet shape change (elongation effect and satellite droplet) at breakup for a 20 percent Glycerine water solution and published data.

**Figure 4.18** Typical data of semi-fluidic liquid Gallium droplet: Numerical Simulation against experiment observation.

**Figure 4.19** Comparison between experimental and numerical data showing the growth of a Gallium droplet:

**Figure 4.20** Effect of the contact angle on the volume of the droplet.

**Figure 4.21** Typical example showing the effect of materials on the formation of satellite drops.

**Figure 4.22** Models and control conditions for producing droplet smaller than the diameter of tube/nozzle.

**Figure 4.23** Typical numerical results showing the generation of droplet smaller than the diameter of the nozzle.

**Figure 4.24** Typical setup of the model for simulating droplet formation in micro channels (water in oil)

**Figure 4.25** Effect of water droplet formation breaking up from a capillary tube. Water Volumetric flow rate of: 0.055kg/sec.

**Figure 4.26** Comparison of droplet interfaces between the five different water flowrates.

**Figure 4.27** Effect of mass flowrate on the size of the droplet generated.

**Figure 4.28** Typical contours showing the difference between the droplet of Water, Glycerine, Gallium and Nickel (high temperature). All these materials have different surface tension and viscosity to illustrate the use of the model to analyse the effect of materials properties on droplet shapes.

**Figure 4.29 (a)** Flow chart to show the main structure for analysing pendant droplet in Matlab.

**Figure 4.29 (b)** Typical feature of the Matlab codes and example outline of droplet.

**Figure 4.30** Typical contour plot for Gallium Droplet at 0.14 Second.

**Figure 4.31** Typical example showing the effect of choice of modelling approach on the modelling of liquid flowing through a nozzle.

**Figure 4.32** Typical cases involving merging of small volume of liquid in welding process.

**Figure 4.33** Typical example numerical result showing the merging of small drops of liquid.

**Figure 4.34** Typical surface roughness analysis and effect of welding currents.

**Figure 4.35** Sample numerical model developed to assess the effect of contact angle (wetting coefficients on the residual of liquid when a tube is pulled from a liquid

**Figure 4.36** Dye penetration process and an effective way of simulating of the dye penetration test.

## Chapter 5

**Figure 5.1** Structure and boundary conditions of the FE indentation model with a flat ended cylindrical rigid indenter.

**Figure 5.2** Deformation fields of the matrix and the embedded shell under indentation with a flat-ended cylindrical indenter.

**Figure 5.3** FE models of indentation with a flat-ended cylindrical indenter on homogenous materials and materials with embedded shells.

**Figure 5.4** Numerical data showing the Enhanced Indentation Resistance of shell embedded system. (a) Positive Poisson's ratio for the matrix; (b) Negative Poisson's ratio for the matrix. (b: indenter diameter,  $\delta$ : indentation depth;  $\mu$ : shear modulus of the matrix; P: force, h: depth of the shell)

**Figure 5.5** Spherical indentation FE model/mesh (a) and deformation field (b); (c) Comparison between numerical and analytical data for indentation of a homogenous material.

**Figure 5.6** Effect of embedded shell on the indentation resistance

**Figure 5.7** Indentation stiffness enhancement of materials with an embedded shell. (ISR is calculated against the load when there is no embedment).

**Figure 5.8** Data showing the effect of Poisson's ratio and depth of the embedment on the enhancement of the indentation resistance represented by the ISR.

**Figure 5.9(a)** Framework for developing analytical solutions (Li et al, 2019, work in progress)

**Figure 5.9(b)** Enhanced Indentation resistance of material with an embedded shell (Analytical data) (Li, 2019, unpublished work)

**Figure 5.10** Typical example showing the comparison of shear stress (S12) of embedded shells between positive and negative Poisson's ratio matrix ( $\nu = \pm 0.1$ ).

**Figure 5.11** Numerical model of droplet interaction with a solid.

**Figure 5.12** Typical loading of the droplet when hitting a matrix. The solid surface was fixed from the bottom face using an ENCASTRE boundary condition; a predefined velocity of 5m/s was defined for the droplet.

**Figure 5.13** Typical deformation stages of the droplet during impact onto a rigid solid. (V=5mm/s)

**Figure 5.14** The difference of liquid-solid interaction between a linear (a) and a non-linear solution study (b).

**Figure 5.15** Typical data showing the process used in developing the meshing schemes and extraction of the force and stresses.

**Figure 5.16** Effect of the droplet speed on the reaction forces. Figure 5.16 (a) Effect of the droplet speed on the force time data. Figure 5.16(b) The maximum reaction force on the target with different droplet speeds.

**Figure 5.17** Effect of the Matrix stiffness on droplet deformation mode.

**Figure 5.18** FE model of spherical water droplet onto a matrix with an embedded shell.

**Figure 5.19** Typical data showing the deformation of the material system of an embedded shell within a positive or negative Poisson's ratio.

**CHAPTER ONE**

**INTRODUCTION**

## 1.1 Introduction

The behaviour of liquid droplet formation and its interaction with other phases is a very important process associated with many natural phenomena and many engineering processes such as medical, oil, general machinery and many more. The volume and the characteristics of droplet formation are generally dependent on various material properties, microfluidics and fluid mechanics considerations. Research on droplet formation offers a unique case for understanding the behaviour of a small volume of liquid, it also offers a simple way to establish the influence of key material properties in particular surface tension, wetting, etc. Increasingly droplet formation is becoming a critical process for new technologies such as drop-in-demand systems and 3D printing (Fathi et al 2013, Guarino 2018). The interaction between droplet and different substrates (for example rigid and deformable surfaces) is also important for manufacturing processes. In addition, many new materials are being developed with novel behaviour, it is essential to have a modelling program to predict the effect of the novel material properties about their interaction with droplets which could be significantly different from rigid subjects. An effective modelling framework for small volumes of liquid such as droplets, could also effectively feed into the modelling of more complex systems for data development, design optimisation as well as for training purposes for relevant engineering processes by integrating works in fluid simulation, materials science and specific engineering practices.

Droplet formation is relevant to many engineering systems and manufacturing processes, such as administration of medicines, welding, 3D printing, inkjet printing, microfluidic analysis, coating/spraying, microchannel. etc. (Shimasaki et al, 2011; Fathi et al 2013; Zhu et al 2016; Chen et al, 2018; Saqib et al 2018). Some typical examples are shown in Figure 1.1. In addition, droplet formation is becoming increasingly important for some emerging areas in materials processing and handling. Typical procedures such as drop-to-drop deposition (Fathi et al 2013) and drop-on-demand (Guarino 2018) approaches are simple and effective methods for producing/utilising droplets over different sizes and scales. The high effectiveness and flexibility of these processes make them promising production methods of small or delicate parts as well as favourable in the fields of tissue engineering, drug delivery, bio-fabrication and sensors (Fathi et al 2013). For example, the drop-on-demand technique has a wide range of applications, such as ink-jet printing, deposit of specific materials on displays or electronic circuits, formation of microarrays on biological chips, etc. The advantages of droplet based manufacturing and printing include its flexibility in controlling the material's volume and

deposition pattern by using different mechanisms such as the Piezo system (Shimasaki et al, 2011; Fathi et al, 2103; Guarino, 2018). In some cases, picolitre or microlitre volumes of aqueous materials can be used to produce series of droplets for deposition of different types of materials at very small scales without contacting the underlying substrates. It can also produce gradient patterns of 3D space by tuning the number, size and spacing of the droplets. All these require an effective modelling approach to suit different situations in order to controlling the size, shape and breaking up times, etc.

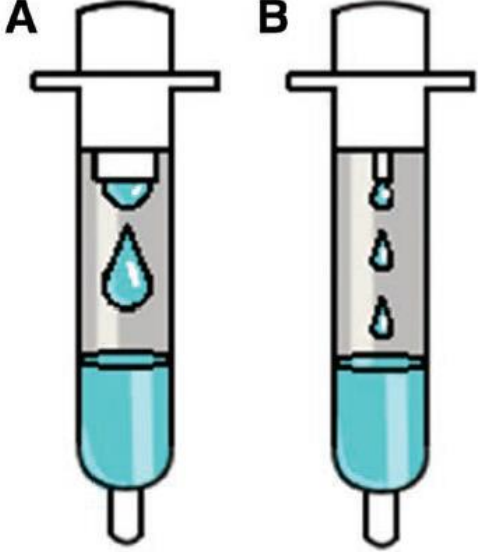
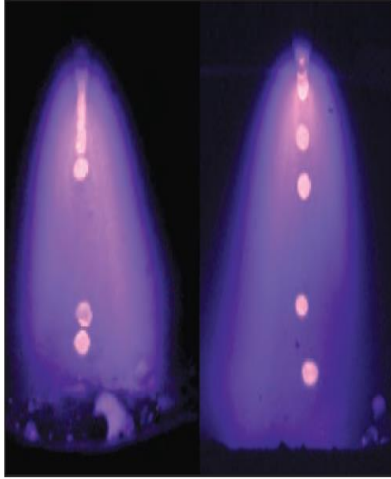
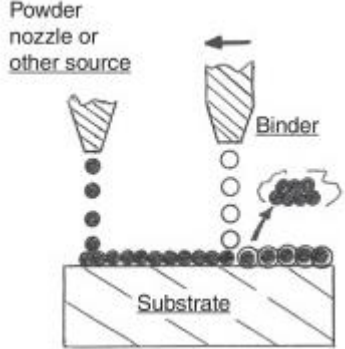
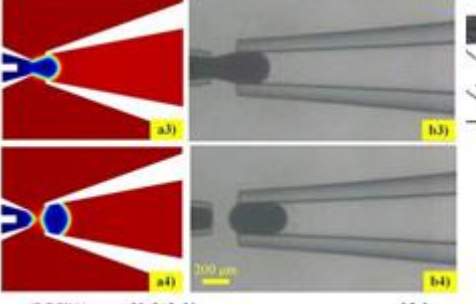
	
<p>(a) Droplet in Medical: Droplet in dose management. (Kim et al 2016);</p>	<p>(b) Droplet in Manufacturing: typical image showing droplet in Gas metal arc welding process at high temperature. (Mcintosh et al, 2017)</p>
	
<p>d) Droplet in Material process. 3D metal droplet printing (Murr et al, 2017).</p>	<p>(e) Microfluidic droplet generation. (Hu et al 2020).</p>

Figure 1.1 Typical cases of small volumes of liquid in different situations relevant to industrial processes.

An extensive range of theoretical studies, experimental work and computational analyses have

been performed to improve the understanding of the droplet's dynamics (Wilkes et al, 1999; Zhang, 1999; Fawehinmi, et al. 2005; Kovalchuk et al 2017; Pardeep et al, 2017). Normally the formability of droplets occurring from a capillary tube end, has two main modes (Zhang et al, 1999): (1) Jetting – (high flow velocity) is the result of a coherent laminar jet, which originates from the tube, before breaking into small separate drops, due to Rayleigh instability. and (2) Dripping – (occurs only within slow flow velocity) is the result of the liquid flowing out of the tube as small periodic drops. The dripping mode can be divided into two main stages. The first stage corresponds with the quasi-static growth of the drop. This stage ends when the surface tension becomes incapable of holding the weight of the drop. The second stage is the necking, which is caused by the destabilizing effect of the surface tension, and it generally starts during the breaking up stage of the droplet. The necking stage results in creating a conical shape in the upper section of the droplet, and a spherical shape in the lower section. The length of the liquid thread that is linking the upper and lower section simultaneously, will increase as the droplet reaches the critical breaking point, where the spherical section is detached from the upper section of the droplet. As for the rest of the fluid, it rapidly withdraws because of the surface tension effect; In some cases, it may lead to another break-up of small droplets called satellite drops, the formation and control of these droplets directly influence the subsequent deposition or interaction between the droplet and target (such as rigid surface, deformable surface) (Ikegawa and Azuma, 2004; Majidi et al, 2016, Al-Sharafi et al 2018). For different engineering process, the different stages of the droplet formation may have different influences. These works highlighted the importance of a detailed model capable of predicting droplet formation to enhance understanding and applications.

The interaction between droplet and other material is also important. A typical example is in the interaction between droplets with embedded systems and the influence of novel material properties such as Auxetic behaviours. Auxetics behaviour is novel behaviour with a negative Poisson's ratio. Poisson's ratio represents the ratio between lateral strain and axial strain when a material is being deformed. For materials with a positive Poisson's ratio, the materials shrink under tension, expand under compression, but negative Poisson's ratio materials expand when being stretched and shrink when under compression. Such a material has been shown to influence the behaviour of material under localised loadings such as indentation (when indented by a sharp/rigid subject). In an indentation process, an indenter is pressed onto the sample surface and deforms the material. It is of interest to study the interaction comparatively between a sample with negative Poisson's ratio with a liquid droplet, which behaves differently from solid subjects. Liquid droplet on soft materials with embedded structures is also of interest.

Such a structure contains a thin insert (re.g. a thin shell as illustrated in Figure 1.2) within a matrix, which is increasingly being used in many applications, in particular in sport and medical systems (*Patton et al, 2015??; Heidner and Adams, 2016??*). This material type refers to systems with a stiffer structure (either in 3D or 2D form) being fully enclosed in a matrix for improving mechanical performance or achieving other functions. For example, a thin stiffer plate could be inserted in a soft insole to increase the strength or pressure distribution (*Kajta et al, 2015??*). A heating element can be used in an insole or midsole for thermal management of shoes. Recently, there has been considerable work in wearable technology in footwear for both research purposes and technological development, in which a thin electronic device or chip is embedded in the sole system (*Crea et al, 2014??*). A detailed understanding of the mechanics of these material systems, subject to both indentation of different shaped rigid indenters and liquid droplets, is important for improving the structure integrity and lifetime reliability.

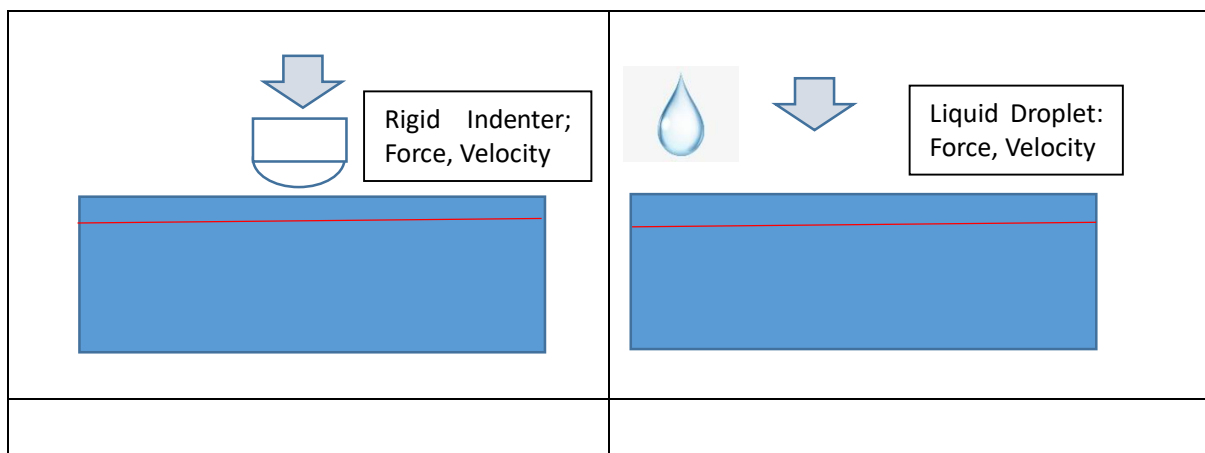


Figure 1.2 Schematics to show the impact of a surface of a rigid indenter and liquid droplets.

## 1.2 Aims and Objectives

This work aims to develop an effective numerical modelling framework for simulating the liquid droplet formation and interaction between liquid droplets with materials of different properties in comparison with rigid indenters.

The main objectives are:

- To develop a numerical CFD modelling approach for simulating droplet formation of liquids with different properties and investigating the effect of material properties
- To model the droplet formation under different conditions within a single phase or multiphase system
- To develop an effective model for simulating the interaction between liquid impacting onto different material systems, and to investigate the effect of Poisson's ratio and Auxeticity on the behaviour of a material with embedded thin layers under indentation in comparison with rigid indenters of different shapes
- To establish an effective modelling approach for engineering systems in which a small volume liquid is critical, such as welding and dye penetration.

### **1.3 Outline of the thesis**

In Chapter 2, the main background and literature related to some key technology and research areas is reviewed. Key parameters controlling the fluid and semifluid behaviours are outlined with reference to different methods and technologies for measuring the surface tensions. The effect of viscosity on fluids and droplets is presented; the key physical attributes and dynamics of droplet formation and their influence on droplet shape and size are reviewed. Wetting between liquid and different surfaces/ Droplet Contact angle and factors affecting droplet interaction are briefly explained. Past and recent numerical modelling approaches of drop formation and coalescence and different numerical solvers suitable for simulating liquid behaviour are compared. Challenges and potential in modelling small volumes of liquid of different material systems and their relevance to different material testing and production processes are highlighted.

Chapter 3 outline the main research works including the experimental and numerical investigation on pendent droplet formation and numerical modelling of small volume of liquid under different conditions and processes (presented in Chapter 4) and comparative studies on the interaction between solid indenters of different shapes (flat ended and spherical) and liquid drop with materials with embedded thin shell and/or auxetic matrix (presented in Chapter 5). The main focus for each part of the research is described. The work presented briefly explains the set-up and details of some key experimental facilities and materials associated with the project. The facilities include liquid droplet testing machines, mixing and viscosity measurements. The materials include glycerine-water mixture and Gallium alloys. Procedures for some property measurement and calculation procedures such as liquid density and the viscosity measurements are explained. Some welding facilities, material preparation and characterisation are presented. The micro welding process of wires and tubes, which involves complex processes including merging of small volumes of liquid when forming a joint, is explained. Surface roughness measurement apparatus were also utilized, to characterise the surface of welded stainless steel tubes. Different modelling programs evaluated and used in the research are detailed including the ANSYS Fluent, ABAQUS, Open foam and CFX.

Chapter 4 presents the details on simulating droplet formation for several different material systems and experimental works. The work concentrated on the development of a multiphase numerical model that can be utilized to develop complex systems. The second section describes

experimental procedures conducted to measure key material properties that are important for numerically modelling the droplet formation and complex multiphase flow. The main work focuses on water, glycerin and glycerin-water mixture, as reference material which offers a broad range of properties for droplet formation. In the discussion, key factors affecting the modelling process and the limitation of the VOF numerical solver are analysed. The effect of the contact angle, which represents the wetting of liquid is analysed. Furthermore, special cases numerical models, extended from the developed droplet model, are presented including; effect of changes in material properties on the formation of multiple satellite drop modes, droplets with a size smaller than the nozzle, as well as the relevance of such models on different applications, including drop on demand and 3D printing techniques. Key procedures and results on modelling continuous droplet formation in microfluidic system are also presented and discussed. Finally, work on using the numerical data for a droplet contour data system in Matlab, its function and potential extension to other complex situations is discussed. A few case studied were presented where the modelling of small volumes of liquid is beneficial and critical, including a case with a study of ABAQUS Coupled Eulerian Lagrangian (CEL) using simplified geometries and material properties to reduce simulation complexity: Modelling of liquid and droplet merge integrated in welding processes is studied; and surface finish of welded stainless tubes and modelling of liquid dripping process is presented. Typical modelling of fluid penetration in small cracks mimicking NDT Dyne penetration test is also presented.

Chapter 5 summarizes the main work and key results in modelling the interaction between a rigid indenter or liquid droplets with homogenous materials and soft materials embedded with thin layers at elastic regimes. In the first part, the work is focused on rigid flat-ended cylindrical indenters and spherical shaped indenters. In the second part, the work was extended to the modelling of liquid droplets onto homogenous materials and soft materials with embedded thin shells through the Smoothed Particle Hydrodynamics method (SPH) approach. The effect of Poisson's ratio and auxeticity of the matrix is highlighted.

In Chapter 6, overall conclusions are given and future works is recommended.

## **CHAPTER TWO**

### **BACKGROUNDS AND LITERATURE REVIEW**

## 2.1 Introduction

The fundamentals of droplet formation are a very important process in many engineering systems and manufacturing procedures, which include welding, biotechnologies, 3D printing, biochemical, biomedical fields and many more (Ikegawa and Azuma, 2004, Guarino 2018). The volume and the characteristics of droplet formation generally depend on various material properties, microfluidics and fluid mechanics considerations. Understanding of droplet formation and an effective way of simulating small volumes of liquid in different processes is important to many manufacturing processes. This chapter reviews the key fundamentals of droplet formation and associated processes. Key topics include: key parameters controlling the fluid and semifluid behaviours, in particular surface tensions; measurement of surface tensions under different configurations; the source of viscosities and its effect on different types of liquid loading and interaction conditions; the droplet's physical attributes and different forms of droplets; difference between jetting and droplet dripping with reference to the dynamics of droplet formation; wetting between liquid and different surfaces and numerical modelling of drop formation and coalescence. It covers past and current development of theoretical, experimental and numerical approaches to quantify the shapes and sizes of droplets. Recent research and development of technological development based on droplet formation is also briefly presented including welding, 3D printing, drop-on-demand, and microchannel methods. The challenges and potential applications in modelling small volumes of liquid of different material systems are also discussed.

## **2.2 Key parameters controlling the fluid and semifluid behaviours**

Understanding the behaviour of fluids is important for many applications over a range of industries, research in such areas is relevant to many engineering applications and technological developments. The behaviour of liquid is controlled by some key properties and service conditions/constraints. The important basic properties of fluids controlling the mechanical behaviour include the density, viscosity, specific weight, surface tension, etc. while external environmental factors include velocity, pressure, temperature ( Batchelor 2012, Elger et al, 2013;). The behaviour of these properties is also influenced by their interaction with different phases either gas, other liquids or solids, represented by the wetting conditions. For droplet formation, surface tension is probably described as the most complex attribute (Tolman, 1949; Yeow et al, 2008).

The surface tension of a liquid is a molecular level phenomenon, it results from the change in energy between the particles of fluid interface compared with the energy for solids made of the same substance. The surface energy of a liquid could be regarded as a measurement unit for how much energy is needed to make a unit area of interface between liquid and solid/gas. The conventional unit for surface energy is Joules per square metre, which is the equivalent to Newton's per metre, the latter is used more commonly. It was established a long time ago (Rayleigh, 1879, Washburn, 1921) that surface tension is a fundamental concept in describing the phenomenon of droplets, directly influencing their size, weight, shape, as well as their stability and velocity. Despite the long history of research into liquid and droplets, the study of liquid at different scales has continued to become more and more important. From the chemistry/molecular/atom level, the surface tension reflects the chemical configuration of fluid interfaces and affects the desorption and adsorption of interfacial active solutes. In other cases, when dealing with microfluidic sizes (such as microchannels), the surface tension is dominated by forces that can be effectively used in advanced liquid handling. Hence, the surface tension is a very important fluidic property with applications relevant to precise measurements for both industry and science.

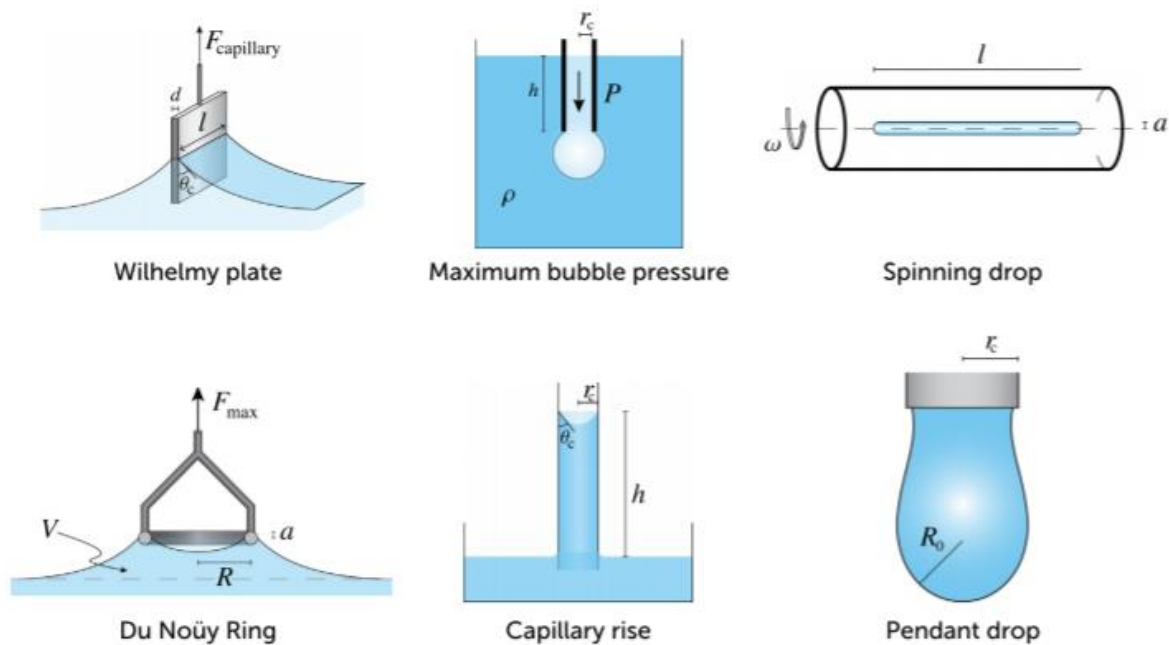


Figure 2.1 Different types of liquid loading condition used to characterise the surface tension. (Berry et al 2015)

Many methodologies have been approached to control/measure the behaviour of surface tension. Some common methods are listed in Figure 2.1. Their qualities and features are defined in detail by Drelich et al (2006). In the Wilhelmy plate method, a thin plate is dipped into a liquid, then the force exerted onto the plate is recorded. The area is normally in the order of a few square centimetres, the materials can be paper, glass or platinum (inert), in the case of the latter two, the surface may be roughed to ensure that a full wetting is produced between the plate and the liquid. The Du Noüy ring method is a method for measuring the surface tension of a liquid and the interfacial tension between two liquids. In this method, a thin wire ring is inserted under the interface (which can be either a liquid-vapour or liquid-liquid interface) and held horizontal. Then the ring is pulled up through the interface. Figure 2.3 illustrates the main stages in (1) initial position, (2) The ring touches the liquid surface, (3) The ring has to be wetted by the liquid. (4) The ring is immersed into the liquid (5) The ring is moved out of the liquid with a constant speed (6) A liquid meniscus is pulled out by the ring; (7) The liquid meniscus increases and the force approaches a maximum; (8) The force passes the maximum and decreases again (9) Further pulling the ring leads to a rupture of the meniscus. The maximum force represents the surface tension of the liquid.

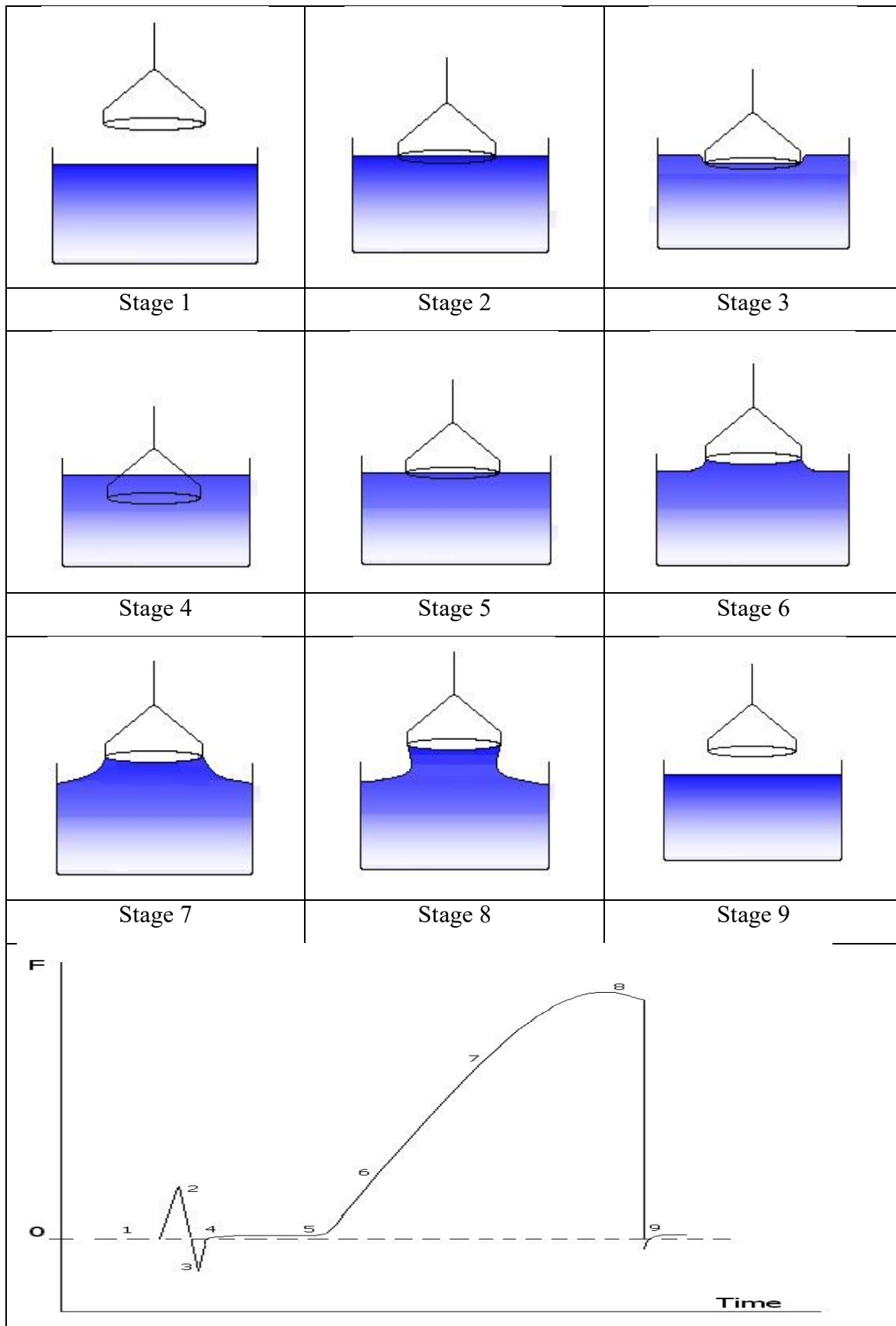
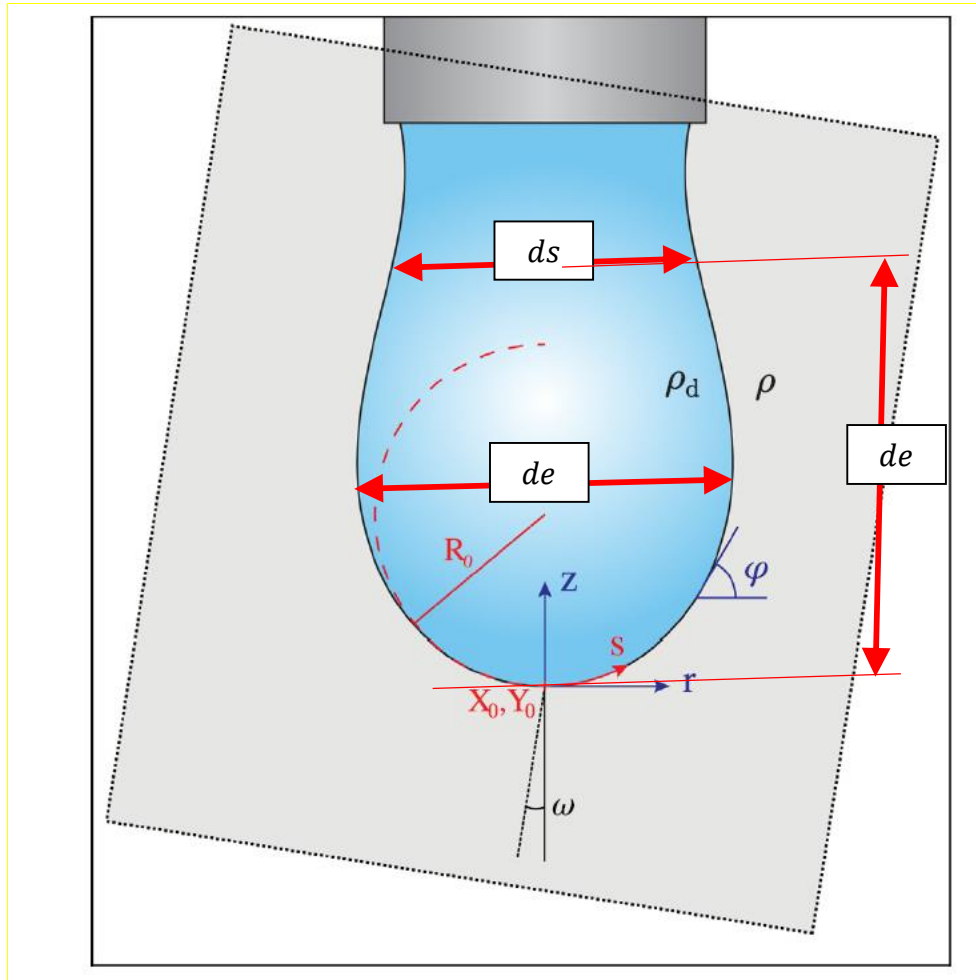


Figure 2.2 Schematic change of the force measured during the process of a ring tensiometer experiment. (<http://www.sinterface.com>).

The Pendant Droplet method is the most versatile, robust and simplest method to measure the surface tension. The technique uses a hanging droplet from a nozzle to produce fluid mechanics measurements. With this method, it is easy to control the process and calculate the surface tension from the shape, volume and size of the liquid pendant droplet. The idea to use gravity was first suggested by Worthington (1881). Modern imaging techniques such as smart phone cameras can also be used to capture and process the image to obtain the shape and volume (Chen et al 2017).

In general, the basic principle for the pendant drop method is based on the principle that the shape of a liquid drop is governed by the competition between gravity and the surface tension of the liquid. The surface tension tries to maintain the droplet as a sphere while the gravity tends to stretch a pendant drop (Berry et al, 2015; Chen, 2017, Gajewski, 2017). There are two approaches associated with the pendant drop method. One is based on measuring the weight of the volume of each drop. i.e.  $W=2\pi r\gamma$  (where  $W$  is the weight,  $r$  is the radius of the tip while  $\gamma$  is the surface tension). This method is easy to use but the accuracy of the method is sensitive to the wetting of the liquid to the tube tip. Another set of methods is optical methods, in which the surface tension is determined from the image of an axisymmetric droplet by analysing the shape of the drop. Compared to other methods the optical pendant method only requires a small volume of materials to perform, thus it is the preferred method.

Surface scientists commonly use an optical goniometer/tensiometer to measure the surface tension and interfacial tension of a liquid using the pendant or sessile drop methods. A drop is produced and captured using a CCD camera. The profile of the drop is subsequently extracted, and sophisticated software routines then fit the theoretical Young-Laplace equation to the experimental drop profile. The surface tension can then be calculated from the fitted parameters. Unlike other methods (such as Wilhelmy plate method, Du Noüy ring method, etc.), this technique requires only a small amount of liquid making it suitable for measuring interfacial tensions of expensive liquids.



**Figure 2.3** Schematic of a pendant drop below a needle. The maximum droplet diameter  $d_e$  and droplet diameter  $d_s$  measured at distance  $d_e$  from the bottom. (Adapted from Berry et al, 2015)

Figure 2.3 schematically illustrates a pendant drop below a needle. In general, the weight of the drop is balanced between the surface tension and the gravity; the internal pressure is also a critical issue when controlling the shape of the droplets. The generated pressure from the pendant droplet across a portion of the rounded interface of a drop suspended from a glass nozzle is important. Early works by Bashforth and Adams (1883), used comprehensive mathematical tables to estimate the solutions of the axisymmetric Young–Laplace equation. These mathematical tables are still in use today. In this method, an appropriate scale is utilized to illustrate that the profile/shape of the axisymmetric pendant drop hinges on a single dimensionless quantity (Equation 2.1):

$$\beta = \frac{\Delta\rho g R_0^2}{\gamma} \quad (2.1)$$

Where:

$\Delta\rho$ : The difference in density.

$g$ : Gravitational force.

$R_0$ : Radii of curvature for a droplet.

$\gamma$ : Interfacial tension.

Bond Number  $\beta$  were defined as the “abstract number” in the work by Bashforth and Adams (1883). The Bond Number has an important physical definition, it is used to represent the relative gravitational force to the interfacial tension/forces (Berry 2015).

It is very hard to accurately calculate the Bond Number for a pendant droplet shape, for a given system, due to the complexity linking the interfacial tension with the gravity, density and drop size. It has gone through several key changes through a history of development. In the early stage, it was Wilfrid Bond (1897 – 1937) who created the relationship between the abstract number and the terminal velocity of water bubbles and drops in 1928. Andreas et al (1938) then created a simple approach for determining the Bond Number term by taking the ratio of two measured experimental quantities (Andreas et al, 1938). As illustrated in Figure 2.3, the concept was based on the maximum droplet diameter  $d_e$  and droplet diameter  $d_s$  measured at distance  $d_e$  from the bottom, which is based on the model by Andreas et al (1938), the Bond Number and the interfacial tension can be determined by measuring the values of the maximum droplet diameter  $d_e$  and droplet diameter  $d_s$  is measured at distance of  $d_e$  from the bottom experimentally. Later work by Fordham et al (1948) and Niederhauser et al, (1950) improved things further from Andreas’ tabulated results through numerical integration of the Young-Laplace equation.

Although both of these approaches introduced a simple methodology for calculating the interfacial tension, it was documented that a large section of the results relating to the actual droplet profile was considered as unusable/unstable. Two more relevant critical publications led by Rotenberg et al (1983) and Huh et al, (1983), introduced computational procedures to exploit the tabulated data, which importantly increased the accuracy of the method. In both approaches, the droplet profile is compared to the theoretical results by assuming the sum of the squared residuals between each experimental and theoretical droplet data point/profile. These techniques share many resemblances, the Huh method (Huh et al, 1983) introduces an imprecise expression that compares the exact expression introduced by Rotenberg et al (1983), which focuses on the position of the droplet apex as an unidentified quantity. This quantity can be determined simultaneously with the shape parameter, Bond Number and Apex radius all together. Other researchers who improved Rotenberg et al (1983) the Bond Number’s method

are Jennings and Pallas (1988), who implemented ‘rotational discrimination’ that can be considered as an enhanced Gauss-Newton method. This technique can produce an optimisation routine that can reduce the computational time requirements drastically. Additionally, the concept by Jennings and Pallas (1988) also provided a detailed error analysis which can produce a conservative, accurate interval that are associated with experimental uncertainty, such as the effect of the interfacial tension between two fluid boundaries. Both of these methods were later redeveloped and reintroduced using an advanced computational method called ADSA (Axisymmetric drop shape analysis). The ADSA was computed by Hoorfar and Neumann (2006). The ADSA method enhanced the droplet experimental set-up and the fitting software. Nowadays, analysing a pendant drop method has been developed further to include a wider variety of drop formations and imaging techniques including smart phones (Chen et al 2017, 2018). Many efforts have also been made to deal with droplets being deformed away from the spherical shape, which is difficult to quantify. More recently, Galerkin Finite Element technique was proposed by many journals, such as Dingle et al (2005), which has the ability of calculating surface tension of a droplet profile. This is a new finite element method (FEM), developed to analyse the structures with more than one parameter behaving in a stochastic manner. This method, however, still requires more computational power to produce reliable results. These developments have provided an important extension to the fluid dynamics of pendant droplets, as they are capable of producing precise interfacial tension readings for very low Bond Numbers. All these development work has highlighted the importance of studying droplet formation and the uncertainty associated with droplet formation.

### **2.3 Viscosity and effect of viscosity on fluids and droplets**

Another important issue associated with droplets, for both static droplets or droplets in dynamic/transition situations, is the viscosity of the liquid. Viscosity refers to the state of a substance being sticky, this is mainly due to internal friction. The distortion of materials is associated with stress and strain involved for solids or liquids. The stresses generated by the deformation of a material, from its rest state, are known as elastic or plastic stresses. Elastic stress is recoverable, while plastic stress is associated with permanent deformation, i.e. non-recoverable. Viscous stresses are another type of material stress that is generated by the rate of change of the deformation over time. In this situation, the present stresses are attributed to the rate of change of the deformation over time. For example, in a fluid (e.g. water), the shearing of the fluid during flowing generates a form of stress, which is influenced by the rate of velocity at which the shearing occurs rather than the distance over which the fluid has been sheared. This is the main source of fluid viscosity; in other words, fluid viscosity is associated with the rate of change of a deformation to the viscous stresses in the material. This behaviour is applicable to all type of flows defined as a simple shearing flow, using the Couette flow concept. (Li et al 2000)

For the situation of a Couette flow, the fluid is located between two substantially large surfaces, one of them in constant parallel motion and the other one fixed (Figure 2.4). When the velocity of the top surface is very low, no turbulence exists, then the fluid particles will move in steady state condition, and their velocities will differ from '0' at the bottom, to 'u' at the top. In this case, the fluid layer moves faster than the layer below it. Friction is produced in such a situation between these layers, the results in a form of force resisting the relative motion between the liquid layers. In other words, viscosity represents the resistance of a fluid to deformation at any given rate. This resistance can be used as a measurement for the frictional forces generated between the different layers of fluid with different flowrates, in some cases.

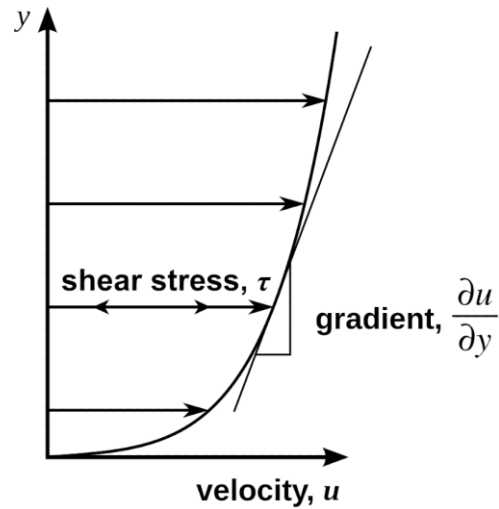
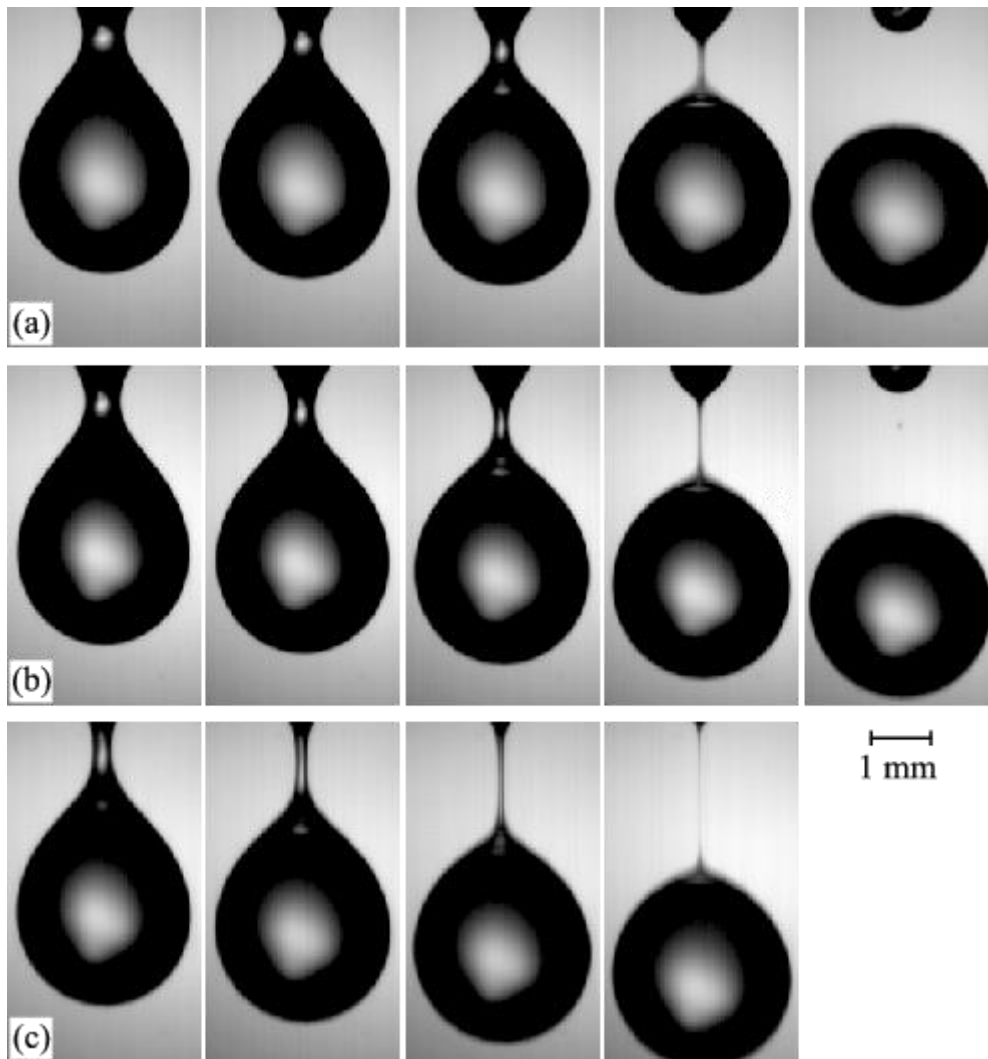


Figure 2.4 Schematic to show a general parallel flow, the gradient of the flow velocity is proportional to the shear stress (Bergman et al 2011).

For the situation with a pendant droplet, fluids with a higher percentage of viscosity tend to have higher droplet volume and size, regardless of the outlet pressure or the flowrate. Similarly, higher values of surface tensions will result in larger fluid droplets (Davidson et al 2006; Omocea et al 2017). The viscosity also directly influences the break-up of droplets (Li et al 2000) and the collision of two droplets (Finotello et al 2018). In addition, the viscosity of a liquid also influences the impact of liquid droplets onto different surfaces (Li et al, 2000, Qin et al, 2019; Almohammadi, et al, 2019).

## 2.4 Different form of droplets and key stages of droplet formation process

The fluid dynamics of droplet formation has been for a long time an important research topic of interest in many engineering systems and manufacturing procedures. It can be considered as an important component of various technologies used in many industries, which include fluid handling, welding, biotechnologies, 3D printing, biochemical, biomedical fields and many more (Heidiger et al, 1986, Shield. et al, 1987, Radiom. et al, 2009). An extensive range of theoretical studies, experimental work and computational analyses, have been performed over the past decade to understand the dynamics of droplets in the dripping mode and other complex situations. As a basic case, the formability of droplets from a capillary tube end, has two main modes (Zhang, 1999): One is jetting, which occurs at a high efflux velocity. Jetting is the result of a coherent laminar jet, starting from the tube, before breaking into a small separate drops. The break-up is mainly due to Rayleigh instability. Another mode of fluid movement from a capillary tube is dripping, this occurs only within slow efflux velocities. It is the result of the liquid flowing out of the tube as small periodic drops, the dripping mode can be divided into two main stages. The first stage of dripping is the quasi-static growth of the drop. This stage ends when the surface tension becomes incapable of holding the weight of the drop as explained in section 2.2. The second stage is called necking, which is caused by the destabilizing effect of the surface tension, necking generally initiates during the breaking up stage of the droplet. A conical shape in the upper section of the droplet, and a spherical shape in the lower section is formed in the necking stage. The length of the liquid thread which links the upper and lower section simultaneously, increases as the droplet reaches the critical breaking point, at this moment, the spherical section is detached from the upper section of the droplet. As for the rest of the fluid attached to the tube, it rapidly withdraws because of the surface tension effect or it may lead to another break-up of small droplets called satellite drops.



**Figure 2.5** Main stages in a single droplet. (Zhang 1999)

Even though the general stages in droplet formation are similar, the profile of the drop and the breaking up process could be different between different liquids and set-ups. A large number of experimental studies have visualized the process of droplet formability before and after the breaking up process (Zhang, 1999, Eggers, 1995). In general, the droplet formation can go through four main sequences of events during droplet formation (Peregrine et al, 1990). These are: Necking, bifurcation, recoil and secondary break-up (as illustrated in Figure 2.5). The exact form a liquid takes also depends on the properties of the liquid. For example, increasing the viscosity may lead to creating more thin liquid line threads during droplet formation. In addition, micro thread lines and smaller necks may lead to creating satellite drops (small droplet formed after the big ones). A typical example can be found in the work by Henderson et al. and Brenner et al. (1997). Their work demonstrated that a series of small necks will be spawned near the break-up for concentrated solutions such as glycerine in water. A representative paper by Zhang and Basaran (1995) also had excellent quantitative data from an experimental study,

which highlighted the influence of the properties of the flowing fluid and the capillary radius effect, both can lead to the formation of satellite drops, for cases with and without surfactants. The published results were later reconfirmed experimentally and computationally by Wilkes et al. (1999) and Zhang (1999). Apart from those common droplet formations reported, another important type is the pneumatic droplet generators. They are specialized in generating droplets smaller than nozzle exist. In general, they depends on the properties of the liquid and the periodic control of the flowrate in junctions/valves and microchannel (Goghari et al 2008; Amirzadeh et al, 2013). These types of droplets are great interest in research laboratories or in industrial applications such as 3D printing, circuit-board manufacturing and solder jetting.

## 2.5 The dynamics of droplet formation and different analysis approaches

Theoretical models describing the dynamics of droplets is a challenging but crucial task to analyse the dynamic behaviour of a pendant droplet. Many academic papers have attempted to work out the droplet volume as a function of the fluid flowrate, material properties and nozzle outlet geometry. One main approach was based on simple macroscopic force balances, in which the breaking up of the droplet and the necking processes are followed by static growth. Nevertheless, this basic approach was deemed inaccurate, with a 20% difference in results. Most of the theoretical work was achieved based on the Rayleigh et al (1887) theoretical model of droplet breaking up, *via* a wide range of axisymmetric one-dimensional models. The information regarding the surface rupture during droplet formation has been obtained by solving the rigorous equations for the momentum conservation and the axial droplet mass (Eggers et al, 1995; Papageorgiou, 1995). Their work has demonstrated that it was able to accurately predict/measure the evolution time of the droplet formation, but it was limited for low flowrates only. The work revealed the formation of thin liquid threads above the hanging droplet, as well as a series of smaller necks with smaller diameter prior to the break-up. The findings from Ambravaneswaran et al. (2002) were further supported by the work by Eggers. (1995). In the work, a comparison study between the one-dimensional and two-dimensional theoretical droplet model formations was conducted. The conclusion of the study proved that the one-dimensional model is sufficient in some case, the two dimensional droplet model was able to provide better outcomes, than the 1D model, with regards to analysing the microscopic fluid features, such as the satellite drops and thin liquid lines.

Numerical modelling *via* Computational Fluid Dynamics software (CFD) provides more comprehensive tools for overcoming /complementing the limitations of theoretical works (Schulkes, 1994; Zhang and Stones, 1997). These methods, supported by high computational power, are able to simulate free surface flow, flow of fluids in a confined space, in contact with other phases or a combination of complex situations. Zhang and Stones (1997), as well as Schulkes (1994) produced a typical computational fluid dynamic study of a two-dimensional axisymmetric model of droplets, *via* the application of boundary conditions/elements and the boundary integral method, which limits the invisible, irrational, Navier-Stokes flows. In another case, Richards et al. (1995) analysed droplet formation within a liquid-liquid system, during the jetting process, using only the Volume of Fluid (VOF) approach. As for solving the full Navier-Stokes equations for an asymmetrical droplet formation of a Newtonian liquid, a similar approach was used by Wilkes et al. (1999) in simulating an ink-jet printing droplet. There are other approaches that can be applied to solve the flowing fluid problem for droplet

simulations. Volume of Fluid (VOF) can be considered as the most reliable code for solving this problem. It can be applied successfully to record fine flow details such as the separation process and the satellite drops. However, numerical difficulties can be encountered if the code is not setup correctly.

## 2.6 Main factors affecting the shape and size of a droplet and analysing approaches.

For many applications, the droplet size and shape are important (Segur et al 1951; Ward et al, 2005; Wang et al 2018). For example, the size can help with the control of the dose of medicines in clinical situations (Kim et al, 2016; Nasser et al, 2018; Melo et al 2019); in a 3D printing process, both the shape and size affect the deposition process (Zhang et al 2015). In a welding process, the size and shape of the metal drops may affect the production speeds (*Hertel. et al, 2013*). For material testing or characterisation, the shape of the droplet could be critical in determining the key properties such as surface tension (He et al 2017). Much of the literature and many published journals investigated common ways of measuring the surface tension theoretically. In general, droplet formation is often connected with fluid flowing through a nozzle or a capillary section. Profiling a pendant droplet geometry can be represented *via* various sets of differential equations. These equations depend heavily on the boundary tension generated on the droplet surface. Hence, the formability of a droplet can be analysed theoretically *via* various methods, such as the Drop Weight (DW) method, the pendant prop (PD) method and the Drop levitation method. The least direct method, which is also the most rapid and persistent, is the pendant proplet method (PD).

In the pendant droplet method, one key aspect for studying droplet or modelling is to determine the profile of a droplet, then this can be used to compare the effect of different conditions based on experimental or numerical data. Some key features were briefly reviewed in this section with reference to the main history developments. This is essential for understanding the key factors or limitations when analysing droplet and droplet interaction with other phases. The pressure generated by the droplet can be linked with the radius of curvature at the drop origin, *via* the following formula (Andreas, 1938; Morita, 2002):

$$p = \frac{2\gamma}{R} - g\sigma z \quad (2.2)$$

Where:  $p$ : The pressure due to the surface of curvature.  $\gamma$ : The boundary tension.  $R$ : The radius of curvature of the droplet.  $g$ : The acceleration of gravity.  $\sigma$ : The difference in density between the multiphase fluids.  $z$ : The vertical coordinate measured away from the droplet origin.

It is to be noted that the pressure caused by the curvature of the droplet is always equal to the product of boundary tension and the mean curvature. Hence, the pressure can be represented as:

$$p = \gamma \left( \frac{1}{R} + \frac{1}{R'} \right) \quad (2.3)$$

Where

$R$  and  $R'$ : two principal radii of curvatures.

Equation 2.3 can be combined to solve the boundary surface tension  $\gamma$  in various ways.

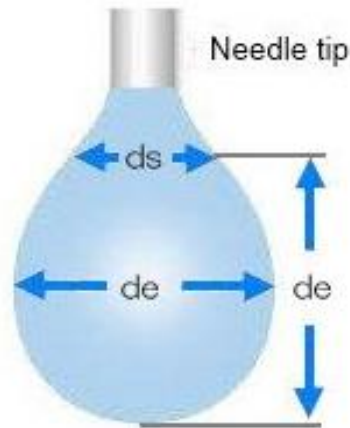


Figure 2.6 Geometry and notation of symbols of a pendant-drop profile. (Song and Springer, 1996)

However, neither the droplet surface pressure nor the boundary tension can be solved without conveniently gauging the droplet size, which can be done by measuring the equator diameter. This figure can only be described by calculating the ratio of the diameters measured at two different horizontal planes. Therefore, Andreas (1938) suggested to measure one diameter at the plane of the equator, and the other from the end of the droplet bottom and into the equatorial diameter. As shown in Figure 2.6, these two diameters can be described as the following ratio:

$$S = \frac{d_s}{d_e} \quad (2.4)$$

Where:

$d_e$ : The diameter at the equator.

$d_s$ : The distance diameter from the arbitrarily plane.

A third and final quantity which must be considered when calculating the droplet size theoretically, is the ratio of the diameter at the equator to the radius of curvature at the origin  $H$ . This can be defined as a new quantity:

$$H = \beta \left( \frac{d_e}{b} \right)^2 \quad (2.5)$$

Which is a function of  $S$ . Because ‘b’ is not known a priori, the integration procedure is iterative: the calculations are performed for various assumed values of b, and the true value of b is determined a posteriori by matching it to the prescribed volume of the droplet (Lubarda and Talke, 2011).

It can be clearly seen that the value of the radius of curvature  $H$ , as a function of  $S$ , can be utilised to solve the boundary surface tension  $\gamma$ .

$$\gamma = \frac{g\sigma b^2}{\beta} = \frac{g\sigma(d_e)}{\beta\left(\frac{d_e}{b}\right)^2} = \frac{g\sigma(d_e)^2}{H} \quad (2.6)$$

Equation 2.6 is convenient and comprehensive, the outcome is subject to the accuracy of the measuring tool used for defining the values of the equator diameter ( $d_e$ ) and the ratio of the diameter at the equator to the radius of the curvature  $H$ .

## 2.7 Wetting between liquid and different surfaces and testing methods

The interaction between a liquid and solid is an important phenomenon relative to the flow, transport and control of fluids (Good et al, 1992; Del Rio et al, 1998). For example, if a fluid residual is attached on steels, it may cause corrosion. If water accumulates on an aeroplane, it can cause icing. In a NDT dye penetration test, the flow of the paint is critical to the penetration depth. While all large-scale volumes of liquid can be defined by the type of volumetric flow, such as flow in pipe or a tank, small scale volume of liquids, including droplets, are defined by the interaction/contact between its molecules and a solid surface. This material characteristic is defined as wetting, which determines the balance of forces between its cohesive and adhesive forces. As illustrated in Figure 2.7, when there is little wetting, the liquid will remain in its original shape, while with stronger wetting, the liquid will spread over a larger area. The wettability of a material can be considered as one of the few advent research topics over the past few decades, due to its applications in many nanomaterials, nanoscience and nanotechnology fields, such as carbon nanotube, graphene and boron nitride nanomesh. (Rafiee et al 2012, Law 2014).

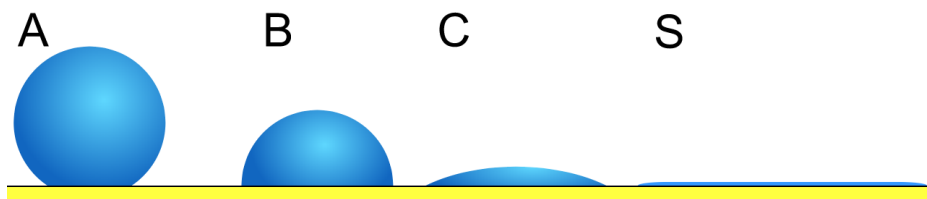


**Figure 2.7** Wetting process for fluids. Drop (A) shows a fluid with very little wetting. Drop (C, S) shows a fluid with more wetting. (Law 2014)

The key feature in wetting is the contact angle ( $\theta$ ) which represents the interface meeting between the liquid-vapour and solid-liquid phases. As seen in Figure 2.8, this is the angle at which the liquid–vapour interface meets the solid-liquid interface. The contact angle represents the balance between the cohesive and adhesive forces between the liquid and the exposed contact surface. As the nature of a drop is to deform over a flat surface, the contact angle decreases and the solid surface increases. Thus, the contact angle provides an inverse measure of wettability (Shafrin, 1960). The wettability of a material can be measured by producing a liquid droplet on a solid surface, then measuring the two dimensional angle formed between the droplet profile vertex and the solid, at the three phase line highlighted in Figure 2.8. The Young Laplace equation used to define the interaction between the adhesion and cohesion forces, is defined as follow:

$$\gamma^{SV} = \gamma^{sl} + \gamma^{lv} \cos\theta \quad (2.7)$$

Where:

$\gamma^{SV}$ : The solid surface free energy

$\theta$ : The contact angle.

$\gamma^{sl}$ : The solid/liquid interfacial free energy

$\gamma^{lv}$ : The liquid surface free energy

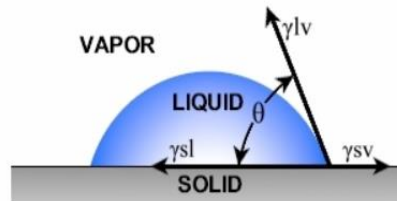


**Figure 2.8** Definition and measurement of contact angle of a droplet on a solid surface. (Law 2014)

When the contact angle of the droplet is over  $90^\circ$ , it is defined as hydrophobic. This means that the wetting process is poor due to the poor force between the free energy of the solid surface and the adhesive forces. Any droplet with an acute contact angle is known as hydrophilic. This condition reflects better wetting adhesiveness, and higher surface energy. Both static and dynamic contact angle measurements are commonly employed to study the wetting, de-wetting, and adhesion characteristics of these surfaces. Figure 2.9 shows different contact angle measurements, including static contact angles, Tilting Plate Method, Add and Remove Volume Method, Wilhelmy Plate Method and Time dependent dynamic studies.

### Static Contact Angle

Static contact angle is known as the most common type of wettability measurement. It is often generated from a sessile droplet and captured during equilibrium conditions of thermodynamics between the three states of gas, liquid and solid. The static contact angle is very useful in providing beneficial data about the conditions of the solid surface. It is also used to measure the surface roughness and the cleanliness. This is because organic and biological contaminants will prevent wetting, which can result in producing larger contact angles on hydrophilic surfaces. Hence, a cleaned and well treated surface will remove any contaminants and this can result in reducing the contact angle as well as improving the wetting process and increasing the surface energy. It can also be used to measure the effects of primers, resins, oxidation, annealing, bonding, and polishing

## **Tilting Plate Method**

The tilting plate method uses an inclined solid surface, typically from  $0^\circ$  to  $90^\circ$ , to record the contact angles of the droplet. Generally, measurements for this method are captured from both the right and the left side of the sessile droplet. Because of the inclined solid surface, gravity will cause the contact angle on the uphill side to decrease and on the downhill side to increase. Correspondingly, the contact angles are referred to receding and advancing angles. The difference between the two angles is known as hysteresis. In some cases, the solid can tilt all the way to  $90^\circ$  without the drop releasing. The final left and right contact angles are used. The graphic below shows a sessile drop as the solid is inclined.

## **Add and Remove Volume Method**

The receding and advancing contact angle, requires the addition of volume to the droplet dynamically, this is to increase the analysed drop volume without increasing the three phase line. This complex method which results in increasing the value of the contact angle, is known as the advanced angle. Once the contact angle/wettability is determined, the additional volume is then removed. The contact angle can also be measured by removing the added volume, without reducing the three-phase line.

## **Wilhelmy Plate Method and Time dependent dynamic studies.**

A more complicated method for measuring the contact angle involves lowering a solid surface into a test liquid and then removing it. During this, the forces generated on the plate can be measured. This method is known as the Wilhelmy Plate Method and it requires large volumes of liquid and the two solid samples be designed to the exact dimensions and have two identical surfaces. This method also needs a precision force scale to produce an accurate reading. This method can be used to investigate and analyse the effect of evaporation, absorption and other phenomena such as the Wenzel to Cassie transitional states.

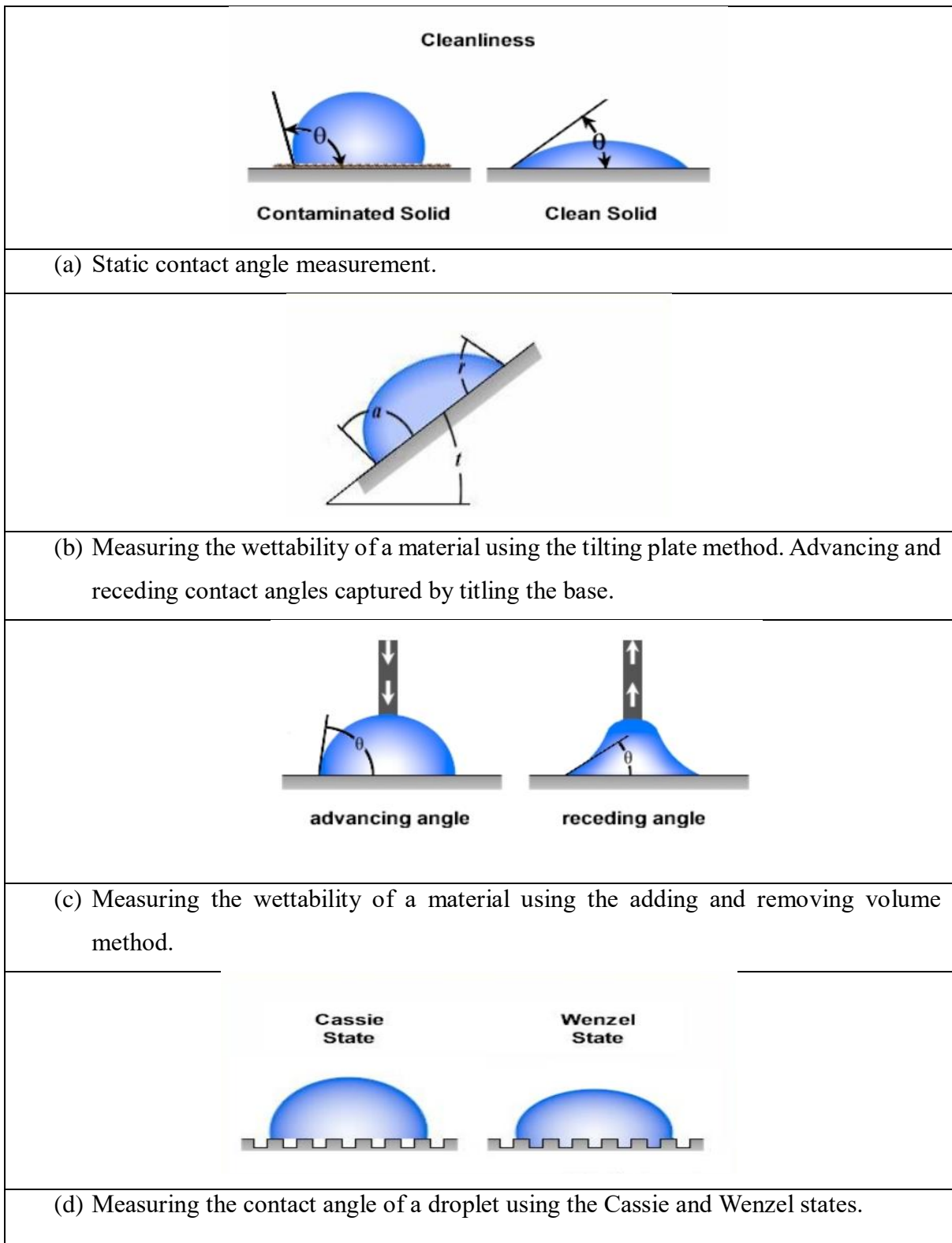


Figure 2.9 Factor affects the fluid behaviour in contact with different types of surfaces. (<http://www.ramehart.com>)

### **Factors influencing the contact angle.**

Many factors may affect the contact angle, for example, surface roughness, heterogeneity factor and adsorption of surfactants. The wetting behaviour and the contact angle of pendant droplet is influenced by chemical and physical factors including both material properties, surface roughness as well as particle shape and size. Many works have been conducted to examine the correlation between these factors and surface wettability (Bartell and Shepard, 1953; Crawford et al, 1987; Drelich et al, 1997).

The surface roughness of the solid surface has a direct effect on the contact angle between liquid/droplet and the surface, this is particularly important on flat surfaces (as compared to curved surfaces). Many practical situations involving wetting and droplet deformation/spreading occur in the real world. Although, it is well understandable that the surface roughness is the main contributing factor to the difference of contact angle measurements, the quantitative correlation and the extent between the contact angle hysteresis and the surface roughness value is difficult to predict (Huh and Mason, 1977). A typical early work by Bartell and Shepard (1953) tested the Wenzel's theory, the work demonstrated that the droplet contact angle on a solid surface can contain roughness within its contact line, and hence, the values are identical to those of clean surfaces. In the early work by Huh (1977), situation for the surface roughness with idealised features (e.g. cross grooves, hexagonal grooves, and radial grooves) was studied systematically and the apparent contact angle and the local contact line positions are approximately predicted. Surfaces having random roughness are also considered and investigated, and a modified form of the well-known Wenzel equation is derived, the approach included a factor for surface texture on top of the conventional roughness factor. There are many factors which affects the uncertainty when linking surface roughness to contact angles (Giese et al 1991; Dang-Vu et al, 2005; Hebbar et al, 2017). This include poor roughness characterisation. The theories only equated roughness with wetting hysteresis, which only applies to idealised models of roughness, and therefore they have limited practical applicability. The difficulty of assigning the "true" apparent contact angle and the inability to distinguish between variations in surface roughness and surface chemistry of heterogeneity and anisotropy are further limitations. Research work is still required to quantify or establish an effective way to implement the effect for engineering problems. Additional significant matter that must be taken into consideration is the Heterogeneity factor. Surface heterogeneity is unavoidable for numerous reasons relating to the presence of contamination. Crawford et al. (1987) investigated the receding and advancing of contact angles for water droplets on quartz plates with a variety of area fractions in a method comparable to that studied by the Cassie

equation (Milne and Amirfazli, 2012). In the work by Milne and Amirfazli (2012), it is shown that the commonly used form of the Cassie–Baxter equation,  $\cos\theta_c = f_1\cos\theta - (1-f)$ , is only correct for the case of flat topped pillar geometry without any penetration of the liquid. Drelich et al. (1997) examined the wetting properties of fluid droplets at well-defined heterogeneous materials containing hydrophilic and hydrophobic regions. The tests in the work were prepared by modelling self-assembled monolayers (SAMs). The work shows that the Cassie equation needs modification in order to take into account the influence of the free energy that is connected with the three-phase contact line. These adjustments are vital for heterogeneities of small sizes within micrometres or less. This requires a high level of modelling linking the behaviour of the liquid at different molecular, micro and macro scales.

## 2.8 Droplet formation in different processes and Numerical modelling of drop formation.

The well-known limitations and complications of theoretical one dimensional models could be overcome by numerical methods. These methods utilize the computational power to simulate free surface flow, via Computational Fluid Dynamics software (CFD). Richards. et al (1995), as well as Schulkes (1994) were some of the first people who produced a computational fluid dynamic study of a two-dimensional axisymmetric model of a droplet, via the application of boundary conditions/elements and the boundary integral method, which limits the inviscid and Navier-Stokes flows. Zhang and Stones (1997) also analysed droplet formation within a liquid-liquid system, during jetting process, using only the VOF approach. As for solving the full Navier-Stokes equations for an asymmetrical droplet formation of a Newtonian liquid, Wilkes et al (1999) were able to verify this, by simulating an ink-jet printing droplet. (Figure 2.10).

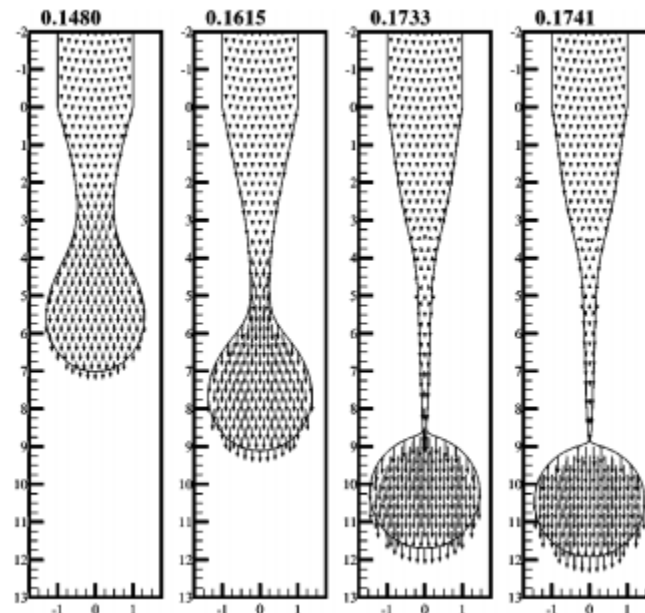


**Figure 2.10** Evolution in time of the computed velocity field in a drop of 85% glycerine in water growing out of a capillary when  $R=50.16$  cm and  $Q=525.0$  ml /min. (Wilkes et al, 1999)

Although it is already known that computational fluid dynamics software is easily capable of simulating complex free surface flows with coalescence and liquid separation/break-up, some researchers prefer to utilize Finite Element (FE) methods due to the successful record in producing accurate simulating results for steady free surface flows. The meshing method used in FE methods is prepared to interpolate the topology of forming droplets, as this will enable the software to record accurately the changing features of the flowing fluids, such as the thin liquid lines before the break up, or the droplet overall volume. Although, running FE models requires a very high mesh density, and more than 350,000 unknown elements, which will

require a lot of computational power and cost to run. Thus Wilkes et al (1999) and Fawehinmi et al (2005) were able to use this method to simulate the challenge of predicting the pinch-off of a low viscosity liquid.

Although various numerical techniques can be applied to solve the flowing fluid problem for droplet simulations, Volume of Fluid can be considered as the most reliable code for solving this problem. This is because it has been applied successfully to record fine flow details such as the separation process and the satellite drops. However, numerical difficulties can be encountered if the code is not set-up correctly. This was demonstrated by Renardy et al. (2002), who faced problems simulating the free surface flow when the surface tension is the dominant force during fluid flow.

The formability of metal droplets is a widely known topic during welding procedures. This has been the focus of many research works (Haidar, 2010, Yamazaki. et al. 2010, Liu. et al, 2010; Liu. et al. 2012, Quinn. et al, 2013). For example, Kovacevic and Bwardsley (1998) studied the process control of 3D welding as a droplet-based rapid prototyping technique. Hertel. et al, (2013) analysed the droplet formation and the transport equations for a semi-fluidic metal during a GMAW system, using high speed videos. Recently, McIntosh et al (2016) reported that a droplet is generated due to the influence of Ar-CO<sub>2</sub> gas on the GMAW process. All of these works, and many more, highlighted the importance of studying the dynamics of droplet formation and its effect on the final welded product. During welding, the physical process is much more complex than a simple multiphase flow simulation. This is because that the heat generation, melting and solidification considerations need to be taken into account when simulating the problem. Figure 2.11 shows a typical modelling work of GMAW in ANSYS, in which the droplet formation and the peak temperature were successfully predicted.

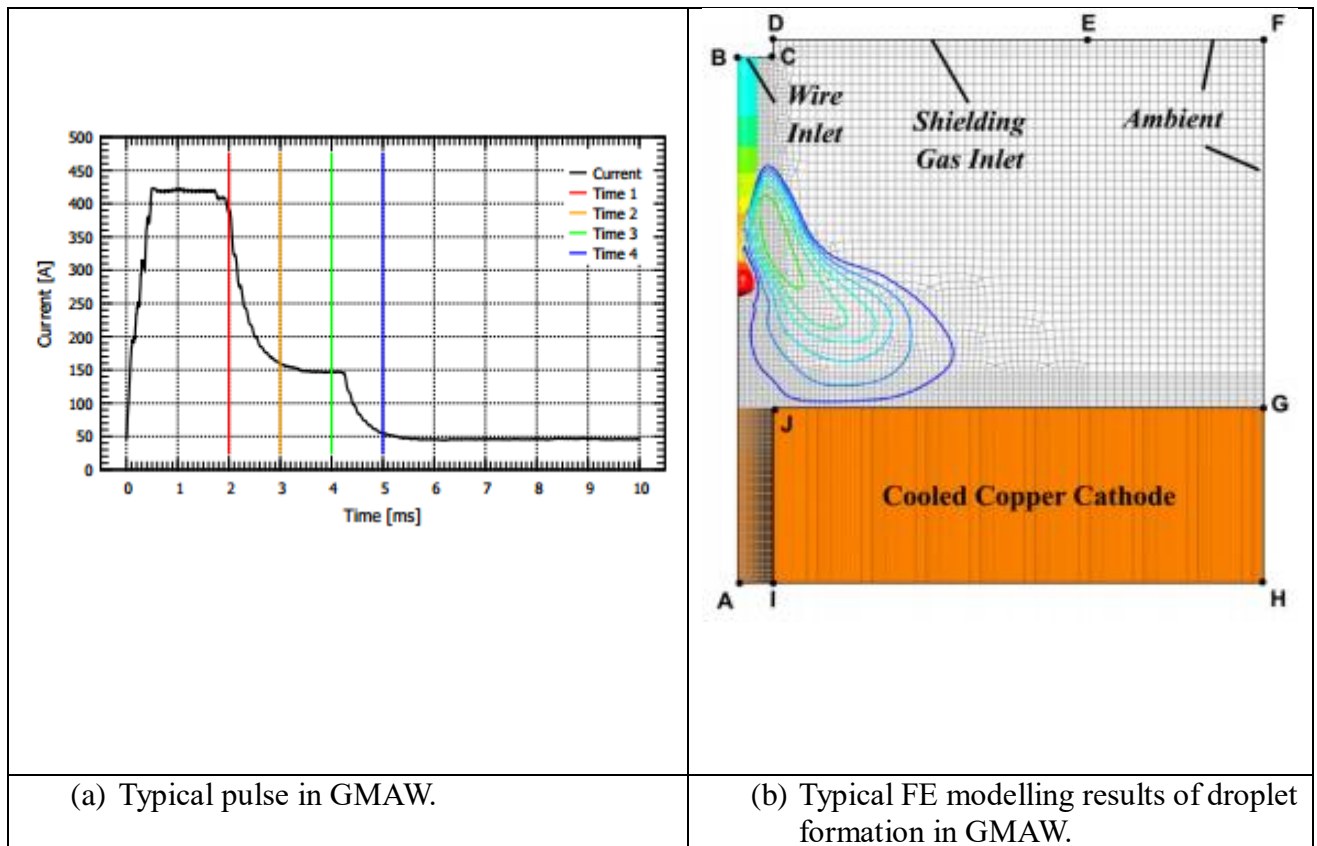
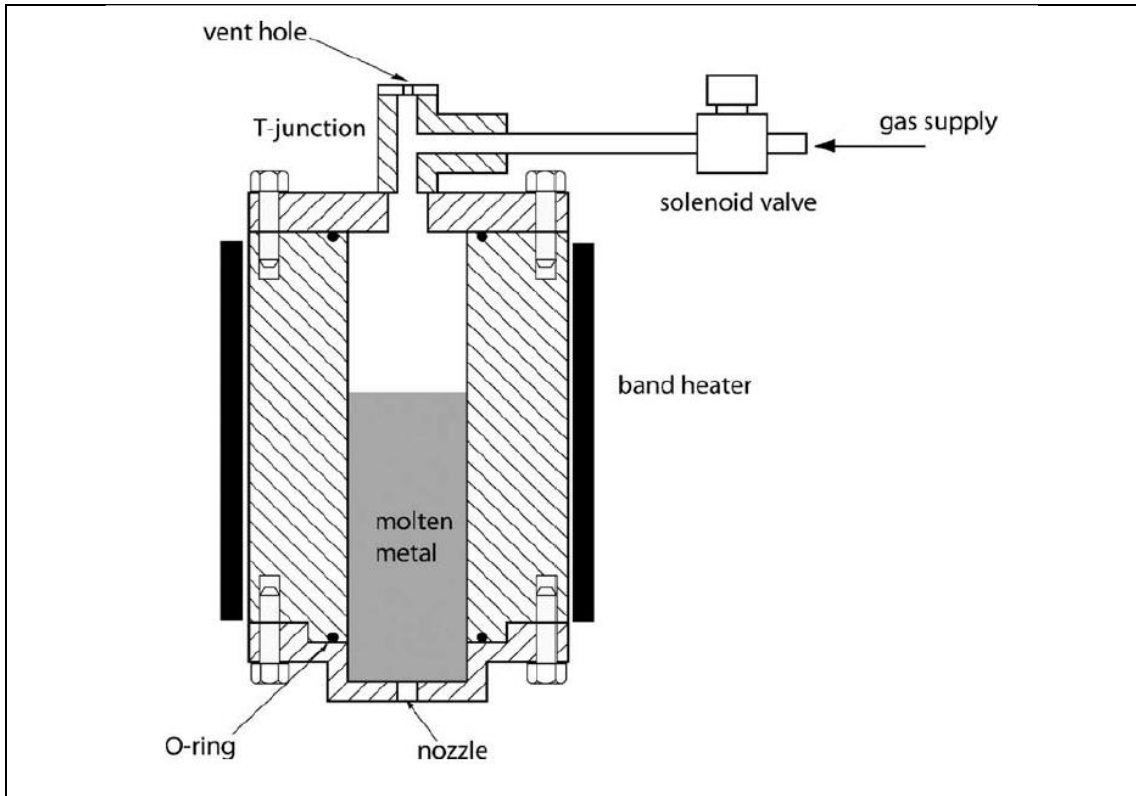
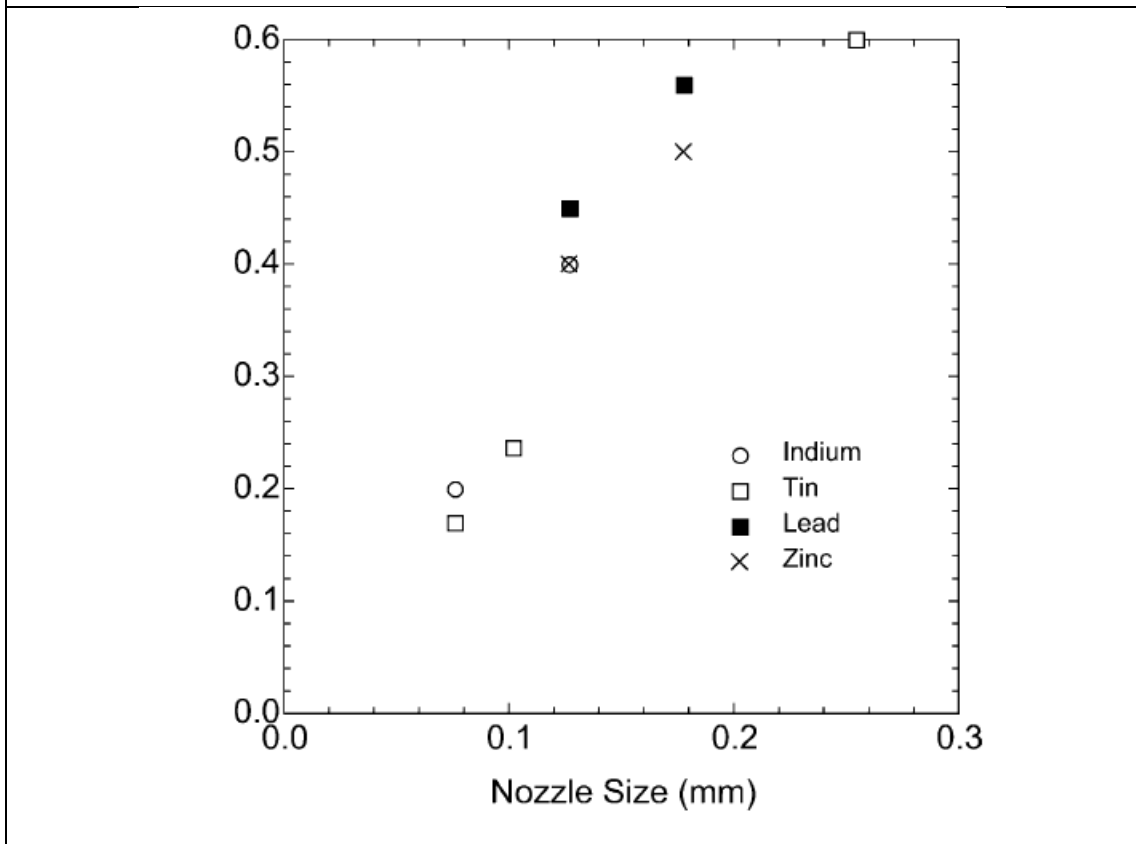


Figure 2.11 FE modelling of droplet formation in a welding process (Hertel. et al, 2013).

There are several other engineering processes that require the production of small, uniform sized droplets of a molten material on demand (Shimasaki and Taniguchi, 2011). A typical case is the deposition of small balls of solders onto printed circuit boards in the electronics industry. The solder is used to attach integrated circuit chips to the boards while providing electrical connections at the same time. Compared to the conventional screen printing techniques, using molten droplet generators to position solder balls directly on boards makes the process far simpler, quicker and more flexible (Cheng et al, 2005; Luo et al 2012; Lass et al, 2013; Amirzadeh et al 2013, Ma et al 2019).



(a) Schematic diagram of droplet generator.



(b) Effect of nozzle size on the size of the droplets.

**Figure 2.12** Typical design of drop generator (a) and the effect of nozzle size on the size of the droplets (b). (Cheng et al; 2005)

Similar types of molten droplet generating processes are also being used in rapid prototyping technology. Components made with wax or metal can be produced in three dimensions (Figure 2.12 & 2.13). As shown in Figure 2.12, in the work by Cheng et al (2005), a cylindrical synthetic sapphire nozzle with an outer diameter of 2.0 mm and an orifice ranging from 0.102 mm to 0.254 mm was inserted into a hole in the bottom plate of the droplet generator and sealed in place using ceramic cement. A range of materials including less corrosive metals (tin, indium or bismuth) and corrosive metal (e.g. Zinc) with the stain-less steel body of the droplet generator were studied. As shown in Figure 2.12(b), the droplet size formed represented by the particle diameters varies between the materials with the same orifice sizes. The work also shows that oxidation affects the size of the droplets.

In this process, fluid instabilities develop along the liquid jet, breaking it up at regularly spaced intervals, thus the droplets are deposited onto the substrate and build up a predefined shape. As illustrated in Figure 2.13, the powder is supplied from the nozzle while the binder is in liquid or semi-liquid form and supplied through a droplet control process. This process is also termed as binder jetting, powder bed/inkjet printing, drop-on-powder printing, etc. The binder/powder product is extracted from the building process, and after removal of excess or unbound powder, is sintered at high temperature as the binder is vaporized. Another area is droplet-on-demand generators which could have different designs. In general, the system requires that a sudden, momentary pressure can be applied to a liquid held in a reservoir, ejecting a single droplet through an orifice (Hieber, 1989; Haferl and Poulikakos, 2002, Cheng et al 2015, Ionkin and Harris, 2018; Ma et al 2019; Wang et al , 2019). Figure 2.14 shows a typical system with electrical field control reported by Wang et al (2019). The electromagnetic force caused by positive current flows through the liquid metal acted as the driving force, which makes the liquid metal flow out from the nozzle. This produce a micro-column near the nozzle. Once the current is switched from positive to negative, the electromagnetic force as restoring force make the micro-column break up into single droplet. All these require practical modelling approaches and materials properties to use the simulation to provide guidance for design and process optimisation.

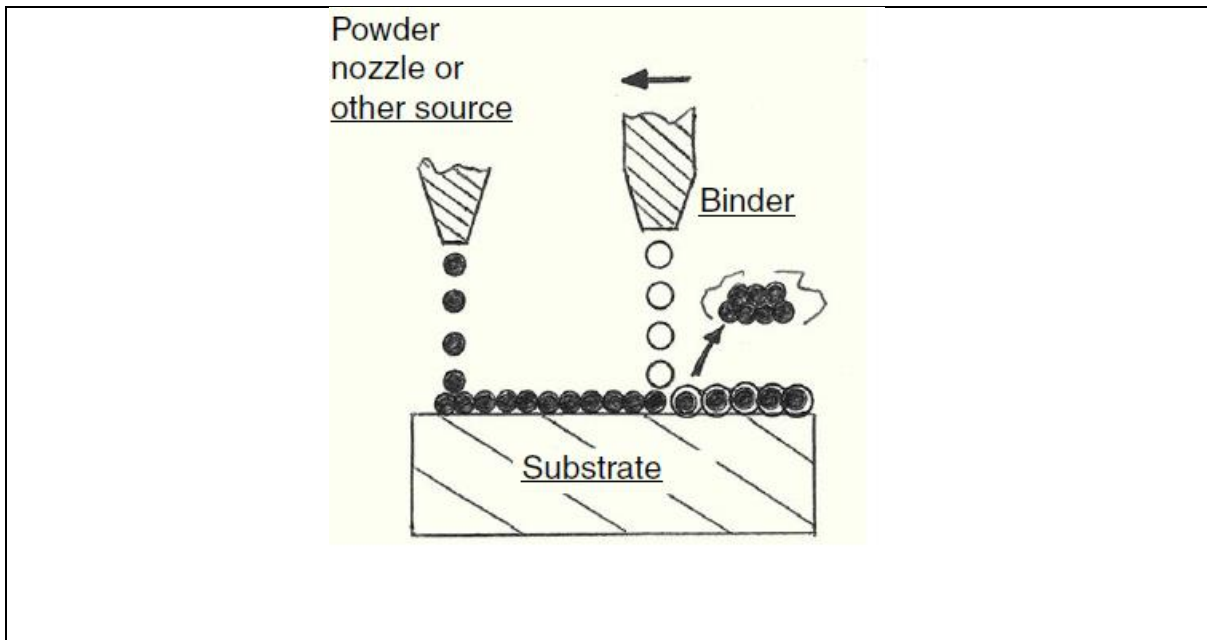


**Figure 2.13** Typical example shows droplet formation in 3D printing. (Murr 2017)

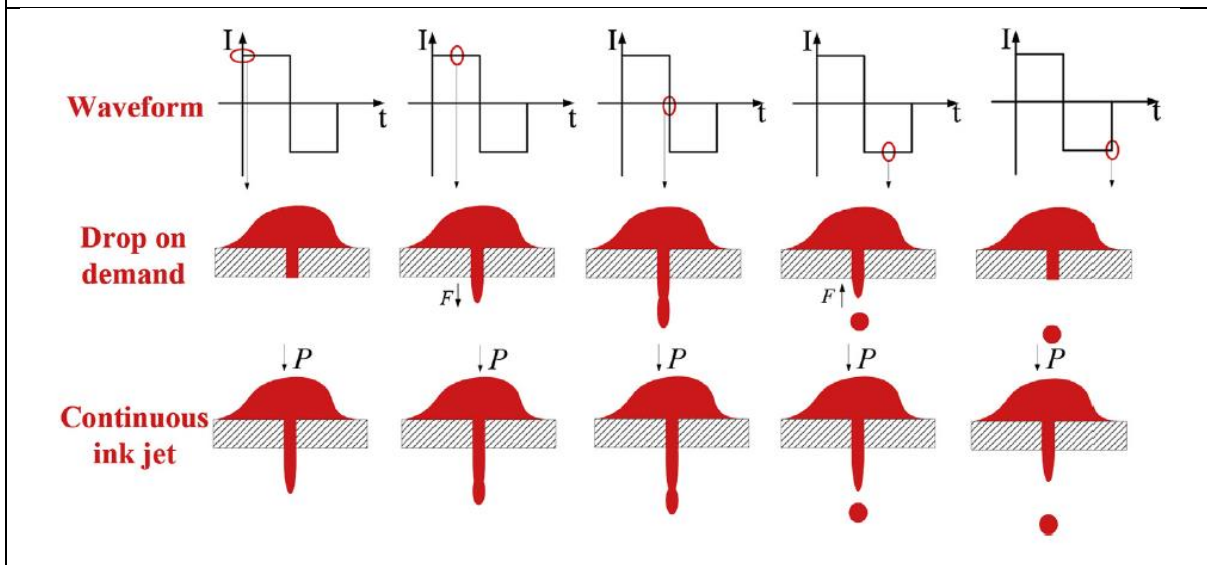


**Figure 2.14** Schematic diagram shows the principle of the droplet formation by the technology of drop-on-demand (DOD) and continuous-ink printing. (Wang. et al, 2019).

More complex issues such as microfluidics is an important area. It is used in liquid handling as well as new material formation and development. It also influences the fluid in other systems such as microfluidic systems (Ward et al 2005; Xu et al, 2008???, Ngo et al, 2016, Anna et al 2016). In addition, microfluidic devices and ways to control droplet generation can also be used for introducing the generation of monodisperse gas bubbles and materials. Despite the apparent simplicity, this approach is a valid tool for the fabrication of several types of advanced materials. Generally, generating droplet and bubbled processes is identical from the point of view of

device employment and physical principles, except for the differences concerning gas liquid interfacial interactions. Garstecki et al (2006) introduced the formation of gas bubbles using microfluidic T-junction and flow-focussing device layouts, similar to the devices used for standard droplet generation. Recently it has been used for more complex systems. A typical example is shown in Figure 2.15. The system is designed to generate droplets of different types of liquid in sequence by controlling the angle of taper ( $0 \leq \alpha \leq 25$  in steps of 5 degrees). Due to the presence of two dispersed phase inlets, sequential alternating droplet generation could be achieved.

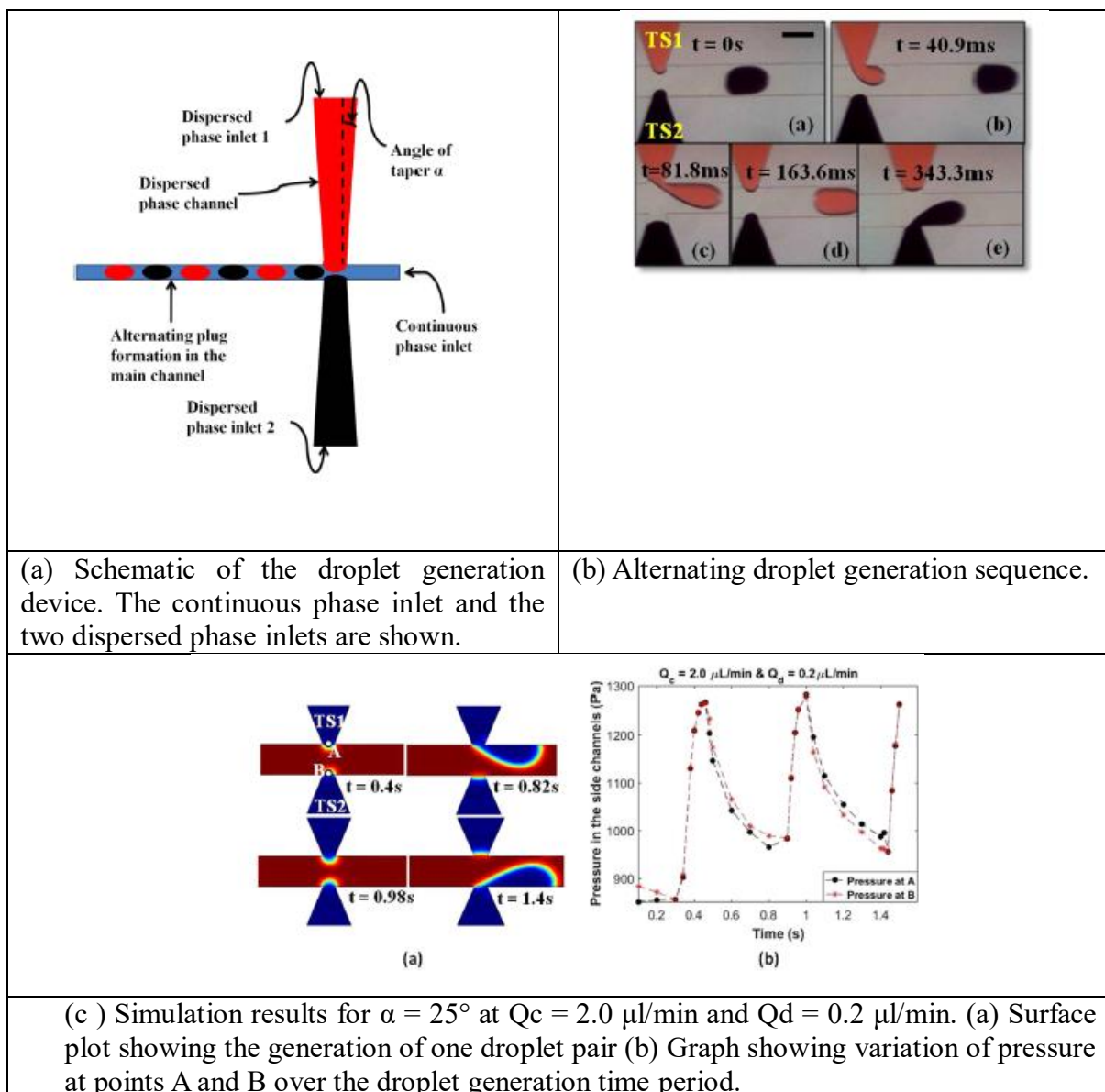


Figure 2.15 Droplet generation for alternating drops of different materials. The continuous phase inlet and the two dispersed phase inlets are shown (Saqib et al, 2018).

## 2.9 Smooth particle hydrodynamics modelling methods and applications

The Smoothed Particle Hydrodynamics (SPH) is a modelling approach developed for dealing with highly deformable materials (Lucy 1977; Druzhinin et al 2016). SPH is a Lagrangian mesh-free method, in which continuous or granular media is represented as a set of discrete particles governed by the appropriate constitutive model. The main parameters assigned to each particle include its mass, internal energy, position, velocity and spatial distance. In the ABAQUS SPH modelling procedure, a size or diameter of a particle is defined which represents these parameters. The SPH method is an effective approach to deal with situation of highly deformable materials under different type of loading conditions. Since the particles are not attached to any grid, this is no issue with mesh distortion. This is an advantage of SPH over other approaches that are developed based on a structured mesh. In a simple term, SPH defines a body by a collection of points, instead of using nodes and elements. The SPH method implemented in ABAQUS uses a cubic spline kernel for interpolation, applying either a fixed or a variable “smoothing” length to particles. Internally, particle connectivity is determined based on smoothing length. The particles can contact Lagrangian bodies through the Abaqus/Explicit general contact feature. In addition, particles can be “glued” to Lagrangian bodies through \*TIE constraints. SPH supports an extensive library of solid and fluid materials, including user materials. (Abaqus Theory Menu (15.2)); Abaqus Technology Brief).

The SPH method has been used to model problems such as metal forming, machining, impact, wear, additive manufacturing, liquid impact, liquid-solid interaction (Li et al 2010; Bojanowski 2011; Zahedi et al 2013; Balbaa 2015; Cercos-Pita 2015; Cercos-Pita et al 2017, Moslemi 2019; Hassoon et al 2019; Cook and Murphy 2020). For different solid or liquid material systems, the parameters need to be tuned to accurately represent the material systems and methodologies. Druzhinin and Vandepitte (2016) used SPH method in modelling sandbags in luggage for virtual drop tests. The SPH method combined with the Mohr-Coulomb material model to simulate granular behaviour of the plastic spheres. The influence of the size of the SPH particles on the resulting stress and strain fields’ smoothness have been investigated. A good correlation between the simulation and experiment data is obtained. In the analysis a ratio  $N$  between the shell element size and the diameter of the SPH particles is found to be the most important characteristic parameter. Cercos-Pita et al (2017) studied the energy conservation properties of the SPH in the presence of fluid–solid interactions. In the work, the whole solid–fluid domain is described as a unique particle system by modelling both the fluid phase and the solid bodies through solid particles. The work showed that, when solid particles are considered, the

energy equation of the particle system contains some extra terms that depend on the pressure–velocity field extensions. However, evident from several prototypical numerical test, the consistency of the SPH model is not affected by the presence of these extra terms, as they tend to vanish when the spatial resolution is increased. The data also shows that the viscous extra term slows the convergence significantly.

Recently Hassoon et al (2019) used SPH method in studying the mechanical performance evaluation of sandwich panels exposed to slamming impacts, in which a high magnitude pulse peak pressure occurs quickly when the ship bottom structure impacting against the sea surface. SPH method was used to simulate the slamming event and the meshed elements of the fluid domain were replaced by particles. A velocity control system was used to calibrate and preserve the approximately uniform velocity throughout the slamming impact. This study focuses on the overall structural response, deformation, and hydrodynamic response of the structure during the dynamic impact designed for naval applications. The model showed very good agreement with detailed experimental works.

The SPH method was used in modelling particle-surface interaction at different angles (Solenthaler et al 2006; Michel et al 2006; Li et al 2010). In the work by Solenthaler et al. (2006), the melting and solidification processes was simulated using the SPH method, in which the merging and splitting of different objects caused by phase change processes is successfully simulated. Michel et al (2006) studied the hypervelocity impact process of a particle on thin brittle targets. The numerical results showed a good agreement with experimental data, damage characteristics and ejection phenomena. The SPH method has also been used to investigate the effect of oblique impact on particle deformation in cold spraying (Li et al 2010). In the study, a systematic examination of the oblique impacting of copper particles in cold spraying was conducted by using SPH method compared to the Lagrangian method. One interesting finding of the work lies in the fact that in the oblique impact, the additional tangential component of particle velocity along the substrate surface could create a tensile force and decrease the total contact area and bonding strength between the particle and the substrate. The model was successfully used to establish an angle range, where the deposition efficiency may be promoted rather than the normal angle. The particle deformation behaviour simulated by the SPH method and the Lagrangian method and the experimental results showed a good agreement.

Another application area for SPH is liquid filled structures (Idelsohn et al, 2009; Oñate et al,

2011, Zhu and Scott, 2014; Sun et al 2010). SPH offers several advantages over CFD and coupled Eulerian-Lagrangian methods in tracking free surface boundaries, handling small material-to-void ratios, and modelling extreme deformation with fragmentation. In the model for simulating Prosthetic Aortic Valve (Sun et al 2010), a finite volume of blood near the aortic valve was modelled with one-node PC3D elements. All particles had the same volume initially. There were 4956 particles, each with a radius of 1 mm. A generic aortic valve was meshed with shell (S4) elements. In another work, SPH is used to simulate the behaviour of blood during valve closure and pressure changes (Sun et al 2010; Abaqus Brief, 2012). In another recent work by Moslemi et al (2019), the Nonlinear sloshing response of liquid-filled rectangular concrete tanks under seismic excitation was studied. The work is able to predict the free surface sloshing height. The model provided a tool to analyse the effect of three-dimensional geometry, corner sloshing, tank aspect ratio, bidirectional loading, and earthquake frequency content.

## 2.10 Droplet formation and materials development

As reviewed in the sections above, droplet formation is related to many design and material issues. The droplets formation is relevant to various manufacturing processes and a range of materials, such as water, glycerines (Segur and Oberstar, 1951; Fawehinmi *et al*, 2005); Low melting temperature metals such as Gallium (Bernstein *et al* 2000; Kim *et al*, 2013, Majidi *et al*, 2016; Zhu *et al*, 2016; Chen *et al* 2018;) and metal materials at high temperatures. In addition to the research on key fundamentals of single droplet formation and associated processes, there are many other emerging areas of more complex systems for material development or handling, such as microfluidic systems (Ngo *et al*, 2016; Anna *et al* 2016; ), and satellite droplet (Kovalchuk *et al* 2017; Pardeep *et al* 2017). Furthermore, droplet collision is becoming an emerging area for material development of hybrid material systems (Jia *et al* 2019). Wetting behaviour is also an important area for material surface development (Khojasteha *et al*, 2016; Tang *et al*, 2017; Al-Sharafi *et al*, 2018; Li *et al*, 2019; Manaf, *et al* 2019). Another direction in the development lies in the interaction between droplets with other materials systems, which can be a combination of physical and mechanical processes. The interaction between droplets on different surface is also important (Moreira *et al* 2010; Mitra *et al* 2013; Cimpeanu *et al* 2018; Khojasteha *et al* 2016). Complex full fluid modelling requires high computation resource and time, and it is difficult to assess the deformation in the materials. A simple more effective way to simulate such process will aid the investigation of water droplet behaviour and material interaction for new material developments and applications.

As outlined in chapter 1, there are some emerging novel materials such as materials with layered systems. Droplet impact represents localised loading onto a material, which resembles the indentation onto a material. One particular interest of this work is negative Poisson's ratios materials. Poisson's ratio represents the lateral deformation of a material under tension or compression. It can be calculated by the negative values of lateral strain over the strain at the loading direction. Conventional materials will shrink when being stretched, and expand when being compressed. Hence, most conventional materials has a positive Poisson's ratio. Some new materials have a novel Poisson's ratio, the materials expand when being stretched and shrink when being compressed (Gaspar *et al*, 2005; Aw *et al*, 2015). Therefore, it is termed as "negative Poisson's ratio" or Auxetic materials. Recent works shows that, negative Poisson's ratio influences the material deformation under localized deformation such as indentation (Lim 2014, Photiou *et al*, 2016;). It is important to study the effect of Poisson's ratio and Auxetic behavior for both rigid indenters and liquid droplets in homogenous materials or more complex material systems, such as materials with embedded thin shells. The recent research and

development works on auxetic have been covered in several review works (Saxena et al 2016; Lake 2017; Duncan et al 2018). Potential applications of this group of materials cover many industries such as aerospace, sport, medical and sensors. The majority of research works had been focused on identifying mechanisms/structures that have negative Poisson's ratio behaviours, such as re-entrant structures, chiral structures, rotating rigid/semi-rigid units; angle-ply laminates; grooved block of metals as single materials, diamond perforation (Grima et al 2012; Brely et al 2015; Wang et al 2019). Some structures have inhomogeneous structures and the auxeticity is caused by the localised deformation, bending or rotation of beams or joints. For example, in a re-entrant honeycomb cells of conventional hexagonal auxetic structure, the auxetic behaviour is controlled by horizontal rib, length of the linking ribs and depth of ribs. For Re-entrant triangular structure, the length of the ribs and the angle between the ribs is very important (Saxena et al 2016). The rotating rigid/semi-rigid units are formed by connecting straight ligaments (ribs) to central nodes which may be in circles or rectangles or other geometrical forms, while Chiral honeycombs displays the auxetic effect for both in-plane and bending loads, which is achieved by arranging the cylinders on the base of a re-entrant structure (Lake 2017; Wang et al 2019).

Some structures have relatively homogenous structure such as auxeticity with entangled single wires, random oriented cuts, diamond perforation. These materials have relative uniform structure. Most known homogeneously auxetic materials are porous foams or artificial macrostructures and there are few examples of inorganic materials that exhibit this behaviour as single crystal or polycrystalline solids. Dagdelen et al (2017) reported a new approach to predict homogeneously auxetic materials as well as a number of compounds with a near-zero Poisson's ratio. It used high performance computer to discover materials with target properties including auxeticity. The finding that many materials have auxetics properties such as  $\text{SO}_2$ ,  $\text{FeV}_3$ ,  $\text{GeO}_2$ . In the work, the Poisson's ratios were derived from the calculated elastic tensor of each material in this reduced set of compounds. In another work, Yu et al (2017) studied negative Poisson's ratio in 1T-type crystalline two-dimensional transition metal dichalcogenides. The work reported that the material groups exhibit an intrinsic in-plane negative Poisson's ratio, which is dominated by electronic effects.

The unique properties of auxetic structures opened a window towards a wide range of functions such as the design of novel biomedical applications, energy-absorbing devices, acoustic dampers, membrane filters with variable permeability, personal protective equipment (e.g. shin

pads, shoe covers, etc.) and smart implants (Sanamia et al 2014; Darwish and Aslam 2014; Aw et al 2015; Mousanezhad et al 2016). One advantage of auxetic structures lies in its high indentation resistance. Indentation refers to the deformation of materials under localised load by a pressure and in contact with indenter of different shapes. The way an auxetics material works (shrinks under compression and expands under tension) greatly influences the material behaviours. Recent works show that, negative Poisson's ratio influences the material deformation under localized deformation such as indentation (Lim 2014, Photiou et al, 2016; Aw et al 2016; Kumar et al 2020). Earlier work by Evans and Andersons (2002a and 200b) on ultra-high molecular weight polyethylene (UHMWPE) exhibits enhanced indentation resistance by up to a factor of three when compared with conventional UHMWPE and enhanced attenuation of ultrasonic signals (Evans 2000; Evans and Anderson 2000). Lim (2014) studied the uniqueness of line and point contacts on auxetic half-space in comparison to conventional ones in terms of displacement and stress fields, and found that the contact area is affected by the Poisson's ratio. Photiou et al (2016) also studied the interaction between a conical indenter and an auxetic material through the finite element modelling method. The work showed that the contact area is reduced as the Poisson's ratio increases, this induced a higher force to penetrate the material. The pressure underneath the indenter is also increased. Aw et al (2015) investigated the effect of Poisson's ratio on the deformation of the thin membranes through FE modelling and establish the influence of parameters including sample thickness, indentation depth and indenter size is analysed. The feasibility and limitation of an analytical solution is also evaluated. Kumar et al (2020) investigated the elasto-plastic indentation of auxetics and metal foams, which established the contributions of yield strain, elastic, and plastic Poisson's ratio on the indentation hardness. The work also reported that there is no effect of elastic Poisson's ratio on the indentation hardness when the plastic Poisson's ratio is more than -0.8. Several work also studied the effect of auxeticity on the impact resistance with different types of indenters. It has been widely reported that the auxetic material densifies under the impact in both the longitudinal and transverse directions (Evans d Anderson 2000; Photiou et al 2016), In the case of a thin shell with fixed boundaries, the deflection profile is slightly different between positive and negative Poisson's ratio, while the contact area for negative poisson's ratio relative smaller (Aw et al 2015). It is important to study the effect of Poisson's ratio and auxetic behavior for both rigid indenters of different shapes and liquid droplets in homogenous materials or complex material systems, such as materials with embedded thin shells.

## **CHAPTER THREE**

# **EXPERIMENTALS, NUMERICAL MODELLING AND DATA ANALYSIS PROGRAMS**

### 3.1 Introduction

Figure 3.1 shows the overall research structure, key approaches and focuses. The topics covered in each chapter are listed in Table 3.1. The material characterisation is focused on measuring the key material parameters and calibration procedures related to the droplet formation and cross-examine the material parameters. This includes using experimental apparatus, set-up procedures and details of some key experimental facilities and materials associated with the thesis work. Details of the work is presented in section 3.2-3.4. The experimental work also helped identifying issues in modelling small volume of liquid in different industrial processes. The numerical modelling investigations covered two inter-linked sections. The first section (main results presented in Chapter 4) focused on the computational fluid dynamics aspects of the research. Different numerical modelling codes and programs are evaluated to develop an effective and efficient method for simulating droplet formation. three different types of CFD multiphase programs and methods were evaluated, each of which behave in a different level of complexity. Hence, it is very important to select the correct numerical solver/code before starting the simulation, so that the numerical model is able to utilize the right continuity equations and efficient use of computation resources. Furthermore, it was important to compare the results from different numerical methods against each other to work out the best efficient and accurate method that are suitable for simulating several droplets conditions. The second section (presented in Chapter 5) focused on developing a Finite Element model, *via* Abaqus, to comparatively study the investigate the interaction behaviour of solid indenter and liquid drops impacting different material systems. Initially, the indentation stiffness/ resistance, of soft material systems with an embedded thin layer under a flat-ended indenter and a spherical indenter were comparatively studied. The effect of the Poisson's ratio (positive and negative Poisson's ratio) on the indentation resistance were systematically analysed theoretically and numerically. The Smoothed particle hydrodynamics (SPH) approach is implemented to simulate liquid droplets impacting onto homogenous materials and structure with an embedded thin layer. Use of the numerical data to explore the development of a parametric MATLAB program for producing a design/processes selection tool. The work also extended to other related issues relevant to research and development in droplet management, beading forming in welding, and fluid flow in cracks.

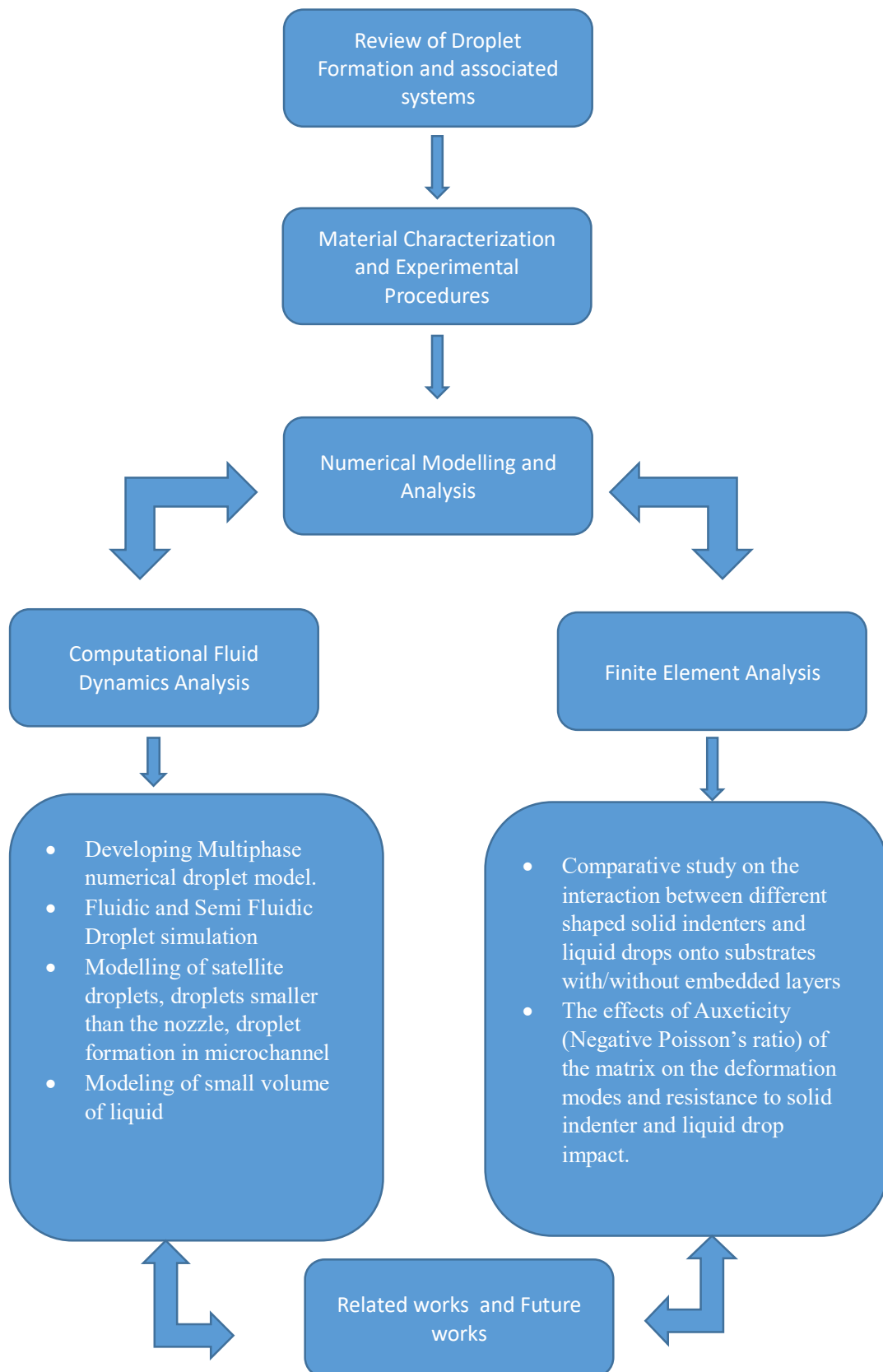


Figure 3-1: Overall structure and research approach.

**Table 3.1 Main Research Works**

#### **Development of Numerical Modelling Program of Droplets (Chapter 4)**

- Development of numerical models of droplets and compare the efficiency of different approaches.
- Evaluation of effect of key modelling parameters and mesh densities.
- Comparison between numerical model and theoretical/analytic calculation
- Comparison between numerical data and experimental data (fluid with known properties)

#### **Experimental and Numerical analysis of droplet formation for different material systems and comparison with numerical data**

- Characterisation of the properties and droplet formation of fluid mixtures
- Investigation of the effects of liquid mixture (water-viscous liquid mixture) on the key parameters of droplet formation
- Experimental and numerical investigation of the droplet formation with satellite drop (fluid mixture)
- Experimental and numerical investigation of the low melting temperature liquid metals
- Parametric numerical modelling of effect of materials

#### **Discussion**

- Key factors affecting the droplet formation approaches, uncertainty and limitation
- Effect of contact angles in droplets and other situations
- Inverse material properties predictions: surface tension estimation from pendent droplets
- Modelling more complex systems (continuous droplets, satellite droplets, droplets smaller than the nozzle and fluid in micro channels)
- Importance and potential use of numerical modelling of droplets and data system development

Case Studies: Modeling of droplet merging in micro welding, dripping of liquid from and stainless steel surface and liquid penetration in cracks in NDT

#### **FE modelling of interaction between rigid indenter with soft substrates with or without embedded systems (Chapter 5):**

- FE modelling of soft material with a flat indenter with/without embedded systems.
- FE modelling of soft materials with a spherical indenter.
- Effect of material properties including Auxetics (Negative Poisson's ratio).
- FE modelling between droplets and different substrates:
- Numerical model development with SPH elements.
- Solver/solution method comparison and meshing scheme development.
- Deformation of droplet with different substrate and embedded systems.

#### **Discussion**

- Effect of indenter shapes on the material deformation.
- Effect of droplet shapes.
- Deformation of droplets and its potential implications

Chapter 6 Conclusions and Future Works

## **3.2 Testing and material preparation**

Sections 3.2-3.3 summarized the set-up and details of some key experimental facilities and materials associated with the project. The facilities include liquid droplet testing apparatus, mixing and viscosity measurements. The materials include glycerine-water mixture and a low melting temperature alloy (Gallium). Procedures for some property measurement and calculation for liquid density and the viscosity measurements are presented. Some welding facilities, material preparation and characterisation are also introduced. The micro welding process of wires and tubes involves a complex process including merging of small volumes of liquid to form a joint. A3D surface roughness measurement apparatus for characterising the surface of welded steel tubes is also presented, the surface features influences wetting between the surface and liquids. Different modelling programs evaluated and used in the research are detailed including the ANSYS Fluent, ABAQUS, OpenFoam and CFX.

### **3.2.1 Pendant Droplet apparatus.**

Figures 3.2&3 show the experimental set-up to generate a pendant droplet of liquid and perform image measurement. The procedure utilized a high speed camera with image analysis to visualize the liquid flow out of the nozzle, as well as yielding quantitative information of the limiting length of the drop, the primary drop volume, and time to break-up. The liquid flow is supplied using a syringe that is located on an anti-vibration table. This is important to ensure that the flow velocity is fully developed during the experiment. The type of nozzle used to produce the pendant droplet has an external diameter of 0.4mm and an internal diameter of 0.325mm. In this experiment, the pendant droplet images were obtained using Eastman Kodak Ektapro with a Meijotech magnification zoom lens (0.7 – 4.5x) and a High Speed Motion Analyser software. This camera has the ability to record full photos at speed of 4,500 frames per second (256 by 256 pixels), as well as 40,500 frames per seconds for partial frames (64 by 64). The camera is also capable of recording videos for viewing images of the drops before, during and after the droplet break-off. The apparatus is lit up with a 250 Watt halogen light source reflected on a white paper to backlight the oil droplet.



Figure 3.2 Experimental arrangement used to visualize droplet formation.



Figure 3.3 Typical captured image of a pendant droplet

Before start generating the droplet, the nozzle was cleared of any liquid or contamination, which may result in creating a disturbed non-uniform flowrate. After that, the syringe head was turned steadily to generate a periodic flow condition, in which the droplet is formed, developed and detached from the nozzle exit. In the preliminary studies, repeating the experiment under the same conditions was performed to assess the repeatability. Frequent values of droplet length and volume were produced. This means that the experiment was reliable with repeatable volumes of the primary droplets. Some tests were performed and results showed agreeable data with other published papers, which is to be detailed in Chapter 4.

### 3.2.2 Material systems

To study the effect of surface tension and viscosity on the formulation of a pendant droplet and provide data to assess the numerical modelling results, Glycerine and Water solutions (Glycerine+stilled water) were utilized for the experiment and computational simulation process as reference/model material. The material system itself is important for many applications (Gonzalez et al 2011). Another reason for choosing this material system as a model/reference material in this work lies in the fact that this type of solution has broad freedom with controlling the viscosity, density and the surface tension, as the content of glycerine increases in the solution from 0 to 100 per cent. This work used five types of Glycerine-Water solutions with different concentration levels. These were prepared by mixing the desired percentage of glycerine with a distilled water, *via* a measuring cylinder. The data reported in the thesis are mainly based on five solutions that had 0, 25, 50 and 100 per cent glycerine oil concentration levels, respectively.

### 3.2.3 Testing procedure for obtaining material properties for pendant droplet test and modelling.

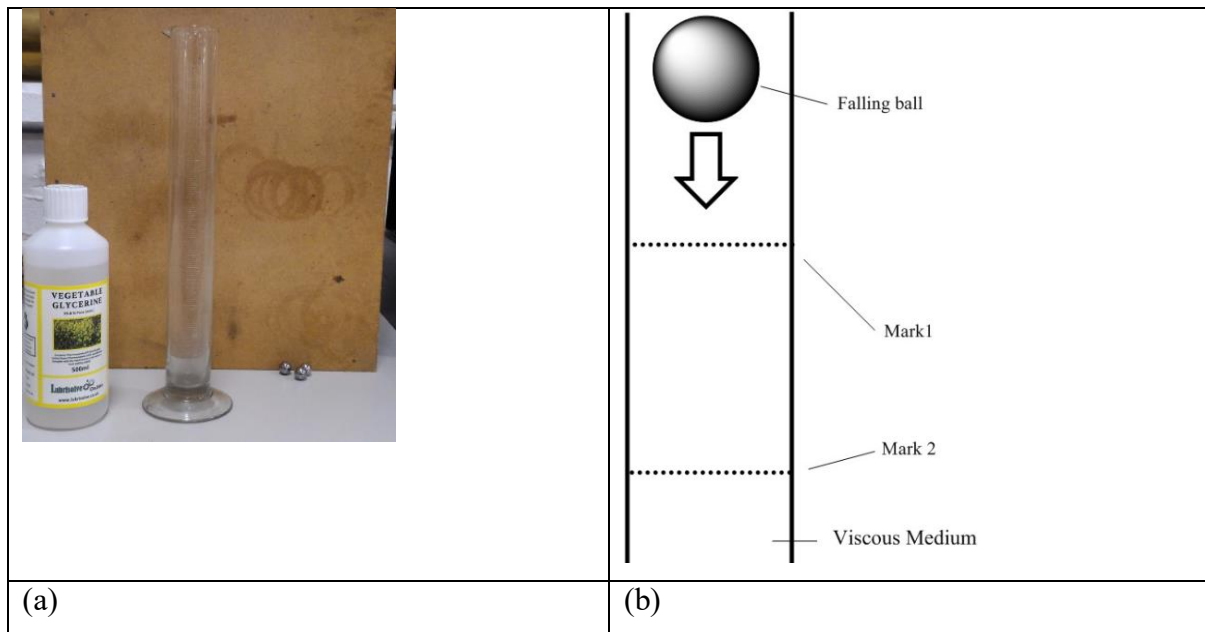


Figure 3.4 Apparatus used to calculate the viscosity of Glycerine-Water solution with various concentration levels.

To investigate the flow of the Glycerine Water Solution within the testing tube, the test involved performing a series of experiments to determine the fluid properties. The aims of the experiment are to determine: (i) The density of the Glycerine Water Solution, at different concentration levels. (ii) The dynamic Viscosity of the Glycerine Water Solutions. The density and the dynamic viscosity were calculated experimentally using Stock's Law ball bearing method. The apparatuses and the principles are shown in Figure 3.3 for the viscosity tests. The equipment required for this experiment is: a large graduated cylinder; a selection of different sizes of ball bearings; a mass balance; a video Camera and a stop watch.

The equations required for this experiment are as follows:

Volume of sphere:

$$V_{volume} = \frac{4}{3}\pi r^2$$

Equation (3.1) – Volume of sphere equation.

Density of the sphere:

$$\rho = \frac{m}{V_{volume}}$$

Equation (3.2) – Density of Sphere equation.

Velocity of the sphere:

$$s = \frac{d}{t}$$

*Equation (3.3) – Velocity of the sphere equation. 'd' is the distance; 't' is time.*

Dynamic viscosity equations:

$$\mu = \frac{\Delta\rho \cdot g \cdot r}{9s}$$

*Equation (3.4) – Dynamic viscosity equation.*

Where:

*s*: Velocity of the ball bearing.

*r*: Radius of the ball bearing.

*m*: Mass of the ball bearing.

*d*: Distance of travel.

*t*: Time of travel.

$\Delta\rho$ : Density difference between bearing and fluid.

*g*: Gravity acceleration.

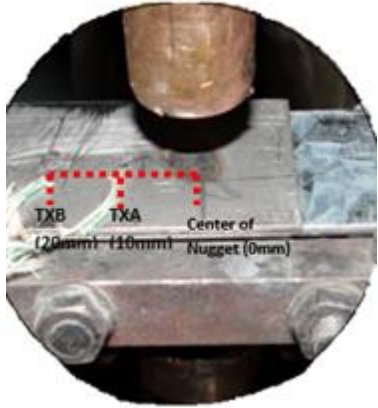
The testing process included: mark a fixed position at the top of the cylinder at around 30mm below the surface of the oil. Measure the distance between the two marks on the cylinder. Set up the video camera so that the entire cylinder is being recorded. Drop the ball bearing into the liquid with the camera filming (Figure 3.3). Using the recorded footage, measure the time it takes for the ball to travel between the two marks on the cylinder. Calculate the velocity of the sphere using Equation 3.3. From the referenced experimental process, an average value from six trails were documented for both the density and the viscosity. Some typical data is listed in Table 3.1. The surface tensions values were measured using the DuNouy ring probe mounted on a torsion balance (Fawehinmi. et al, 2005). It is to be noted that the results from this experiment is applied in the developed numerical model.

**Table 3-1-** Main material findings from the Stock Law experiments (error percentage  $\pm 0.1$ ).

% Glycerine (v/v)	Density of Solution ( $g/m^3$ )	Viscosity of Solution ( $Pa\ s$ )	Surface Tension ( $N/m$ )
0% Glycerine	0.973	0.001	0.070
25% Glycerine	1.114	0.017	0.0660
50% Glycerine	1.225	0.17	0.0625
100% Glycerine	1.231	0.3	0.0620

### **3.3. Facilities and process for studying the bead formation in welding Processes and surface finishes.**

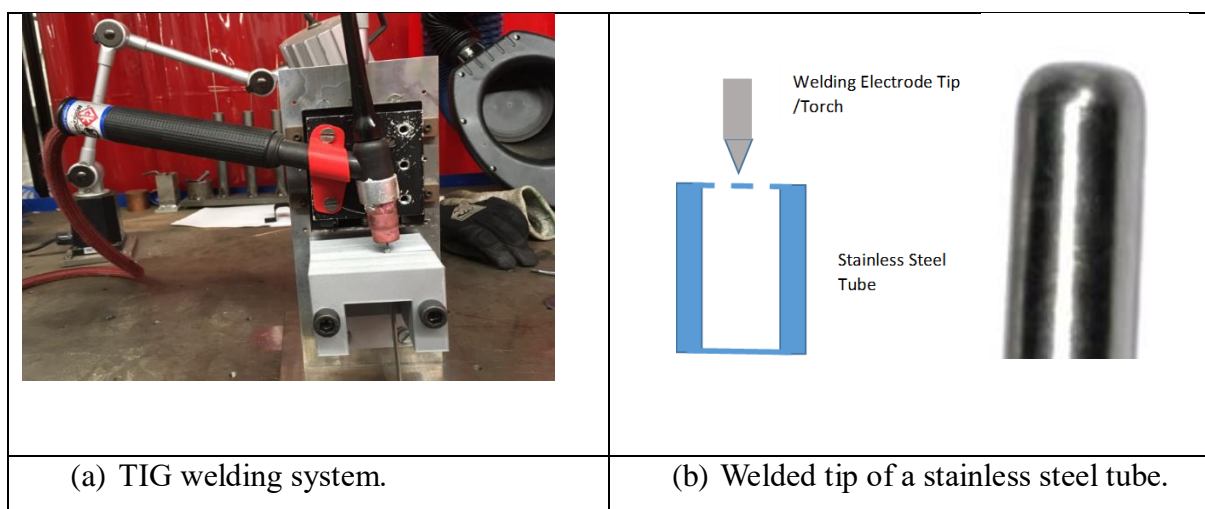
As a part of a major project in developing integrated modelling of micro welding process and temperature sensors including developing ways of using effective modelling for training, a range of practice and experiments have been performed during the project. Typical processes includes: the welding process has been evaluated with a particular focus on the nature of the bead forming process from two thin wires in Capacitor Discharge Welding (CDW) of K-type thermocouple sensors; tungsten inert gas (TIG) welding of thin stainless steel tubes and structure analysis of sheathed thermocouples (Norbury, 2018); Some typical cases representative of small volumes of liquid in different conditions are also evaluated. For example, in non-destructive testing (NDT) dye penetration tests (paint flow into small cracks); the use of welded thermocouples in remote temperature is examined, to analyse the effect of bead size and shape on the temperature response rate. Thermocouple bead represents a case where the shape and the size of bead, formed through fluid drops merging are important for its sensitivity of measurement (Norbury, 2017). Merging liquid from two nozzles at an angle; generation of droplets in flowing liquids is studied to aid the development of numerical models, effect of the surface roughness on the wetting and dripping of liquid when a sensor is measuring temperature is also tested as part of the project and linked to other new projects which evolved from the outcome of this project.

	
<p>Figure 3.5(a) Capacitor Discharge welding apparatus used to join two thin wires for thermocouples.</p>	<p>Figure 3.5 (b) Typical welded joint of two wires. The tip is formed by merging liquid drop of melted metals in the welding process.</p>
	
<p>Figure 3.5 (c) Typical remote thermocouple used in measuring the temperature in electrical resistance spot welding of steel plates.</p>	<p>Figure 3.5 (d) Data logger used to record the temperatures with thermocouple as in (c).</p>

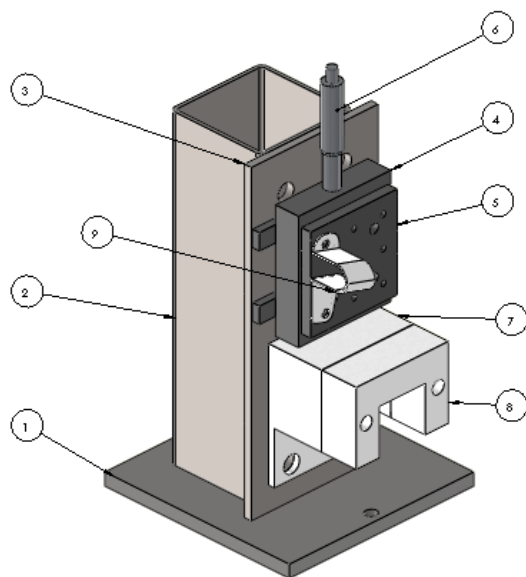
**Figure 3.5** Typical facilities used in welding tests and evaluation of the metal melting bead formation.

Figure 3.4 (a) shows an auto pin welder apparatus, manufactured by TMS Europe. This Capacitor Discharge Welding machine was used to produce the thermocouple samples. It contains a battery that is being powered by six capacitors, which can provide up to 250 Joules of energy output. It features two main welding cables, a large magnet pot and interchangeable pliers, as well as a controlling unit panel, which is used to regulate the consumed power during the welding process. The Auto Pin Welder works by connecting the output leads through the wires/piers to the workpiece, and into the return magnet. Then three short distinct beeps will be declared, followed by the discharged energy, in which the welding will occur. Some typical examples are shown in Figure 3.4 including a bead formed through melting two wires (Figure

3.4(b)) and welding thin wires on a plate used for measuring the temperature in electrical spot welding (Figure 3.4c). In the case of a welded bead, the two thin wires were melted in the welding process, the droplet at the end of the two wires then merge to form the bead. In some cases of welding a thermocouple onto a steel plate, the process also involves metal welding and mixing. This allows users to position, the bead of the two thin wires close to the welding spot, which is important to provide data for developing finite element thermal modelling of the temperature history using a remote thermocouple (Norbury 2017). The produced numerical modelling of the droplets is potentially able to provide basic tool for modelling complex liquid drops merging in industrial practice such as shape forming in the welded bead process.



**Figure 3.6** Welding apparatus designed to hold the TIG and Capacitor Discharge Welding (CDW) torches (a) and typical tube closure (b)



ITEM NO.	PART NUMBER	QTY.
1	Apparatus Base	1
2	Back Cylinder	1
3	Back Sheet Metal	1
4	Front Sheet Metal	1
5	Adjustable height square	1
6	Micromanometer	1
7	Vice Base 1	1
8	Vice Base 2	1
9	TIG / CDW bracket	1

**Figure 3.7** Bill of Material for the Welding Apparatus designed.

Figure 3.5 shows a TIG welding set-up process method. This in-house designed apparatus use

a 'one arrangement system' to conduct repeatable tests with controlled positions and angles of the electrodes. The TIG welding apparatus is utilised to study the welding closure of a thin stainless steel tubes as the sheath of insulated thermocouples. As shown in Figure 3.5(b), the tip of the electrode needs to be controlled when in the welding process when conducting closure welding of thin stainless steel tubes. The welding apparatus (Figure 3.6) consists mainly of the following sections: (1) Height control unit (Micrometre). Here the height of the electrode can be controlled using an attached Micrometre, which controls the predefined height required for accurate welding procedures. The torches for the TIG and CDW welds, are attached to a metal block via a 3D printed clamp, which ensures that the welding process is performed at 90 degrees vertically, towards the specimens. As noted before, the brackets are attached to a metal block which is connected to the Micrometre using a vertical spring. The height of the spring controls the height of the welding torches. The apparatus also has a mechanical vice, made from copper and Tungsten sheets, which holds the Stainless Steel tubes and the bare thermocouple wires. (2) TIG Welding Torch – Torch is fixed with the height adjustable block unit. A tungsten electrode is fixed to the torch and Argon gas flows through the torch. (3) TIG Welding machine – This is the main part of the TIG welding set-up, by which a controlled amount of current and voltage is supplied during the welding. A Rectifier (made by FRONIUS) with current range 10-180 A and voltage up to 230V, depending on the current setting has been selected. (4) Gas cylinder – For TIG welding, Ar gas is supplied to the welding torch with a particular flow rate, so that an inert atmosphere formed and stable arc is created for welding. Gas flow is controlled via a valve and a regulator. 5. Typical tubes used in the test include stainless tubes of different sizes. As shown in Figure 3.7(a), 316 Stainless steel tubes with a wall thickness of 2mm were selected as the main workpiece material for presenting results. The stainless steel tube has an outside diameter of 3mm and 100mm length. Before the start of the experiment, the surface of the tube was cleaned and polished with emery paper to ensure the removal of any dirt or contaminations. Once the preparation of the samples is completed, the Stainless steel tubes are fixed into the mechanical vice, with 5mm exposed at the top end, so that the tube end is welded.

The electrode used in the TIG welding process is 2.0% lanthanated tungsten electrode. It has an excellent arc starting control, low-burn-off rate, good arc stability, and excellent re-ignition characteristics — many of the advantages for a material to be used as electrodes. 2.0% lanthanated electrodes also closely resemble the conductivity characteristics of 1.5% thoriated tungsten. In some cases, it can replace 2% thoriated without having to make significant welding program changes. These electrodes follow an American Welding Society (AWS) classification of EWLa-2.0 and contain a minimum of 97.80% tungsten and 1.30 to 1.70% lanthanum, or lanthana. The 2% lanthanated electrodes work well on AC or DC electrode negative with a pointed end, or they can be prepared for use with AC sine wave power sources. They also maintain a sharpened point well, which is an advantage when welding steel and stainless steel on DC or the AC from square wave power sources. The steel tube used is **316 steel**, an austenitic chromium-nickel stainless **steel** that contains between two and 3% molybdenum.

The welding parameters for the first section of the experiments are shown in Table 3-2. However, before starting the experiment, a number of tests have been performed to evaluate the applicable parameters range, over which the welding could be possible, and to avoid any observable defects like porosity and undercutting during the procedures. The distance between the electrode tip and the centre of the tube end is important to generate the arc and control shape of the welded tube closure.

**Table 3-2** – Welding parameters used for initial experiment.

Parameters	Range
Welding Current	(10 - 50) A
Voltage	74 v
Distance of tip from weld centre	1mm- 2mm – 3mm
Gas Flow rate	(8-10) l/min
Current Type	CD
Dimension	400mm x 0.125mm(OD) x 0.2mm



Figure 3.8 Struers Prontopress machine used to prepare welded nuggets for analysing the shape of the weldment and flow feature of the liquid during the welding process.

To analyse the shape of the welded joints, samples were mounted and studied in detail to analyse the final shapes, which will provide information on the shape and flow of liquid during their molten state. The metallographic specimen of the welded drops/nuggets samples were prepared using a CitoPress machine. This is a hot mounting machine where a clean and dry specimen is placed inside a mounting cylinder in a hot mounting press and the appropriate mounting resin is added. A temperature of 180°C is applied to embed the specimen firmly in the resin before grinding with abrasive papers and polished with diamond paste. (6 and 1micron). Water cooling is used to obtain the shortest possible mounting time.

### **Surface measurement: Brukker GT-K Surface measurement system.**

One important issue for small liquid flow is the wetting. In the numerical modelling process, this is represented by the contact angle as a general parameter. The wetting behaviour is affected by the surface finish, and the surface roughness is affected by the welding process. So preliminary work has been conducted to assess the effect of welding on the surface finish of the tube. This is a material characteristic that may affect the dripping process from the side/end, which is relevant to the maintenance and control when using a stainless temperature measurement probe to measure the temperature in liquid particularly in sensitive/hazardous liquid.

A ContourGT-K 3D Optical Microscope (Brukker GT-K) was used to measure and produce Surface Roughness values of the welded tubes for all specimens. The Brukker GT-K is a versatile bench-top optical surface profiling system, with a 3D optical microscope. It can produce readings of step heights, roughness and surface profiling scans for different material profiles. It also has the ability to produce surface measurements with 1-2 $\mu$ m resolution and 1nm vertical resolution. The reason for utilising this particular apparatus is to scan and analyse different welding profiles. As well as highlighting micro-level defects associated with various welding parameters.



Figure 3.9 ContourGT-K 3D Optical Microscope used to measure the surface roughness.

The Bruker GT-K can produce two measurement methods: Phase Shifting Interferometry (PSI) and Vertical Scanning interferometry (VSI). The PSI method uses a narrow band green light source to test smooth surface finish for various smooth products such as optics, mirrors and highly polished samples. This method cannot obtain data from objects that have large step-up like height changes. As for the VSI, it uses a white light source to produce effective measurements from materials with a rough surface finish, as well as these with adjacent pixel height differences greater than 135nm. The translator inside the system moves the objective to a certain point until it reaches a maximum, and then tapers off as the objective passes through focus. For this work, PSI method was applied to measure the surface roughness of the welded stainless tube.

### 3.4 Numerical modelling and data analysis programs

The general purpose of this project is to develop effective numerical models and framework for modelling small volumes of liquids and develop their relevance to industrial practice. It can be used for R&D or training purposes. Part of the work includes comparing numerical programs as well as evaluating the accuracy of some data based programs such as Matlab. The main design tool used is Solidwork, and the main numerical modelling is ANSYS Fluent and CFX. The use of the open source program OpenFoam is also evaluated. ABAQUS is used to model interaction between a solid indenter or liquid droplets onto a material with/without an embedded thin shell. Matlab is used to develop the framework of a data system to incorporate realistic droplet shapes based on data from the numerical model developed. Some key features and main functions of each program are briefly summarised in this section.

There are numerous Computational Fluid Dynamic codes that allow for simulating of multiphase flow behaviour. Software such as ANSYS CFX, FLUENT and ABAQUS CEL are used heavily in research and industry to design and optimise new apparatus and to test already existing installations. The computational fluid dynamics (CFD) analysis for ANSYS can produce solutions for many engineering problems including single, multi-phase, and compressible and many more fluid problems. The CFD solver in ANSYS is divided into two main sections, These are: ANSYS FLUENT and ANSYS CFX, both are reliable and widely used for different situations. The technologies used in both numerical codes are highly scalable, which allow efficient parallel calculations to be resolved by using large numbers of processing cores. Using FLUENT or CFX with the full featured ANSYS CFD post-processing tool allows the user to perform advanced quantitative analysis or create high quality visualizations and animations.

Furthermore, multi-phase flow is an analysis technique which allows for multiple flows to be applied in a simulation. These flows can be different materials with different input pressures that allows for complex simulations to be carried out. Modelling a multi-phase flow in ANSYS poses a couple of challenges that must be evaluated closely. This is because fluid flow exerts hydrodynamic forces on a structure which can results in deforming/translating the structure. Fluid flow can also modify thermal stresses within a structure. Therefore, it is important to select the correct CFD coupling scheme that are associated with the investigated case. For instance, dealing with fluid couplings simulation, which is the interaction between gas-liquid

or liquid-liquid phases requires a two way coupling scheme. Furthermore, fluid structure interactions, which involve coupling of fluid dynamic and structure mechanics disciplines, requires a four way coupling scheme. In general, Table 3-4 illustrate the difference between the three main coupling schemes that can be utilized in CFD simulations.

**Table 3-3** - Main three different coupling schemes used in Multiphase Flow

Coupling Scheme	Description
One way coupling	Primary phase affects flow of secondary phase, secondary phase does NOT affect flow of primary phase.
Two way coupling	Primary phase affects flow of secondary phase, secondary phase affects flow of primary phase, particles of secondary phase do NOT interact with one another.
Four way coupling	Primary phase affects flow of secondary phase, secondary phase affects flow of primary phase, and particles of secondary phase interact with one another.

There are different types of multi-phase models which each behave in a different level of complexity. It is important to select the correct multi-phase model before starting a simulation, so that the code is able to utilize the right continuity equation to produce accurate results. Each type is used in different situations to increase the complexity of the simulation. The models are described as follows: **Lagrangian Mode:** It solves the primary phase by using the continuity equations as a whole entity, while individual particles from the secondary phase are tracked throughout the flow and are assumed not to interact with one another. **Algebraic Slip Model:** Primary and secondary phases are treated as one composite mixture and one momentum equation is solved for the combined phases. **Eulerian-Eulerian Model:** Primary and secondary phases are treated individually as being continuous and separate momentum equations are solved for each phase. **Volume of Fluid (VOF) Model:** An Eulerian-Eulerian variation in which the secondary phase is not dispersed within the primary phase but rather there is an interface between the phases and so the interface must be tracked while also solving a momentum equation for each phase. **Discrete Element Method:** The most complex multiphase model in which momentum equations are applied to individual particles of the

secondary phase as well as to the primary phase as a whole. Each one of the multi-phase flow models has its own application for when it is best used and adapted. This depends on the typical flow regime present in a particular multi-phase flow system. The most frequently used multi-phase models are the Eulerian-Eulerian, VOF and the algebraic-slip models. Table 3.5 shows examples of the multi-phased models and their physical systems which can be analysed using ANSYS FLUENT.

**Table 3-4** -Application of important multi-phase models.

Multi-phase Model	Applications
Algebraic-slip model	Bubble column design, gas-liquid mixing vessels.
Eulerian-Eulerian/VOF model	Fluidized bed systems, which encompass catalytic reactions such as hydrocarbon cracking and non-catalytic reaction, both homo and heterogeneous.

The major scientific challenge lies in modelling accurate prediction of the shape, size and volume of the droplet, which is directly influenced by the material properties and boundary conditions. Setting up a numerical simulation is very similar across many commercial engineering problem solvers. Firstly, the geometry of the nozzle is designed and modelled in a computer aided design software. In the case of this work, SolidWorks was used due to its available license for this research. The 3D model is then imported to the numerical solver which has the capability to define the boundary conditions of the physical problem. After that, the model is meshed, to divide the geometry into very small discrete elements, which the selected solver will use to iterate via its mathematical language. For different models, detailed mesh size sensitivity is conducted before being used to study the effect of material and processing parameters. Then, an investigation was started into the capabilities of various numerical software with a set of simple models. The materials properties of glycerines-water is enalayed based on detailed testing and validation with testing data and published works. In the post processing process, the contour of the droplet were exported into excel and MATLAB programs. The velocity profile is also analysed. The formulation of these simple models and the process of employing them in simulations are discussed in Chapters 4 and 5.

The FE modelling of interaction between rigid indenters and liquid droplets is performed

using ABAQUS software. The main numerical works include indentation of a thin shell embedded in an elastic matrix with different shaped indenters, including flat ended cylindrical indenters and spherical indenters. The work is aimed at improving the fundamental understanding of the mechanical behaviour and the influence of an embedded thin shell on the indentation resistance of the material system. The interaction of liquid drops on to homogenous systems and systems with an embedded shell is also comparatively studied using ABAQUS Smoothed particle hydrodynamics (SPH) approaches. The SPH method is a practical way of modelling complex liquid-solid interaction. Some theoretical details are to be presented in Chapter 5 together with the results. The model was built in ABAQUS based on the droplet profile from the droplet simulation, and then it is built with a solid model before being converted into SPH elements. The post processing process include in assessing the deformation profiles, the solution times, the reaction-displacement data, these data is used to analyse the effect of the indenter types and the Poisson's ratio of the matrix on the on the indentation resistance .

**CHAPTER FOUR**

**NUMERICAL AND EXPERIMENTAL STUDIES  
OF DROPLET FORMATION OF DIFFERENT  
MATERIAL SYSTEMS UNDER VARIOUS  
CONDITIONS**

#### **4.1 Introduction and main research works**

As listed in Table 4.1, this chapter details the work on simulating droplet formation for several different material systems and experimental works. The work will concentrate on the development of a multiphase numerical model that can be utilized to simulate different complex systems.

In this work, ANSYS FLUENT will be utilized to form a droplet using a 2-D quarter axis-symmetric model via Volume of Fluid solver. The work will investigate factors influencing the overall shape and size of the droplet (e.g. density, surface tension and dynamic viscosity). The results from the numerical investigation will be assessed against experimental data and other published results conducted with Water-Glycerine solutions. The effect of key material parameters and process design, on the droplet formation in simple cases and further complex systems are investigated. It is also used to evaluate the uncertainty of shapes when inversely calculating the surface tension of liquids. A Matlab based data system is also developed based on the numerical model and the potential use of the approach to more complex systems is discussed. As listed in Table 4.1, the first part of the work concentrated on the development of the Multiphase numerical model using the Volume of Fluid (VOF) solver. This section also explores some of the modelling solver techniques, which were considered to simulate the outlined problem. Furthermore, mesh sensitivity study was performed to analyse the effect of number of elements (NOE) and number of nodes (NON), as well as the boundary conditions on the key modelling results. This includes flow velocity, generated pressure and running time of the study.

The second section described experimental procedures conducted to measure the key material properties that are important for numerically modelling of the droplet formation and complex multiphase flow. The main work focused on water, glycerine and glycerine-water mixture, to investigate potential improvements of droplet formation. This includes measuring the density, viscosity and surface tension for various concentration levels of Glycerine-Water solutions. After this, a qualitative comparison study was performed to validate the numerical results, produced by ANSYS FLUENT, against experimental data and other published results with different modelling programs (e.g. CFX and flow 3D) under comparable conditions. Further credibility to the work is added, by performing a quantitative comparison analysis, which investigated the effect of changing material properties on the droplet formation, such as droplet length, volumetric flow rate and separation time. The verification of the numerical modelling is achieved by comparing surface tension values, for various droplet contours, experimentally,

theoretically and numerically.

The following section discussed numerical methods that can be utilized to simulate droplet formation for low melting temperature metals (Such as Gallium) and high melting point metals (e.g. Nickel).

The effects of key factors affecting the modelling process and the limitation of the VOF numerical solver are analysed. The effect of the contact angle, which represents the wetting of liquid is debated and analysed. Furthermore, special cases of numerical models, extended from the developed droplet model, are presented including; effect of changes in material properties on the formation of multiple satellite drop models, droplet with a size smaller than the nozzle, as well as the relevance of such models on different applications. This includes drop on demand and 3D printing. Preliminary work on model development of droplet formation in microfluidic systems is also presented and discussed. Finally, a data system based on the numerical data is developed in Matlab and its functions compared and potential extension to other more complex situations is discussed. Several cases of modelling small volume of liquid is presented including droplets merging in micro welding, dripping of liquid from and stainless steel surface and liquid penetration in cracks in NDT. The properties of water-glycerine mixtures is cross-compared with data from different sources, the key factors affecting droplet formation and modelling is discussed.

**Table 4.1 Main Research Works**

<p><b>Development of Numerical Modelling Program of Droplets</b></p> <ul style="list-style-type: none"><li>➤ Development of numerical models of droplets and compare the efficiency of different approaches.</li><li>➤ Evaluation of effect of key modelling parameters and mesh densities.</li><li>➤ Comparison between numerical model and theoretical/analytic calculation</li><li>➤ Comparison between numerical data and experimental data (fluid with known properties)</li></ul>
<p><b>Experimental and Numerical analysis of droplet formation for different material systems and comparison with numerical data</b></p> <ul style="list-style-type: none"><li>➤ Characterisation of the properties and droplet formation of fluid mixtures</li><li>➤ Investigation of the effects of liquid mixture (water-viscose liquid mixture) on the key parameters of droplet formation</li><li>➤ Experimental and numerical investigation of the droplet formation with satellite drop (fluid mixture)</li><li>➤ Experimental and numerical investigation of the low melting temperature liquid metals</li><li>➤ Parametric numerical modelling of effect of materials</li></ul>
<p><b>Discussion</b></p> <ul style="list-style-type: none"><li>➤ Key factors affecting the droplet formation approaches, uncertainty and limitation</li><li>➤ Effect of contact angles in droplets and other situations</li><li>➤ Inverse material properties predictions: surface tension estimation from pendent droplets</li><li>➤ Modelling more complex systems (continuous droplets, satellite droplets, droplets smaller than the nozzle and fluid in micro channels)</li><li>➤ Importance and potential use of numerical modelling of droplets and data system development</li><li>➤ Case Studies: modeling of droplet merging in micro welding, dripping of liquid from stainless steel surface and liquid penetration in cracks in NDT.</li></ul>

## 4.2 Numerical modelling of droplet: Model development and analysis

Figure 4.1 shows a typical example 2D-asymmetrical model created in SolidWorks and imported to ANSYS FLUENT, which has the capability to simulate the flowing fluid inside the model. In the initial stage of the project, several approaches have been evaluated to develop the model (e.g. sketching the model directly in ANSYS, etc.). It was decided that best approach was to use SolidWorks as the main software to design the geometry and then import the model to FLUENT for the CFD study. This is because Solidworks offers more flexibility in dealing with different geometries and the capacity to edit the model for complex assembly in any future works.

Figure 4.1 clearly elaborates on some of the important boundary conditions, such as the inlet, outlet, walls and symmetrical axis of the model. The mass flowrate used in the model is 0.17ml/sec (A range of flow rate has been assessed in the work), which was set up as an inlet boundary condition. An outlet boundary condition was also assigned in the opposite condition of the inlet. This was specified so that the pressure drop, across the boundary, becomes negative and the solver will assume a virtual wall to stop the multiphase flow from flowing back out of the model. The interaction between the wall and the fluid is controlled by a contact angle in the model. Other key details on the terms of the computational fluid dynamics for the droplet simulation are also listed in Figure 4.1.

Extensive preliminary work shows that the main challenge in simulating the multi-phase free surface flow of the droplet formation, *via* computation fluid dynamics lies in defining the boundary conditions within the mathematical model. The explicit Volume of Fluid Eulerian model is the best option for simulating the referenced problem (ANSYS Theory Manual, Version 17). Eulerian model (EM) is preferred over the Lagrangian model (LM), because it requires fewer meshed elements to solve the interface movements of the flowing fluid. Based on the EM model, pure liquid flow has a value of one (Red colour in Figure 4.2) while pure air has a value of zero (Blue colour in Figure 4.2). Therefore, the free surface separating the liquid and the gas phases is defined as the cross-over region, in which the value of the volume function of water and air fluctuates between zero and one. So an accurate representation, from the simulation, depends on fine mesh elements, which have small discrete volumes, so it can represent the separate phase better. This will also make it easier and more accurate when extracting the coordinates for the profiles of the droplet, which is part of the thesis aim when calculating the volume and building databases with more realistic droplet contours. Details will be presented in later sections.

This approach is considered as the most suitable method for simulating complex behaviours of droplet dynamics (e.g. necking, breaking up and satellite droplets). As illustrated in Figure 4.2, the model is capable of predicting the change of shapes at increments of 0.05 and 1.2 and 2.4 seconds, consisting of the critical stages of the droplet formation before the break-off occurs. More quantitative analysis will be presented at a later section with different mesh densities.

#### 4.2.1 Mesh sensitivity study

Figure 4.3 (a) shows three typical models with different mesh densities for simulating a water in air system, which was used to produce the mesh sensitivity study for the droplet. One of the main problems that was found during the CFD simulation was the smearing of the oil droplet formation for a various number of cells at the outlet of the nozzle. Consequently, an appropriate value of mesh density value needs to be determined to obtain the required number of elements/nodes for converged computed solutions. In the mesh sensitivity study, the Number of Elements (NOE) and Nodes (NON), play important role in defining some of the key functional parameters for the analysis. This includes the droplet shape, rate of convergence for the pressure and velocity plots, as well as the processing time to simulate the problem. Furthermore, the effect of mesh size on the contour and grid generation, which is important for post-processing of results was evaluated. It is important to automatically extract coordinates of the boundary systematically/accurately for calculating the percentage error of the contour, as well as providing data for comparing the numerical data from this work with experimental measurement and published data (*Wilkes et al, 1999*).

Typical comparison results between different levels of Mesh contours are shown in Figure 4.4. A contour plot is a series of lines linking points with equal values of a given variable, or points within a narrow range of values. In this case, the smearing of the fluid flow is plotted into a number of contours. It can be seen that Mesh C was able to produce the steady plots in terms of contour consistency and resemblance with experimental data (e.g. Droplet length, volume, shape) other published data (*Wilkes et al, 1999, Fawehinmi et al, 2005*). This is due to the high number of NOE and NON values it contain, when compared to Mesh A and Mesh B.

Figures 4.5 and 4.6 confirm the mesh convergence behaviour for the maximum generated pressure and fluid velocity plots, from the nozzle outlet, for the ten different types of studies. These values were probed from a point at the centre of the nozzle exit. It can also be seen that the maximum pressure values kept on decreasing as the number of elements is increased. The data of the pressure kept decreasing throughout the first six attempts of the study until it reached

a point where the change of pressure is limited, close to the horizontal line. This straight line behaviour between studies 6,7,8,9 and 10 proves that the simulation is able to produce precise results and the mesh is capable of achieving convergence. Similar mesh sensitivity studies have been applied to other material systems, a similar level of mesh size effect was also defined. The results are not shown to avoid repetitive presentation and preserve clarity.

Figure 4.7 shows how long the central processing unit (CPU) time solver took for each study to produce results. It can be seen clearly that as the density of the mesh kept on rising for each study, the time taken to solve every study increased with it. Although accurate outcomes are vital and significant when simulating a CFD problem, the cost of increasing the number of nodes and elements will result in increasing the computational and CPU time, which is expensive to accomplish. Please note that the comparison is based on a single workstation (3.4GHz Quad Core Processor with 16Gb ram). Hence, the ratio on the effect of element size is representative when the simulation is performed on different systems with high capability of processing power. The data in Figure 4.7 shows that the mesh size is critical to the CFD simulation. A similar approaches has been applied to all the numerical models presented in the work, details are not going to be repeated to focus on the main works.

#### 4.2.2 Theoretical validation of the initial numerical model

A simple analytical work has been conducted to further assess the accuracy of the computational fluid dynamic simulation results. As illustrated in Figure 4.8, the momentum equation and Bernoulli's equation are used to calculate the velocity of the flow, exiting the nozzle, theoretically. The calculated results can then be compared against the numerical data by calculating the percentage of difference between the two methods.

To calculate the mass flow rate at point A:

$$\dot{m} = \rho \cdot A \cdot s1 = 1000 \times 1.25 \times 10^{-3} \times 2 = 2.5 \text{ kg/s} \quad (4.1)$$

Now to use the continuity equation to calculate the outlet velocity at point B:

$$\rho 1 \cdot A1 \cdot s1 = \rho 2 \cdot A2 \cdot s2 \quad (4.2)$$

$$s2 = \frac{A1 \cdot s1}{A2} = \frac{(1.25 \times 10^{-3} \times 2)}{78.5 \times 10^{-6}} = 3.185 \text{ m/s} \quad (4.3)$$

This value is very close to the average value of exit of nozzle (Figure 3.27). A typical single

data is illustrated in Figure 4.8 probed from the numerical code. The value is 3.27m/s and is very similar to the theoretical calculated values, with a relative error of 3%. Similar work had been performed on Nozzles of other sizes and shapes (e.g. straight tube used on the droplet imaging machine as detailed in Chapter 3; and tapered nozzle of Syringes), and a similar level of accuracy can be observed.

### **4.3 Experimental tests and data**

This section will investigate droplet formation shape generated by different material systems which include water, pure Glycerine as well as metal Gallium. Droplet formations generated from these materials are important due to the many vital applications they are involved in. Most of these applications necessitate the need for producing very small and rapid droplet volumes, such as those involved in removing oil drops from solid surfaces, ink-jet printing, DNA microarraying and many other applications (Bernstein et al 2000; Bleiwas et al 2010). The measured material properties were used in the numerical simulation, to compare the accuracy and error range generated from the VOF model. Low melting temperature metal based on Gallium is also used as a model material to study the droplet formation. It is an interesting material relevant to 3D printing as well as conductive rubbers (mixture of conducting drops and silicone rubber, which is the topic of another PhD project (Kaid, 2019, PhD Project).

To start, five different concentration levels of Glycerine-Water Solution were used in the numerical model to simulate the droplet effect. The reason for using this type of solutions is because of the various material properties they possess, which can affect the overall formability of the droplet. Therefore, an experimental procedure is performed to determine the density and the dynamic viscosity of the glycerine water solution. The worked out values from the experiments, will be utilized in the numerical code to model the multiphase flow correctly. The analysed glycerine water solutions droplets were created, using the material properties documented in Table 4.2. These were prepared by mixing the desired percentage of glycerine with distilled water, via a measuring cylinder. The five solutions had 0, 25, 50 and 100 per cent glycerine oil concentration levels (Volume fraction, vol%). The density and the dynamic viscosity were calculated experimentally using Stock's Law ball bearing method. The scales were checked and found to have an error of 2.3%, which was compensated for within the calculations. It is to be noted that the calculated results are based on an assumption that the mixed Water Glycerine solution, is homogeneous. The effect of the volume fraction on the density is plotted in Figure 4.9.

After determining the density of various concentration levels of the Glycerine-Water solution, an experiment to determine the viscosity was also performed. A detailed procedure and the calculations for this experiment are presented in Wilkes, et al (1999). The facilities used in the measurement are detailed in Chapter 3, including Graduated Cylinder 100mL, Water, Glycerine, Measuring Balance in grams; Dropper. Falling ball viscometer method is covered in international standards (Tanner, 1963). This repeated experiment involved the ball bearing being dropped into the oil 11 times and the time recorded for each attempt averaged. The data is comparable to published works. For example, for pure Glycerine, the results from the experiment gave an average viscosity of 1.176 Pa s. Typical reported data of the Viscosity of Glycerine oil is between 0.97-1.412 Pa S (*Segur and Oberstar, 1951*). The data measured in this work is comparable.

**Table 4.2** Physical properties of Glycerine-Water solution used to study the formability of droplets.

% Glycerine (v/v)	Density of Solution ( $g/m^3$ )	Viscosity of Solution ( $Pa s$ )	Surface Tension (N/m)
0% Glycerine	0.973	0.001	0.070
25% Glycerine	1.114	0.017	0.0660
50% Glycerine	1.225	0.17	0.0625
100% Glycerine	1.231	0.3	0.0620

The experiment also studied the changes in the viscosity behaviour when increasing the temperature of the oil up to 50°C . This water range is relevant to the working temperature of the liquid, which also gives a reasonable range of viscosity to be used as model material data for validating the numerical prediction and estimating the range of accuracy. The presented data can be seen in Figure 4.10, which demonstrates how the viscosity is reduced when the temperature increases, and rate of change in viscosity reduces as the temperature becomes higher.

#### **4.4 Experimental works and droplet test**

Once the material properties for the glycerine water solutions were determined, a typical droplet experiment was performed and compared to the developed numerical method, as shown in Figure 4.11. This initial investigation used a plastic syringe with a tapered nozzle (OD = 1.2mm), to generate fluidic droplet. Then the developed numerical code is used to simulate the droplet under similar conditions to the initial experiment. Once the initial model was validated, different numerical syringe designs (outlet diameter = 0.8mm, 1.6mm and 2.75mm) are used to analyse the difference in behaviour during droplet growth. The results from these numerical investigations are cross-referenced with published work (Hirt et al, 1981; Fawehinmi, O. B, 2003). This suggests that the models and properties are effective in accurately predicting the trend of droplet formation. More accurate measurement has been conducted on the Theta Optical Tensiometer apparatus with straight steel tubes of different sizes (stainless steel tubes, 1.6mm and a 0.8mm outlet diameter). As stated previously, the apparatus used to generate pendant droplets, used a stabilized table and a high-speed motion analysis software to process droplet images produced 4,500 frames per second. As well as measuring various droplet properties such as length, width, volume and surface tension. It can be noticed from Figure 4.12, the droplet volume is gradually increased throughout the plastic syringe tapered nozzle. When repeating the experiment under the same conditions, frequency, length and volume of the droplets were reproducible. The image obtained from experimental data shows a good agreement with the initial predicted droplet model. In addition, these images provided are used to extract quantitative data of the key dimension of the droplet to be compared with numerical data and other published works.

Two main studies have been performed to establish the validity of the work. These are Qualitative and Quantitative methods. The qualitative method will focus on analysing the effect of changing the syringe's existing dimensions, increasing the volumetric flow rate and the influence of the Dynamic Viscosity. As for the quantitative study, it will focus on changes within the droplet length, interface shape and elongation effect and secondary satellite droplets.

##### **4.4.1 Experimental work with Glycerine-Water solution and comparison with numerical models**

More detailed quantitative droplet tests have been performed with a straight stainless steel tube on the Theta Optical Tensiometer apparatus. Quantitative information has been generated in regards to the overall droplet length of the hanging droplet, estimation of the overall droplet

volume, as well as the breaking up time.

During the experiment, the volume is gradually increased throughout the stainless steel tube with an internal diameter of 1.6mm. Figure 4.12(b) shows some typical results of the droplet formation process. When repeating the experiment under the same conditions, the values of droplet length and volume were reproducible. The image obtained from experimental data shows a good agreement with the numerical results. In addition, these images were used to extract quantitative data of the key dimension of the droplet to be compared with numerical data and other published work.

#### **4.4.2 Quantitative analysis of the droplet dimension and shape and effect of material properties**

This section will produce a quantitative investigation, into the resemblance in behaviour between the generated numerical FLUENT data, experimental outcomes and other published results, regarding numerous measurable droplet properties. Figure 4.13 illustrates key dimensions measured including the droplet length, separation time and factors affecting them. Figure 4.14(a) compared the length of the droplet from the numerical modelling, experimental and published data. It confirms the high resemblance in behaviour between the numerical results and the experimental values for the droplet length. It can be noted that the overall droplet size increases as the viscosity level increases across all four different types of study. Another noted point is that, as the viscosity value increases, the difference between the numerical and the experimental results increases as well. Figure 4.14(b) investigates the difference between break-up times, as the flowrate is increased from 1ml/min to 10ml/min, for solutions with a 50 percent glycerine concentration levels. The good agreement in behaviour between the FLUENT numerical results and the experimental data can be considered as excellent for both solutions, which also shows that time of droplets break-up is relatively proportional to the value of flow rate  $Q$ .

Figure 4.15 illustrate the effects of changing the nozzle diameter on two different types of glycerine water solution concentration levels (25% and 50%). In this test, three different syringe were used with different outside diameters: 0.8mm, 1.6mm and 2.75mm. In the experiment, the flow rate of the solution is controlled by a pump attached to the apparatus tube. It is to be noted that the time between subsequent break-offs decreases rapidly when the nozzle diameter exist is reduced. This 10% decrease between subsequent break-off times is due to the viscous effect which is higher in the 50% glycerine-water solution than the 25% solution. It

can also be noted that increasing the value of the flowrate resulted in reducing the time between break-offs. This decreasing effect was noted in all simulation results, except the smaller nozzle (OD=0.8mm) in which the flow was very close to reach the jetting mode.

Figure 4.16 (a) and (b) shows the stages and elongation effect during droplet formation, for a 50% glycerine water solution with a flowrate of 1ml/min. The interface shape obtained from FLUENT is compared against CFX and FLOW-3D simulations from reference Fawehinmi et al, (2005). The obtained values of droplet length (L) and separation times from the FLUENT-3D simulations are in a reasonable agreement with other published papers (Wilkes et al, 1999). More demonstration of the free surface shape/interface, during the droplet breaking up process, can be seen in Figure 4.16 (c&d), which compares the shape before the break-up process between the three numerical codes, for the same multiphase material properties used by Fawehinmi. et al (2005). It is very apparent that FLUENT was able to simulate the long thin liquid lines, for solutions with high surface tension values. These lines are very obvious during the experimental photos. The failure in simulating the long thin liquid lines, for fluids with high surface tension values, can be blamed on the limitations of the CSF algorithms applied by FLUENT.

Figure 4.17 also demonstrated the predicted behaviour in the break-up process of glycerine (20 percent Glycerine water solution) including the elongation effect, the secondary droplets and the satellite droplet effect. Such processes are important, in most applications, such a behaviour may have a negative effect, such as reducing the print resolution during an Inkjet printing process. So a program capable of predicting such processes is important. The plotted results from FLUENT showed a clear similarity in the droplet shape, within a similar timescale between different programs from this work and published data. Both numerical codes also highlighted the presence of the satellite droplet effect, as well as the time in which it forms. To predict the 3D volume and the speed of the satellite droplet, it would require the use of more computational power, finer mesh elements and a longer timescale to simulate their effect within the relevant region.

#### 4.4.3 Droplet simulation of semi fluidic materials.

In this section, the numerical modelling method was tested to simulate semi fluidic metals with similar flow characteristics to the Glycerine-Water solution that was analysed in the previous sections. Metals with excellent semi-fluidic properties and material conductivities, such as aluminium, mercury, gallium, tin and many more, are regularly used in industry for their liquid states characteristics, at room temperature, though the choices are very limited. For example, most of the alloys derived from Galinstan, always remain within their liquid states at room temperature. Another a popular non-toxic, ultra-low vapour pressure, liquid metal that is being used lately for many applications is Gallium.

Table 4.3 Properties of the properties of metals.

Material Name	Gallium (Ga)	Nickel (Ni)
Melting Point	29.7 °C	1566 °C
Density (Solid phase)	5.91 $g/cm^3$	8.909 $g/cm^3$
Density (Liquid phase)	6.09 $g/cm^3$	7.81 $g/cm^3$
Molar heat capacity	25.86 $J/mol.K$	26.07 $J/(mol.K)$
Young Modulus	9.8 $GPa$	200 $GPa$
Poisson ratio	0.47	0.31

This liquid metal alloy contains 68.5% Galinstan, 10% Tin and 21.5% Indium, which makes it better for applications such as coolants, thermometers, electromechanical replays, ion sources. Though, due to its recent discovery, it has failed to meet many microelectromechanical system regulations, which are being adapted in today's micro-devices manufacturing. Gallium is known for its low melting temperature and high surface tension value. When simulated, it showed similar dynamic behaviour to the glycerine-water solution droplet, with regards to the dominance capillary effect and separation time. A clear droplet shape of a Gallium droplet can be seen in Figure 4.18. Figure 4.19 shows a typical agreement between experimental results and extracted FLUENT coordinate data of the numerical model at different timescales. This suggests that the CFD model is effective in predicting the droplet formation of semi fluidic materials.

#### **4.5 Modelling of the formation of different types of droplets**

Modelling fluid droplets is a complicated process, as it is affected by many parameters. Although the literature review highlights findings from academic journals, on the material changes during pendant droplet formation, predicting the precise location of satellite droplets and their volume can be difficult. Various numerical and open source codes can be used to simulate pendant droplets, however, selecting the right CFD solver to mimic the free surface smearing and the dynamics of the droplets, can be a challenging task. Furthermore, the accuracy of the simulated results, heavily depends on the computational cost and time spent to produce the desired output.

Five different droplet types with different levels of Glycerine-Water solution concentration have been analysed experimentally, with an aim of producing a numerical model with similar fluid dynamic behaviour, as well as examining the limitation of various popular commercial CFD codes (ANSYS FLUENT, CFX and 3D Flow). The CFD simulations focused on highlighting the free surface smearing of a multiphase flow, droplet length, separation time and subsequent satellite drops. The overall results from the qualitative comparison study, showed a clear resemblance with other referenced work.

##### **Effect of contact angle/wetting factor on droplet formation**

The developed numerical model provided a tool to assess and predict droplet formation at different timescales and volumes. Hence, one of the most important factors that the numerical model can predict is the effect of contact angle on the droplet's overall volume. As shown in Figure 4.20, the contact angle or wetting factor effects on the volume is relatively limited. As detailed in the literature review, the wettability of real surfaces is subject to many factors, both physical and chemical. For the flotation process, the effect of four main factors; surface roughness, heterogeneity, particle shape and particle size, on contact angle measurements are of importance. Wetting is a critical issue between liquid and solid. It can be affected by many factors, this may become more important to application cases such as dye penetration in which the liquid needs to flow into confined spaces under constant pressure.

##### **Effect of viscosity and surface on satellite Droplets**

Satellite drops are an important phenomenon in droplet formation. This secondary effect is caused by the surface tension of the liquid/air interface. As the liquid thread, also known as the

elongation effect, starts thinning/necking, between the developed pendant droplet and the fluid stream, the fluid molecules start to stretch at the surface. When the drop breaks free, the stretched region rebounds. Depending on the material properties and the boundary conditions, the thread of the fluid can sometimes stay as a single mass, or separate to single entities due to the recoil disturbance force resulted from the separation of the problem near the final stages of thread break-up. While predicting the many shapes and sizes of droplet formation can be simulated and computed numerically, predicting the precise location of satellite droplets and their volume can be challenging. Depending on the application, secondary droplets are generally considered as unwanted incidents, especially during precise deposition. The production of secondary droplets is administered by the non-linear dynamics of the liquid metal smearing near the final stages of thread break-up. Figure 4.21 illustrates the secondary droplets phenomenon, which is also known as the satellite droplet, produced throughout the breaking up process of the main large droplet. For glycerine, the numerical model is accurate in predicting the formation of satellite drops, which is comparable to experimental and published data. As shown in the figure, the model is able to predict the effect of material properties on the satellite drops. It is noticed that when the glycerine content increases, more satellite droplets are formed.

#### **Use of the modelling approach to predict droplets with smaller sizes**

Another area of work that the numerical model is able to predict is droplets smaller than the nozzle diameter. Many established and emerging technologies require the production, on demand, of mono-sized liquid droplets, which are a few tens of microns in diameter. All of these droplet-based technologies are improved by reducing droplet size, which enhances the resolution of components produced by droplet deposition, or decreases the amount of material used for analysis. The simplest way of decreasing droplet size is to use a smaller nozzle diameter; but very fine nozzles are prone to blockage, and so it is advantageous to be able to produce droplets that are smaller than the nozzle from which they emerge (Goghari, 2008). The satellite drop and the size can be controlled by the flow mode. Figure 4.22 and 4.23 show a model developed with a nozzle size of 0.02 mm. The numerical code for controlling the droplet size is referenced in Figure 4.22. The numerical model demonstrated the ability of producing very small droplets in the range of a few microns. This proves the numerical model can be used as a tool for designing nozzles and parameter optimisations.

### **Modelling microfluidic droplet generation and effect of parameters**

The numerical model of the droplet has been extended to study the droplet formation in microchannel, which is an important area. Some typical results are presented briefly in this section. Figure 4.24 focused on analysing droplet formation within a microfluidic flow focusing channel. This numerical model was achieved by compiling published data and experimental results (Anna et al, 2016; Kim et al 2013). The numerical model focused on analysing the effect of variation in volumetric flowrate on the droplet size, outlet velocity and the dynamics of droplet formation during the dripping procedure.

This numerical geometry is based on a relief mould which has the capability of producing soft lithography techniques, by using flow focusing shape with a single output channel for both fluids. The numerical model has three inlet channels with a width of 100um, height of 75um and a one outlet of 100um. The mould also has a concentration section with a width of 50um to direct the multiphase flow. The results from the computational simulation were used to further validate droplet formation within a stream of another fluid. This study also looked at other data such as separation time, elongation effect, satellite drops, splitting and fusing, which have the ability of providing multipurpose outcomes for analysis within the engineering, fabrication, 3D printing, chemical and biological systems.

The effect of the different flowrate, between the continuous oil phase (in Blue colour) and the dispersed water phase (in Red colour), on the interface shape and growth of the droplet is illustrated in Figure 4.26, in which there is a clear agreement between referenced published data (Ward et al, 2005; Xu et al, 2008) and the contours of the developed numerical model. The elongation effect is very apparent above the primary droplet volume. This is due to the viscous effect that causes a significant lengthening of the liquid necking/thread between the liquid cone and the primary drop. Moreover, the contour plots highlight the increasing in volume and the dramatic size that the interface takes close to the point of breaking up. Furthermore, the increasing of the dispersed phase flow rate results in increasing of the volume size of the droplet. This can be seen clearly, in Figure 4.26, where the droplet volume size increases significantly, with the increase of the water mass flow rate value, while the continuous phase remains constant.

From the numerical model, it is apparent that the water droplets are formed due to the flowrate of the continuous oil phase and that it moves within the channel at a certain speed. Although Ward et al (2005) measured the formability and the velocity of the droplets by directly counting from camera recording, the developed numerical model was able to produce similar results, *via*

high mesh density and multiphase volume of fluid modelling, which allows the simulation of different types of flow to behave at different levels of complexity. Figure 4.27 shows the relationship between velocity of drops and the oil flow rate. The ratio of the multiphase volumetric flow rate against the velocity of the water droplet, is investigated for different continuous phase conditions. The open symbols represent published experimental data from Ward et al (2005), while the closed data represent figures from the developed numerical FLUENT model. The graph also illustrates and compares the difference in behaviour between four different dispersed flows, while the continuous oil phase was left constant. In all three studies, it is seeming that there is a small difference in velocity between the experimental and the computational velocity results, due to similar hydrodynamic behaviour between the multiphase flows. From Figure 4.27, it can also be noted that the average drop speed increased with the volumetric flow rate of the water linearly, this is agrees with the published experimental results (Ward et al, 2005).

## **Use the numerical model in developing a data based program and effect of material properties**

The formation of droplet is affected by many material specifications and factors, an effective cost/resource efficient method of plotting droplets, for specific materials and boundary conditions, is important for research and training purposes. For example, the overall droplet shape and formation for different materials could be quite different. This is due to the effect of different material properties. Figure 4.28 shows a contour plot summary of the investigated materials. The developed VOF numerical method has provided a clear framework which can be used to generate droplets for any multiphase situation. Molten nickel is used as an example of a semi fluidic material that was considered for this simulation. This material is used profoundly for thermal spray coating applications and it is known for its important effect on coating qualities, and hence, analysing the shape and volume regularity, of its droplet behaviour, is an important process that will lead to controlling the transition from irregular shape to more consistent and repeatable droplet volumes. Such information is important in materials development or training. The applications of the Young Laplace equation state the fundamental set of differential equations that define the forces and geometries of the pendant droplet. The developed numerical code in FLUENT is used to solve the Young Laplace equations and to plot an approximate shape parameter that is taken from systematic data produced by the CFD solver. A Matlab program has been developed to incorporate the data extracted from the developed FLUENT method, to a real time user friendly Droplet calculator that plots a contour of the droplet interface shape and output the values of the droplet length and volume at specific time intervals. The developed program aims to reduce the dependence on the numerical solvers, which can be costly and inconvenient to view the contours, and is much more suitable for research and training purposes. Figure 4.29 (a) illustrates the development stages of the Droplet Contour System in Matlab. The process started by running a simple numerical code of Water droplet, which was cross-referenced against experimental data (Section 4.4). Once the initial model was validated, the effect of changing boundary conditions was investigated. This include changing outlet diameter of the Nozzle exist and the material properties of various materials. After authenticating the results of many numerical studies for various materials, two different database were created for Fluidic and Semi Fluidic Materials.

After running numerous numerical models and simulations in ANSYS FLUENT, several hundred contours have been extracted and a large database has been created to develop the Droplet Contour System program. In many trials, the errors for the selected materials and time intervals were within 5-15% difference of the actual experimental set-up. The contour plots

generated by FLUENT are a good comparison to track and predict droplet shape, size and volumes. The Matlab code can also produce an approximate shape factor that can resemble real life pendant droplet experiments, and hence, this program was created. As illustrated in Figure 4.30, the program “Droplet Contour System” starts by accepting input parameters for the needle exit (e.g. an OD of 0.8 or 1.6 mm). After this, a material is selected from the four options “Water, Glycerine, Nickel and Gallium”. Next, the program is run and the droplet contour is generated, via database callback function. The pseudocode command used in the Matlab program can be used to evaluate shape factor values which is helpful as a comparison tool between experimentally generated results and other published literature values. Overall, the Droplet Contour System runs as intended and can be used for training and R&D to easily work out droplet properties. For future work, the program can be developed further to include calculation of interfacial tension, droplet into fluid-fluid systems, satellite drops and other features that can lead to more accurate and precise contour plots. The concept can also be applied to other situations such as smaller droplets, microchannel based on the numerical models developed.

#### **4.6 Modelling of small volumes of liquid and their interaction with different types of materials**

The behaviour of a small volume of liquid with multiphase interface or limited space can be a complex process affected by many factors. Compared to general solid structures, simulating liquid behaviour is much more complicated and can be particularly time consuming and costly. The accuracy level is also not as close to the experimental data since there are many parameters of liquid are empirical data. The choice of program is also critical and important. In the initial stage of the project, a range of programs have been evaluated including ANSYS Fluid, Abaqus CEL(Coupled Eulerian Lagrangian) as well open source programs (such as Open foam). These numerical simulation programs are widely used in different situations. As shown in previous sections, the work on droplet formation with Fluent showed a reasonable agreement with the published works from CFX and flow 3D as the solver. For simple case, such as droplet formation in Air, the choice of CFD solver is relatively flexible, however with more complex cases, establishing the feasibility is crucial. The capabilities of various fluid flow codes have been investigated, a typical case is the study of Abaqus CEL using simplified geometries and material properties to reduce simulation complexity and run times. Abaqus CEL is utilised for the first stage of the plan to simulate water being forced through a simple nozzle. The CEL code allows each cell in the mesh to contain both fluid and void. This makes the code appropriate for showing the intricacies of the spray pattern.

Modelling in Abaqus requires that the detailed geometry representing the fluid in its initial state. Suitable boundary conditions must be provided to simulate walls. Figure 4.31(a) shows the boundary conditions used. The red arrows show the displacement boundary condition which moves the plunger the length of the fluid body. It moves according to an amplitude to minimise inertial effects. The results from the first CEL model are shown at time increments of 0.5 seconds. Figure 4.31(b) shows how the model progresses. The first CEL model ran successfully for only 4.34 seconds of the 10 second total simulation but the results obtained show that this simulation method is unsuitable for these types of modelling conditions. When the modelling begins, the plunger pushes fluid from the nozzle at high velocity. During this time it can also be seen that the fluid is moving away from the plunger leaving a void in the body of the model. As the simulation continues up to 1.5 seconds, the void next to the plunger continues to grow as the fluid continues to move faster than the plunger. During this time the velocity of the fluid coming out of the nozzle decreases, however the flow becomes steadier with fewer drops forming. Between 1.5 and 2 seconds into the simulation the fluid within the body of the nozzle

slows sufficiently. The plunger continues at the same velocity until contact is made with the body of fluid reducing the size of the void. Between 2 and 2.5 seconds the plunger and fluid make contact again and more energy is passed into the fluid. This very quickly causes another large void next to the plunger and causes the velocity of the fluid leaving the nozzle to increase dramatically. The velocity of the fluid in the main body of the nozzle also increases at this time as can be seen in Figure 4.31(c). At 3 seconds into the simulation the void has grown much larger again. As the velocity in the nozzle in Figure 4.31(c) increases, some areas move further from the plunger and leave small drops of water separated from the main body of fluid. The output velocity of the fluid at this point also dropped dramatically again, and the shape of the output is no longer parallel to the nozzle due to the changes in fluid velocity before it exits the nozzle. The remainder of the simulation shows the entire body of fluid reducing in velocity with the void reducing in size. The shape of the output also becomes less constant before the model fails. From the initial investigation, it can be seen that using that a CEL model cannot overcome the inertial effect present when the plunger begins moving. This results in the fluid rebounding away from the plunger and causing the void in the body of the nozzle.

### **Modelling of liquid and droplet merging integrated in welding process studies**

Droplet formation is an important process that is relevant to many industrial processes such as managing the dose of medicine, inkjet and 3D printing. Numerical Fluid modelling is extremely expensive in terms of computation resources and time. Therefore, it is important to develop an effective process for R&D or in some case purely for training purposes. The modelling program developed in this thesis has set up a base which can be used to provide an effective simulation tool for modelling the shape formation processes, effectively integrated materials and manufacturing research.

A typical case is for the manufacturing of thermocouples. Figure 4.32 (a) shows a typical case of bare wire thermocouples, in which two thin wires are joined together. The electrical resistance changes with the temperature of the tip formed by two dissimilar metals. Depending on the configuration, these sensors are often connected to a thermometer or a temperature reading measuring device, to record changes in temperature behaviour for a certain amount of time. For the K type thermocouples, the two wire metals are Chromel {90% nickel and 10% chromium} and Alumel {95% nickel, 2% manganese, 2% aluminium and 1% silicon}. The bead is formed through a capacitor discharge (CD) welding process, in which a current pulse

is provided by the release of electric energy stored in a large capacitor bank that can be up to 1 million amps, and the pulse is typically about 10 milliseconds or less. The heat melts the two wires and joins them together. Figure 4.32 (b) shows the cross section of the welded bead. The welded tip was mounted in plastic resin, then sectioned and polished to reveal the detailed shape of the bead. The size of the bead has direct influence on the sensitivity of the temperature measurement. The properties and structure directly influences the structural integrity and also influences the response time when it is used in measuring the temperature in the spot welding process (Andrew 2016, PhD thesis). Therefore representation of the bead forming process is important. Another case where the merging of liquid is important, is the welding closure of thin stainless tubes for sheathed thermocouples as shown in Figure 4.32 (c). In a sheathed thermocouple, the welding bead of two thin wires was embedded in MgO powder (for insulation) within a stainless steel tube. The end of the tube is then welded together. The tube closure is formed by TIG welding. Details of the welding process is described in Chapter 3. In the welding process, the wall of the tube is melted, which flows and merges into a closed end as a dome. The structure and cross-sectional shape are illustrated in Figure 4.32 (c) and (d). The results show that there is complex fluid flowing and merging process during the welding, which can be challenging to represent this process accurately. A numerical model simulating this process is important for materials/manufacturing research as well as for training purposes (Figure 4.33 (a) and (b). Figure 4.33 (a) shows the merging of the two droplets in the initial stage, while Figure 4.33 (b) shows the stage when a spherical beam is formed. The liquid shows a clear down flow, resembling what is observed in the cross-section of the tube end. Future work will refine the material properties to be able to accurately predict this process.

### **Surface finish of stainless tubes and modelling of liquid dripping from a tube end**

The surface roughness of stainless steel tubes is a matter of critical importance for thermocouple sensor performance and reliability when measuring the temperature of a liquid. For example, there will be residual liquid on the surface of the probe after the probe is taken out of the liquid which needs to be cleared. This could be critical when the liquid is acidic or poisonous. A rough surface finish can result in inaccurate temperature recordings, difficulties in the cleaning process and shorter life time span due to corrosion. Therefore, it can be understood that high surface roughness value is very undesirable. During TIG welding procedures, surface roughness is strongly influenced by complex interaction between welding parameters, such as the current, height of the torch, shielding gas flowrate and welding speed. Hence, a series of welding tests have been performed as listed in Table 4.2. Surface roughness of the weld zone for all the tested samples was measured and the average surface roughness value was calculated from three readings.

Table 4.2 Surface roughness value for different welded samples.

Welding Height	Sample No	Reading 1(um)	Reading 2 (um)	Reading 3 (um)	Average Roughness Value (um)
1mm	1	3.411	3.358	3.034	3.26
	2	1.929	1.19	1.189	1.4
	3	1.72	1.381	1.376	1.49
	4	0.704	1.382	1.395	1.16
	5	2.812	2.791	1.22	2.27
2mm	6	1.9	4.615	3.258	3.26
	7	2.363	2.192	2.174	2.24
	8	3.563	3.575	3.583	3.57
	9	3.248	3.311	4.151	3.57
	10	1.311	1.236	1.21	1.25
3mm	11	3	3.5	3.2	3.3
	12	2.7	3	3.1	3
	13	2.6	2.7	2.2	2.5
	14	3.52	3.42	3.6	3.5
	15	2.3	2.6	2.4	2.5

Figure 4.34 illustrates a comparison between three 3D scan samples (Bukker GT-K surface texture system), of tubes across the welded ends, taken from analysed thermocouple sensor tips. These samples were prepared using different welding parameters, i.e. sample series-A: difference in height (position of electrode tip to the end of the tube), Sample Series-B: different in current. It can be noticed from the scans that there are no specific changes observed from

the weld specimen, though, the cross section of the 3D weld zone scan demonstrates a clear effect of the welding parameters changes. For example, the surface roughness value decreases as the welding height increases throughout all the investigated figures. Similar remarks cannot be observed when investigating the welding current. Also from the referenced scans produced by the Bukker GTK surface texture system, it can be noticed that the welding penetration changes with the adjustment of the welding height and current settings. This is apparent from the surface roughness value, which increased with the welding current, and decreased with the welding height. Again, for a particular value of welding current, surface roughness readings decreased as the welding height is increased.

As an extension of this project, an analysis model has been initiated to study the effect of surface wetting on the tip of the thermocouple sensor. A wetting process is the ability of the solid surface to maintain contact with the liquid. This phenomenon often occurs due to intermolecular interactions when the liquid and solid are brought together. The hypothesis is that surface roughness can affect the adhesive forces between the solid and the liquid, which can cause dripping residuals during operation. Consequently, further investigation will be performed by another ongoing project, which systematically study the link between surface roughness and the wetting process for various materials (stainless steels).

Two typical examples are shown in Figure 3.35, which illustrate the dripping of a liquid from the thermocouple stainless steel tube. This model is able to assess the effect of contact angle and wetting characteristics on the liquid flow and droplet formation. Initial simulation results showed that when the thermocouple is plunged into liquid at an angle of  $0^{\circ}$ , full wetting is achieved and a residual on both sides of the tip can be observed. This can cause the probe to produce inaccurate temperature readings due to the wetting affect. On the other hand, at a  $60^{\circ}$  contact angle, the residual effect is only apparent on one side, which is less significant than the  $0^{\circ}$  contact angle but still effective. Hence, when the contact angle increases, the liquid residual decreases. These results illustrate that the numerical model can be used to systematically map the effect of the contact angle. This initial finding will help in producing a map or a database of wetting characteristics for different materials and surface finishes. Future work will focus on developing systematic studies on the contact angle of flat and curved face with different roughness, then use the contact angle as an input to guide the product analysis or material development.

### **Modelling fluid penetration in small cracks mimicking NDT Dye penetration test.**

Flow of a small volume of liquid in a confined space is relevant to many material systems or engineering situations, a typical example is the Dye penetration test as it is commonly used in Non-Destructive-testing (NDT) of welded structure. Dye penetration testing is a popular way of testing the quality of welded joints in oil industries and it is an important part of the structural inspection. As shown in Figure 4.36, the principle of dye penetrant testing is that the liquid penetrant is drawn into the surface-breaking flaw by capillary/nozzle action, excess surface penetrant is then removed. A developer is applied to the surface to draw out any penetrant in a flaw and to produce a surface indication. Cracks as narrow as 150 nanometres can be detected. The indications produced are much broader than the actual flaw and are therefore more easily visible. When a crack or other surface breaking discontinuity is present in a non-porous material, the penetrant will be drawn into the flaw by capillary action. This is the phenomenon of a liquid rising or climbing when confined to small openings due to surface wetting properties of the liquid. A similar example of this application is apparent in plants and trees drawing water up from the ground to their branches and leaves to supply their nourishment. Furthermore, the human body has miles of capillaries that carry life sustaining blood to our entire body. The Dye penetration process represents a typical case of the flow of a small volume of liquid into a confined space. A model has been developed and used to simulate and effectively represent this process. A typical example is shown in Figure 4.36. As shown in (b - f), the model is able to effectively represent the flow of dye in the crack opening. This numerical model can be used as a tool in a current project for developing new training manuals for NDT methods.

## 4.7 Discussion

The work reported in this chapter focused on developing numerical models for simulating small volumes of liquid relevant to different technical situations such as dimension, load and boundary. The behaviour of a small volume of liquid with multiphase interface or limited space can be a complex process affected by many factors. Compared to general solid structures, simulating liquid behaviour is much more challenging and can be particularly time consuming and computationally costly. Therefore, selecting an appropriate numerical code is critical for balancing both accuracy and efficiency. As detailed in section 4.4, the work on droplet formation, using the numerical simulator FLUENT, showed a reasonable agreement with other published works with different numerical codes such as CFX and flow 3D (Figure 4.16). The overall structure of the research has covered different areas following a progressive structure. Initially, the work focused on modelling the dynamic behaviour of pendent droplet supported by detailed experimental and modelling work. Then FE models for a range of important industrial and research cases were developed. These include droplet for semifluid material systems, formation of satellite droplets, multiphase liquid in micro channels and generating droplets smaller than the outlet diameter of nozzles with controlled flow rate and cycles. The numerical modelling of these cases are relevant to liquid control applications in medicine and 3D printing (Kim et al 2013; Carrier et al 2015; Anna et al, 2016; Kovalchuk et al 2017; Zhong et al 2018; Guo et al 2019). Furthermore, usages of computational fluid dynamics in simulating droplet merging in micro welding, liquid dripping from stainless tubes, and modelling of fluid penetration in small cracks mimicking NDT Dye penetration inspection method, are all relevant to important industrial, research and development applications.

Modeling droplet formation was a critical part of this work, in regards to integrating both numerical and experimental findings. Analyzing the dynamic behavior of a droplet formation and the nature of the free surface flow associated with droplets is important for a wide range of applications within the engineering, industrial and medical fields. The developed numerical model, using the Volume Of Fluid (VOF) solver in FLUENT, was validated *via* both qualitative and quantitative approaches (e.g. droplet shape, length, volume, separation time). This was achieved by comparing analytical solution, experimental results and published data with different modelling approaches. Even though, there are many CFD packages that are used nowadays to simulate droplet formation and changes in material flow patterns across various intervals. A detailed validation process of the material properties and boundary conditions is

still essential for the credibility of the work. In addition, the performance of the simulation process, in terms of computational power, total cost and time, are also affected by these factors, which has been addressed to produce consistent data when modelling fluid at small scales.

In this work, the numerical model was correlated with analytical solutions based on pressure and velocity calculations from Bernoulli's theory. The model was also assessed in comparison with other methods with similar reference material systems and showed a good agreement in simulating the dynamic behaviour of both pendant droplets and droplets with satellite effects. In addition, the work compared the produced data against other published results from various numerical softwares (such as CFX and FLOW 3D), in regards to simulating the free surface smearing of a multiphase flow, droplet length, separation time and subsequent satellite drops. Achieving this provided an effective approach for validating and using of the numerical VOF code for a wide variety of applications. A range of pure and mixture liquids (mainly water-glycerine solutions and low melting temperature metals) was used to evaluate the developed numerical model and to study the effect of change in properties within different conditions.

One of the key challenges faced in this work is defining the properties of fluid mixtures, which were measured and controlled using volume fraction/mole fraction techniques. The approached drop ball method is simple but versatile, when compared to other measuring devices such as rotary viscometer. Methods such as rotary viscometer can only provide readings for translucent fluids, i.e. distilled water or low viscosity fluids (Michal et al 2017; Ali et al 2019; Mograne et al 2019). An advantage of using glycerine water solutions lies in the fact that it offers different viscosities by changing the concentration levels. Table 4.2 showed the viscosity is low at lower concentrations and increased dramatically at 85% and 100% concentrations. The values of the viscosities are in a close agreement with published data from different measurement approaches (Shankar and Kumar, 1994; Michal et al 2017). Shankar and Kumar (1994) compared data for pure Glycerol at different temperatures, the reported viscosities of 1.2 Pa.s and 0.2 Pa.s at 20 °C and 50 °C, respectively, which is very close to the measured values from this work for pure Glycerol (Figure 4.10). The viscosity data of glycerine-water mixture and its changing trend with the temperature is also close to the values reported by several researchers (Segur and Oberstar, 1951, Cheng et al 2008, Michal et al 2017). Work by Cheng et al (2008) revealed that the viscosity for the glycerol-water mixture can be calculated by an exponential formula, which reflects a steep increase in viscosity values at high glycerine concentrations. The

produced data for the 85% glycerine-water solution of this work is also in a close agreement with recorded values by rotary viscometer (Michal et al 2017). The work also shows that the effect volume/mole fraction of glycerine on viscosity can be represented by different mathematical models with the natural logarithm being the most suitable one to describe the significant increase in viscosity when the volume fraction increased from 80%. The detailed mechanism for the significant change in viscosity with the water-glycerol concentration change is still a subject to scientific research mainly in chemistry science. It is believed to be associated the complex interaction between hydrogen bond acceptor. A potential approach to establish the full mechanisms is to establish the structure effect through a complex molecular modelling (Baz et al 2019).

The work compared the effect of viscosity, surface tension and contact angles (wetting) in different situations associated with droplet formation. One key part is qualitative and quantitative comparison of pendant droplet against experimental data and polished work with different modelling approaches (as detailed in section 4.1.1 and 4.4.2). The results clearly show that the numerical model can successfully predict key stages of droplet formation. The numerical model demonstrated the dominance of the capillary effect and separation time. In early stages, the droplet is round in shape due to its high surface tension values. At later stages, the droplet is significantly elongated due to the density effect. From the experimental and numerical results, it was noted that the viscosity limits effect on the droplet length. The main controlling factor for the droplet size is the surface tension and density. As discussed in section 2.2 and 2.6, the weight of the pendent droplet is balanced by the surface tension. However, since the VOF solver is based on atmospheric boundary conditions, therefore, the density of the liquid is dominating. One of the important features for the developed simulation method is the ability to simulate complex multiphase material systems such as water in oil, or liquid metal in a liquid. All of this can be achieved by simply replacing the air values with other liquid used. The investigation also showed that the volumetric flow rate plays an important role on controlling the droplet volume and the break up time. As the volumetric flowrate increases, the overall volume of the droplet decreases rapidly, until the velocity of the flow approaches to the jetting mode. Similar results have been reported by other works (Guillot et al 2005; Lu et al 2018). Hence, this developed numerical method can also be used for designing and optimising Micro-Liquid Jetting systems (Ghodsi, et al 2017; Lu et al 2018).

The work shows that the viscosity directly influences the formulating satellite droplets, and

droplet smaller than the size of the nozzle. The process of drop detachment from a capillary tip and formation of satellite droplets is a complex process that has been studied by other works (Carrier et al 2012; Kovalchuk et al 2017). The formation of satellite droplet is caused by surface tension of the air/liquid interface. As shown in 4.16, 4.17 and 4.22, a neck between the main jet and the developing drop is formed when the jet starts to pinch off. This neck is stretched under the weight of the moving droplet until it is broken. After this, the stretched region rebounds when the drop is completely separated. The rupture of the neck results in forming satellite drops. As shown in Figure 4.22, as the viscosity increases (higher glycerine content), more satellite drops are formed. In general, satellite droplets are known as an unwanted effect when trying to control droplet volume. For example, in electro hydrodynamic jet (e-jet) printing, the patterns on the substrate will be contaminated if the satellite drop falls onto the substrate (Guo 2019). A parametric numerical could help to predict and control these processes by establishing optimum conditions for situation such as liquid jetting or microsphere formation (Lu et al 2018)

The droplet smaller than the nozzle can be considered as a progressive method of regulating droplet sizes uniformly, which is important to many research and industrial areas (Amirzadeh et al 2008; Castrejón-Pita et al 2012; Goghari et al, 2008; A.Amirzadeh et al 2013; Wang et al 2020). These include modelling and developing drop-on-demand (as outline in section 2.8). As illustrated in Figures 4.2-3, the key feature is the velocity and cyclical loading patterns. This is particular relevant to metal based systems as general flow of molten metal in a thin tube is difficult. The capacity of generating metal drops smaller than the nozzle could significantly improve the technicalities (Wang et al 2020). The developed numerical method is also relevant to developing liquid encapsulated spheres for micro-sphere composites or self-repairing materials, in which as small volume of liquid needs to be encapsulated in a thin shell (Liu et al, 2019).

Modelling of small volumes of liquid in open or confined spaces is a challenging but important area (Baroud. et al 2010; Benet and Vernerey 2016). Typical cases presented in the work include merging of welding bead in joining of two dissimilar thin wires, the dripping liquid from metal surface and penetration of fluids in crack openings. These are important engineering, industrial and R&D applications, for which numerical modelling methods are effective and efficient. In a longer term, the numerical model could also be used for potential fit-for-purpose engineering training applications. In the case of welding applications, as shown in welding for thin wires

and stainless tubes, the model is able to predict key stages of the bead forming process as well as the formation of void between two droplets. Previous works (Norbury et al 2018) show that the shape of thermocouple beads directly affect the sensitivity and accuracy of the temperature measurements. Future work could extend these into areas where the shape and the volume rather than the microstructure (Norbury, et al 2018; Xiong et al 2017).

As for the dripping test, the model shows the residual of the liquid on a tube surface with different wetting coefficients and contact angles. This has laid a foundation for future work on quantifying the link between surface finish and wetting behaviour, which is currently being developed by other members of the research team. In the case for the dye penetration test, the developed numerical model illustrates the important uses of CFD for representing complex process in an effective way. This finding is also used for research and training purposes.

Although the work focused on the droplet formation process in atmospheric conditions, the numerical code is also applicable for droplet in other medium/envrionment. In a continuing project, the droplet formation of water in oil and liquid metal in different oxidation preventing liquid is being studied based on the program developed in this work (Kaid et al thesis 2020). The work by Kaid (2020) also used the droplets formation model to predict the rebound and droplet formation process of low melting temperature metals used for conductive rubbers (metal beads in silicone rubber). The numerical model can also be extended to modelling droplet formation of complex chemical/polymers for forming polymer spheres and liquid encapsulated in polymer shells for self-repairing composites (Liu et al 2019).

## 4.8 Summary

This work focused on developing effective modelling approaches for simulating the behaviour of small volumes of liquid and their interaction with other phases under different conditions with a particular focus on droplets and their interaction with different material systems. Various commercial CFD approaches (ANSYS Fluent, CFX and 3D Flow) have been evaluated for modelling the droplet formation process. An effective modelling approach has been developed in ANSYS Fluent to simulate pendant droplet formation via the Volume of Fluid approach. The results from the numerical investigation were assessed against experimental data (viscosity/density tests and droplet tests) of selected model materials (mainly Water-Glycerine mixture solution and low melting point metals). Systematic droplet tests were conducted with a range of Glycerine-water solutions, the results show a good agreement with the numerical prediction and published data. The numerical model was applied to material with high viscosities using low melting point metals (Gallium) as experimental materials. A quantitative analysis of the data from the numerical approach and experimental data established the effects of viscosity and surface tension of the solution on the shape and key characteristics (droplet length, breaking up point, overall volume of the droplets). Designated case studies, with specifically built models and codes, relevant to various engineering processes have been developed, including satellite droplets, droplets smaller than nozzle diameter and microfluidic droplets in a multiphase flow system. The results show that the developed approach is effective in simulating different systems and potentially used as a tool for mapping the effect of design or material parameters (as illustrated in the effect of flow on microchannel droplet formation), including the limiting parameters for generating quality droplets. Comparative data shows that at the macro level, for the conventional droplet system, the volumetric flow rate is inversely proportional to the overall volume of the droplet, up to the point where the flow approaches the jetting mode; whereas at the micro level, this relationship is found to be non-applicable. A Matlab data system has been developed incorporating the realistic droplet shapes from the numerical modelling. The modelling approach is shown to be effective in simulating small volumes of liquid in open or confined spaces based on cases of the bead forming process for thin wires; the residual of the liquid on a tube surface as well as the dye penetration process. The parameters of liquid mixtures obtained was cross compared with data from different approaches, and work to further improve the fundamental understanding of liquid properties is discussed. The main factors affecting droplet formation and small volume liquid modelling and futures work is also discussed.

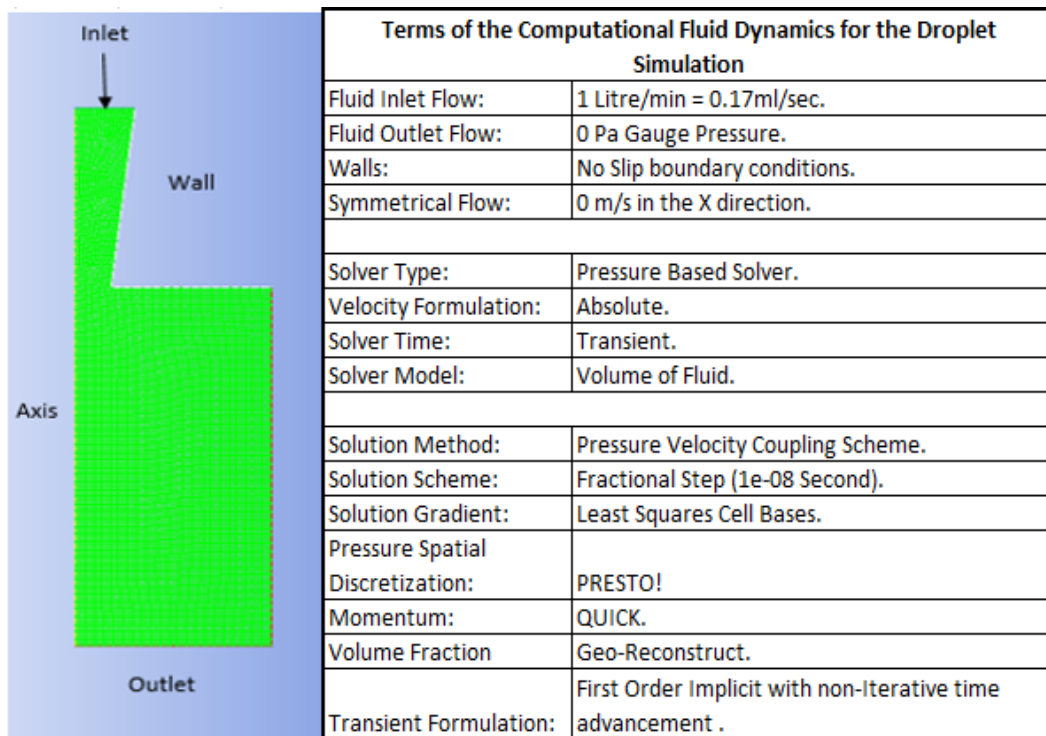


**Figure 4.1** Numerical properties and boundary conditions for the CFD model of the multiphase flow.

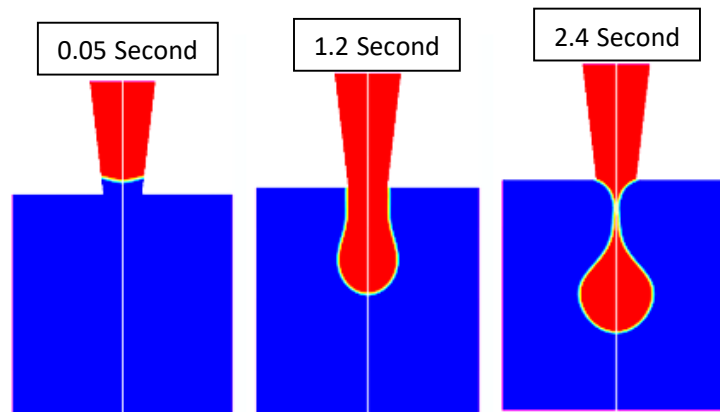


**Figure 4.2** Typical simulation results showing the droplet growth and detachment process (time=0.05, 1.2, 2.45 s) using FLUENT. The air is blue in colour and the water is red in colour based on the EM model).

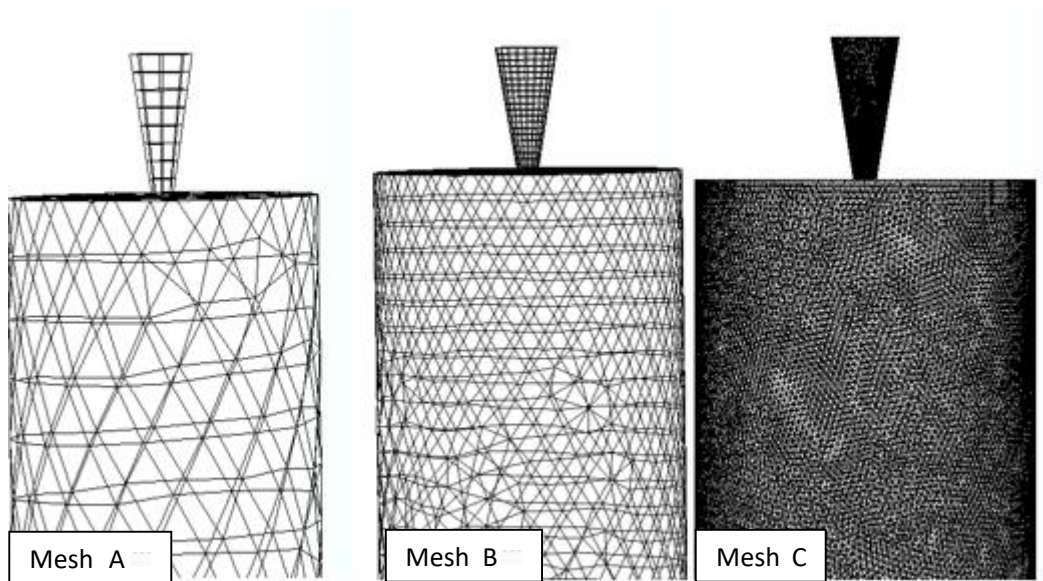


Figure 4.3 Typical different mesh densities/scheme used in the mesh sensitivity/convergence study.

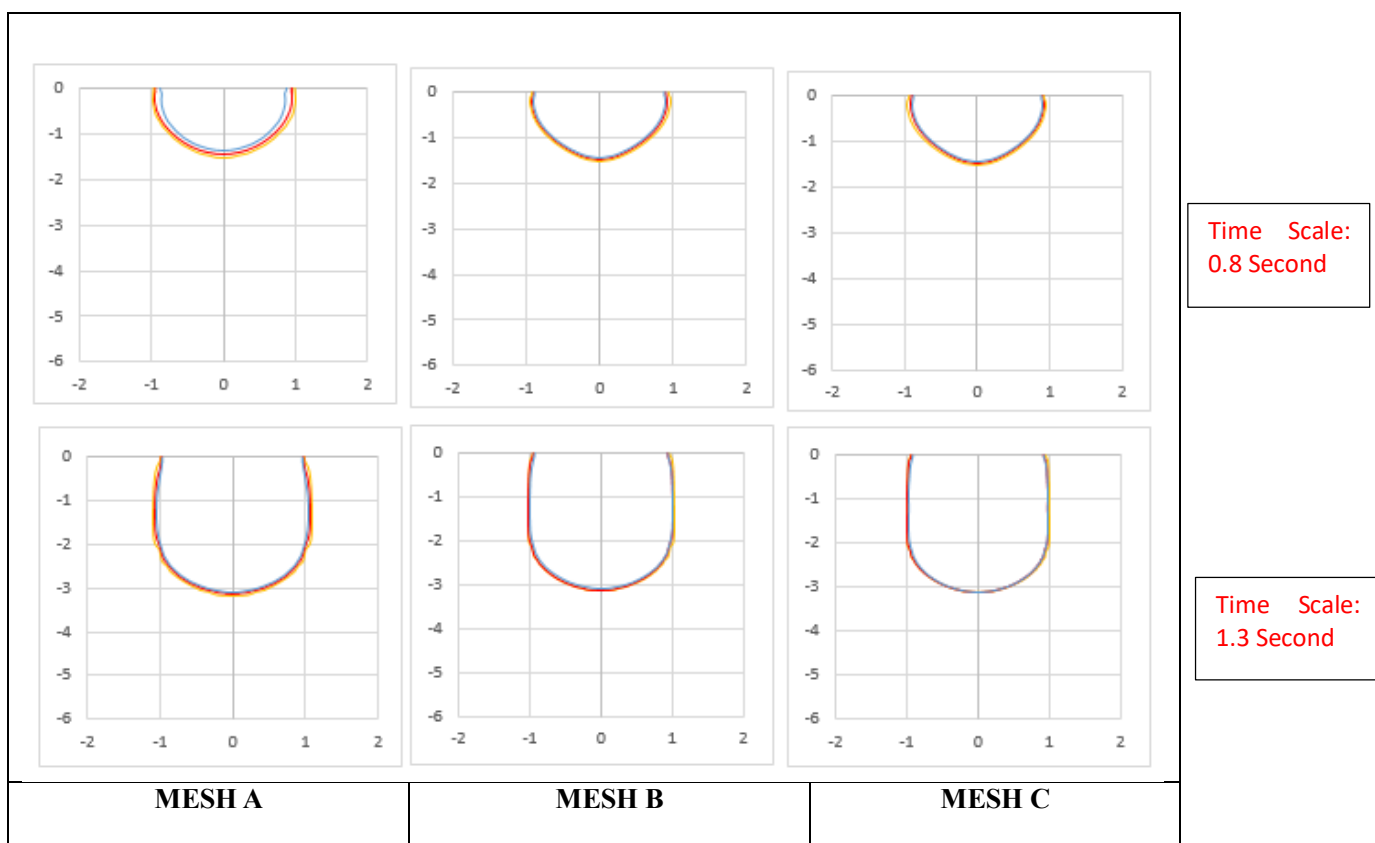
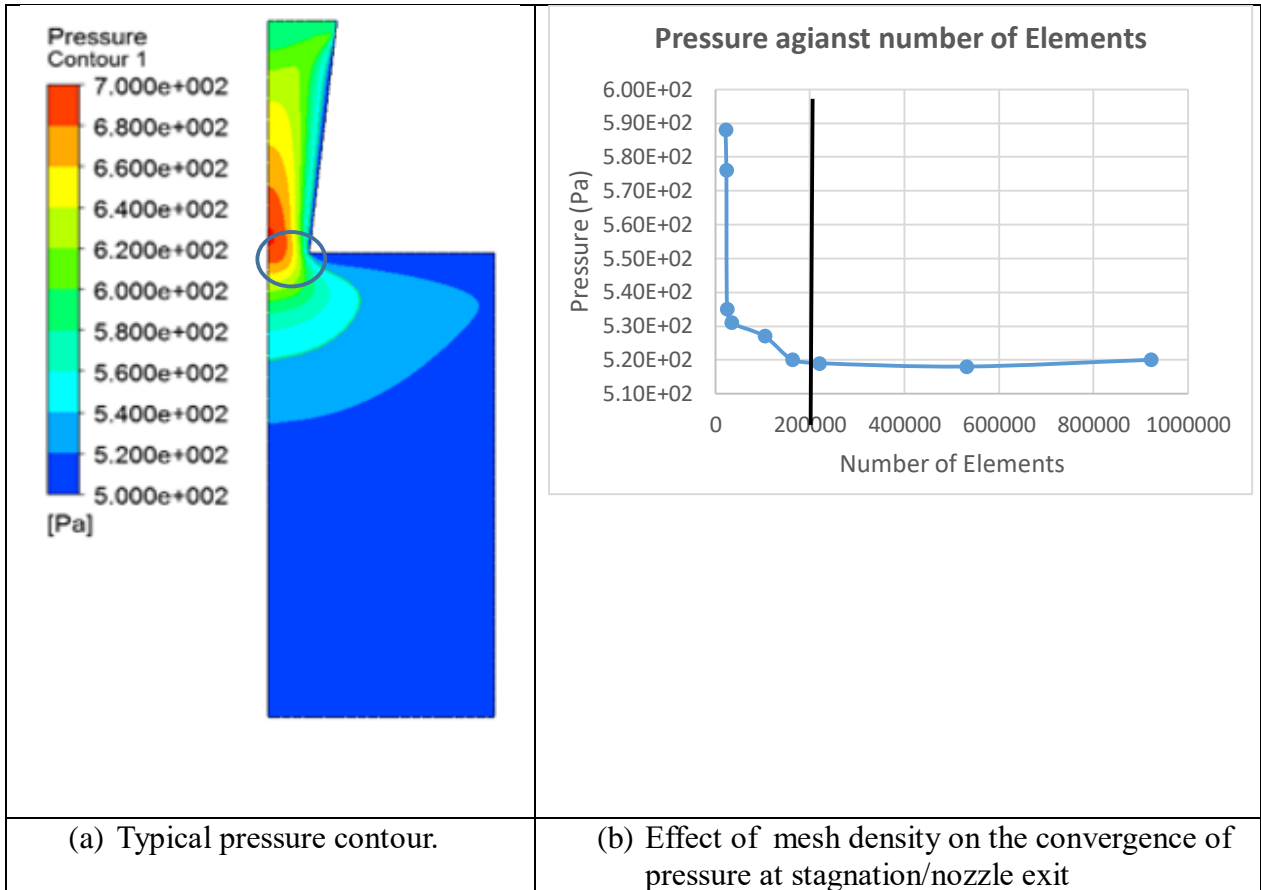
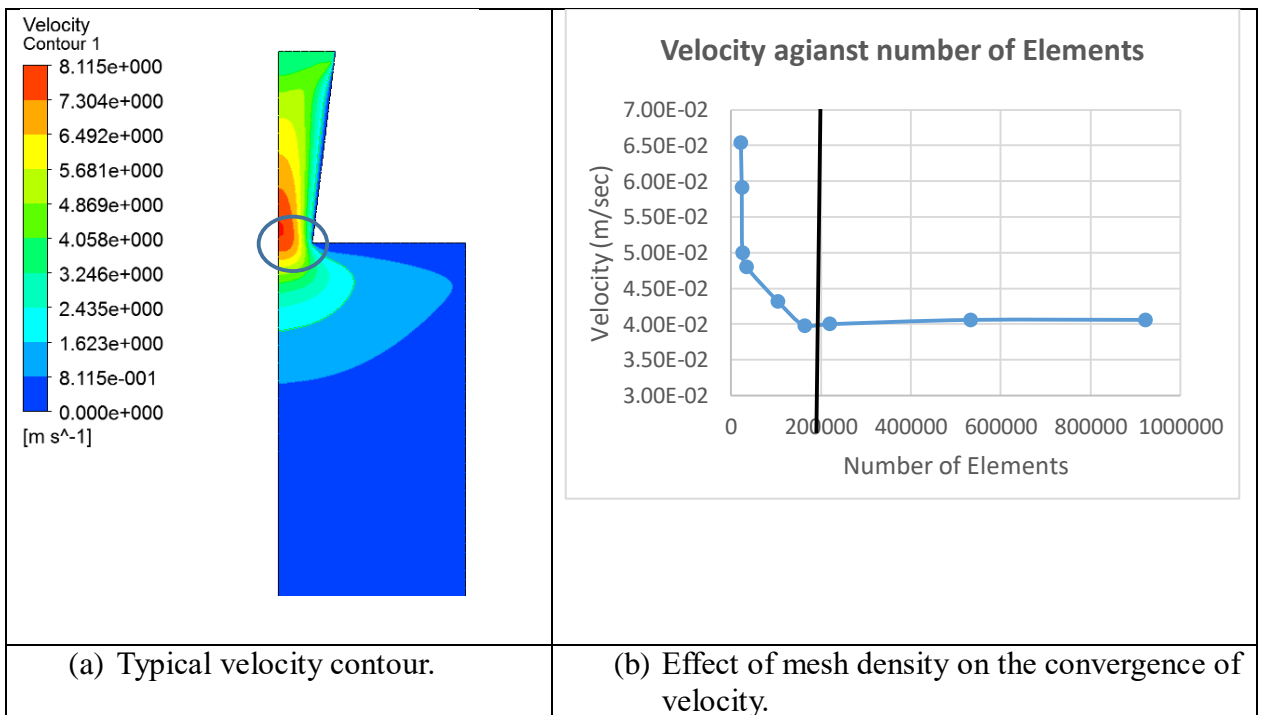


Figure 4.4 Typical example of droplet contour plots at different time scales showing the effect of mesh density on interface shapes obtained using FLUENT. The difference in colours represents the difference.



**Figure 4.5** Typical pressure contour of a tapered nozzle and data showing the effect of mesh density on the convergence of the pressure at the stagnation/nozzle exit.



**Figure 4.6** Typical velocity contour and effect of mesh density on the convergence of the velocity at stagnation/nozzle exit.

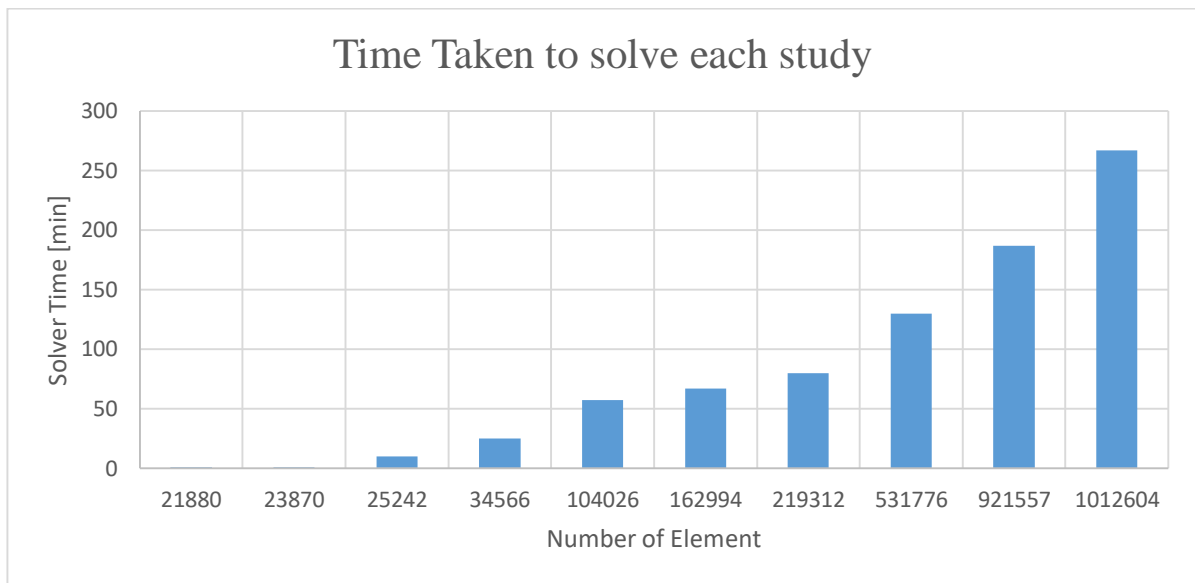


**Figure 4.7** Typical data on a single PC showing that the time taken for each study is increasing nonlinearly when the density of mesh is increased. The data is representative (i.e. the ratio) to other cases when a more powerful computer system is used.

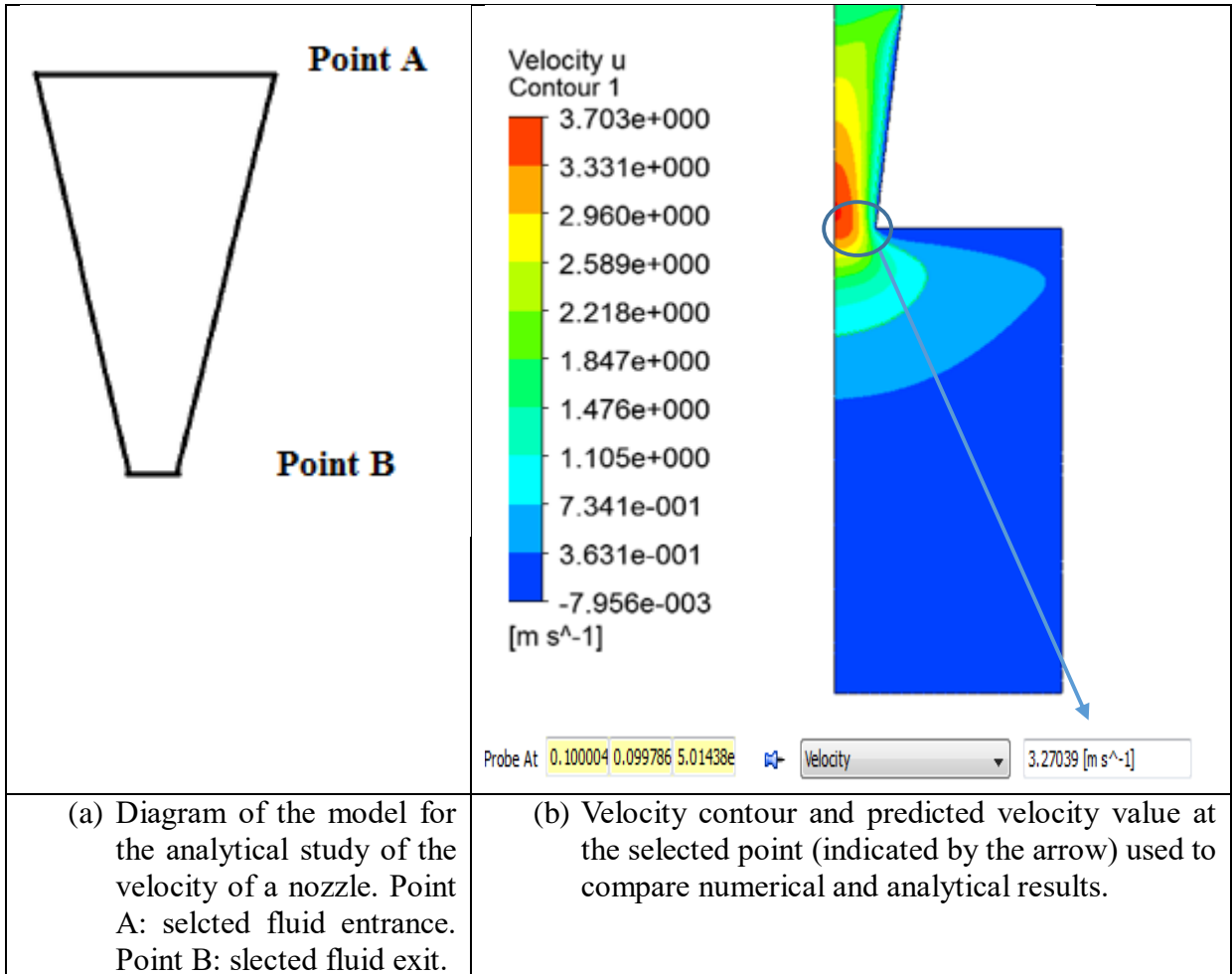


**Figure 4.8** Diagram of the nozzle used in the analytical analysis and the numerical contour. The velocity data at a typical preselected point (coordinates (0.1, 0.099, 5.01) is extracted to be compared with analytical calculation.

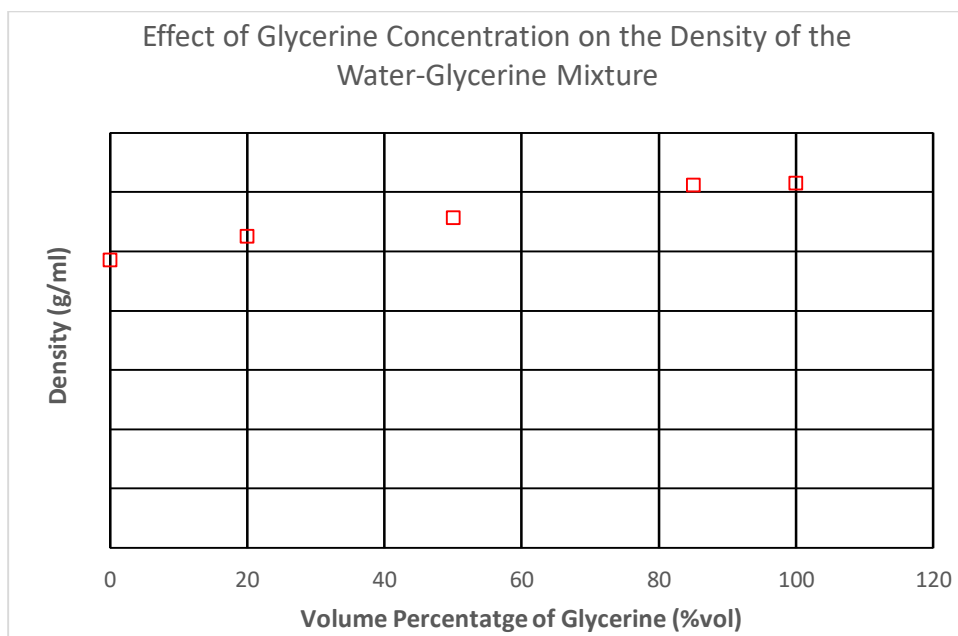
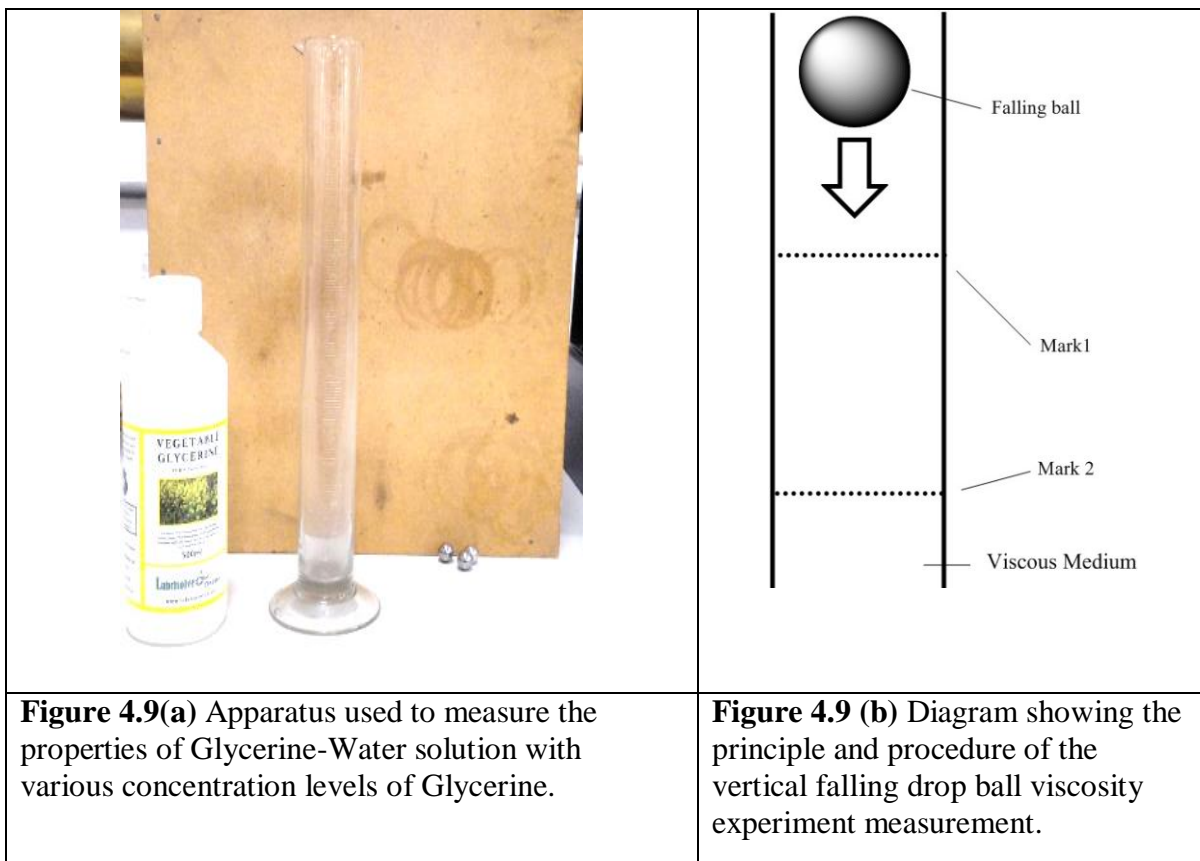


**Figure 4.9(c)** Measured data showing the effect of Glycerine concentration on the density of the Glycerine-Water mixture solution.

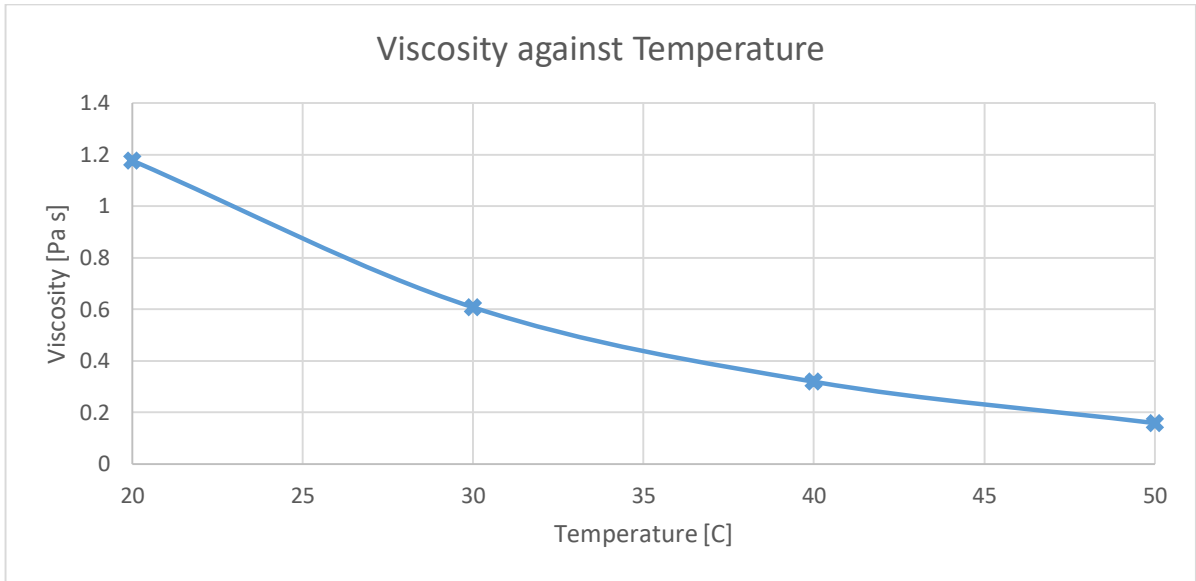


**Figure 4.10** Effect of temperatures on the viscosity of pure Glycerine oil.

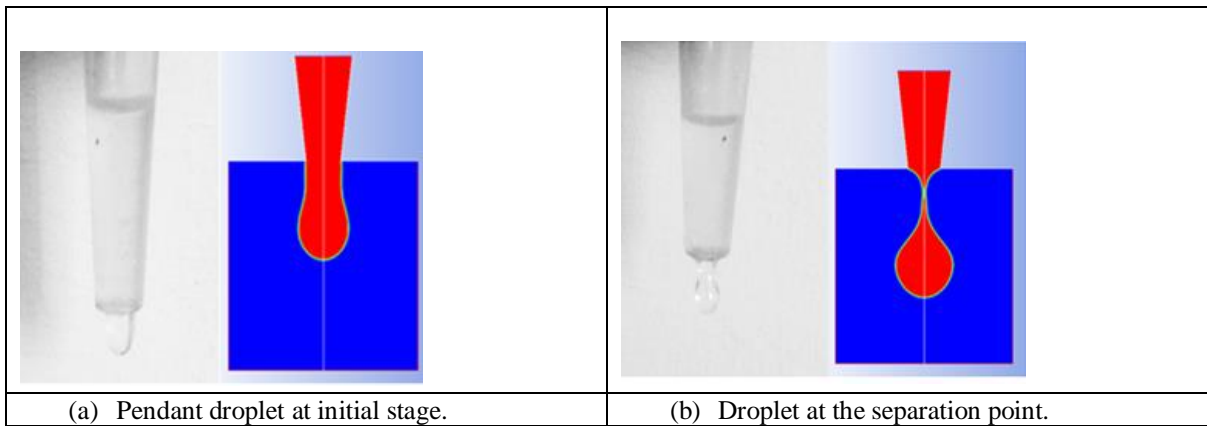
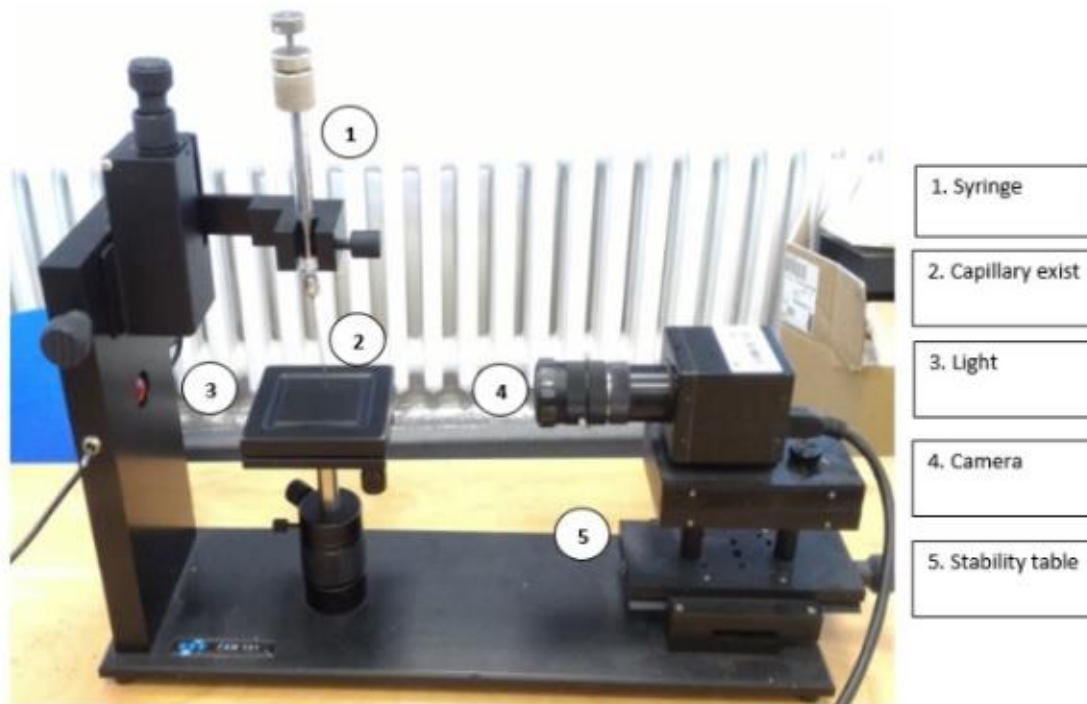
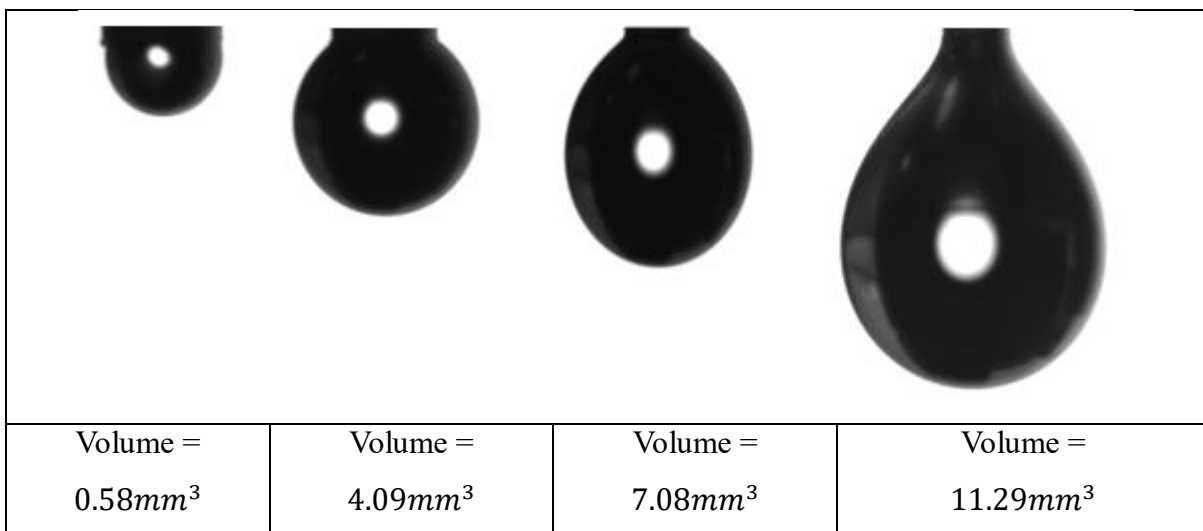


**Figure 4.11** Typical results comparing between experimental and numerically predicted droplet shapes at different stages (a plastic syringe with a tapered nozzle)



- 1. Syringe
- 2. Capillary exist
- 3. Light
- 4. Camera
- 5. Stability table

(a) Experimental arrangement used to visualize droplet formation.



(b) Typical images showing the growth of the droplet with controlled increasing liquid volume. (Straight tube,  $D=1.6\text{mm}$ ).

**Figure 4.12** Typical images showing the growth of the pendant droplet with increasing liquid volume. (Straight stainless tube).

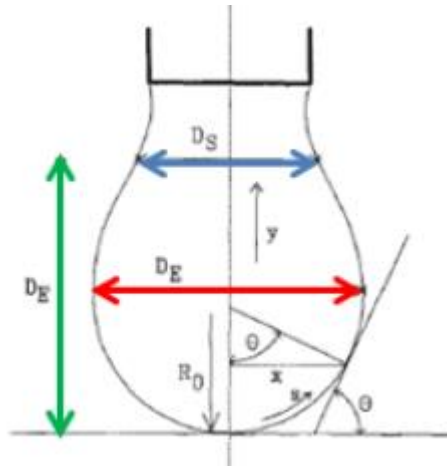


**Figure 4.13** Drawn definition of the key parameters of a droplet for quantitative analysis.

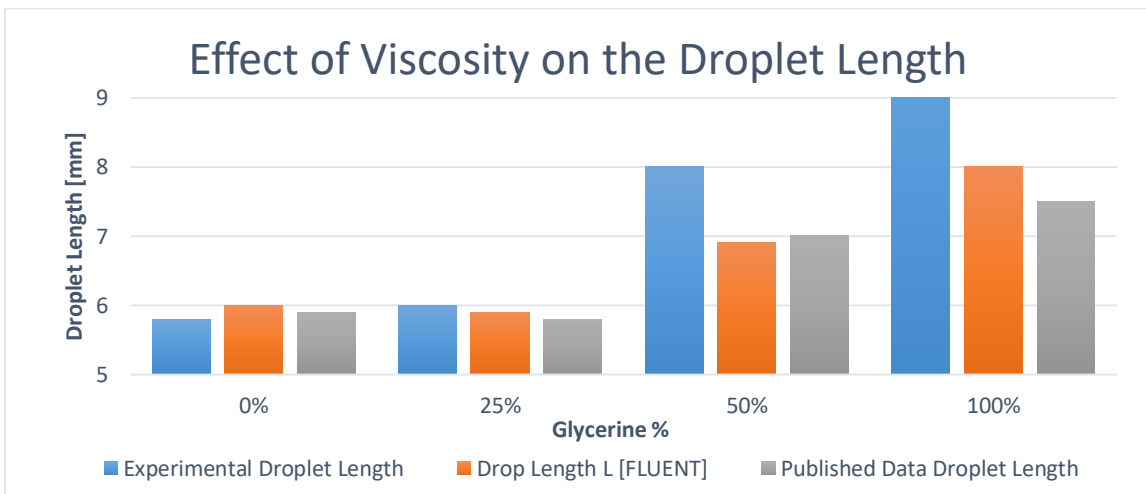


**Figure 4.14(a)** The effect of increasing the viscosity of the liquid on the droplet length.

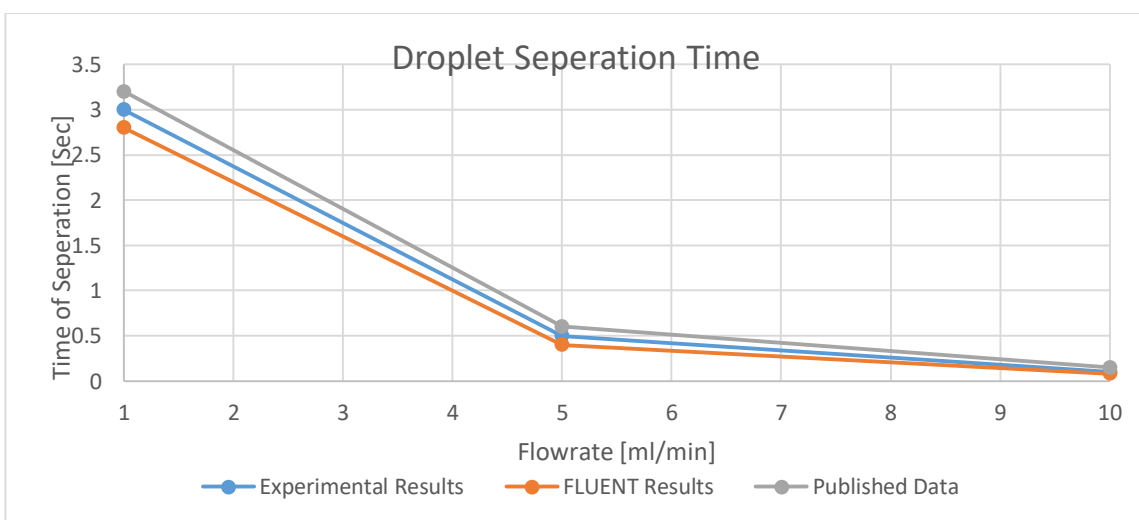
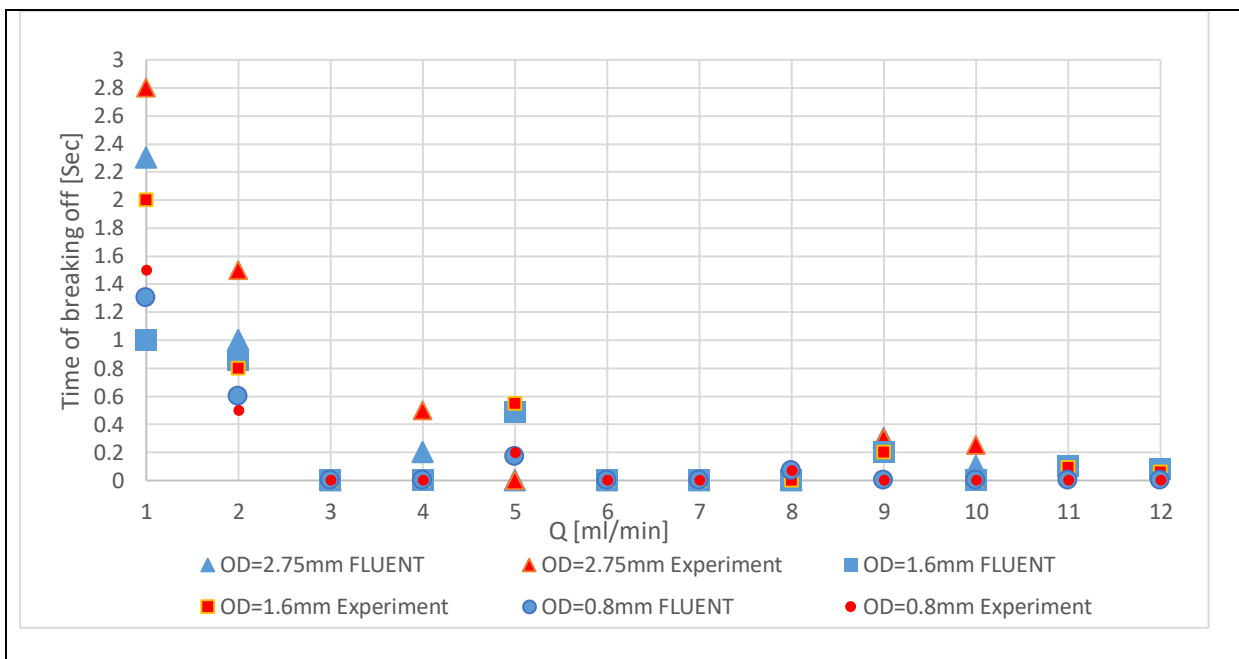
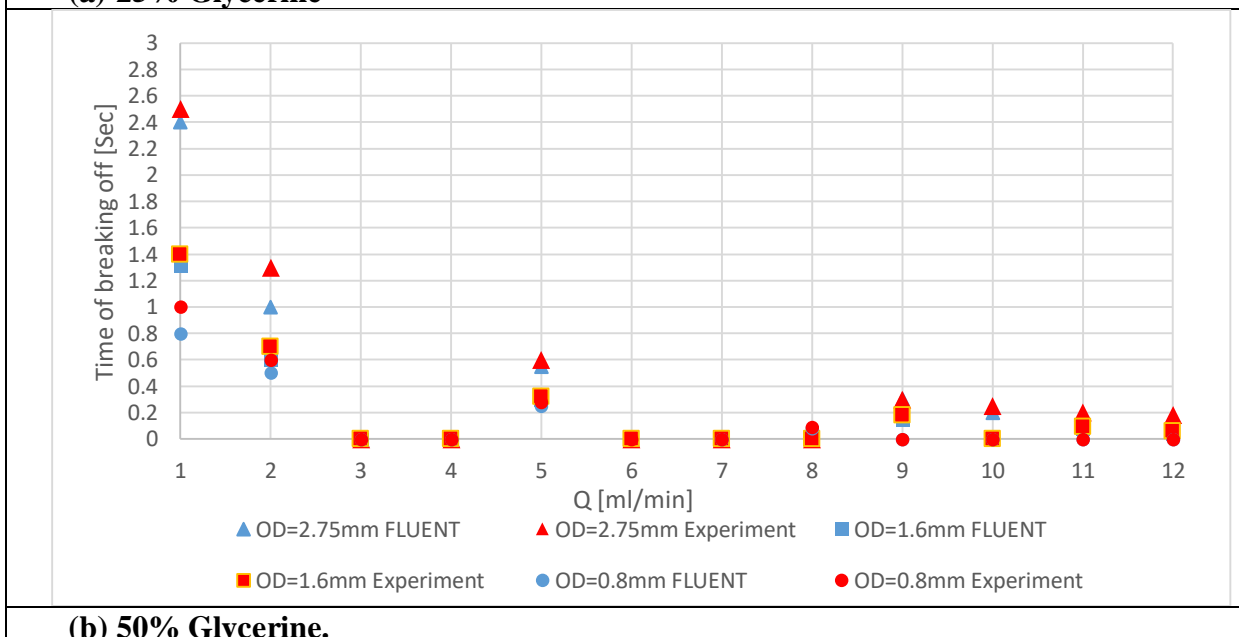


**Figure 4.14 (b)** The effect of volumetric flowrate on the separation time of droplet.



**(a) 25% Glycerine**



**(b) 50% Glycerine.**

**Figure 4.15** The effect of changing the nozzle exit size and the volumetric flow rate on the dynamics behaviour of the droplet.

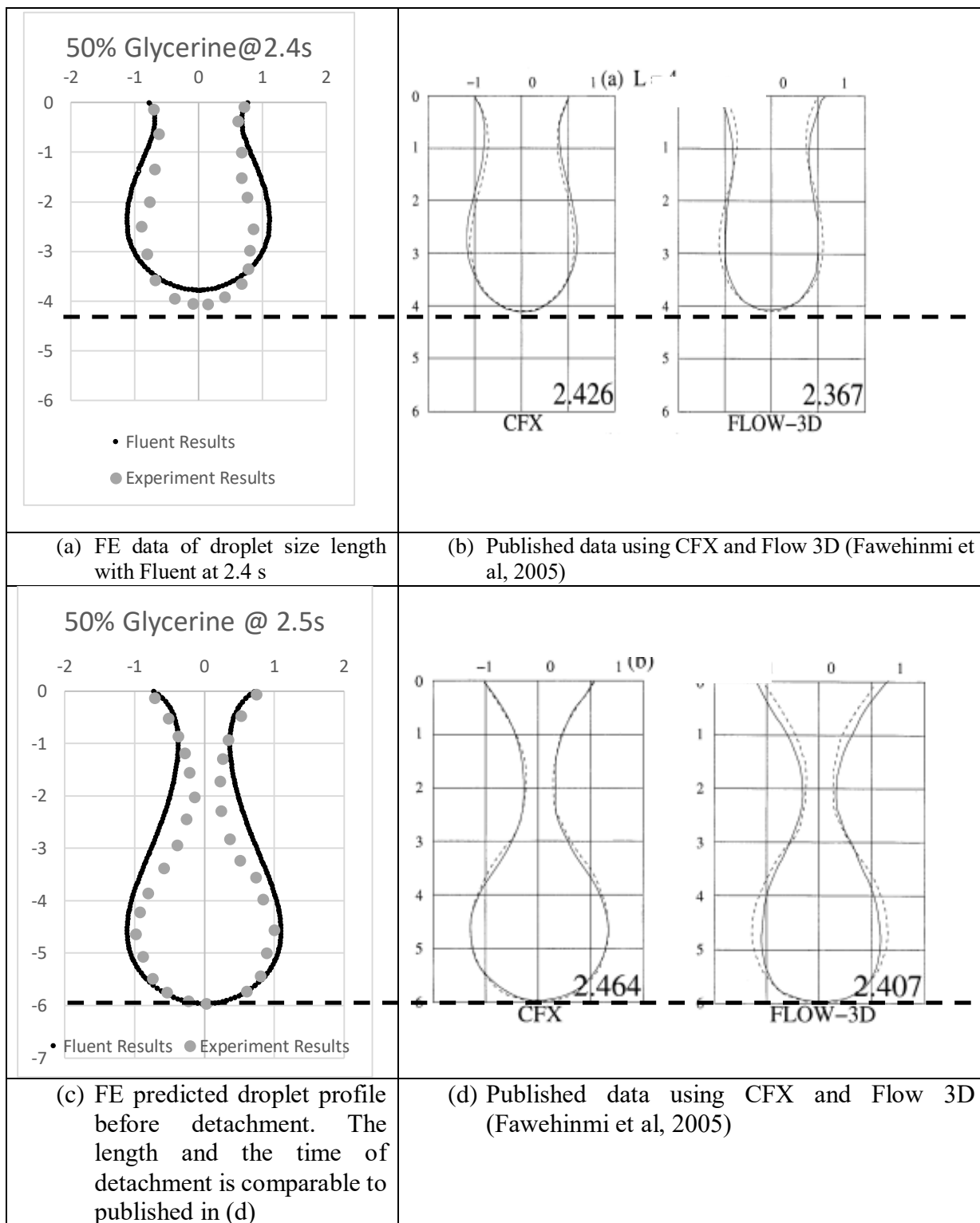


**Figure 4.16** Interface shape comparison between FLUENT results and published data with CFX and Flow 3D. (all based on 50% Glycerine data)

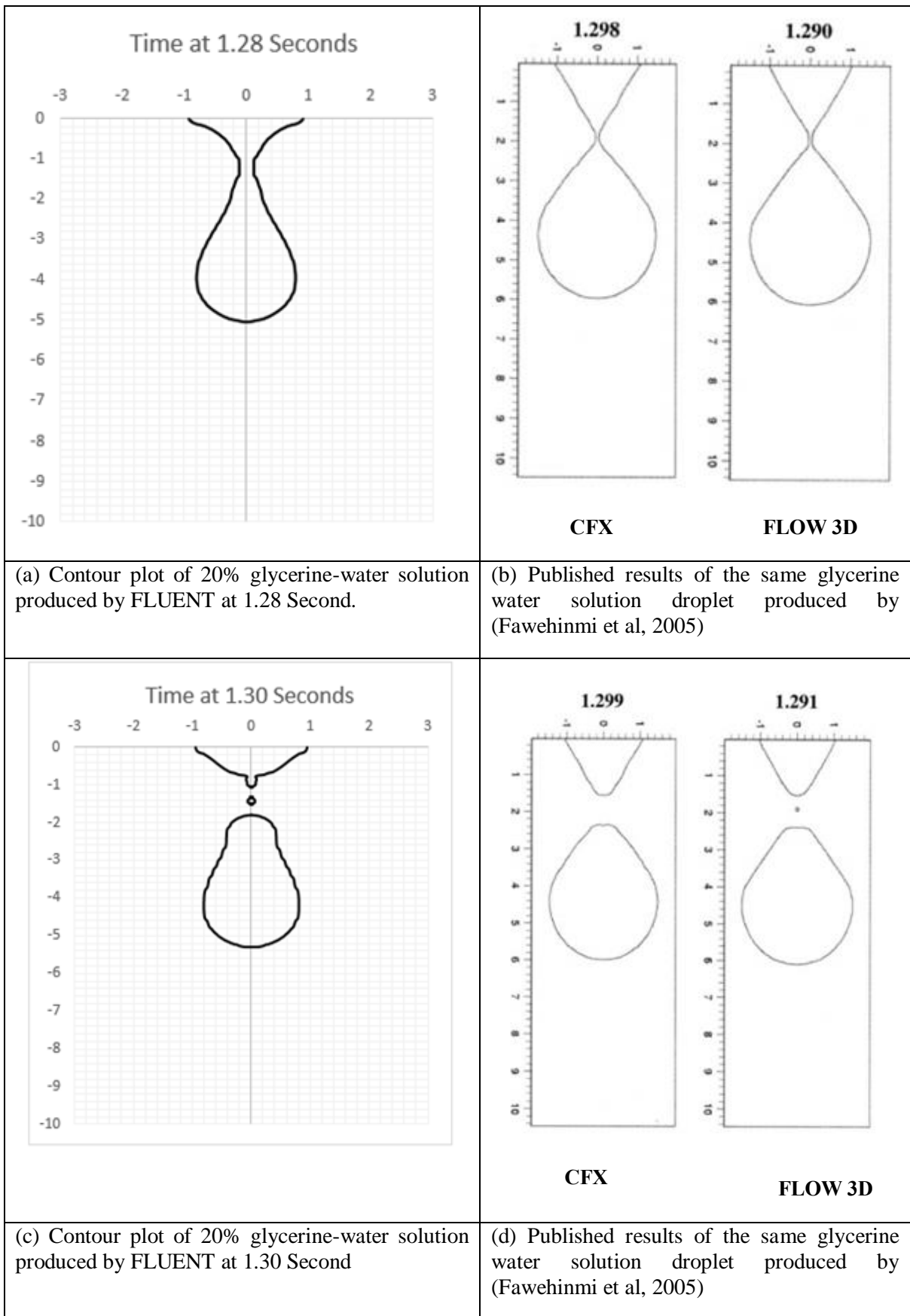


**Figure 4.17** Comparison between FLUENT predicted droplet shape change (elongation effect and satellite droplet) at breakup for a 20 percent Glycerine water solution and published data.

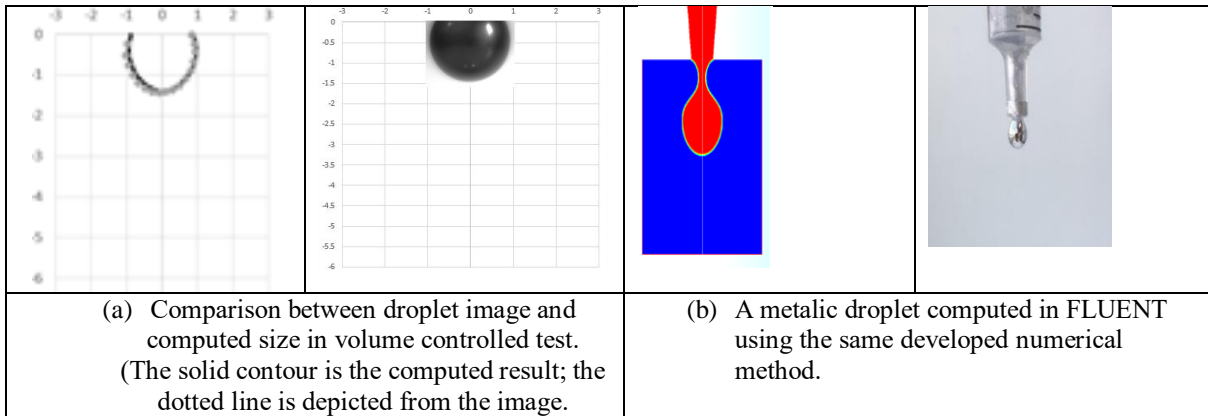


**Figure 4.18** Typical data of semi-fluidic liquid Gallium droplet: Numerical Simulation against experiment observation.

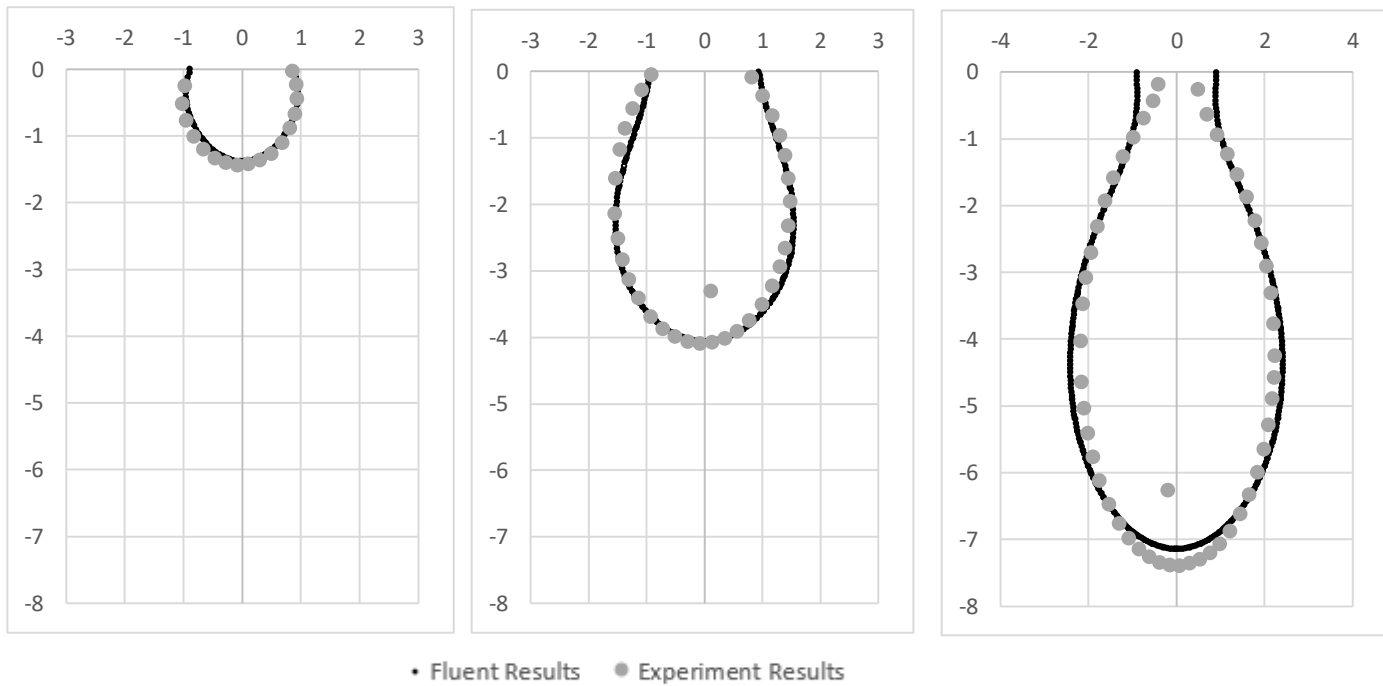


**Figure 4.19** Comparison between experimental and numerical data showing the growth of a Gallium droplet:

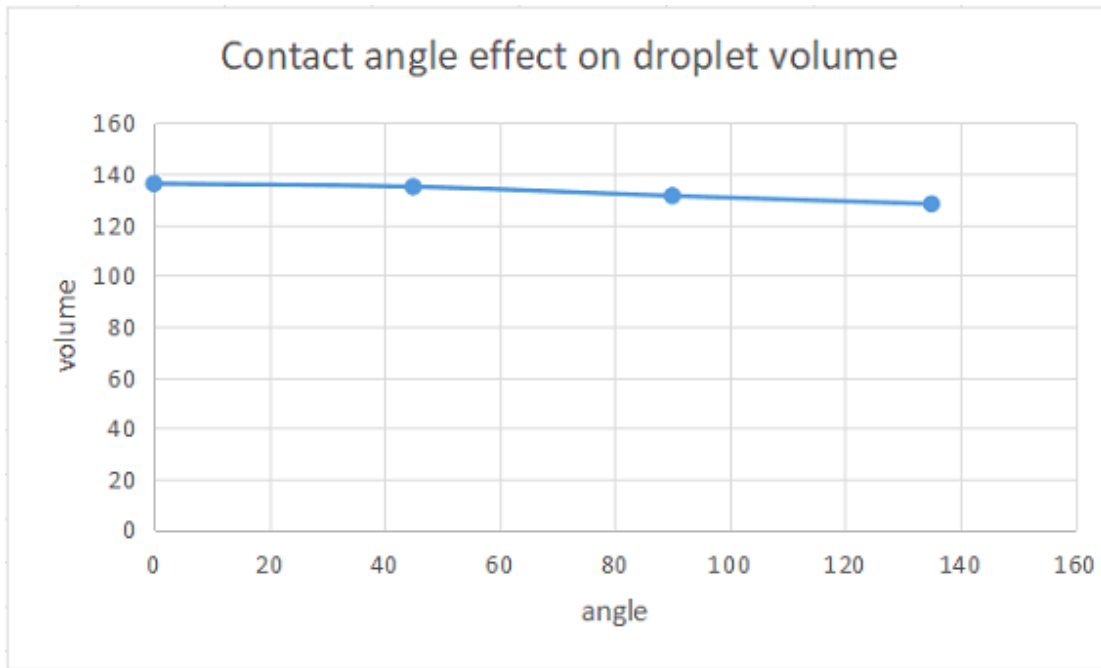


**Figure 4.20** Effect of the contact angle on the volume of the droplet.

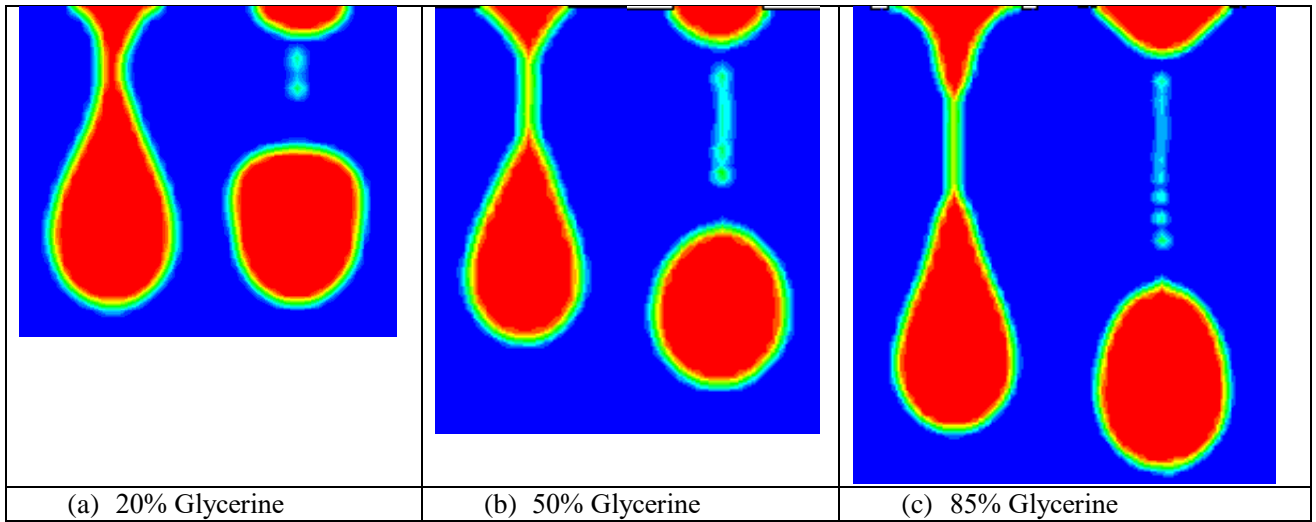
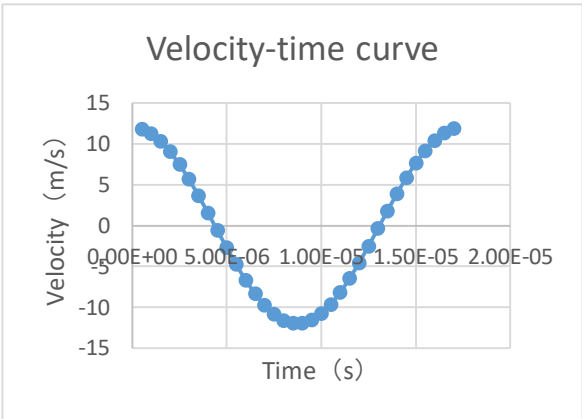
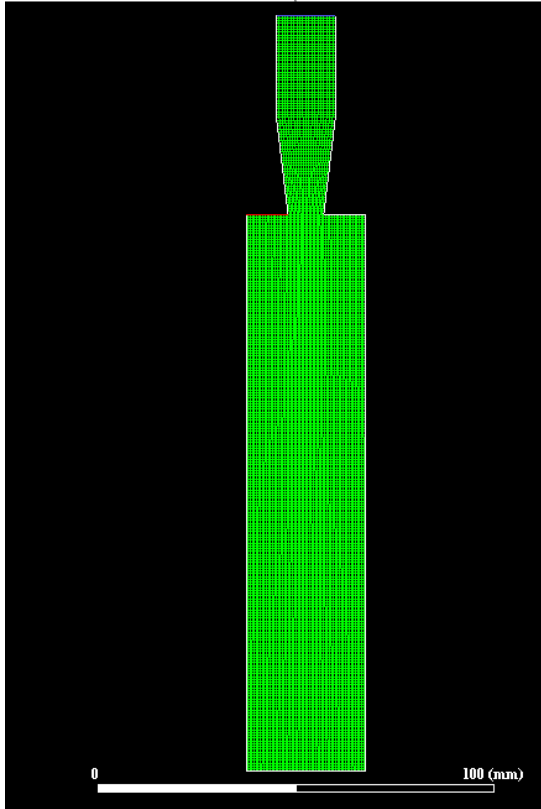


**Figure 4.21** Typical example showing the effect of materials on the formation of satellite drops.



```
#include "udf.h"
DEFINE_PROFILE(unsteady_velocity, thread, position)
{
    face_t f;
    begin_f_loop(f, thread)
    {
        real t = RP_Get_Real("flow-time");
        F_PROFILE(f, thread, position) =
12*cos(1000* 360*t);
    }
    end_f_loop(f, thread)
}
```

(a) Numerical Model for investigating producing droplet smaller than the nozzle.

(b) Loading curves and code  
Velocity curve  $V = 12 \cdot \cos(1000 \cdot 360 \cdot t)$ ;

**Figure 4.22** Models and control conditions for producing pneumatic droplets smaller than the diameter of the tube/nozzle.

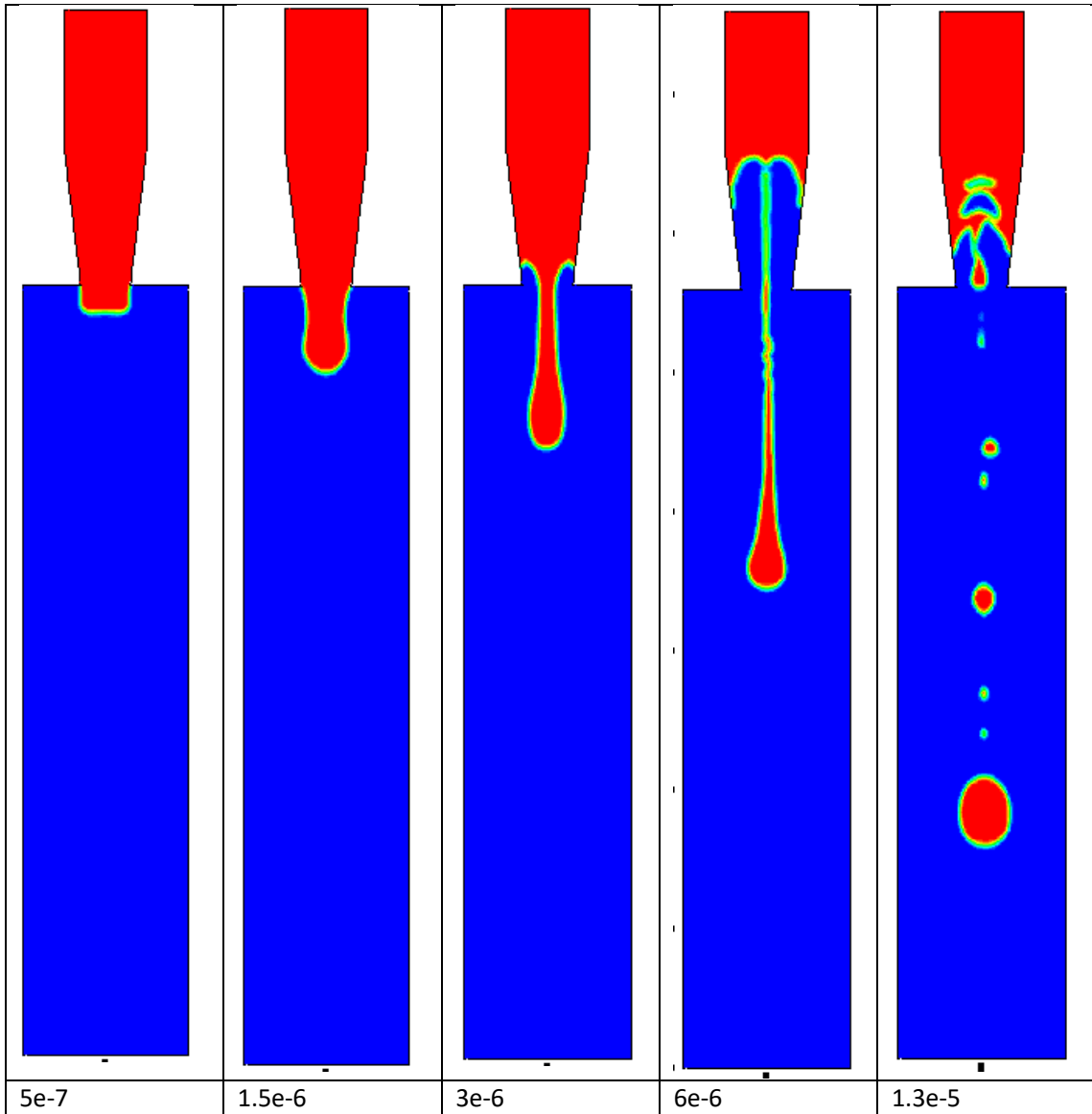


**Figure 4.23** Typical numerical results showing the generation of droplet smaller than the diameter of the nozzle.

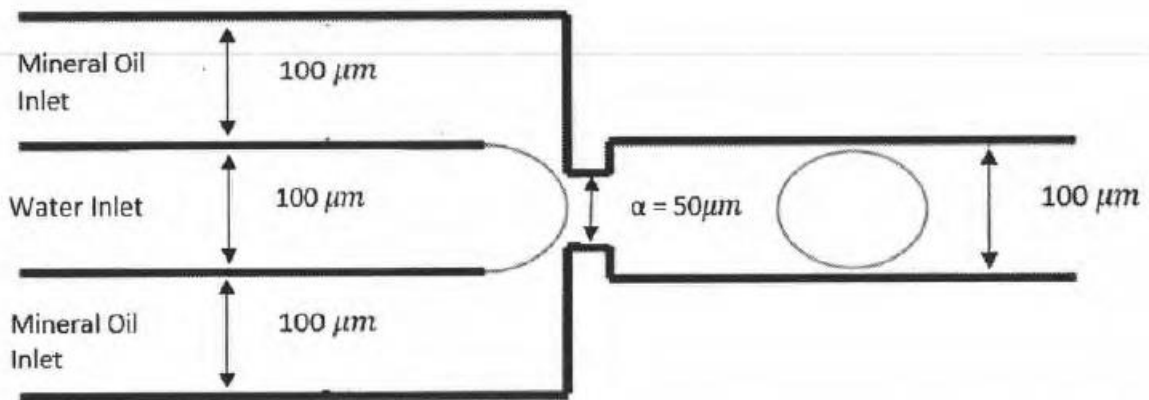


**Figure 4.24** Typical set-up of the model for simulating droplet formation in micro channels (water in oil).

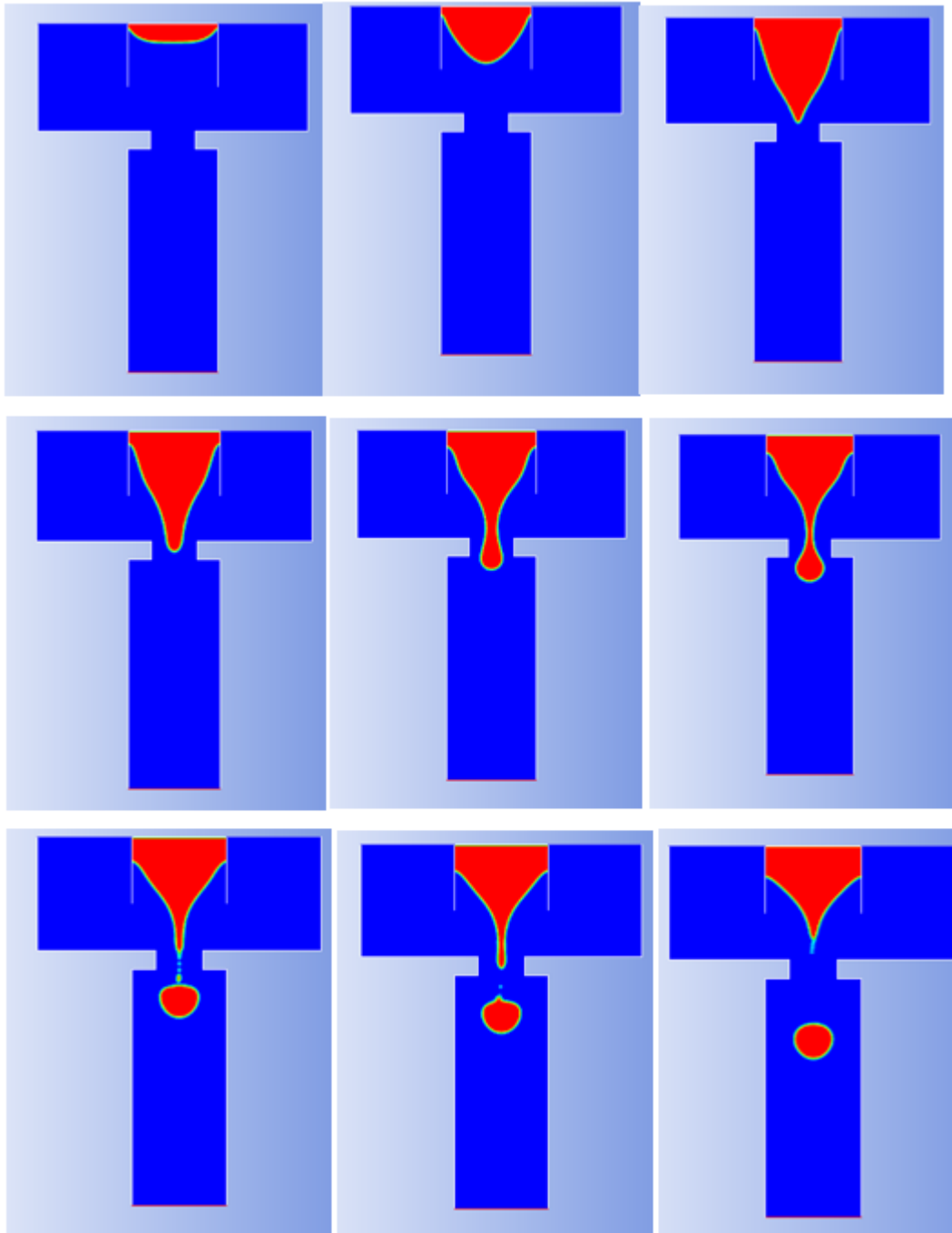


**Figure 4.25** Effect of water droplet formation breaking up in a multiphase flow reduction tube. (Continues Oil phase = **Blue**. Dispersed Water phase = **Red**). Water Volumetric flow rate of: 0.055kg/sec.

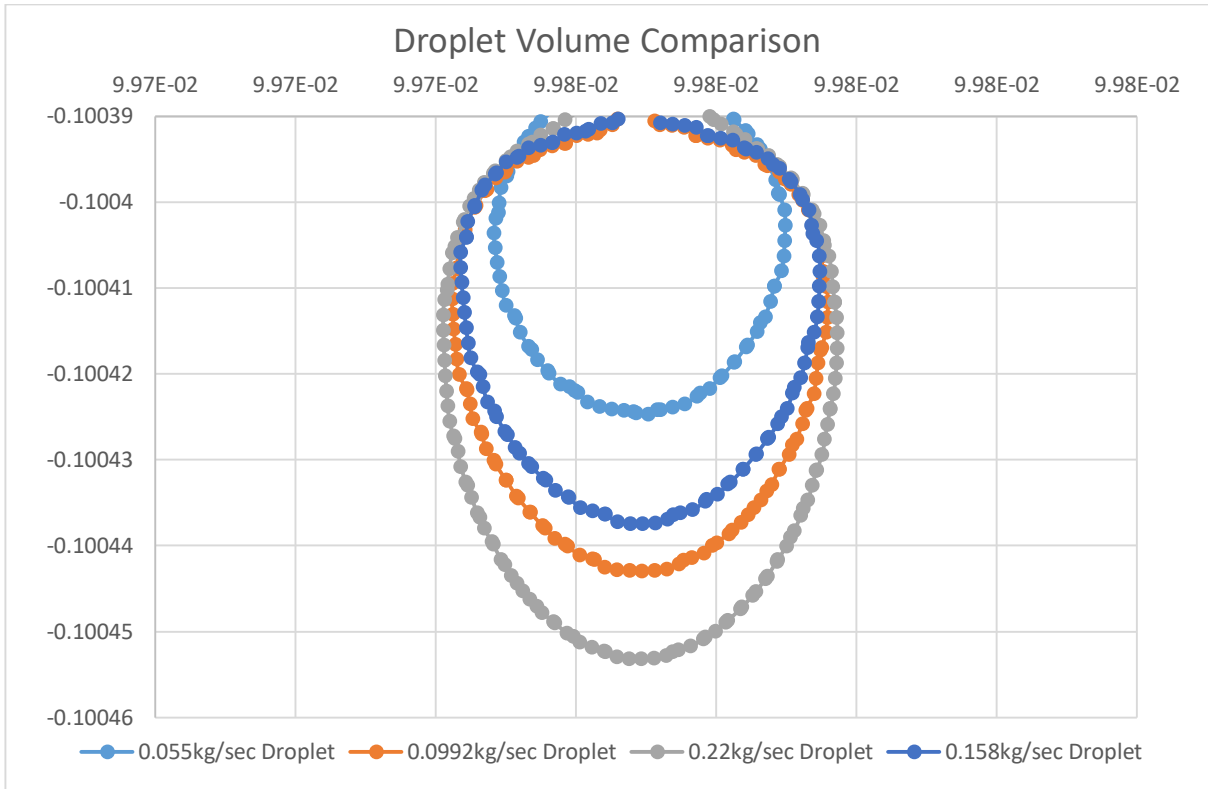


**Figure 4.26** Comparison of droplet interfaces between the five different water flowrates.

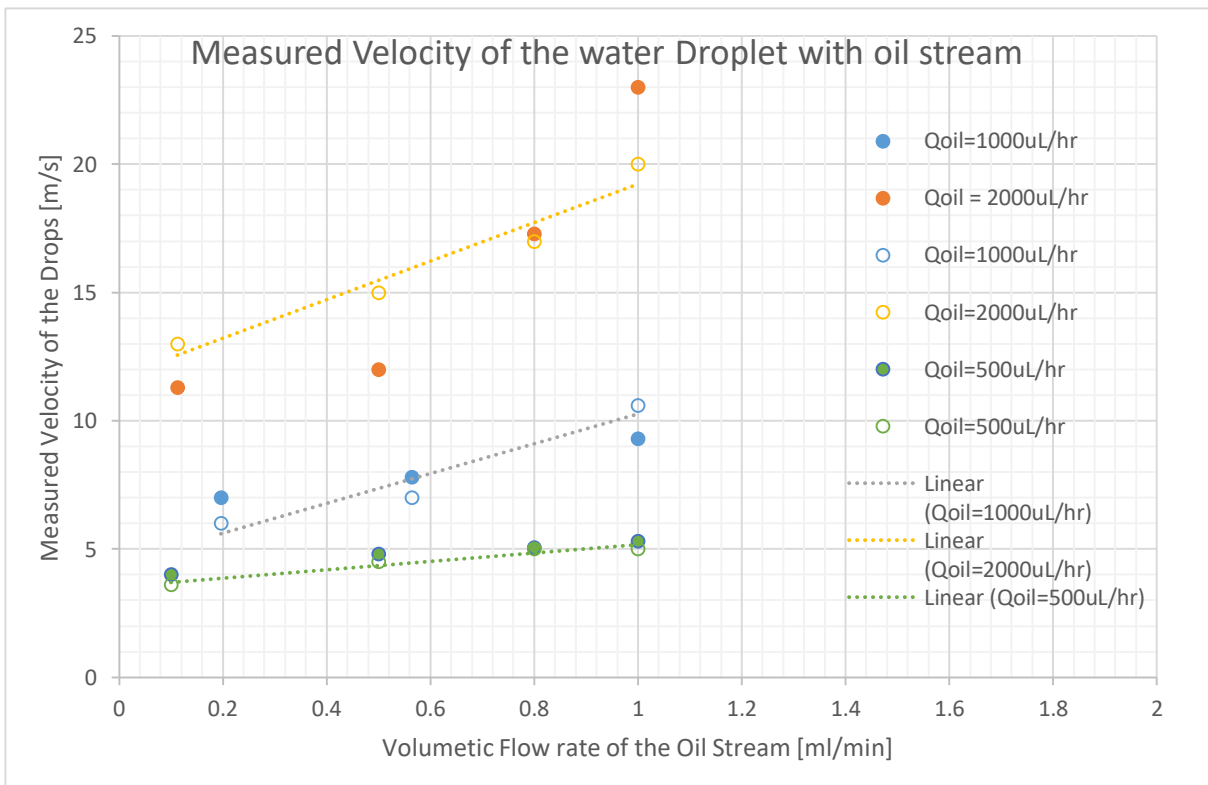


**Figure 4.27** Effect of mass flow rate on the size of the droplet.

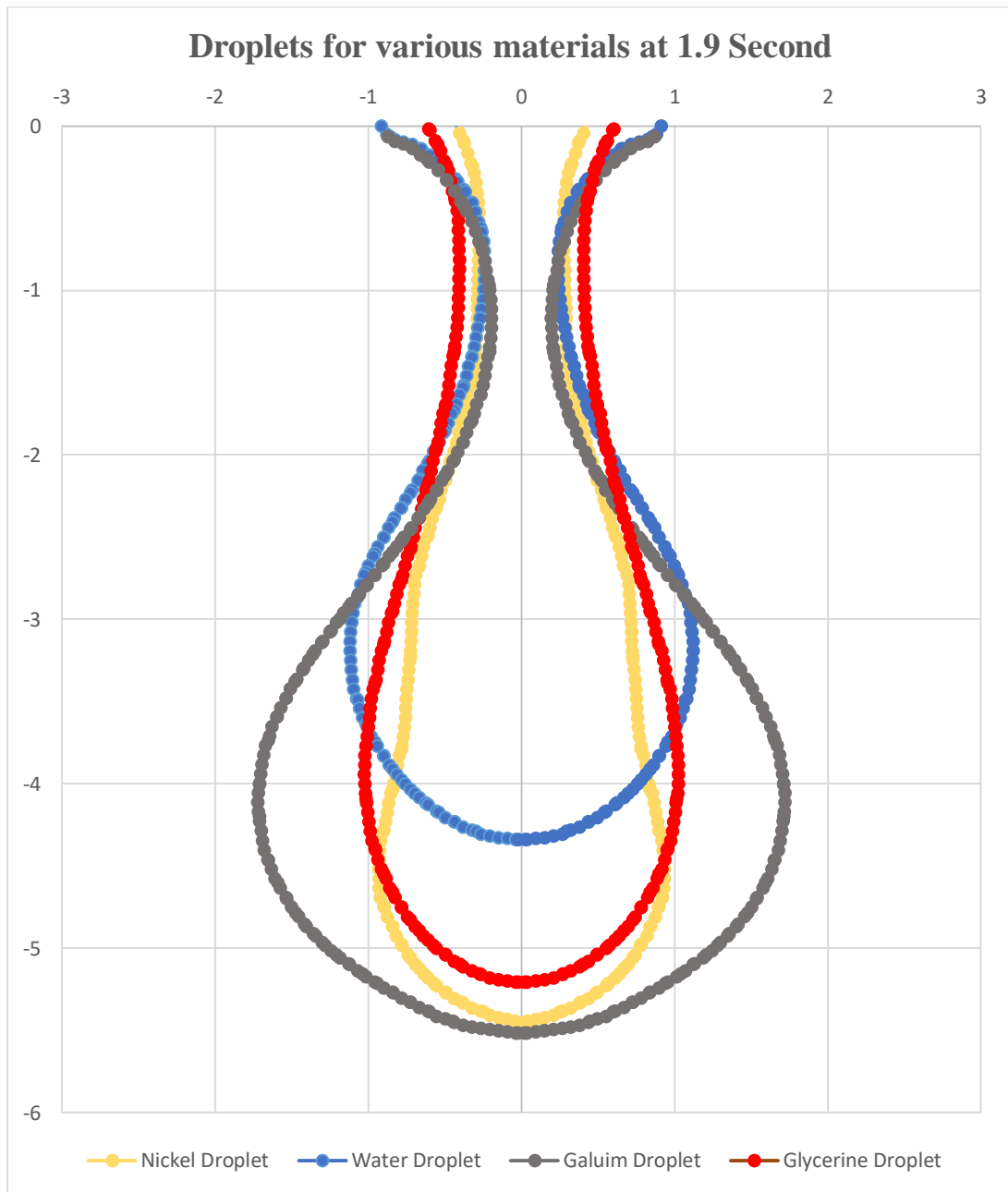


**Figure 4.28** Typical contours showing the difference between the droplet of Water, Glycerine, Gallium and Nickel (high temperature). All these materials have different surface tension and viscosity to illustrate the use of the model to analyse the effect of materials' properties on droplet shapes.

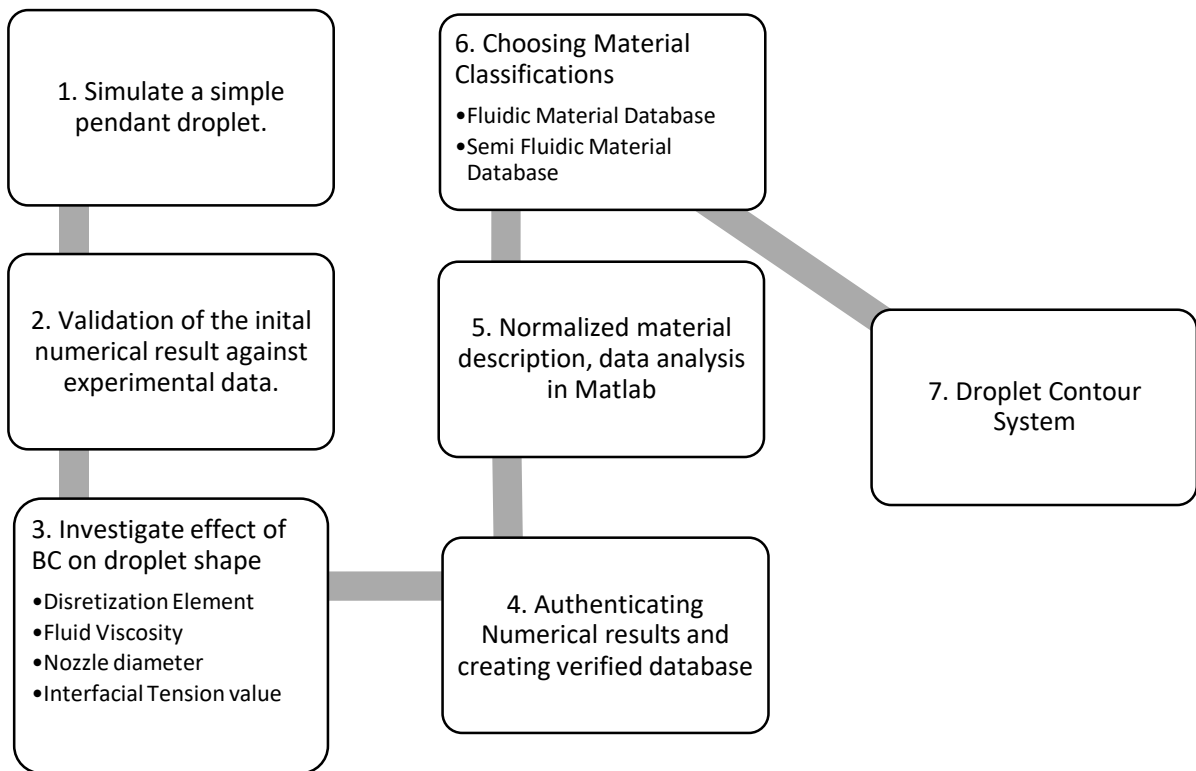


**Figure 4.29 (a)** Flow chart to show the main structure for analysing pendent droplets in Matlab.

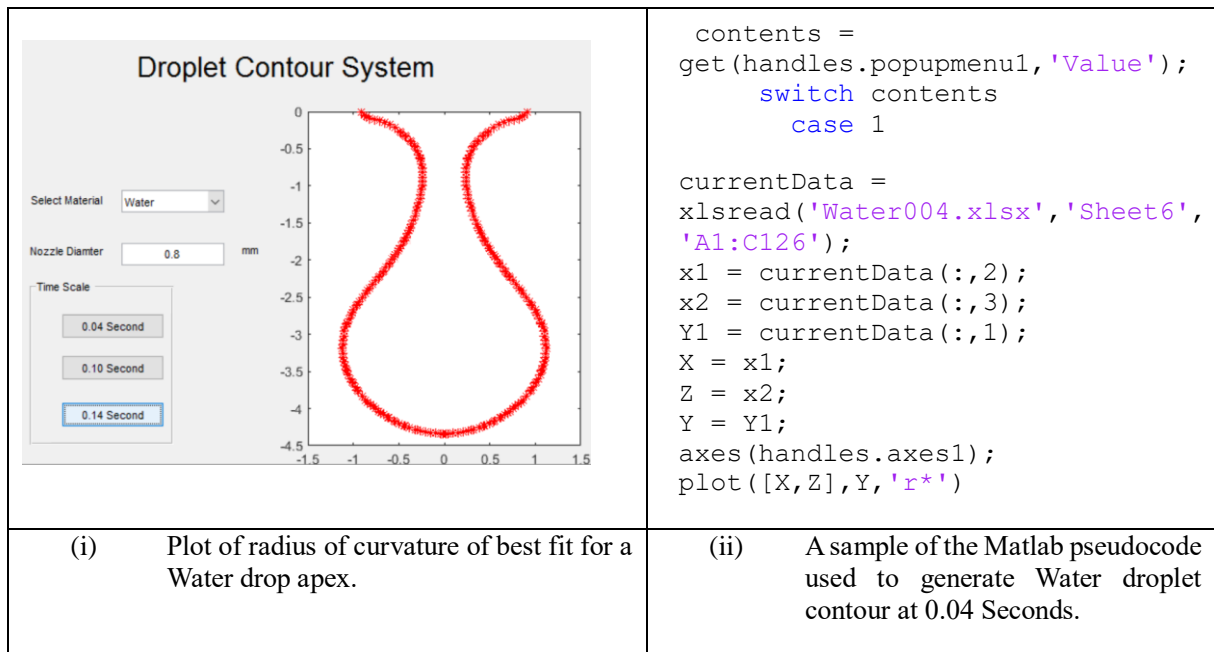


**Figure 4.29 (b)** Typical feature of the Matlab codes and example contour plot.

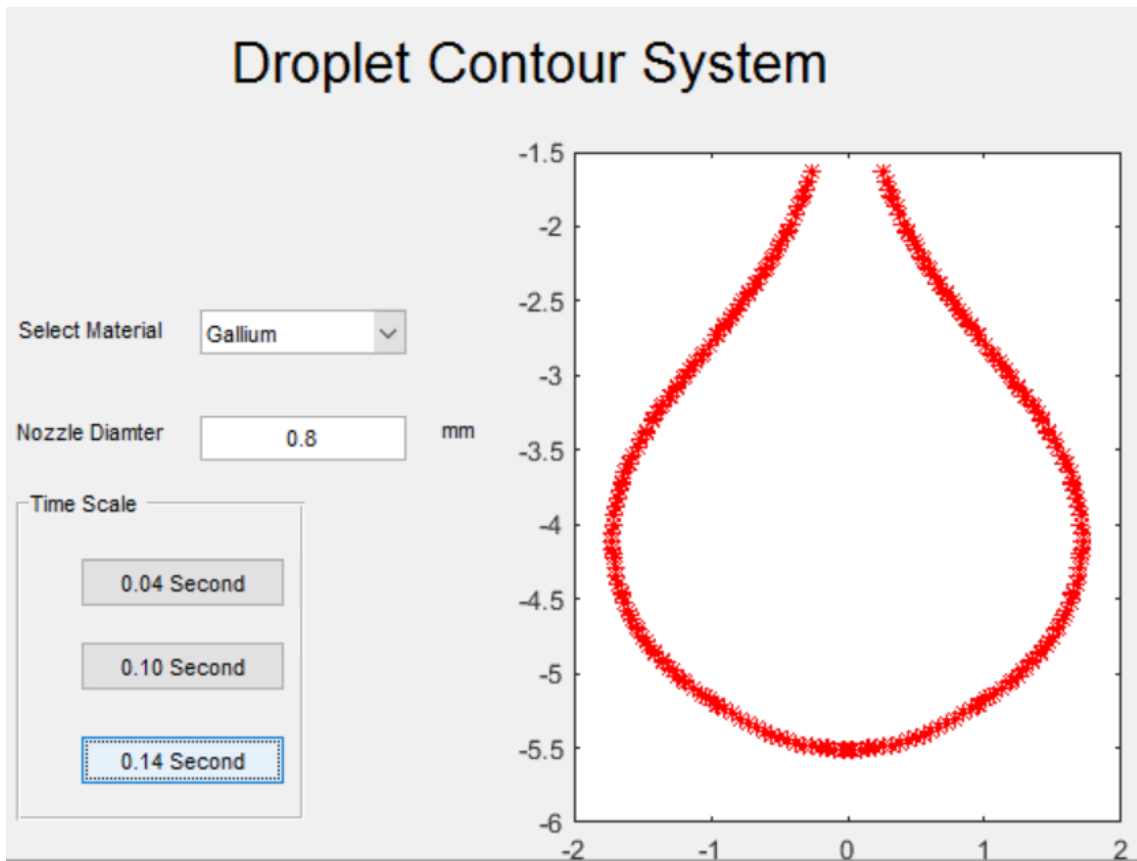


**Figure 4.30** Typical contour plot for Gallium Droplet at 0.14 Second.

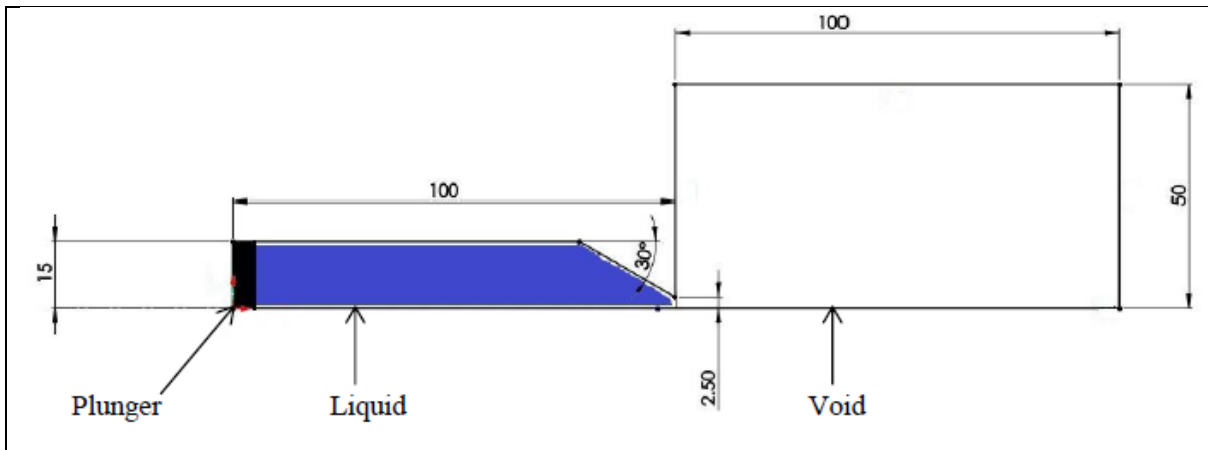


Figure 4.31 (a) Nozzle model used in assessing the efficiency of different modelling programs.

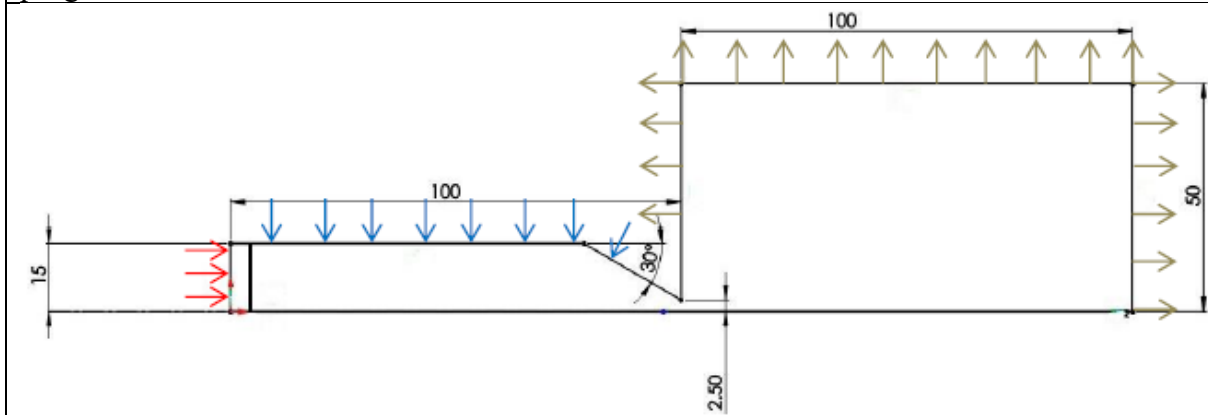


Figure 4.31 (b) Boundary conditions used to simulate a model in ABAQUS CEL.

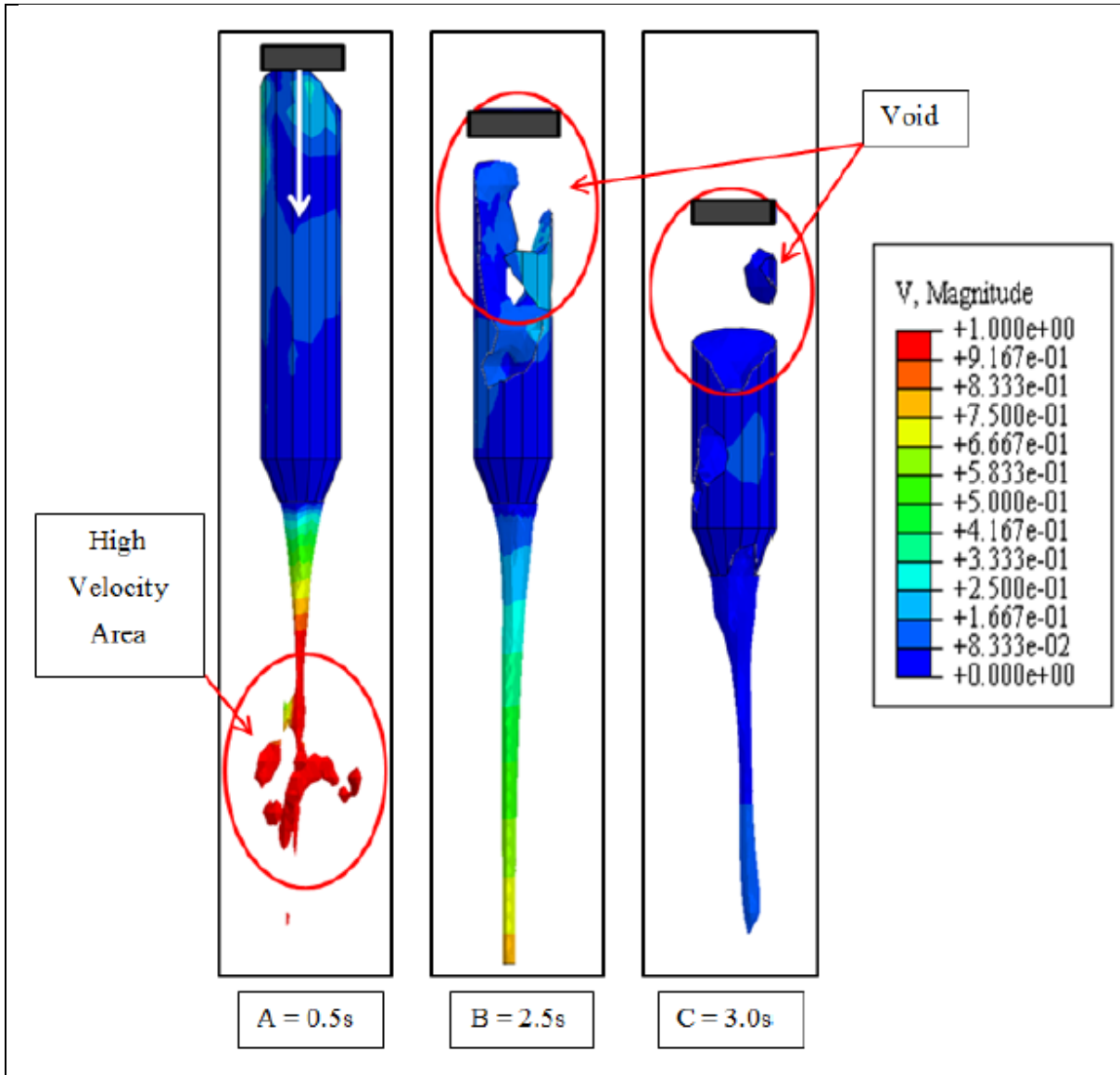
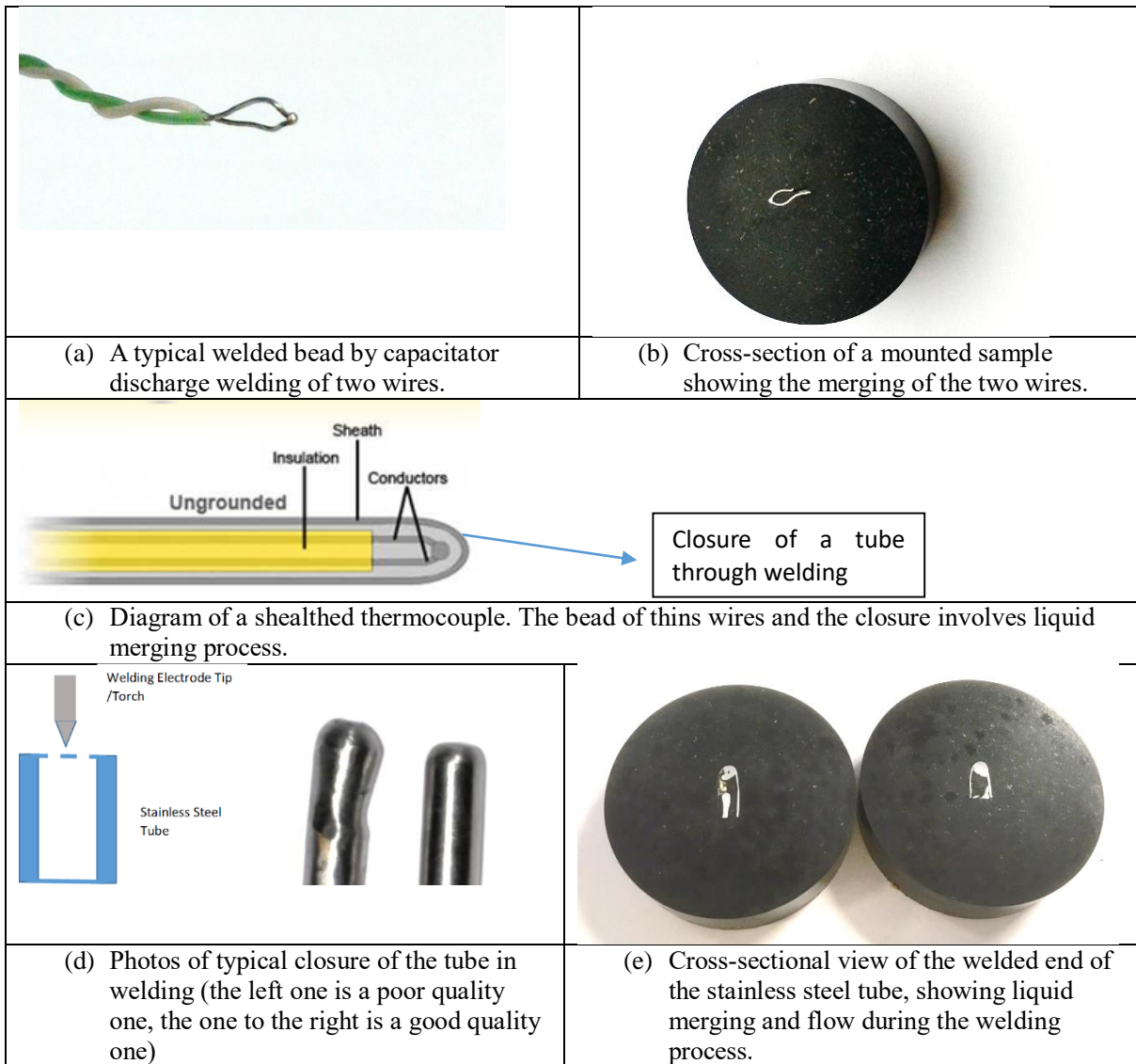
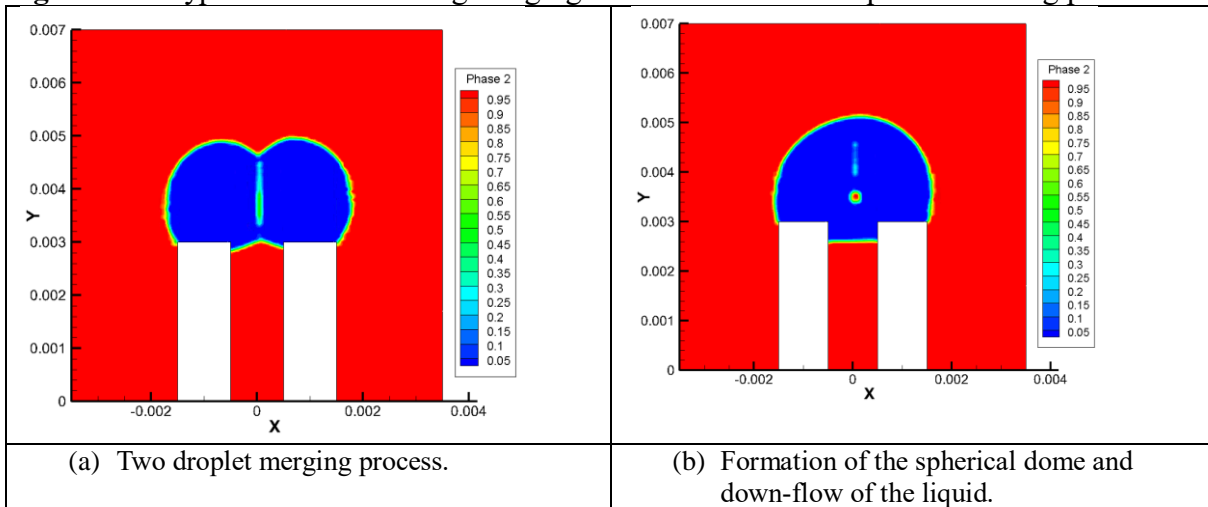


Figure 4.31 (c) Modelling liquid flow through a nozzle using ABAQUS CEL.

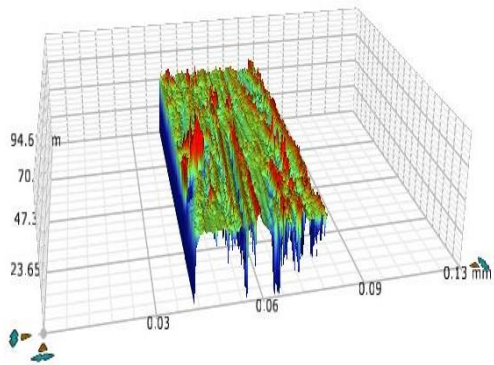
**Figure 4.31** Typical example showing the effect of choice of modelling approach on the modelling of liquid flowing through a nozzle.



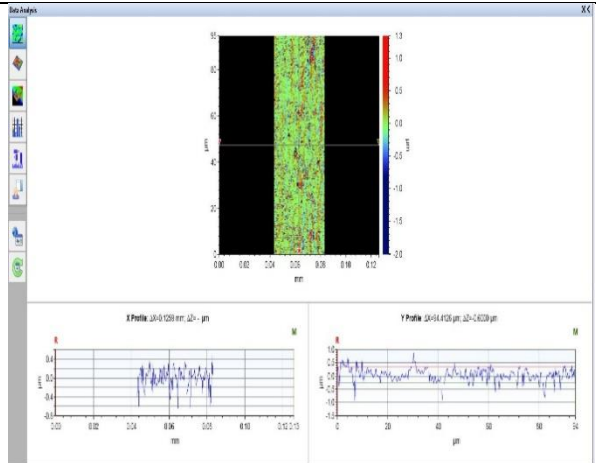
**Figure 4.32** Typical cases involving merging of small volume of liquid in welding process.



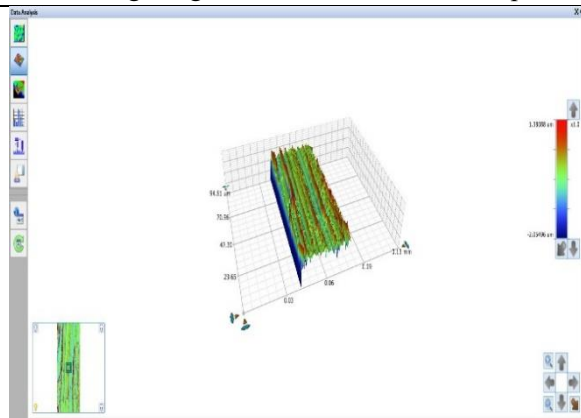
**Figure 4.33** Typical example numerical result showing the merging of small drops of liquid.



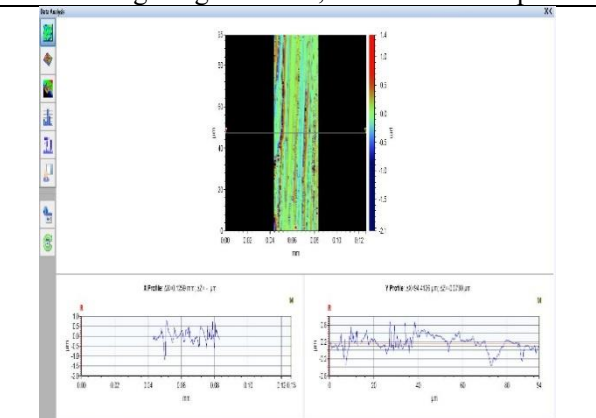
Welding Height = 2mm, Current = 30Amps



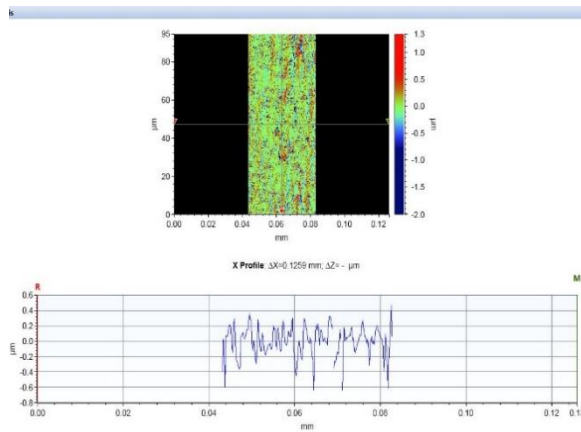
Welding Height = 2mm, Current = 30Amps



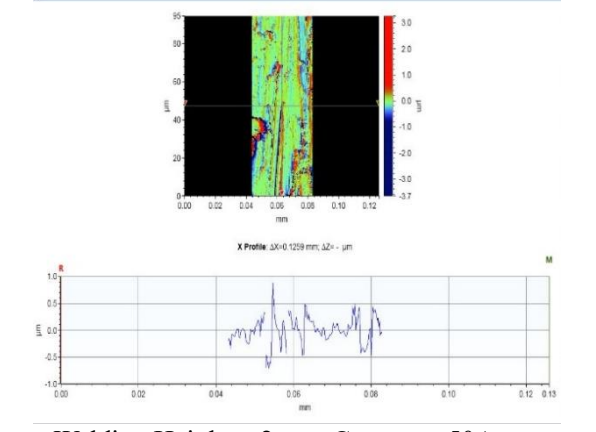
Welding Height = 3mm, Current = 30Amps



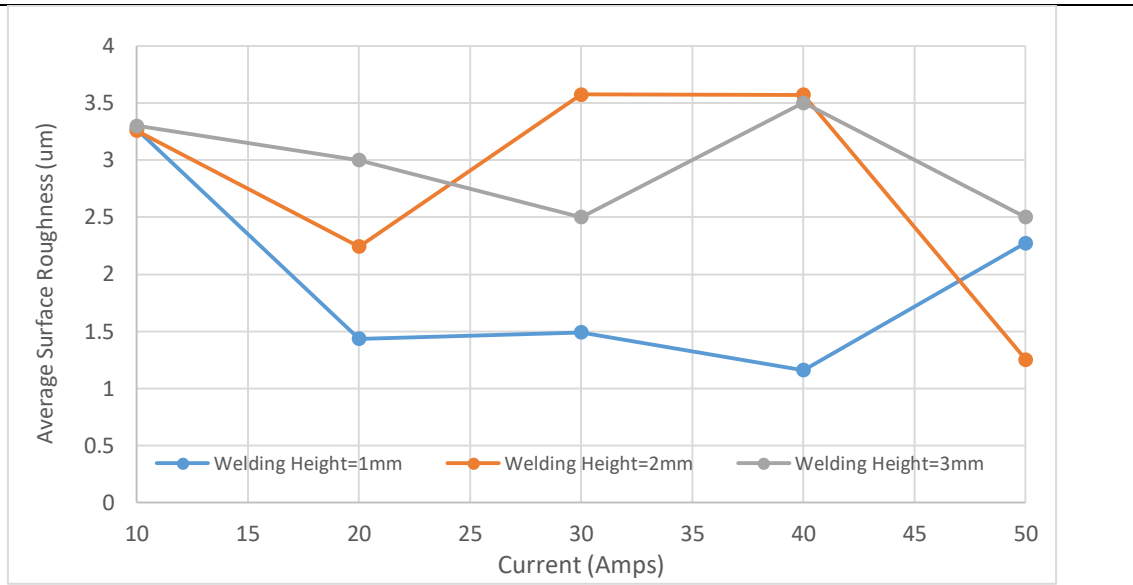
Welding Height = 3mm, Current = 30Amps



Welding Height = 2mm, Current = 30Amps

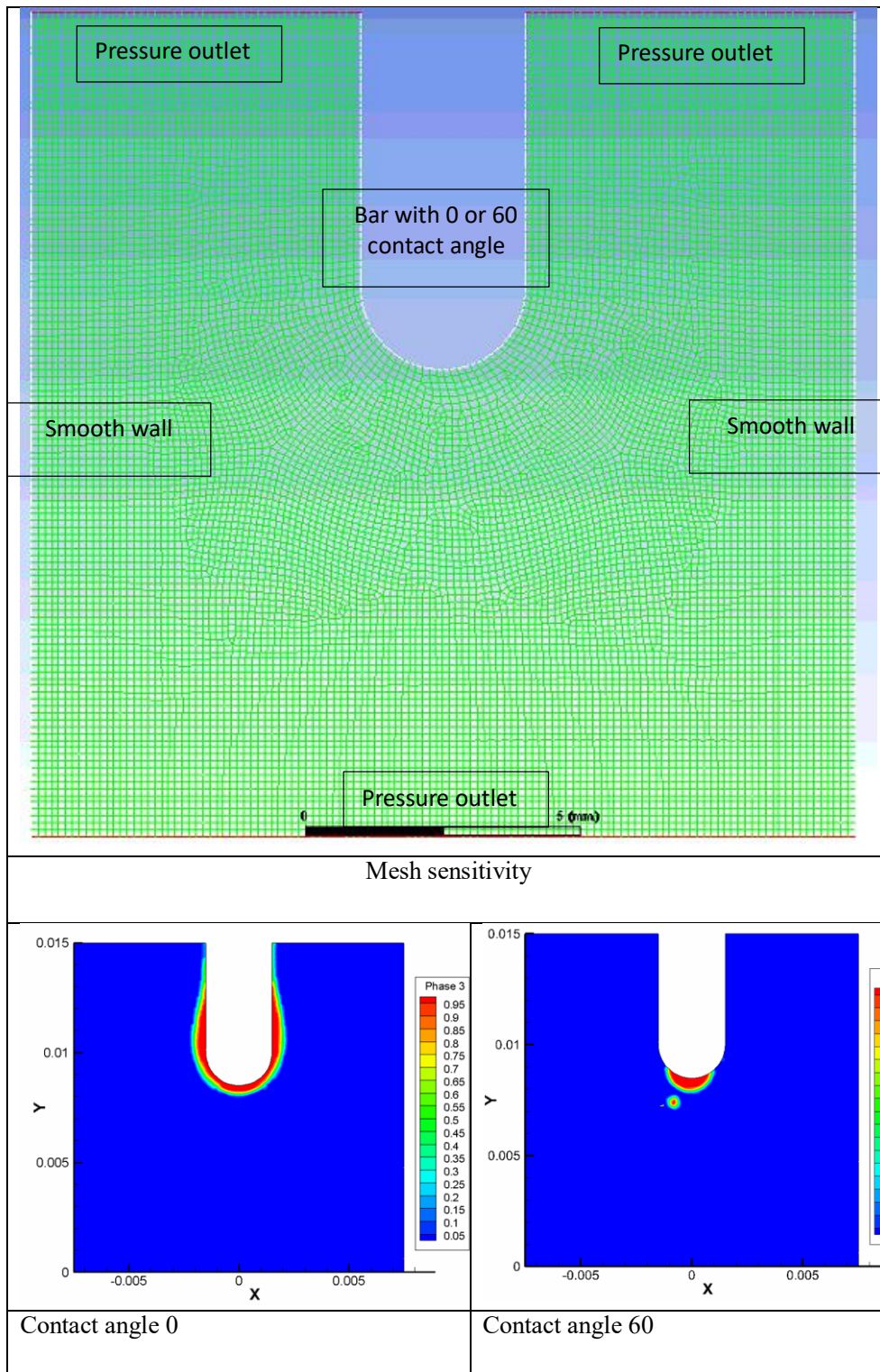


Welding Height = 2mm, Current = 50Amps

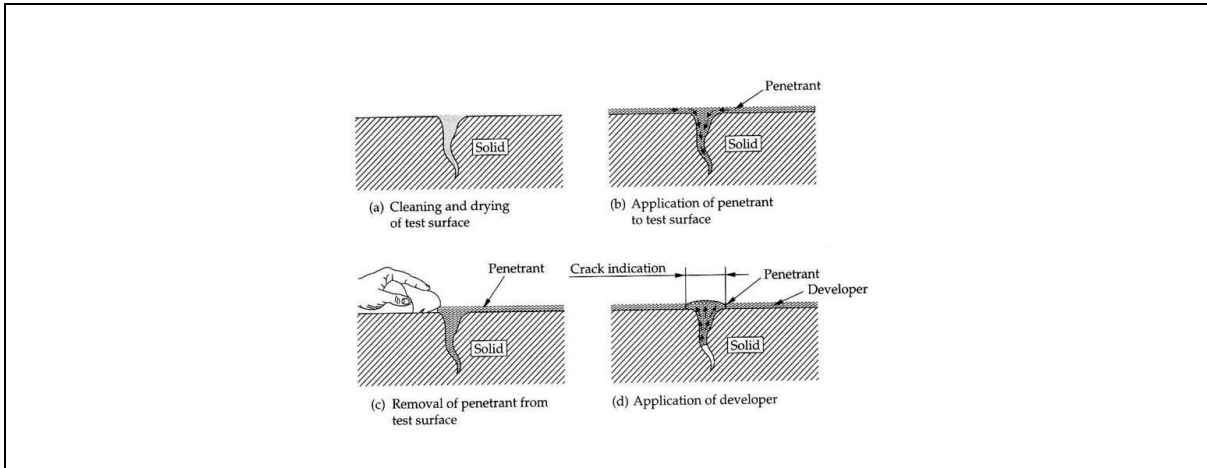


Average surface roughness of the samples with different welding current and welding height conditions.

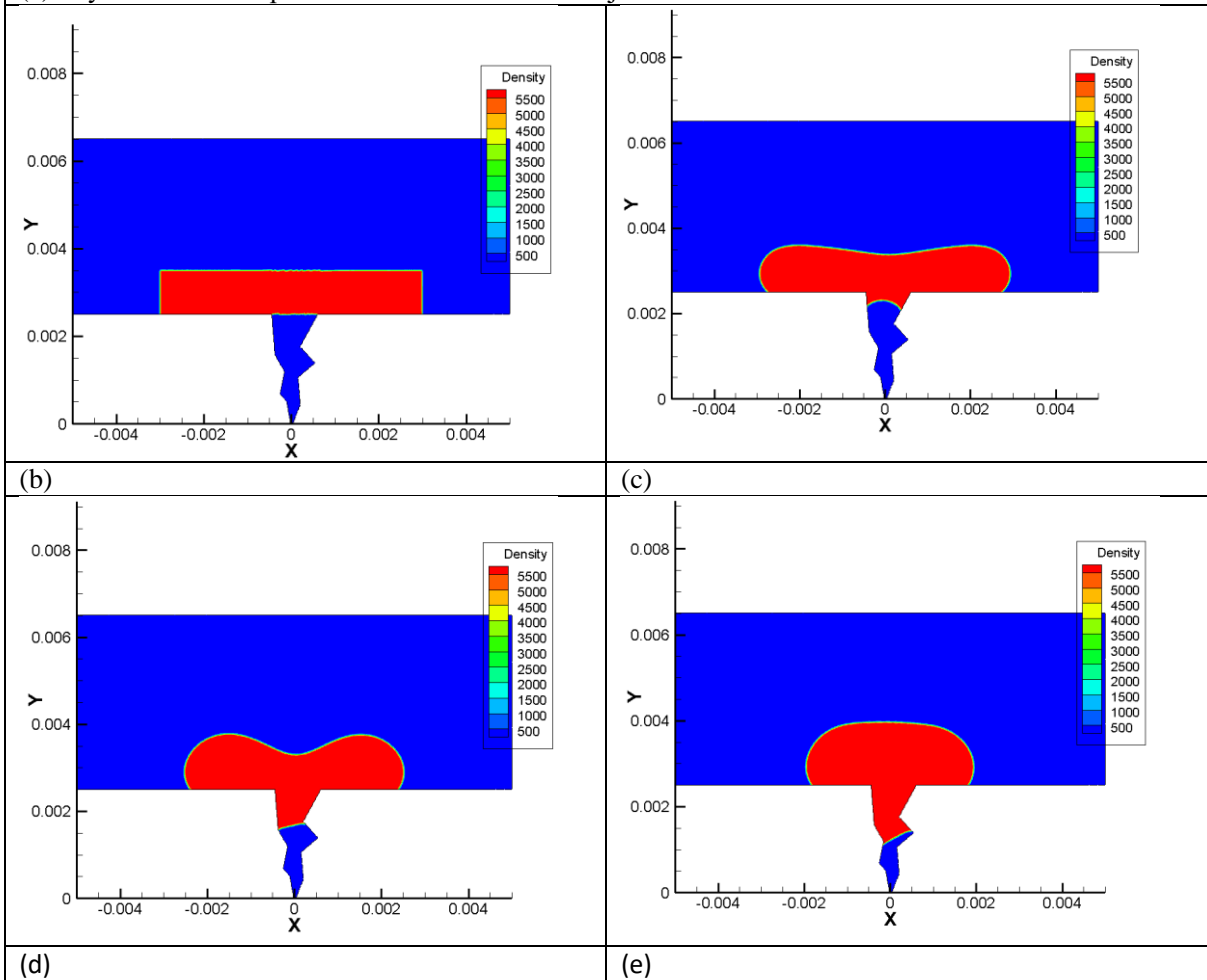
**Figure 4.34** Typical surface roughness analysis and effect of welding currents.



**Figure 4.35** Sample numerical model developed to assess the effect of contact angle (wetting coefficients) on the residual of liquid when a tube is pulled from a liquid



(a) Dye Penetration procedures in NDT of welded joints



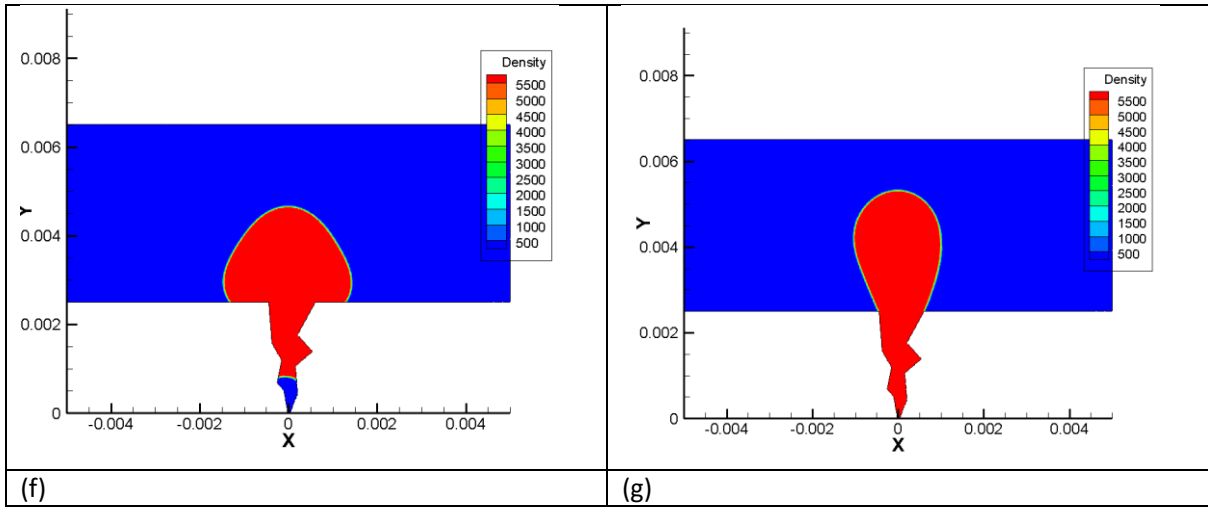


**Figure 4.36** Dye penetration process and an effective way of simulating of the dye penetration test.

**CHAPTER FIVE**

**NUMERICAL STUDIES OF THE INTERACTION**

**BETWEEN SOLID INDENTER/LIQUID**

**DROPLETS WITH DIFFERENT FORMS OF**

**SUBSTRATES AND EFFECTS OF MATERIAL**

**PROPERTIES**

## 5.1 Introduction

The work in this chapter will focus on modelling the interaction between rigid indenter and liquid droplets with both homogenous and soft materials with thin embedded layers at elastic regimes. In the first part, the work is focused on rigid flat-ended cylindrical indenters and spherical shaped indenters. This is important for materials testing and understanding the mechanics of materials with embedded systems, which is becoming more and more important such as flexible sensors. The deformation of both homogenous materials and soft materials with embedded structures is studied. The effect of embedment depth, as well as the effect of the Poisson' ratio of the matrix is also established and analyzed.

In the second part, the work was extended to the modelling of liquid droplets onto homogenous materials and soft materials with embedded thin shells through the Smoothed Particle Hydrodynamics method (SPH) approach. The dynamics of droplet impacting matrix is investigated using SPH particle element approach. The modelling focused on analysing the droplet behaviour, such as splashing, recoiling and spreading. The dynamics of droplets impacting a surface are important in many industrial and medical applications. This include spray cooling, anti-icing, ink jet printing, herbicide delivery systems and many other procedures. The deformation of droplets, which is governed by Laplace surface tension and fluid flow equations, depends heavily on material properties and boundary conditions. In general, during a droplet surface impact moment, the kinetic energy is transmitted towards the horizontal direction, deforming the impacted surface and converting the kinetic energy into other forms. An effective modelling approach of droplets with different substrates could be used as an effective tool for investigating the interaction between the liquid drop and substrate.

Soft materials with embedded structures are widely used in many applications, in particular in sport and medical systems (*Patton et al, 2015; Heidner and Adams, 2016*). This material type refers to systems with a stiffer structure (either in 3D or 2D form) being fully enclosed in a matrix for improving mechanical performance or achieving other functions. For example, a thin stiffer plate could be inserted in a soft insole to increase the strength or pressure distribution (*Kajtaz et al, 2015*). A heating element can also be used in an insole or midsole for thermal management of shoes. Recently, there has been considerable work in wearable technology in footwear for both research purposes and technological development, in which a thin electronic device or chip is embedded in the sole system (*Crea et al, 2014*). A detailed understanding of the mechanics of these material systems is important for improving the structure integrity and

lifetime reliability. Typically, embedded systems can be made of a deformable material (i.e. the insert is not significantly stiffer than the matrix) or an inextensible material (where the insert is much stiffer than the matrix). In service, the system could be under different loading modes, such as torsion, bending and indentation (*Oyen and Cook, 2003; Siivola et al, 2016*), which poses a new challenge in material selection and design. Studying the deformation of the systems under an indentation process is particularly important for such a system. In an indentation process, an indenter is pressed onto the sample surface and deforms the material. This process similar to a situation when a sharp object (such as a stone) deforms a shoe sole system, which may directly influence the embedded structures. Many works have studied the indentation of soft material such as rubbers (*Wu et al, 2016; Needleman et al, 2015*), foams (*Siivola et al, 2016; Duncan et al, 2015*) or composites (*Zhang et al, 2016*) with a range of indenter shapes such as spherical or flat indenters. Indentation is a typical localized loading on materials, in which the stress and strain condition underneath the indenter are not well defined. The deformation of an embedded system in a matrix make the deformation even more complex. Recent work from the group has focused on embedding sensors such as Pizelectrcial sensors and force resistor sensors. The pizelectrical sensors are ceramic coating on a thin copper sheet.. Force resistor sensors (FRC) is a thin flexible sensor for measuring pressure, it is a thin plastic with conductive coating on the surface (*Li, 2018*). When the FRC is compressed, the electrical resistance of the sensor changes that reflects the pressure variation. Protection of these sensors for some situation are important including unintended impact from either liquid or solid substances. In addition, if these sensors are in direct contact with liquid or hazardous environments, it will affect its function and accuracy. An active research area is to protect those thin sensors with soft materials such as silicone rubber (*Kaid, 2020*). The embedded system is also relevant to deformable or flexible electronics, where the wires and chips are inserted in soft rubber or soft plastics. Hence, the deformation of the systems under both rigid indentation and soft liquid drops are important for protection, as well as sensitivity of the system with an in rigid thin layer in a soft matrix.

Another new area regarding the material properties, lies in the investigation of the influence of the Poisson's ratio including novel Auextic behaviour. Poisson's ratio is an important property, it is defined by the negative ratio between axial stain and lateral strain when a material is being stretched or compressed. Most materials shrink in tension and expand when being compressed, so the Poisson's ratio of most materials is positive. For example, for metals, the Poisson's ratio is between 0.2-0.3 while rubber has Poisson's ratio has a ratio close to 0.5, representing that

the material is incompressible. Recently new materials are being developed which have an abnormal Poisson's ratio, the materials expand when being stretched and shrink when being compressed. The Poisson's ratio of this type of material is negative, so called negative Poisson's ratio or Auxetic materials. Materials with negative Poisson's ratio have been the topic of research and development for several decades (Gaspar et al, 2005; Aw et al, 2015). Many different mechanisms have been designed and explored, which has opened up more opportunities to develop negative Poisson's ratio materials at different length scales, in some cases, the material can be treated as a homogeneous system. Poisson's ratio is an important material property, reflecting the lateral deformation of the material when the material is under load. It is calculated by the ratio of the lateral strain to the axial strain. For the Simple loading conditions, such as tension or compression, this is can be directly derived from standard tests uniaxial compression or tension tests. But the effect of Poisson ratio in complex loading conditions (such as localised contact, shear, indentation) is difficult to predict as the stress-strain condition and volume of materials involved is not well defined. Most materials has a positive Poisson's ratio, but there are a new group of materials with negative Poisson's ratios. This new property directly affect the material behaviour in particular for shear or indentations (*Needleman et al, 2015, Lim, 2014, Photiou et al, 2016*), foams (*Siivola et al, 2016; Duncan et al, 2015*) or composites (*Zhang et al, 2016*). In these works, a range of indenter of different shapes such as conical, spherical or flat indenters have been involved. Indentation is a typical localized loading condition, in which the stress-strain condition is not well defined. With a negative Poisson's ratio, the material under that indenter will contract rather being pushed away, this could significantly affect the material deformation and resistance. The effect of the Poisson's ratio could be more significant for mixed structures due to the mismatch of property between the embedded phase and the matrix. For example in composite, the auxeticity of the matrix is known to influence the interaction fibre-matrix interface (*Zhang et al 201, Lake 2017*). It is important to study the effect of Poisson's ratio and Auxetic behavior for both rigid indenters and liquid droplets, as highly deformable cases.

As listed in Table 5.1, chapter 5 will firstly focus on the effect of materials and embedment on the indentation resistance, in soft matrix with indenters of different shapes. A practical modelling methodology of an embedded 2D structure has been developed. The modelling results were compared to the prediction of analytical solutions for both flat ended and spherical indenters. Parametric FE models have been developed to study the influence of different embedded structures and layer depths on the indentation process. The findings from this study were also compared to analytical solutions. The second part of this section focused on

developing a framework of modelling droplets into materials with embedded layers using the SPH element approach. The computed numerical model was able to simulate droplet deformation with different volume and substrate properties. The changes in deformation modes such as the initial contact, spreading, recoiling and splashing is also analysed, in terms of substrate properties. Key numerical issues and future work is also discussed - the effect of indenter shape on the material deformation, deformation of droplets and potential publications.

**Table 5.1 Main research works**

<p><b>FE modelling of interaction between rigid indenter and soft substrates with or without embedded systems:</b></p> <ul style="list-style-type: none"> <li>✓ FE modelling of soft material with/without embedded systems under a flat indenter.</li> <li>✓ FE modelling of deformation of soft materials under a spherical solid indenter.</li> <li>✓ Effect of material properties including Auxetics (negative Poisson's ratio).</li> </ul>
<p>FE modelling between droplets and different substrates:</p> <ul style="list-style-type: none"> <li>✓ Numerical model development with SPH elements.</li> <li>✓ Solver/solution method comparison and meshing scheme development.</li> <li>✓ Deformation of droplet with different substrates and embedded systems.</li> </ul>
<p><b>Discussion</b></p> <ul style="list-style-type: none"> <li>✓ Effect of indenter shapes on the material deformation.</li> <li>✓ Effect of droplet shapes.</li> <li>✓ Deformation of droplets and its potential implications</li> </ul>

## 5.2 Indentation of soft materials with flat ended and spherical indenters

Figures 5.1&2 show the structure and FE model with a thin stiffer layer embedded in a homogenous matrix. The FE model is developed using the explicit code in Simulia ABAQUS (*version 2017*) (*Abaqus manual*). The modelling work was focused data with an indenter with a radius of 1 and 2 mm. The sample is at least 10 times the indenter radius to avoid the sample size effect. As shown in the figure, a thin shell is built, and then embedded in a square block sample (40x40x20mm). The indenter is modelled as a rigid body as it is much stiffer than the sample. The embedded layer is modelled by a finite-strain shell element S4R with 5 integration points. The matrix is modelled by C3D8 elements. The procedure used the constraint type of “Embedded Region” to model the interaction between the thin layer within the “whole model” (*Abaqus Theory Manual*). This approach allows the user to insert a structure within a “host” region of the model or within the whole model. The matrix is the host element while the shell elements of the embedment are treated as the embedded elements. A standard Weight factor round-off tolerance (1E-06) is used. During the FE model development stage, a range of shell thicknesses have been used (0.1-1mm). With this procedure, the position and thickness of the shell can be modified within the system without the need to change the meshing of the matrix. With such an approach, the model can be modified flexibly through parametric studies to simulate indentation tests of different situations, such as sample size, indenter size, shell thickness, position of the shell from the surface, mechanical properties of the shell and matrix, etc. In the FE model, the bottom face of the sample is fixed on all degrees of freedom (DOFs.), the displacement of the indenter is controlled by the applied velocity and the total time.

Three conditions have been investigated to establish the validity of the model and to analyse the effect of key material and dimensional parameters on the indentation process. The first model, which is designated as the homogenous material, is a model with no thin shell embedment. This allows a direct comparison between the numerical results and known analytical solutions for indentation of an elastic half space with a circular flat-ended indenter. The second model, designated as the inextensible shell model, consists of a sample with an embedded shell, which is much stiffer than the matrix (in this case,  $E_s$  is over 100 times that of  $E_m$ ). The third model is similar to the inextensible model, but in this case, a shell with lower stiffness is used. This model is designated as the “deformable shell model”. The flat-ended cylindrical indenter is modelled as a rigid material with a changeable indenter size, the majority of the results presented are based on data for indenter radius of 1 or 2mm, as they are more relevant to situations where a sharper object poses more problems to an embedded

systems. A fixed displacement is applied on the indenter to move it onto the sample, with no rotation or lateral movement being allowed. The results reported in this work are based on a quarter symmetric model. Mesh sensitivity studies have been performed by changing the element size in the model until there is no significant change of the modelling results (force within 2%) with mesh size. In the presented case, the matrix is modelled with over 20,000 elements and the embedded shell is modelled with 1,845 shell elements. A parametric program (ABAQUS-Plugin, Explicit) has been developed, which can alter various key elements within the 3D model, such as the indenter/sample size, thickness, material properties and the position of the embedded shell. The indenter is modelled as a rigid body as it is much stiffer than the sample. The stiffness ( $E_m$ ) is fixed at 3MPa, the effect of the matrix Poisson's ratio is investigated systematically, by changing its value between -0.5 and 0.5.

Figure 5.3(a&b) shows typical data comparing the results from two modelling conditions against the analytical data based on the equation of a homogeneous sample (Equation 5.1). One FE data is for the model without embedded shell, the other FE data is for the sample with an embedded shell, which has the same material properties as the matrix. In both cases, the two FE data (one is with shell and one is without embedded shell) are in good agreement with the analytical solution (Equation 5.1) for flat-ended cylindrical indentation on a homogeneous material (Sneddon, 1965).

$$P = \frac{2bE\Delta}{(1-\nu^2)} \quad (5.1)$$

Where 'P' is the load on the indenter, 'b' is the radius of the cylindrical indenter; 'E' is the Young's Modulus of the matrix. 'ν' is the Poisson's ratio of the matrix. 'Δ' is the displacement of the indenter. For the data presented in Figure 5.3, the Young's Modulus used is 3MPa, and the Poisson's ratio is 0.3. A similar level of agreement could be found in other material properties or shell depth combinations. The close agreement between the homogenous model and the FE model with the embedded shell of the same material property, shows that the modelling approach using an "Embedded Region" in the interaction module is sufficiently accurate. In the preliminary investigation, a full solid model has been developed in which the shell is modelled by solid elements. The results are similar to the previous study (within 5%) with full solid model approach but a very fine mesh is required due to the large ratio of the in-plane and out-of-plane dimension of the embedded layers, which cause a much higher demand on the computational resource and time than the "embedded region" approach. In all cases, the

force and displacement follow a linear relationship. The force-displacement ratio ( $P/\Delta$ ) is used to represent the indentation stiffness.

To analyse the influence of the Poisson's ratio's effect and the depth of the embedment on the indentation stiffness, the ratio between the indentation stiffness for a model with an embedment and that for a homogenous material is defined as the "Indentation Stiffness Ratio".

For the model with an embedded layer, the indentation stiffness ratio could be represented in the form of a dimensionless formula ( $\frac{P(1-\nu)}{4\mu\Delta b}$ ), where ' $\mu$ ' is the shear modulus of the matrix. The formula can be obtained following an integral transformation technique (Selvadurai 2009). Briefly, in the mathematical procedure, a Hankel transformation is used to solve the governing partial differential equation for the mixed boundary conditions of the matrix and the embedded layer. The dual integral equation for the region in contact with the indenter and the outside region consists of a single unknown function which can be represented by a finite Fourier cosine transformation. The mixed boundary value problem was reduced to the solution of a Fredholm integral equation of the second-kind (i.e. no closed form solution), which is solved numerically in Matlab (Matlab 9.0, The MathWorks Inc., Natick, MA, 2016) following the procedure in Sneddon (1965) by fitting the N values (Li, 2018). The numerical solution of the integral equations provides results that illustrate the influence of the depth of embedment of the reinforcing membrane and Poisson's ratio of the matrix material on the indentation stiffness. A N=5 was used for the numerical solution, which provided repeatable results, further details of the mathematical procedure and comparison with numerical data can be found in Li (2018).

Figure 5.4 (a&b) is a typical set of data from the FE modelling (thickness of the embedded layer is 0.1mm,  $E_m=3\text{MPa}$ ;  $E_s=300\text{MPa}$ , Poisson's ratio is 0.3). As shown in the Figure, the value for  $\frac{P(1-\nu)}{4\mu\Delta b}$  varies with the depth of the embedment as represented by the ratio of the depth (h) and the indenter radius (b). The FE data shows that, when the embedment is closer to the surface (i.e. lower h/b), the indentation stiffness ratio is higher than 1. When the shell is deeper (i.e. higher h/b), the indentation stiffness ratio is closer to 1. In other words, the embedment has less effect on the indentation resistance. The figures also show the indentation resistance of the shell embedded matrix with different positive Poisson's ratio. The value on the x axial  $\frac{P(1-\nu)}{4\mu\Delta b}$  represents the indentation resistance of the shell embedded matrix over the same condition of a homogeneous material without a shell. From the selected data of the

indentation resistance, it is understood that when the matrix has a negative Poisson's ratio the resistance is significantly increased. This can be seen when  $\nu_{matrix} = -0.4$ , the indentation resistance is significantly enhanced the shell is close to the top surface.

### 5.3 Indentation resistance of soft elastic materials with embedded shell under a Spherical indenter

A typical example of the spherical indenter FE model is shown in Figure 5.5 (a&b). The model was built with a similar approach as the flat-ended cylindrical indenter, with a difference in the contact area angle that changes with indentation depth for the spherical indenter. In order to validate the numerical model, a comparison with the analytical solution was performed. One set of FE data is for a homogenous matrix with embedded shell of the same material properties (This is similar to a case with no-embedment), the other data from analytical solutions (equation 5.2).

$$P = \frac{4Eb^{\frac{1}{2}}\Delta^{\frac{3}{2}}}{3(1-\nu^2)} \quad (5.2)$$

Where ‘P’ is the load on indenter, ‘b’ is the radius of the spherical indenter; ‘E’ is the Young’s Modulus of the sample. ‘ $\nu$ ’ is the Poisson’s ratio of the matrix. ‘ $\Delta$ ’ is the displacement of the indenter. The close agreement between the FE model of a homogenous model and the analytical solution shows that the modelling approach is sufficiently accurate. Different from that data for a flat-ended indenter, the force-indentation depth data for a spherical indenter is nonlinear, while for a flat-ended indenter, the force-displacement data is close to a linear line (Figure 5.3). It also should be noted that the numerical data is close to the analytical solution up to a depth about 1R. (the radius of the indenter in the model is 2mm). This set the limit for the data used in the work, even though for the problem studied here, the results are focused on developing an effective modelling approach for quantifying the trend rather than the absolute values. Figure 5.6 (a) illustrates the deformation of the matrix and the embedded shell under the spherical indenter, in which the contact area is clearly curved following the profile of the indenter, due to the forces applied by the spherical shape. It can also be noticed from figure 5.6 (a) that the deformation of the embedded shell is also curved. Figure 5.6 (b) are two typical sets of data, one is with the embedded shell, the one with no shell (thickness of the embedded layer is 0.1mm,  $E_m=3\text{MPa}$ ;  $E_s=300\text{ MPa}$ , Poisson’s ratio is 0.495). The presented data clearly shows that the generated forces are higher with an embedded thin shell. In other words, the embedded shell has enhanced the indentation resistance of the system.

The effect of the Poisson’s’ ratio is systematically studied through parametric modelling. The change of indentation stiffness is represented by the ratio of the force over identical indentation depth. As force displacement data from the spherical indenter follows a nonlinear

pattern, the Indentation Stiffness (IS) (the force-displacement ratio ( $P/\Delta$ )) would be studied at 4 different depths, i.e. the depth of the indenter at  $1/4R$ ,  $1/2R$ ,  $3/4R$ ,  $R$ . Some typical results are shown in Figure 5.7. It is understood that when the data at different depths is used, the enhancement of indentation stiffness is synchronizing with the depth value. For both positive (a) or negative Poisson's ratio (b), the enhancement is more significant for the case at a lower shell depth than when the indentation depth is high. This confirms that the effect of the Poisson's ratio is depth dependent and this is probably due to more significant deformation to the matrix and the shell under the indenter. Consequently, the average value of the four different indentation depths was used and the results is shown in Figure 5.8. The data illustrates that there is a clear enhancement of the indentation resistance and when the matrix has a negative Poisson's ratio, the enhancement of the indentation stiffness is much more significant. Comparing the data in Figure 5.4 and 5.8, it can be clearly demonstrated that the enhancement of the indentation resistance for spherical and flat indenter, follows a similar trend. The numerical results are also used to provide a validation means for the development of an analytical solution for indentation of soft material with embedded thin shells. The numerical data in Figure 5.4 and Figure 5.8 shows a good agreement with analytical solutions developed as part of another project. (Li, 2019, in process). The theoretical framework and some typical results are shown in Figure 5.9. Compared to the data in Figure 5.9(b), the level of enhancement of the indentation resistance when a matrix with high negative Poisson's ratio is used, is comparable between the numerical and analytical analysis data. The data indicated that the indentation resistance can be significantly improved, which offers a new direction for material developments. Apart from the influence of auxeticity on the indentation resistance ratio, the deformation and stresses of the embedment are also important, as they may influence the function of the embedment. Figure 5.10 compares the stresses of the embedded layer between matrixes with positive and negative Poisson's ratios, using shear stress as a typical example (please note  $S_{12}$  represents the in-plane shear stress). The overall deformation of the embedded layer is similar but there is a difference in the distribution of the maximum stress. As shown in Equation 5.1 and 5.2, for homogenous materials, when the Poisson's ratio is negative or positive, theoretically there is no effect as the term is square in the equation. So the work showed that the embedded thin layer has changed the material behaviour. Further detailed works are required to establish the detailed mechanisms for the resistance increase due to the auxeticity of the matrix, which is associated with the fact that with a non-auxetic matrix, the embedded layer underneath the indenter is being pulled,

## **5.4 Numerical modelling investigation of interaction between liquid droplet and different forms of material systems**

### **5.4.1 FE model**

This section of the work discussed the modelling of the interaction between a liquid droplet and a solid surface, in terms of design, meshing, selecting the appropriate boundary conditions, applying the load and choosing the required number of elements, nodes and solvers so the simulation can produce accurate results. A main focus is to establish the key procedure and feasibility of using the Smoothed Particle Hydrodynamics method (SPH). Smoothed-particle hydrodynamics (SPH) is an effective computational method used for simulating the mechanics of fluid (Abaqus Theory Manual). It offers a much more effective and efficient way of modelling fluid-solid interaction than the pure fluid based approach. Before starting the initial static analysis, which is used to analyse and validate the impact of the droplet on the solid surface, as well as investigating the splashing and the reaction force, a procedure is developed to build the geometry of the droplet and the solid surface. As shown in Figure 5.11, the droplet geometry was designed by exporting the coordinate data from Ansys FLUENT. These coordinates were used in Abaqus to extract the droplet geometry. Once the dimensions of the 3D model were verified, a datum point and two reference points were identified within the structure of the assembly. As can be seen in Figure 5.12, the position of the datum point was placed in the centre of the solid surface. The datum point is used as an orientation origin to take measurements data from. As for the other reference points, it was used to measure the distance and the velocity of the falling droplet.

### **5.4.2 Droplet modelling with Smoothed Particle Hydrodynamics method (SPH)**

The droplet FE model used a computational method known as the Smoothed Particle Hydrodynamics method (SPH) to simulate the mechanics of continuum particles such as fluid flows and solid mechanics. This numerical method was developed by Monaghan (Lucy 1977; Gingold and Monaghan, 1977; Libersky and Petschek, 1991) for basic astrophysical problems. However, the method has been under constant development by academics and physicists to include many fields of research such as oceanography, ballistics, volcanology, finite element and astrophysics. One of its main advantages includes using free mesh techniques that are compatible with the LaGrange method in which the coordinate of the SPH particles move with the fluid flow. Libersky and Petschek (1991) were some of the first people to extend the SPH method to FE solid mechanics applications such as the possibility of simulating large local

distortion than complex grid based method. This beneficial feature has been explored in many solid mechanics simulations within metal forming, crack growth, impact and fragmentation. Many recent works have used this approach in different applications. Some basic theory is listed briefly in the section below (Wendland, 1995. Quinlan et al 2006)

For the referenced droplet model, the SPH method works by dividing the volume of the droplet into a set of discrete elements  $i, j$ , which are defined as particles. The lagrangian nature permits setting up the particle's position  $r_i$ , by integrating the velocity vectors:

$$\frac{dr_i}{dt} = v_i \quad (5.3)$$

A kernel function is used to describe the interaction particles with distinctive radius identified as the "smoothing length". This is typically represented in equations by  $h$ . This means that the amount of physical weight of all particles can be calculated by summing the relevant properties of all the particles that lie within the range of the kernel. This summation is known as the weighting function  $W$ . This function can be illustrated in two steps. The first step is an arbitrary field  $A$ , which can be calculated as follows:

$$A(r) = \int A(r')W(|r - r'|, h)dV(r') \quad (5.4)$$

The second step is the integral of using Riemann summation over the particles:

$$A(r) = \sum_i V_j A_j W(|r - r_j|, h) \quad (5.5)$$

The summation over  $j$  includes all particles in the simulation.  $A_j$  is the value of the quantity  $A$  for particle  $r$  and  $j$  denotes position,  $V_j$  is the volume of particle  $j$ . As for the density of the particles, it can be expressed as follows:

$$\rho_i = \rho(r_i) = \sum_j m_j W_{ij} \quad (5.6)$$

Where  $m_j = \rho_j V_j$  denotes the particle mass and  $\rho_j$  the particle density and  $W_{ij}$  is equivalent to  $W_{ji}$  which is a short notation for  $W(|r - r_j|, h)$ . A correction value is added by approximating the integral by a discrete sum depending on  $h$ , on the size of the particle  $V_j^{1/d}$ ,  $d$  being the space dimension as well as the arrangements of particles in space.

### 5.4.3 Boundary Conditions

Defining the boundary conditions is a very important step during the finite element analysis; it represents the step which describes the effect of constraints and the interaction between different parts. The boundary conditions for the investigation were applied to the assembled geometries via the two reference points (RF1 and RF2), which were used to represent the mass of the droplet and the constraints on the solid surface. The solid section was fixed from its base using a symmetrically encastred boundary condition. By doing this, the solver will assume that the geometry of the solid section is vertically fixed during the static analysis. Once the boundary conditions were defined by fixing corners of the solid section “Encastre”, the load was applied to the droplet geometry as a predefined field of 5m/s initial velocity. After this, an automatic initial coarse mesh was applied to the geometry of the droplet and the solid section. The simulation was prepared to run and the initial results for the first static analysis was extracted from the result section. Figure 5.13 shows a typical droplet deformation process onto the surface of a rigid substrate ( $E=1000\text{GPa}$ ). As shown in the figure, the model can effectively simulate the droplet deformation and the splashing process.

### 5.4.4 Effect of linear and nonlinear solver based on analysing the Initial results

Although, the initial study had an automatic coarse mesh of 1,001 nodes and 469 elements, the main aim of this run is to compare between a linear and non-linear analysis (Figure 5.14), as well as verifying whether the output displacement value is or is not directly proportional to the input data of the study. From the image shown, it can be seen that the linear study produced a maximum displacement of 8.693mm, while the non-linear study produced a 9.055mm displacement. This makes a difference of 0.8mm between the linear and non-linear solvers. Given the liquid deformation is a large displacement process. Therefore, it can be concluded that there are no big differences between the linear and the nonlinear solvers and this small verity between the two methods can be neglected. The Abaqus starter guide stated that linear solvers, which reduce integration element, tend to be too flexible because they suffer from their own numerical problem called hourglassing. Hence, the linear solver method was used throughout the static analysis study.

#### 5.4.5 Effect of Meshing schemes

Ten different types of studies were attempted to work out the required number of elements and nodes to produce a static analysis with accurate results. As listed in Table 5.2, the first three studies used an automatic applied mesh, while the rest of the seven studies used a manually applied mesh. The following methods were compared:

- A normal quadratic mesh: This analysis was done using the default meshing technique, which is automatic quadrilateral coarse mesh. This method was used as the first attempt to extrude the initial results of the static analyses, as well as comparing between linear and non-linear static results.
- Tetrahedral mesh: Another automatic mesh applied by Abaqus with an increased number of cells. This mesh uses a balanced number of tetrahedral and triangular solid elements for full integration.
- Refined mesh: A semi-automatic structured mesh applied by the user around important areas within the geometry.
- Refined mesh: A total of seven studies were tested using this method. This approach is based on the results from the previous three runs. The main aim behind the manual refined mesh study is to increase the number of elements and the number of nodes manually in certain parts to produce accurate results.

The main aim behind designing the manual mesh is to increase the number of cells around important areas, such as the droplet impact position, as well as balancing the cell numbers in the non-important areas to produce more accurate results. The final mesh used C38DR structured type elements, which was concentrated around the centre of the solid section due to the high stress figures that can be produced when the solid surface is undergoing sufficient amount of load. The mesh was also concentrated around the top and bottom corners, to record the behaviour of the reaction forces. These corners are also important because they produced high stress values throughout the previous studies, which could lead to failure.

**Table 5.2: Results of the static study under different meshing.**

Number of Attempts	Mesh	Maximum Von Mises Stress	Number of Element	Number of Nodes	Time (Sec)
1	Coarse Mesh	2.21E+08	1001	469	2
2	Coarse Mesh	2.26E+08	4218	2611	3
3	Refined Mesh	2.7E+08	6251	3210	8
4	Tetrahedral Mesh	3.55E+08	15901	7652	13
5	Tetrahedral Mesh	3.43E+08	35487	9608	15
6	Refined Mesh	3.40E+08	42458	52197	18
7	Refined Mesh	3.30E+08	52642	624832	20
8	Refined Mesh	3.30E+08	60240	1547613	35
9	Refined Mesh	3.30E+08	76893	1765421	60
10	Refined Mesh	3.30E+08	82135	2265482	110

As shown in Figure 5.15, the graph confirms the mesh converged behaviour for the maximum Von Mises Stress, generated by the solid section after droplet impact, for ten different types of studies. From the graph it can be understood that increasing the density of the mesh will result in increasing the number of elements in the numerical model. The maximum Von Mises stress values kept on increasing as the number of elements increased. The line kept on rising throughout the various attempts until the variation becomes limited. The straight line behaviour in the graph means that the values produced in the simulation are precise and the mesh convergence has been achieved.

### 5.5 Effect of the velocity and material properties

Figure 5.16 shows the effect of the droplet velocity on the reaction forces. In this study, the velocity of the water droplets were analysed for 5, 6, 7, 8 and 9m/s. The height for the corresponding droplets were 1mm, 2mm, 3mm, 4mm and 5mm respectively. This analysis was conducted to illustrate the effect of reaction forces generated by the droplet deformation during impact. From Figure 5.16a, it can be clearly seen that all 5 cases experienced a fast rise to a maximum value during impact, followed by a period of rapid decreasing in the forces before levelling off. The highest reaction force values can be used to validate the FE model theoretically. The basic procedure is briefly explained in the section below.

The result verification that can be checked during the static analysis is to calculate the total reaction forces of the droplet impacting on the solid surface. Hence, the reaction forces figures generated from the initial FE model should be equal to the theoretical calculations.

The volume of the droplet is estimated to be  $0.2mm^3$  from the FE model.

Hence the mass of the droplet can be calculated using the following formula:

$$m = \rho \times V \quad (5.7)$$

Where:

$m$ : The mass of the droplet [ $kg$ ].

$\rho$ : The density of the fluid [ $kg/m^3$ ]

$V$ : Volume of the Droplet [ $m^3$ ]

$$Mass = 1000 \times (0.2 \times 10^{-3}) = 0.016kg$$

Hence the theoretical reaction force can be calculated as follows:

$$F = m \times a \quad (5.8)$$

Where:

$F$ : The reaction force [ $N$ ].

$m$ : Mass of the droplet [ $kg$ ].

$a$ : Acceleration [ $mm/s^2$ ]

$$F = 0.016 \times 1666 = 26N$$

As shown in Figure 5.16 (b), this result is close to the maximum recorded reaction force of 18N, which proves that the extruded FE results are remotely close to the theoretical force calculations. The graph below shows the variation between FE results and theoretical reaction force calculations, across five different droplet velocities. A small difference in value was noted

for the 5, 7 and 10m/s velocities. However, the difference of reaction forces between the calculated and FE results increased for the 15 and 20m/s to a noticeable percentage difference of 30% and 20%. This difference in values between theoretical calculations and the simulated data can be associated on the limited number of meshing elements used for this analysis, thus fine mesh is essential.

### **Effect of impact velocity and the matrix properties**

Figure 5.17 shows some typical data showing that the model is used to study the effect of velocity on the deformation of the soft substrate ( $E=5\text{MPa}$ ). This is based on another project in developing conductive silicones for sensor applications (Kaid, 2020). When the velocity of the droplet is increased, the maximum depth from the droplet impact is increased. The model is capable of showing the trend line as shown Figure 5.17(e). When the matrix is relatively soft ( $\sim$ below 20MPa), there is significant change of deformation with the stiffness of the matrix, while over 20MPa, the trend line is close to a linear line. Future work will systematically investigate the effect of materials' properties on the maximum deformation of the droplet based on the modelling approach developed.

Another example of using the model on soft material with embedded shell is illustrated in Figure 5.18. In the model, a simplified sphere droplet is used. The set-up of the matrix is similar to that for the indentation studies with rigid indenters in section 5.2. As shown in Figure 5.19, when a matrix of a positive or negative Poisson's ratio is used, the deformation and stress in the shell is significantly different. Comparing Figure 5.19 (a) and (c), the contour of displacement shows that the vertical displacement of the embedded shell is much higher than in the case with a matrix with a positive Poisson's ratio than in the case with a negative Poisson's ratio. The same trend is with the stress. The peak stress with a negative Poisson's ratio matrix is lower, 0.94MPa vs. 1.6MPa. This suggests that the negative Poisson's ratio of the matrix has enhanced the indentation resistance. The details are still to be quantified, however, the work showed clearly that the droplet impact onto materials with negative Poisson's ratio has high resistance.

## 5.6 Discussion

Localised contact between a rigid, or a deformable indenter, onto deformable substrates, is a common loading mode to many materials/structures. The indentation resistance of materials (homogenous or more complex structures), is affected by the size and the shape of indenters. As shown in the work presented, numerical modelling offered an effective mean to analyse the behaviour of these matters and distinguish the effect of the indenter shapes and materials on the indentation resistance, and more importantly the difference between the rigid indenters and water drops. In this work, the FE model was validated against analytical solutions for both simple (homogenous materials) and complex cases in the form of a thin layer embedded in a soft matrix at different depth. Equation (5.1) and (5.2) are for Flat Cylindrical and Spherical Indenter, respectively. These equations were developed based on classic Hertz theories (Sneddon 1965; Yan et al 2003; Photiou et al 2016 ), which is only applicable to deformation within an elastic half space (infinite large samples). In this FE model, the indenter size was set as at least 5 times smaller than the sample size, to ensure that that effect of the sample is minimised. As shown in Figure 5.3 and 5.4, the numerical data illustrated good agreement with the analytical solution, after detailed mesh sensitivity studies. The numerical model also indicated that, for a flat ended indenter, the force displacement follows a linear relationship. While the data for the spherical indenter follows a nonlinear trend related to the radius of the indenter and the indentation depth. This is due to the fact that the contact area for the spherical indenter varies with the radius and the indentation depth. The pressure distribution also varies with the indentation depth, thus contribute to the nonlinearity of the effective indentation resistance. (Kang et al 2009).

The difference in the contact areas between a flat indenter and a spherical indenter also influences the effect of the embedded thin layers on the indentation stiffness. The comparison between the analytical solution for a system with an embedded layer and FE models showed that the embedded region approach used in the FE model is effective. For an elastic medium with an embedded shell, the stress-strain field under the indenter becomes much more complicated than a homogenous sample. It is also difficult to simulate due to the difference between the stiffness of the embedded layer and the matrix (in other word, the existence of property discontinuity). The work used an embedded region approach which effectively reduced the requirements on the computation resource. The numerical data in Figures 5.3(b), 5.8 & 5.9, showed a good agreement with the analytical solutions for situations when a stiffer layer is located at different depths. The work showed that the indenter shape has a significant effect on the resistance with an embedded layer. The case for quantitatively representing the

enhance ratio for the flat ended indenter is relatively easy as there is no major change in the contact area with the depth, but this is more challenging for spherical indenter as the contact between the indenter and the sample is varying with the depth. As illustrated in Figure 5.7, a new approach was used by depicting the force ratio at different indentation depth (as the ratio between the indentation depths to the diameter of the indenter). As shown in Figure 5.7, when force data at different indentation depth is used, the indentation stiffness ratio (representing the enhancement of the indentation resistance) is different at different depth. More significant effect is observed when the depth of the embedded layer is close to the radius of the indenter. This is reasonable as it is known that the maximum shear stress is maximum at is 0.49 of the indenter contact length (Shaw and Desalvo, 2012). The thin layer embedded at this position could alter the distribution of the shear stresses significantly, thus changing the indentation resistance. The work shows that, for both flat ended and spherical indenter, there is a clear effect of the Poisson's ratio and auxeticity of the matrix on the indentation resistance. The results in this work clearly suggest that, with the embedment of thin layer close to the surface, the influence of the auxeticity of the matrix becomes more significant as shown in Figures 5.5-6 and 5.10. The reason for this enhanced effect of auxeticity with embedded layer is subject to further study. The increase the effective indentation resistance could be a beneficial influence of the embedded layer in material design. Further studies are required to investigate these issues by combining the effect Auxeticity and embedded layers (Lim, 2014, Zhu et al 2015, Wojciechowski et al 2016; Aw et al 2016).

The interaction between liquid droplets and substrate surfaces represents a case in which the contact area varies significantly during the impact process (Laan et al 2014; Eggers et al 2010). The work showed that the SPH numerical method is an effective approach to study the effect of material parameters/behaviours, during the interaction between a droplet and a rigid surface or deformable materials. The deformation mode and the reaction forces are affected by the material properties of the matrix. For rigid substrate, the main deformation mode of the liquid is splashing. Less splashing is observed during the impact of the liquid drop on soft materials as the liquid is restrained due to the crater formed. This is an important phenomena in many products or material loading situation such as embedded heating elements, sensors, in silicone rubbers (Cannata et al. 2016; Kaid 2020). The modelling is helping another project on developing flexible sensors embedded in silicone rubber (Kaid PhD Thesis, 2020). In the work, thin pressure sensors embedded in silicon rubber is being developed for applications of measuring impacts of droplets without contaminations (avoiding direct metal-liquid contact).

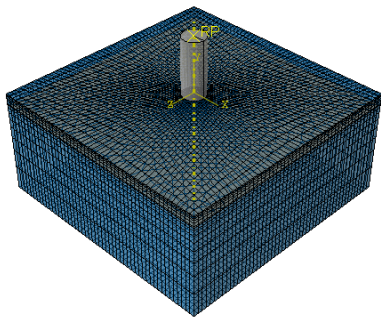
For such case, protection of the embedded element is important. The modelling data (Figure 5.19) shows the clear influence of auxeticity on the deformation mode and force data. The different deformation mode of the liquid drop from rigid indenter will affect the loading condition onto the target. It is noted from the rigid indenter study, the applied force is transferred to the material directly, while the deformation of the indenter is negligible. With water, the reaction force goes through complex stages, as well as the contact area, thus the effect of the auxetics is widely distributed. The developed model can be utilised as a tool for further systematic study on the effect of different fluid and temperature.

The effect of auxeticity on the indentation resistance (as a case for localised contact) is in agreement with many published works for different conditions (Lim 2014; Wojciechowski et al 2016). Most of the earlier work has been focused on foam structures (Lim 2014), while recent investigation/predictions on the isotropic auxetic materials have increased with the development of new auxetic material systems at different scales (Zhu et al 2015; Wojciechowski et al 2016; Li et al, 2018]. The study performed by Argatov et al (2012) investigated indentation and impact compliance of isotropic auxetic materials from the continuum mechanics viewpoint. It was found that the effect of Poisson's ratio and auxeticity is dependent on the shape of the indenter. Furthermore, a stronger effect of Poisson's ratio from the flat ended indenter is observed, more than that for a spherical indenter. Photiou et al (2016) reported that, *via* theoretical investigation and numerical modelling analysis, the negative Poisson's ratio has much stronger influence on the normalised hardness than the positive Poisson's ratio. The work also shows that evolution of different material constants (Young's Modulus 'E', Shear Modulus 'G' and Bulk Modulus 'K') as a function of Poisson's ratio, follow a different trend over the positive to negative domains. Previous work (Aw et al 2015) highlighted that negative Poisson's ratios have direct influence on the deformation, the force–displacement curve, the deflection profile and the contact area for thin membranes with fixed circular boundary conditions which is a situation also relevant to the embedded thin membranes. It should be noted that when a thin membrane/shell is embedded in a matrix, the deformation of the system (matrix and embedment) under localised/pointed deformation (indentation) is much more complex due to the combined interaction from the matrix, the properties of the shell and the position of the shell embedded. Future work is to be conducted based on the developed FE model, to systematically study the effect of material properties through parametric studies (systematically change the properties) when different liquid is used. In addition, the modelling program can also be used in materials with more complex system such as 2D mesh based Auxetics structures embedded in a silicone rubber to establish the deformation of the material

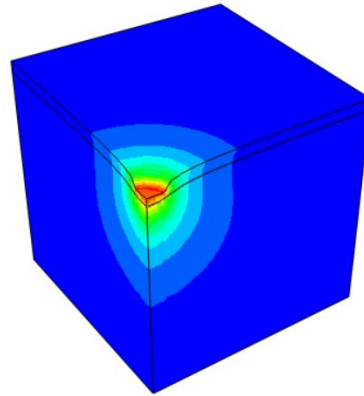
system and factors affecting the indentation resistance/stiffness, which are critical factors for the design and application of such systems as well as developing new material systems.

## 5.7 Summary

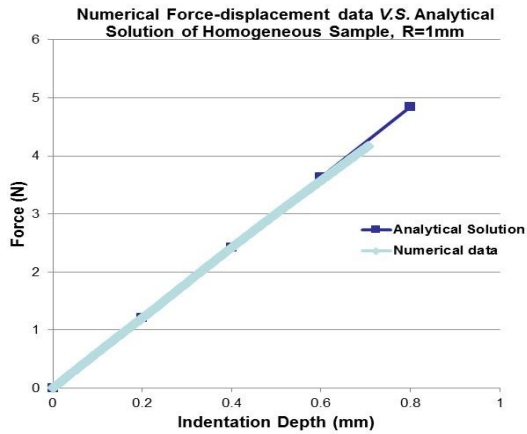
In this section, the deformation of a soft material with an embedded thin stiffer layer under a rigid indenter or liquid droplet was investigated through FE modelling. The indentation stiffness/ resistance, of soft material systems with an embedded thin layer under a flat-ended indenter and a spherical indenter for matrixes of both positive and negative Poisson's ratio values, was systematically studied. The influence of auxeticity on the indentation stiffness ratio and the deformation of the embedded system under different conditions was established and key mechanisms of the Poisson's ratio effect are highlighted. The results show that the auxeticity of the matrix has a direct influence on the indentation stiffness of the system with an embedded stiffer thin layer. The enhancement of indentation resistance due to embedment increases, as the matrix's Poisson's ratio is decreased to zero and to negative values. The indentation stiffness could be increased by over 30% with a thin inextensible shell close to the of a negative Poisson's ratio matrix. The deformation of the embedded layer is significantly influenced by the auxeticity of the matrix. With a non-auxetic matrix, the embedded layer underneath the indenter is being pulled, while for auxetic matrix, the embedded layer is being pushed due to the combined influence of the deformation of the auxetic matrix. The Smoothed particle hydrodynamics (SPH) approach is effectively used to simulate the interaction between liquid droplet and different material system, including systems with thin embedded shells in comparison with rigid flat ended and spherical shaped indenter. The results show that the SPH approach is effective when used to simulate the main droplet deformation stages, which offers a much more efficient approach for modelling liquid-solid interaction. The data shows that Auxeticity of the matrix has a direct influence on the resistance to the droplet impact from both rigid indenter and liquid droplet, which offers new insight for materials developments through combining the use of negative Poisson's ratio material and reinforcement through layered embedment.



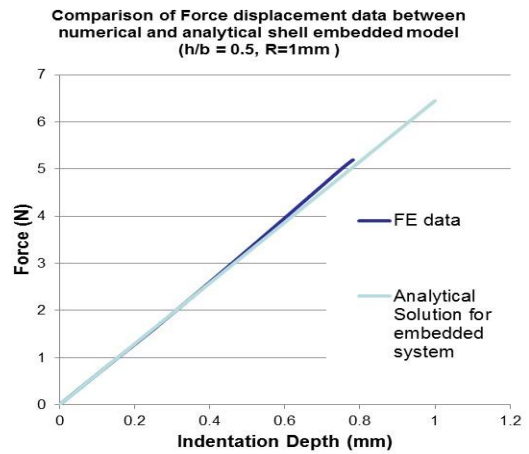
**Figure 5.1** Structure and boundary conditions of the FE indentation model with a flat ended cylindrical rigid indenter.



**Figure 5.2** Deformation fields of the matrix and the embedded shell under indentation with a flat-ended cylindrical indenter.

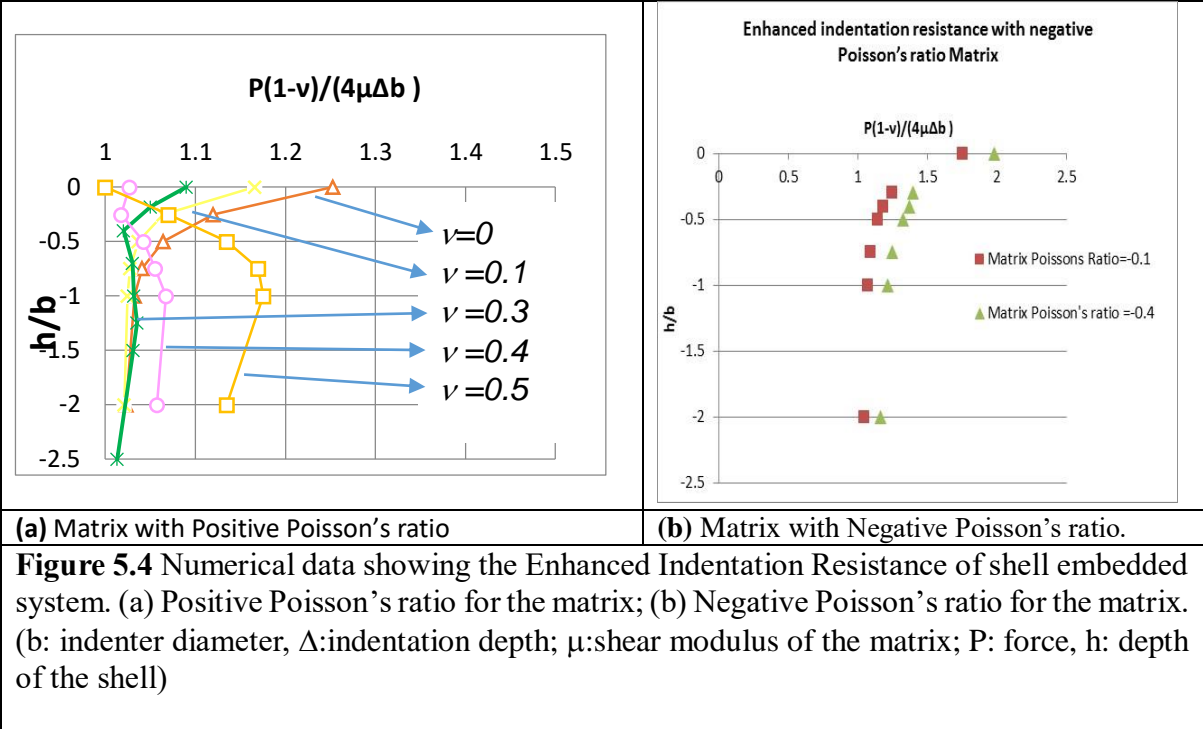


**Figure 5.3 (a)** Comparison between numerical indentation force-displacement data and analytical data of a homogenous model. (no embedment)



**Figure 5.3 (b)** Comparison between FE modelling and published analytical solutions of indentation of elastic matrix with embedded shell.

**Figure 5.3** FE models of indentation with a flat-ended cylindrical indenter on homogenous materials and materials with embedded shells.



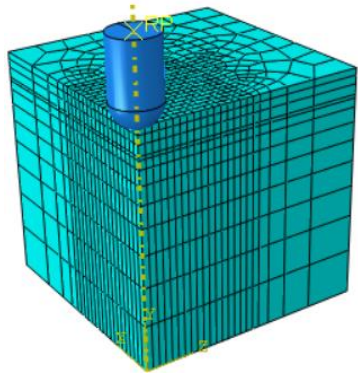


Figure 5.5 (a) FE Mesh of indentation model with a rigid spherical indenter.

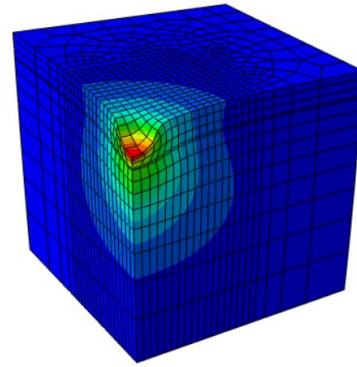


Figure 5.5(b) Displacement field underneath the spherical indenter.

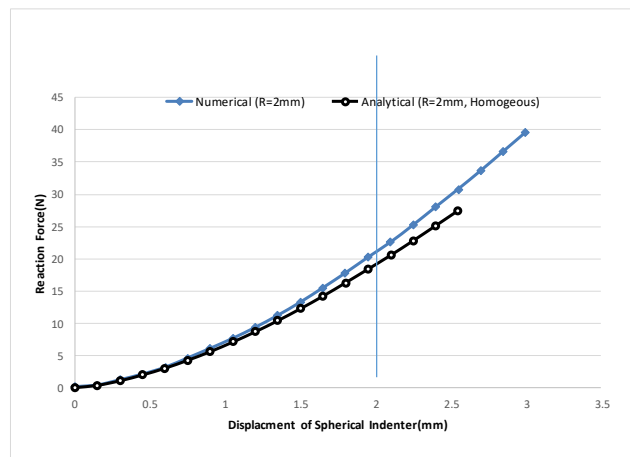
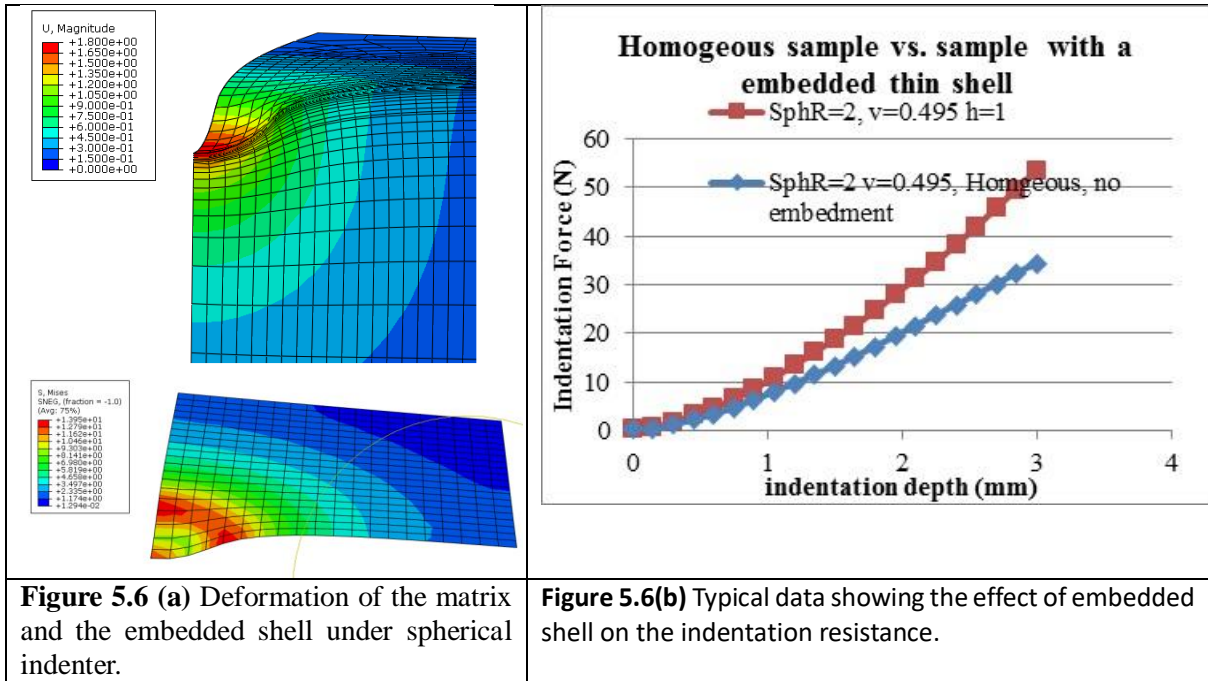


Figure 5.5 (c) Comparison between the numerical data and the analytical solution for homogenous material. The model is accurate up to an indentation depth equal to  $1R$ .

**Figure 5.5** Spherical indentation FE model/mesh (a) and deformation field (b); (c) Comparison between numerical and analytical data for indentation of a homogenous material.



**Figure 5.6** Effect of embedded shell on the indentation resistance

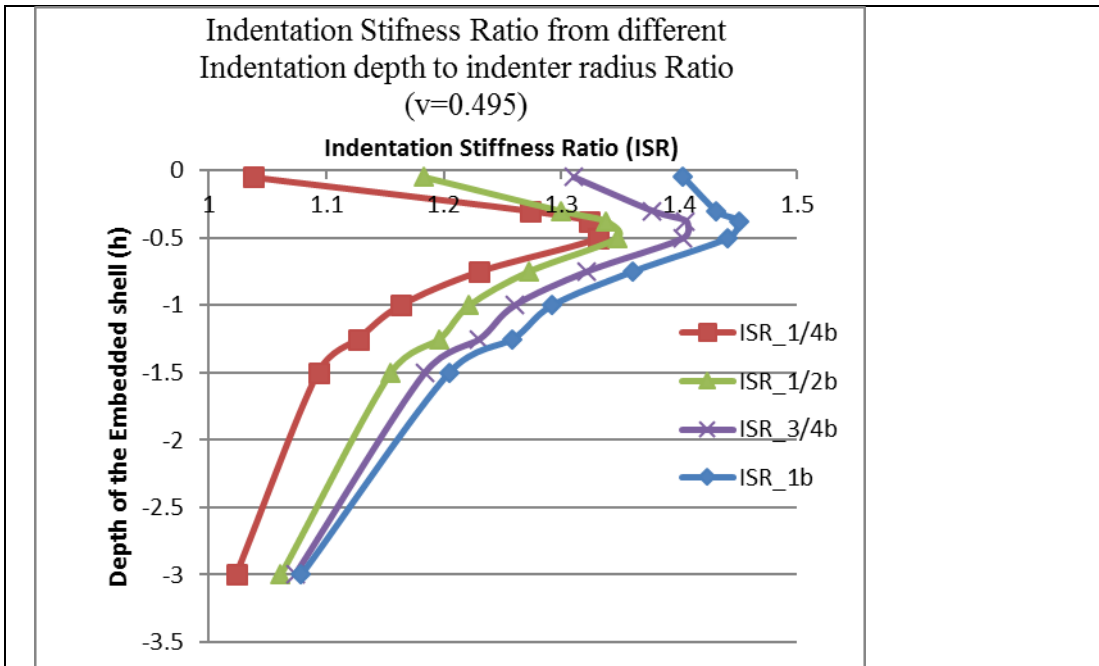


Figure 5.7(a) Data showing the effect of choice of indentation depth on the calculated Indentation Stiffness ratio (ISR) when using force data from different indentation depth.

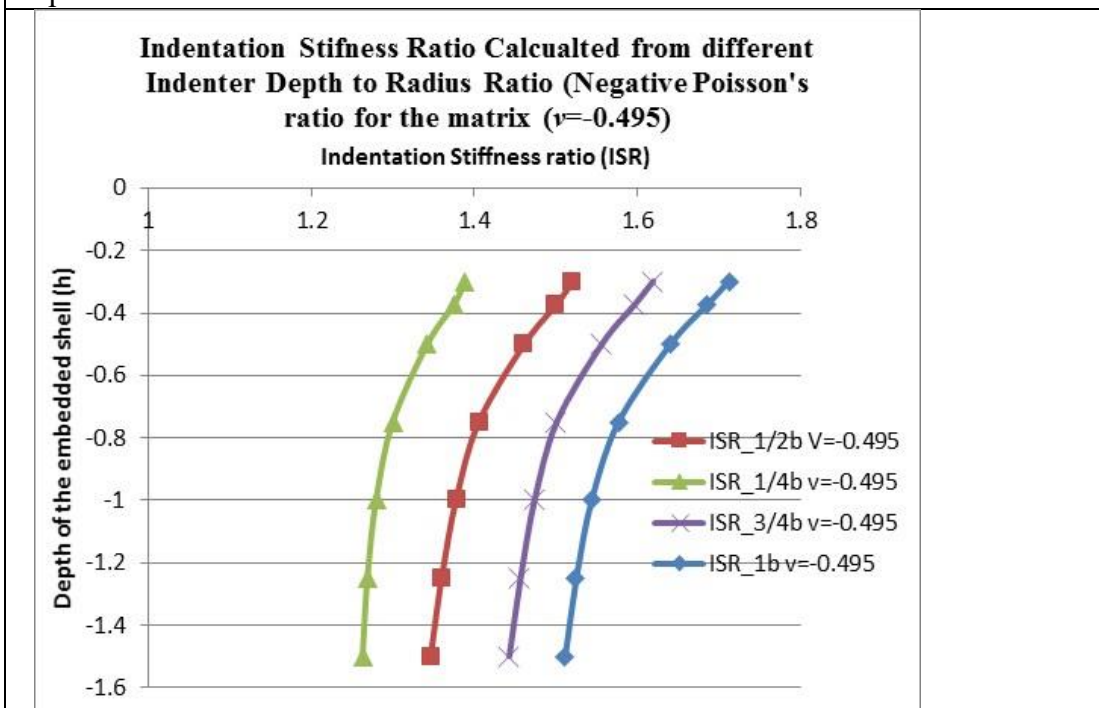
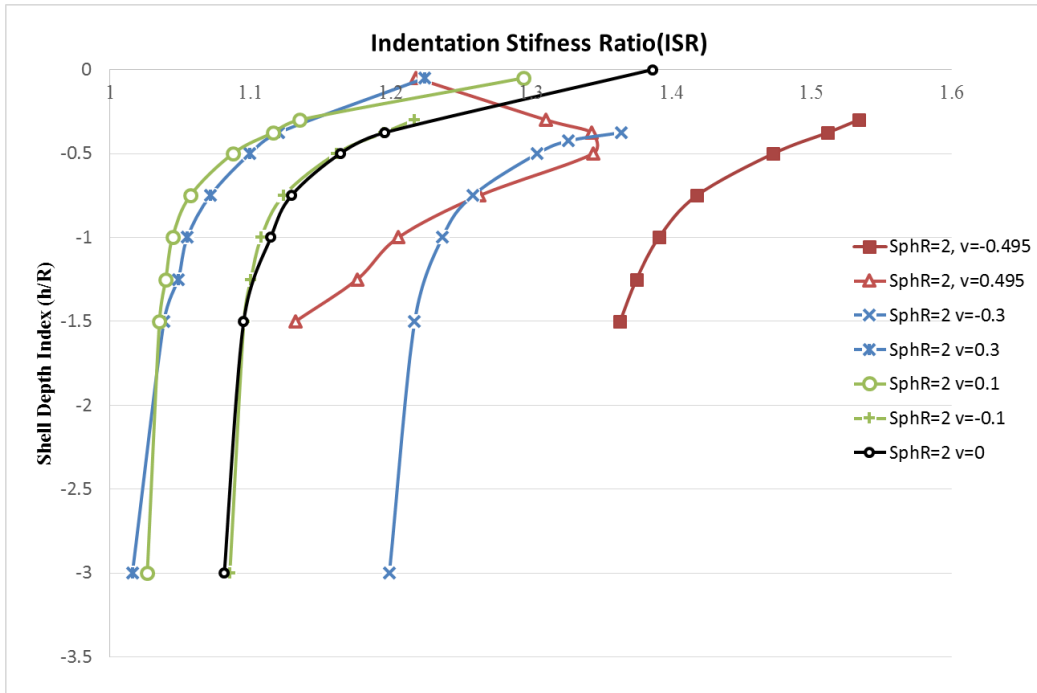


Figure 5.7(b) Indentation Stiffness ratio calculated from data at different indenter depth when the matrix has a negative Poisson's ratio.

**Figure 5.7** Indentation stiffness enhancement of materials with an embedded shell. (ISR is calculated against the load when there is no embedment).



**Figure 5.8** Data showing the effect of Poisson's ratio and depth of the embedment on the enhancement of the indentation resistance represented by the ISR.

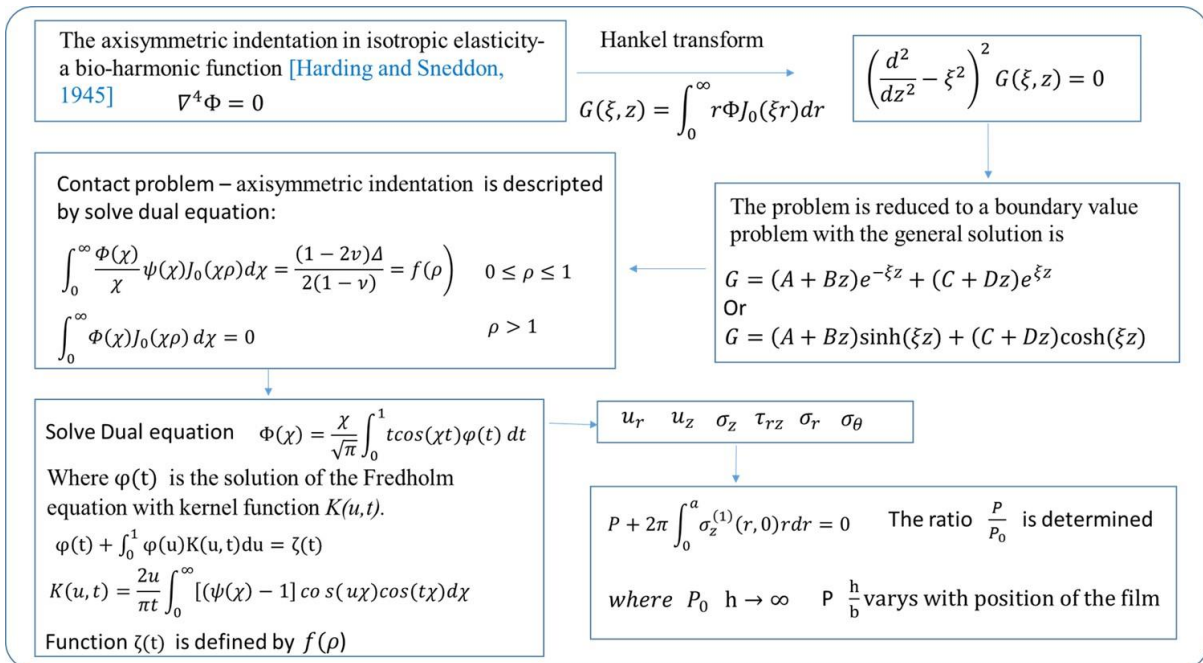


Figure 5.9(a) Framework for developing analytical solutions (Li et al, 2019, work in progress)

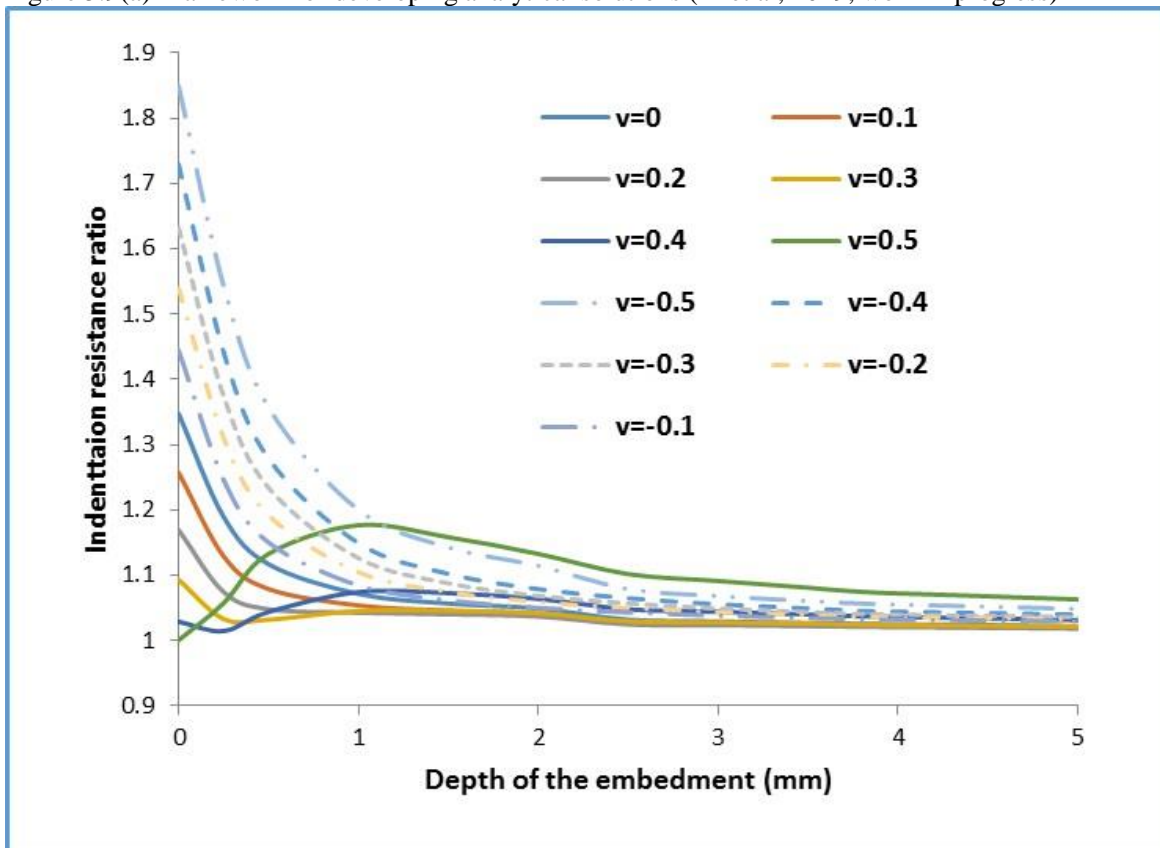


Figure 5.9(b) Enhanced Indentation resistance of material with an embedded shell (Analytical data) (Li, 2019, unpublished work)

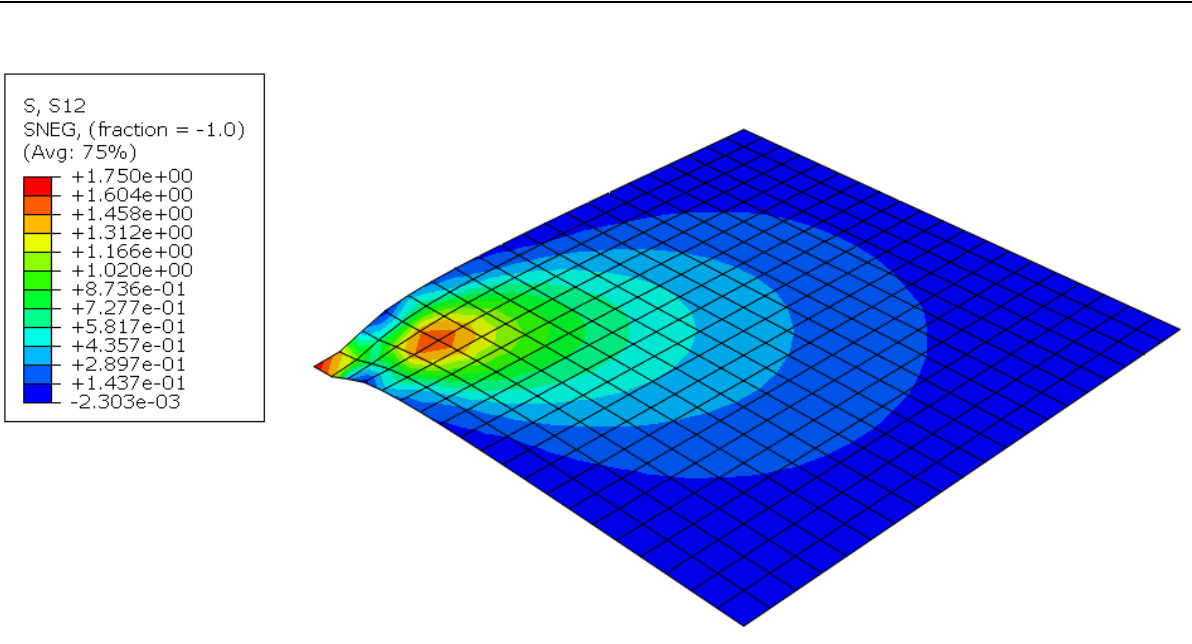


Figure 5.10 (a) Shear stress in the embedded shell when the Matrix has a positive Poisson's ratio ( $\nu=0.1$ )

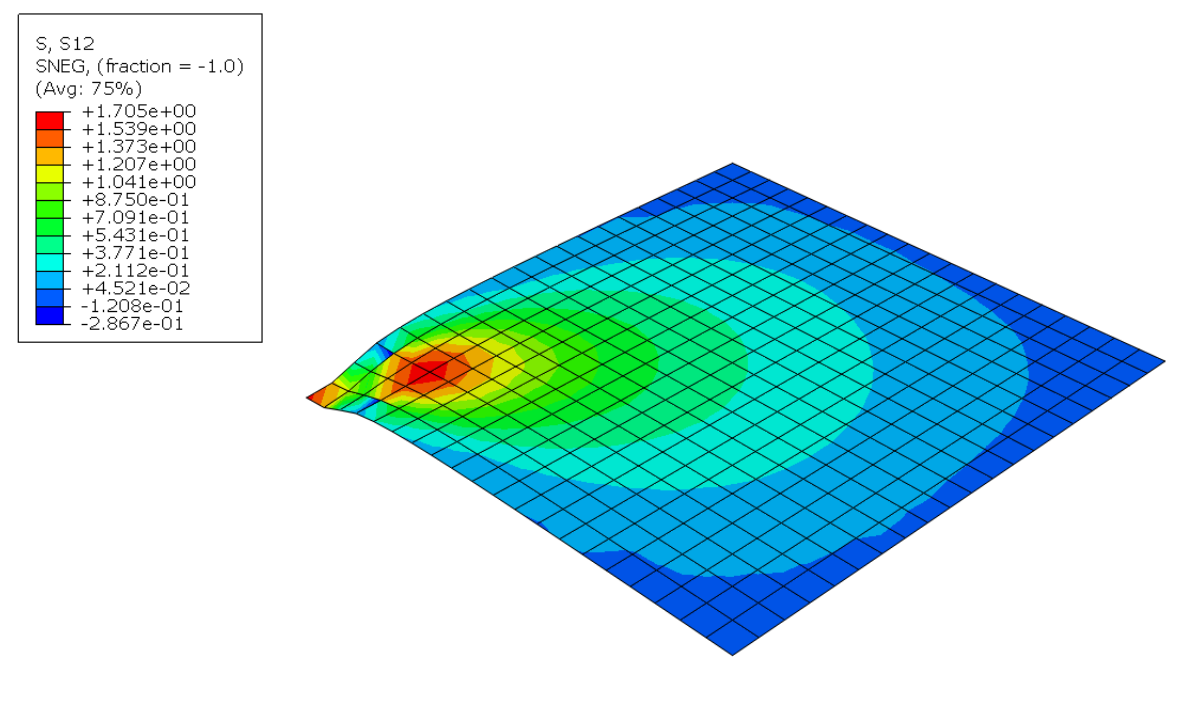


Figure 5.10 (b) Shear stress in the embedded shell when the Matrix has a negative Poisson's ratio ( $\nu=0.1$ )

**Figure 5.10** Typical example showing the comparison of shear stress (S12) of embedded shells between positive and negative Poisson's ratio matrix ( $\nu=\pm 0.1$ ).

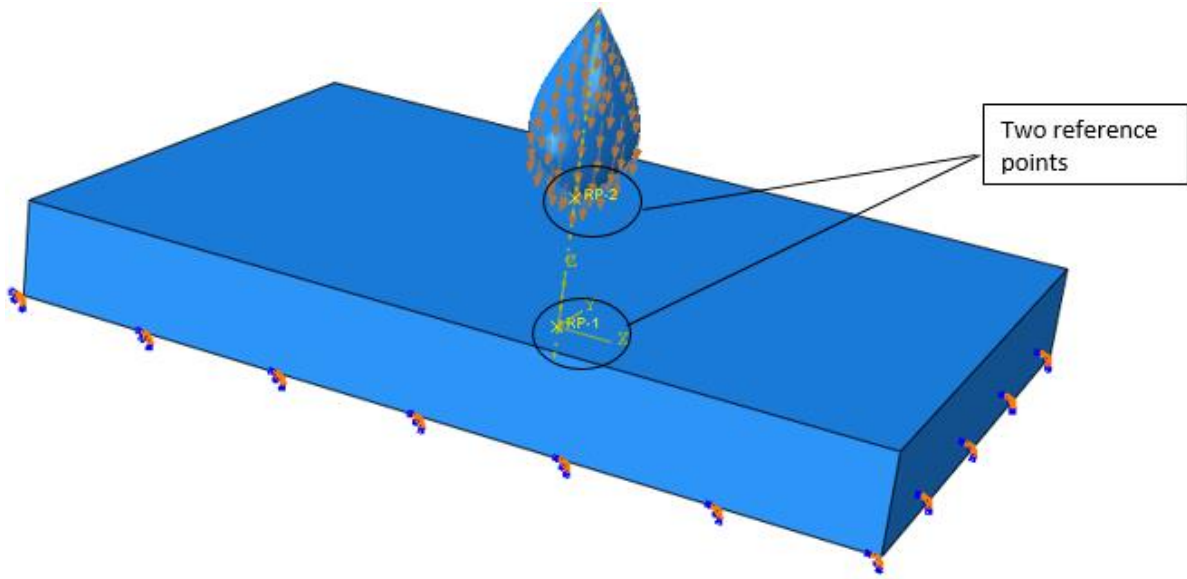
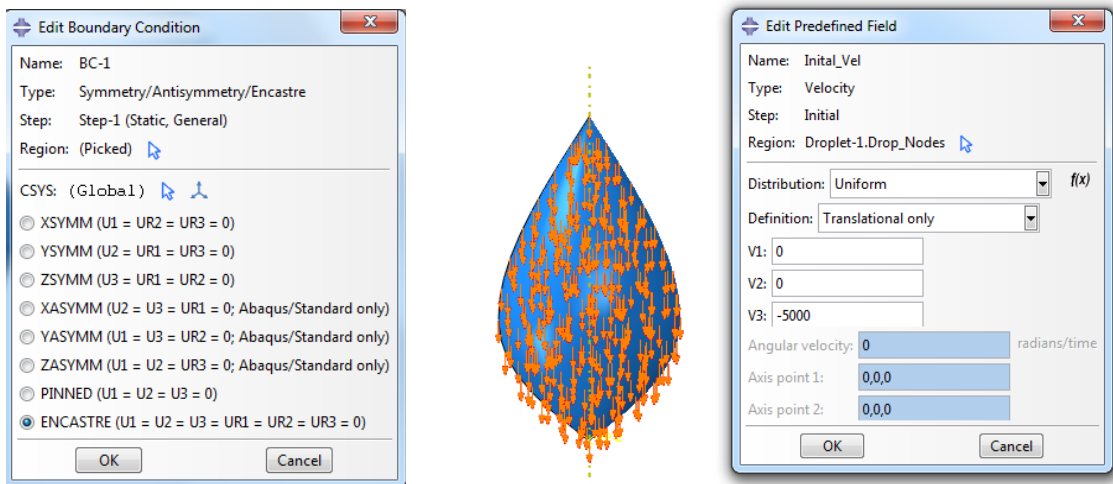
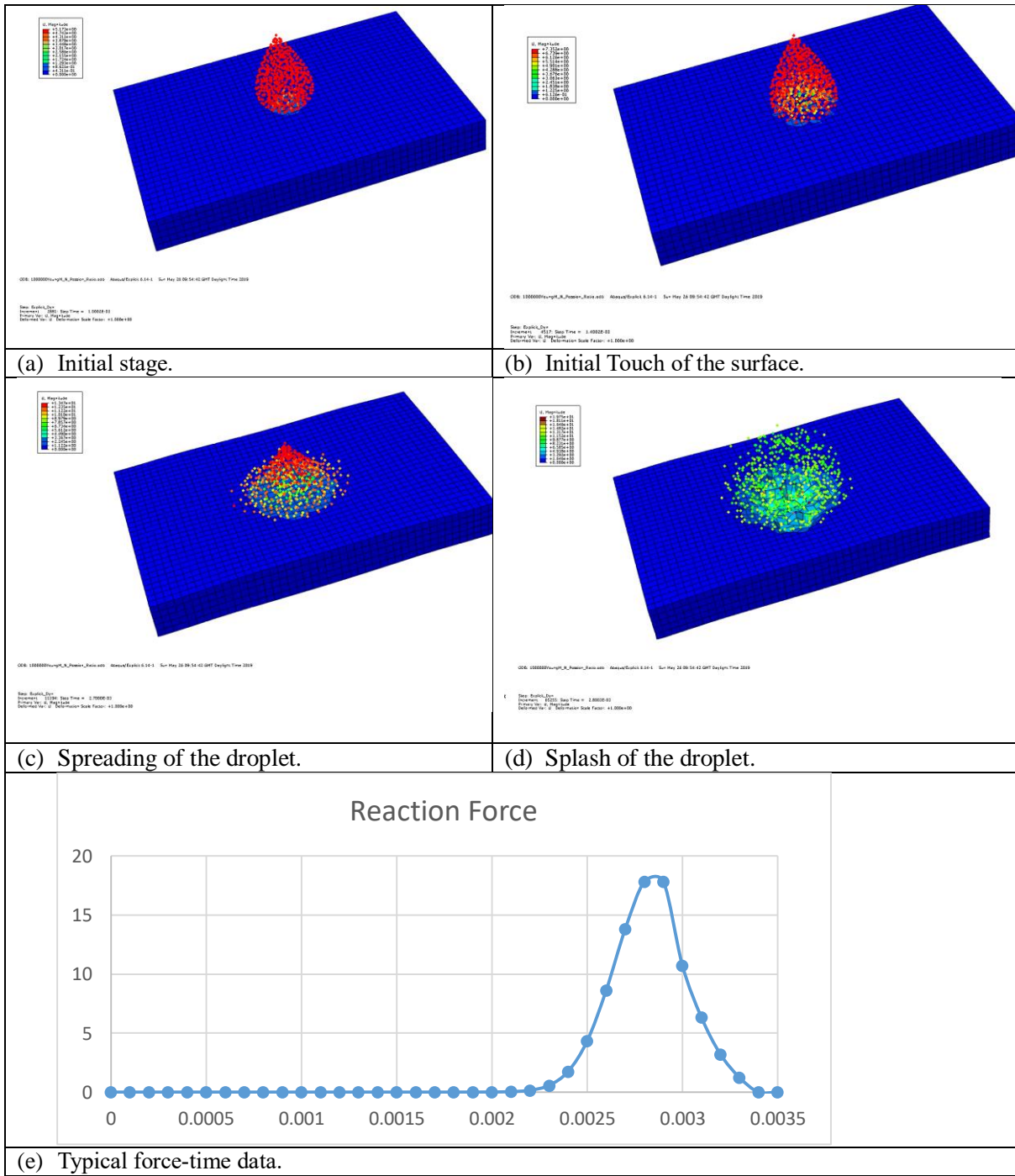


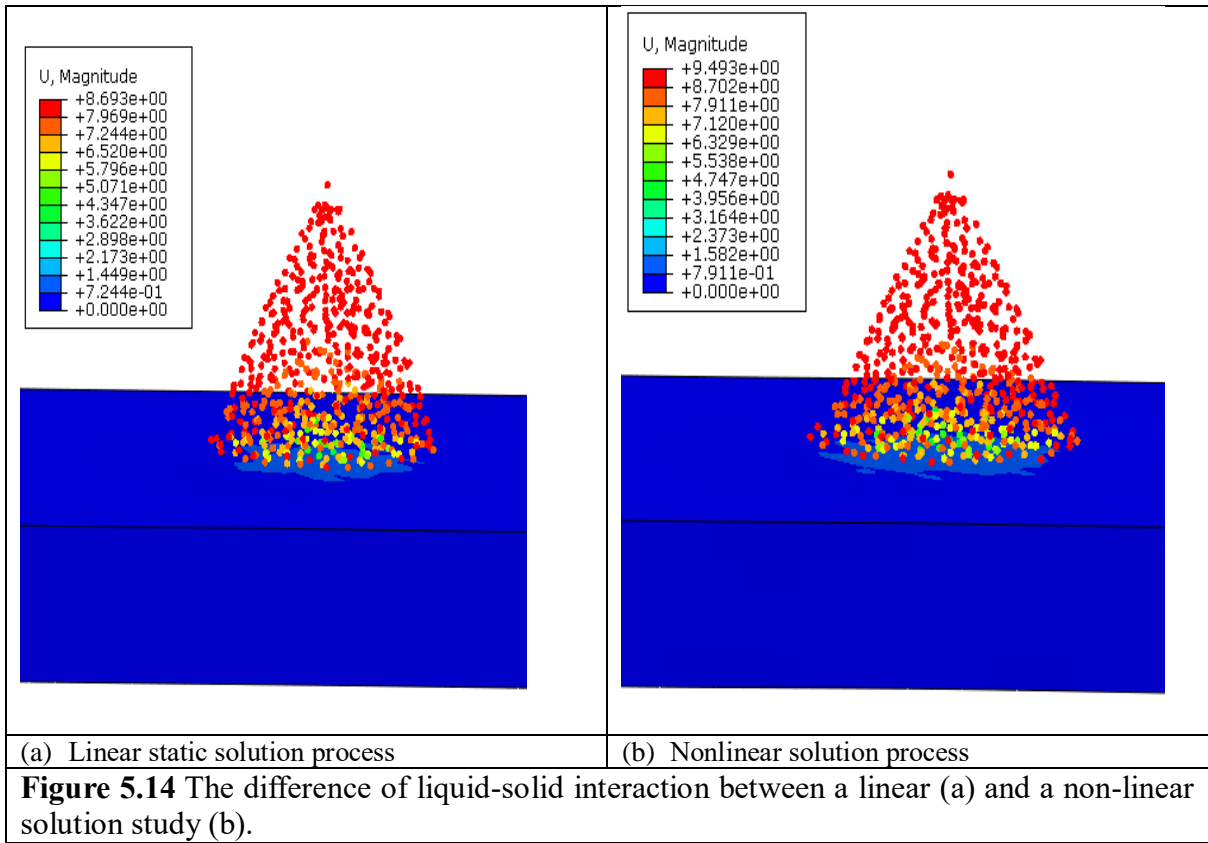
Figure 5.11 Numerical model of droplet interaction with a solid.



**Figure 5.12** Typical loading of the droplet when hitting a matrix. The solid surface was fixed from the bottom face using an ENCASTRE boundary condition; a predefined velocity of 5m/s was defined for the droplet.



**Figure 5.13** Typical deformation stages of the droplet during impact onto a rigid solid. ( $V=5\text{mm/s}$ )



(a) Linear static solution process

(b) Nonlinear solution process

**Figure 5.14** The difference of liquid-solid interaction between a linear (a) and a non-linear solution study (b).

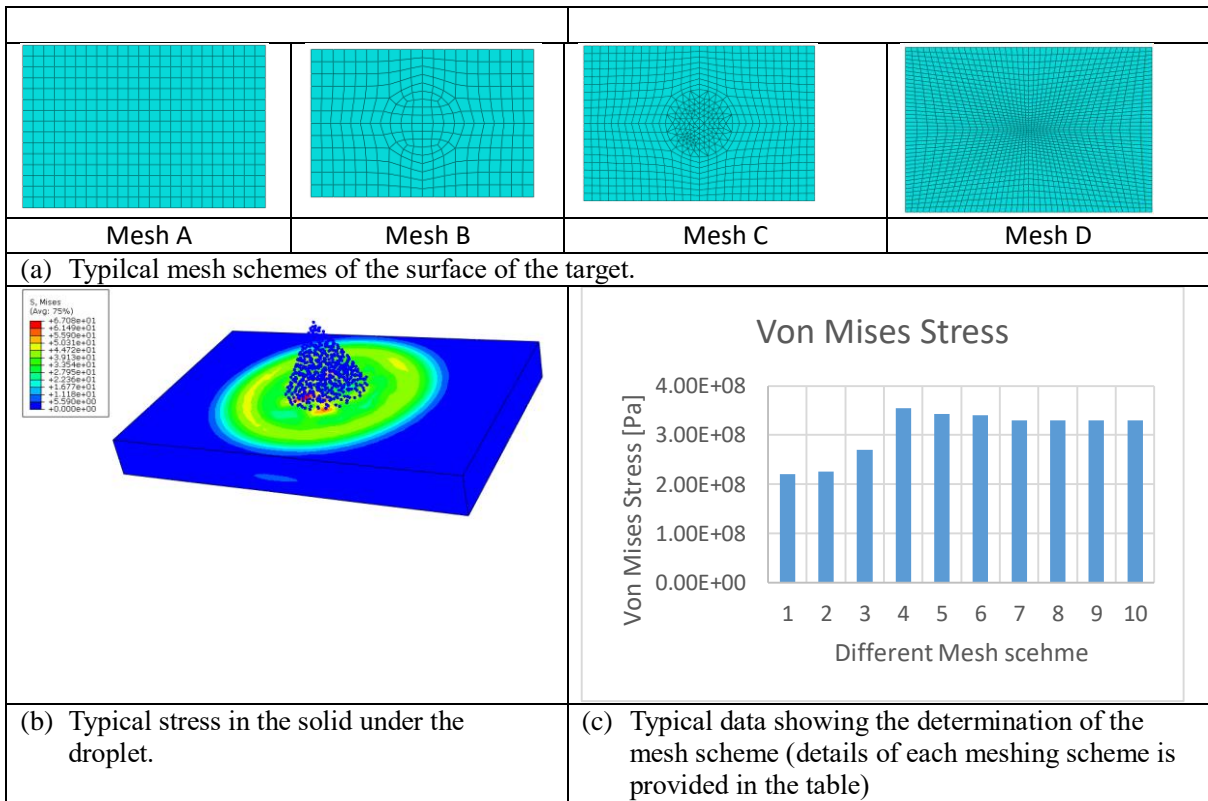


**Figure 5.15** Typical data showing the process used in developing the meshing schemes and extraction of the force and stresses.

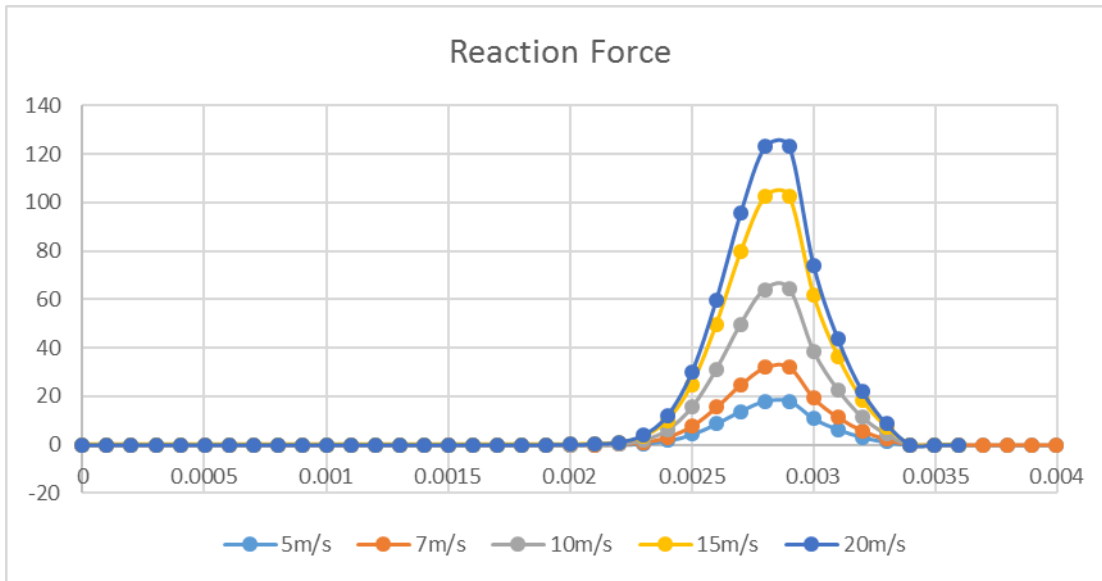


Figure 5.16 (a) Effect of the droplet speed on the force time data.

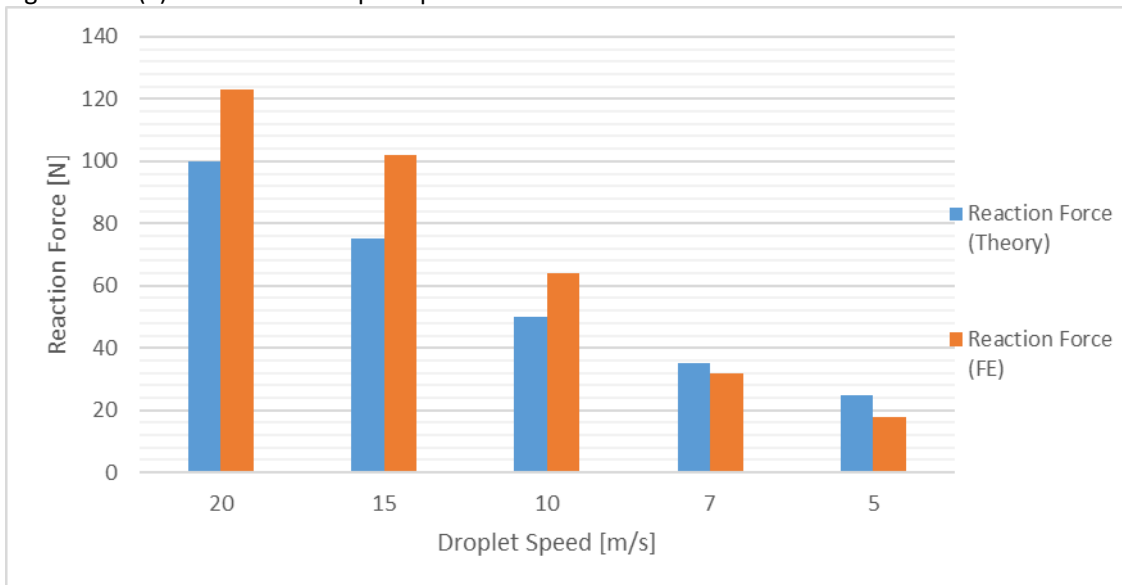
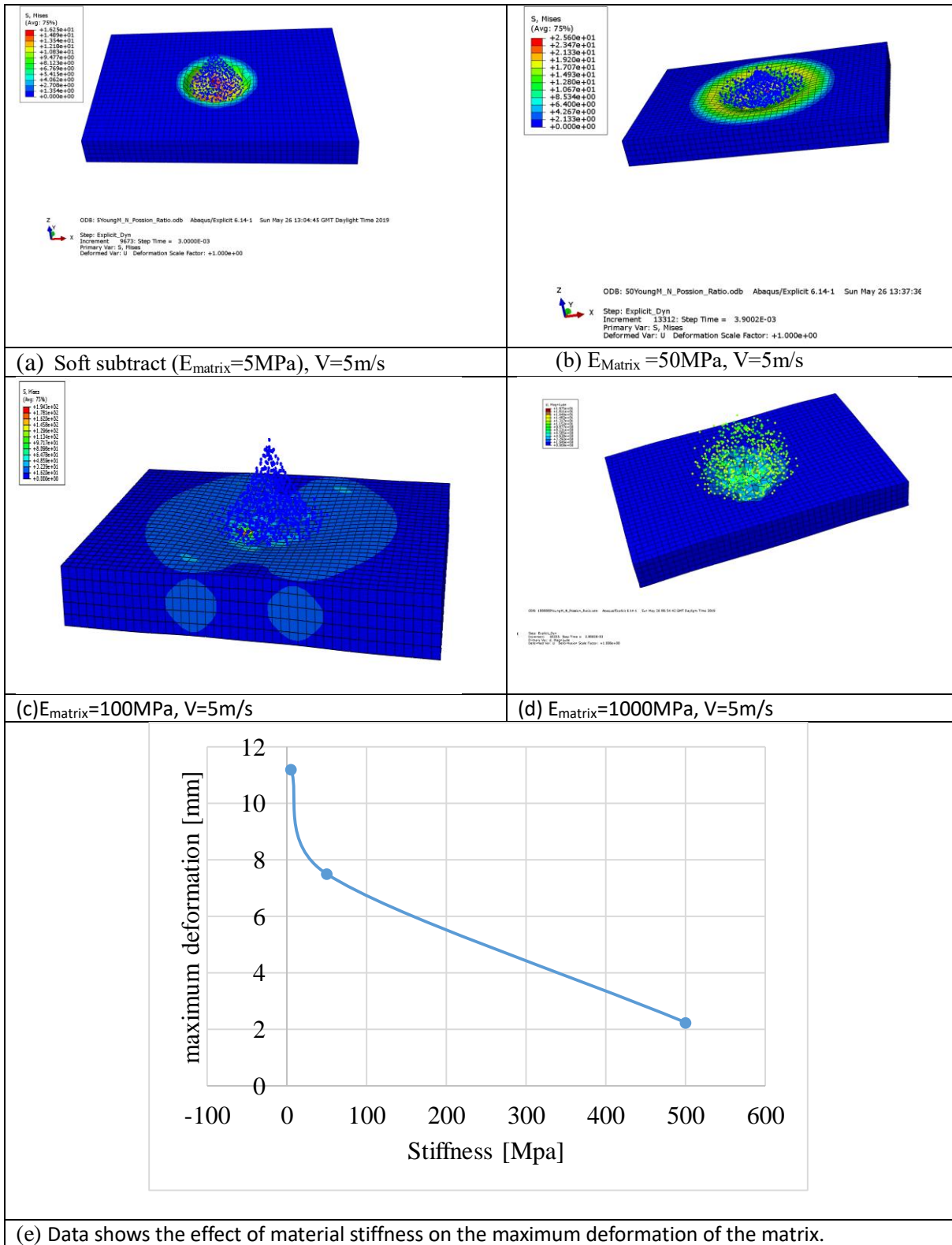
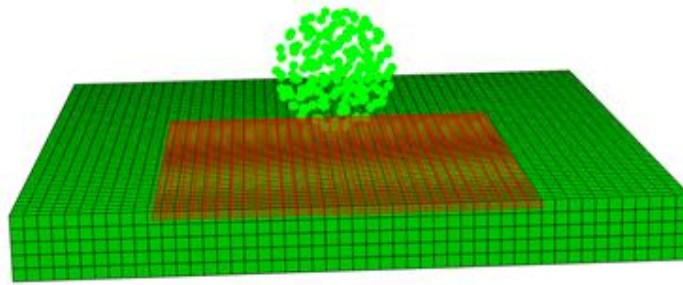


Figure 5.16(b) The maximum reaction force on the target with different droplet speeds.

**Figure 5.16** Effect of the droplet speed on the reaction forces.



**Figure 5.17** Effect of the Matrix stiffness on droplet deformation mode.



**Figure 5.18** FE model of spherical water droplet onto a matrix with an embedded shell.

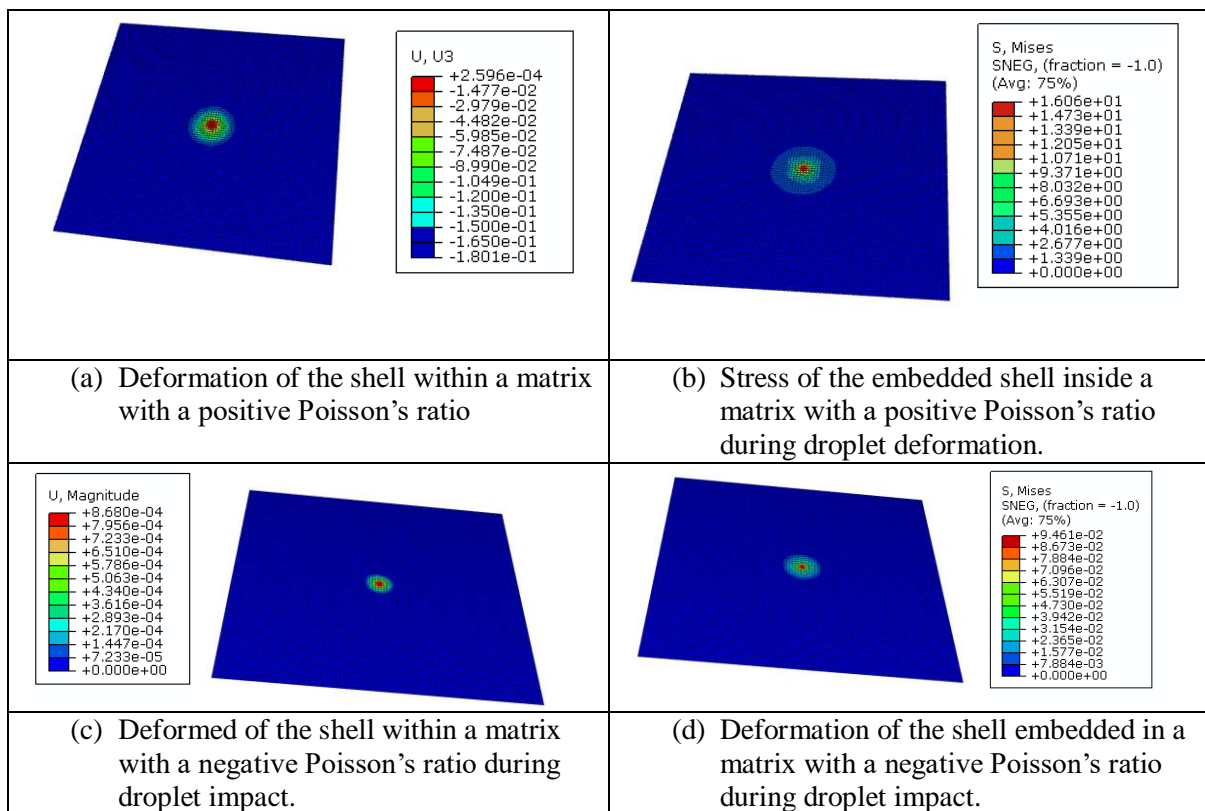


**Figure 5.19** Typical data showing the deformation of the material system of an embedded shell within a positive or negative Poisson's ratio. The maximum deformation of both the matrix and shell for the negative Poisson's ratio is lower than the matrix with a positive ratio suggesting that the negative Poisson's ratio has enhanced the indentation resistance. ( $E_{\text{shell}}=300\text{MPa}$ ;  $E_{\text{matrix}}=3\text{MPa}$ ).

CHAPTER SEVEN  
CONCLUSIONS AND FUTURE  
WORK

## 7.1 Summary and Conclusions

This work focused on developing effective modelling approaches for simulating the behaviour of small volumes of liquid and their interaction with other phases under different conditions with a particular focus on droplets and their interaction with different material systems. The effectiveness and efficiency of various commercial CFD approaches (ANSYS Fluent, CFX and 3D Flow) in modelling the droplet formation process have been evaluated. An effective modelling approach has been developed in ANSYS Fluent to simulate pendant droplet formation via the Volume of Fluid approach. The results from the numerical investigation were assessed against experimental data (viscosity/density tests and droplet tests) of selected model materials (mainly Water-Glycerine mixture solution and low melting point metals). Systematic droplet tests were conducted with a range of Glycerine-water solutions, the results show a good agreement with the numerical prediction and published data. The numerical model was applied to material with high viscosities using low melting point metals (Gallium) as an experimental material. A quantitative analysis of the data from the numerical approach and experimental data established the effects of viscosity and surface tension of the solution on the shape and key droplet characteristics (droplet length, breaking up point, overall volume of the droplets). Designated case studies, with specifically built models and codes, relevant to various engineering processes have been developed, including satellite droplets, droplets smaller than the nozzle diameter and microfluidic droplets in a multiphase flow system. The results show that the developed approach is effective in simulating different systems and can be potentially used as a computational tool for mapping the effect of design or material parameters (as illustrated in the effect of flow on microchannel droplet formation), including the limiting parameters for generating quality droplets. Comparative data shows that at the macro level, for the conventional droplet system, the volumetric flow rate is inversely proportional to the overall volume of the droplet, up to the point where the flow approaches the jetting mode; whereas at the micro level, this relationship is found to be non-applicable. A Matlab data system has been developed incorporating the realistic droplet shapes from the numerical modelling. The potential use of the modelling approach and data system for more complex systems is discussed, with reference to merging of droplets in micro closure welding of thin tubes and dye penetration into small cracks.

The Smoothed particle hydrodynamics (SPH) approach is effectively used to simulate the interaction between liquid droplets and different material systems, including systems with thin embedded shells of a high stiffness in comparison with solid flat-ended and spherical shaped indenters. A particular area has been focused on the indentation resistance enhancement

associated with embedded thin layers and Auxeticity of the matrix (i.e. the matrix with a negative Poisson's ratio) represented by the indentation stiffness ratio (ISR). The numerical result is correlated with the data based on analytical approaches for both homogeneous materials and elastic half space with an embedded stiffer layer. The influence of auxeticity on the indentation stiffness ratio and the deformation of the embedded system under different conditions (indenter size, and depth of the embedded layer) was established and key mechanisms of the Poisson's ratio effect are highlighted. The results confirm that the auxeticity of the matrix has a direct influence on the indentation stiffness of the system with an embedded thin layer. The indentation stiffness could be increased by over 30% with a thin stiffer shell on/close to the top of a negative Poisson's ratio matrix. With liquid droplets, a negative Poisson's ratio matrix provided a higher protection to the embedded shell, the deformation of the shell and stress level is much lower for the shell embedded in an auxetic matrix.

## 7.2 Recommendations for further works

This work has established a framework for modelling small volumes of liquid and their interaction with different material systems. Work on some typical cases such as welding, dripping and liquid penetration into cracks is also established. The work can be extended into the following areas:

1. Molecular modeling can be used to predict the viscosity and surface tension fluids water-glycerin mixture. The data measured in this work showed that the viscosity change dramatically with high glycerin concentration, future molecular modeling is required to simulate the interaction between the molecule and correlate the properties of the mixture to structure and bonding within water and glycerin.
2. The work has established effective modelling approach for liquid in droplet formation d other conditions. The model can be converted into an open source program with parametric interfaces for predicting droplet formation, satellite drops, merging of liquid drops and microchannel. The open source code can be used to generate data for different systems such as microchannel, or droplet smaller than the nozzle size. Such a parametric programs in python can help make the design process more efficient.
3. More detailed study on low melting temperature liquid metals. As part of another project, work is being conducted on using alloys with different low melting temperatures to generate conductive particles. The developed numerical model has provided an effective tool in predicting the droplet formation of liquid metals in air or in other liquid, which showed that the shape of the drop could be controlled more accurately with the assistance of the CFD modelling. This is critical for 3D printing and conductive rubbers. The model developed for interaction between droplets and surface can help analysing the conduction of heat by the droplet.
4. The findings on the effect of the Auxetics materials is an interesting topic, which potentially could offer a new area for materials development and a matrix for protecting embedded sensors. Another area is to model the transportation of liquid in auxetic structure, which potentially can be used as filter material; the ability of the cell to open under tension load will help to maintain a regular cell size and shape.

## References

- Abaqus Analysis User's Guide (15.2.1), Smoothed particle hydrodynamic analyses (accessed 11.2019)
- Abaqus Technology Brief, 2012, Fluid-Structure Interaction Analysis of a Prosthetic Aortic Valve using Abaqus/Explicit Smoothed Particle Hydrodynamics.
- Abaqus Theory Manual, Version 2017, BS Dassault Systems.
- Ali S, Al-Zuky A , Al-Saleh A and Mohamad H, 2019, Measure liquid viscosity by tracking falling ball automatically depending on image processing algorithm, IOP Conf. Series: Journal of Physics: Conf. Series 1294, 022002.
- Almohammadi H., Amirfazli A., 2019, Droplet impact: Viscosity and wettability effects on splashing, Journal of Colloid and Interface Science, 553, 1, 22-30.
- Al-Sharafi A., Yilbas B., Haider Ali H., AlAqeeli N., 2018, A Water Droplet Pinning and Heat Transfer Characteristics on an Inclined Hydrophobic Surface, Scientific reports, 8, 3061-3071.
- Ambravaneswaran B., Wilkes E. D., and Basaran O. A., 2002, Drop formation from a capillary tube: comparison of one-dimensional and two-dimensional analyses and occurrence of satellite drops. Phys. Fluids, 14(8), 2606 –2621
- Amirzadeh A, Chandra S, 2008, Producing droplets smaller than the nozzle diameter by using a pneumatic drop-on-demand droplet generator Article in Experiments in Fluids 44(1):105-114.
- Amirzadeh A, Raessi M, Chandra S, 2013, Producing molten metal droplets smaller than the nozzle diameter using a pneumatic drop-on-demand generator, Experimental Thermal and Fluid Science, 47, 26-33.
- Amirzadeh A., Raessi M., Chandra S., 2013, Producing molten metal droplets smaller than the nozzle diameter using a pneumatic drop-on-demand generator, Experimental Thermal and Fluid Science, 47, 26-33.
- Andreas J. M., Hauser E. A., and Tucker W. B., 1938, Boundary tension by pendant drops, The Journal of Physical Chemistry, 42(8), 1001-1019.
- Andreas J.M., E.A. Hauser, W.B. Tucker, 1938, Boundary Tension by Pendant Drops, J. Phys. Chem. 42 (8), 1001–1019.
- Anna S L, 2016, Droplets and bubbles in microfluidic devices. Annual Review of Fluid Mechanics, 48, 285-309.
- Anna S.L., 2016, Droplets and bubbles in microfluidic devices. Annual Review of Fluid Mechanics, 48, 285-309.
- Argatov I I, Guinovart-Díaz R, Sabina F J, 2012, On local indentation and impact compliance of isotropic auxetic materials from the continuum mechanics viewpoint, International Journal of Engineering Science, 54, 42–57.
- Aw J, Zhao H, Norbury A, Li L, Rothwell G, Ren J. 2015. Effects of Poisson's ratio on the deformation of thin membrane structures under indentation, Physica Status Solids B-Basic Solid State Physics, 252:1526-1532.
- Aw J, Zhao H, Norbury A, Li L, Rothwell G, Ren J. 2015. Effects of Poisson's ratio on the deformation of thin membrane structures under indentation PHYSICA STATUS SOLIDI B-BASIC SOLID STATE PHYSICS, 252:1526-1532.
- Balbaa M A and Nasr M N A, 2015, Prediction of Residual Stresses after Laser-assisted Machining of Inconel 718 Using SPH, Procedia CIRP, 31, ( 2015 ),19 – 23.
- Baroud N, Gallaire F and Dangla R, 2010, Dynamics of microfluidic droplets. Lab on a Chip, 16, 2032-2045.
- Bartell F.E. and Shepard J.W., 1953, The effect of surface roughness on apparent contact angles and on contact angle hysteresis of the system paraffin–water–air, *The Journal of Physical Chemistry*, 57(2), 211-215.
- Bashforth F., Adams J.C., 1883, An Attempt to Test the Theories of Capillary Action: By

Comparing the Theoretical and Measured Forms of Drops of Fluid, University Press.

Batchelor G.K., 2012, An introduction to fluid dynamics. Cambridge university press.

Baz J, Held C, Pleiss J and Hansen N, 2019, Thermophysical properties of glyceline–water mixtures investigated by molecular modelling, *Phys.Chem.Chem.Phys*, 21, 6467-6476.

Benet E and Vernerey F, 2016, Mechanics and stability of vesicles and droplets in confined spaces. *Physical Review E*, 94(6), 1-25.

Bergman T.L., Incropera F.P., DeWitt D.P. and Lavine A.S., 2011, *Fundamentals of heat and mass transfer*. John Wiley & Sons.

Bernstein L.R., Tanner T., Godfrey C. and Noll B., 2000. Chemistry and pharmacokinetics of gallium maltolate, a compound with high oral gallium bioavailability. *Metal-based drugs*, 7(1), 33-47.

Berry J.D., Neeson M.J., Dagastine R.R., Chan D., Rico F., Berry R.F., Joseph D., 2015, Measurement of surface and interfacial tension using pendant drop tensionmetry, *Journal of colloid and interface science*, 454, 226-237.

Bojanowski C and Kulak R F, 2010, *Modeling of Cone Penetration Test Using SPH and MM-ALE Approaches*, 8th European LS-DYNA Users Conference (2011).

Braun, B.J., Veith, N.T., Hell, R., Döbele, S., Roland, M., Rollmann, M., Holstein, J. and Pohlemann, T., 2015. Validation and reliability testing of a new, fully integrated gait analysis insole. *Journal of foot and ankle research*, 8(1), pp.1-7.

Brely L, Bosia F and Pugno N M, 2015, A hierarchical lattice spring model to simulate the mechanics of 2-D materials-based composites, *Frontiers in Materials*, 2, 1-10.

Carrier O, Dervin E, Funfschilling D and Li H, 2015, Formation of satellite droplets in flow-focusing junctions volume and neck rupture, *Microsyst Technol* 21:499–507.

Castrejón-Pita AA, Castrejón-Pita JR and Martin GD, 2012, A novel method to produce small droplets from large nozzles, *Rev Sci Instrum*;83(11):115105.

Cercos-Pita J L, 2015, AQUAgpusph, a new free 3D SPH solver accelerated with OpenCL, *Computer Physics Communications*, 192 (2015) 295–312.

Cercos-Pita J L, Antuono M, Colagrossi A and Souto-Iglesias A, 2017, SPH energy conservation for fluid–solid interactions, *Comput. Methods Appl. Mech. Eng.* 317, 771–791.

Chen H., Muros-Cobos J., Holgado-Terriza J.A., and Amirfazli A., 2017, Surface tension measurement with a smartphone using a pendant drop, *Colloids and Surface A*, 533, 213-217.

Chen L., Xiao Z., Chan P., Lee Y., Li Z., 2011, A comparative study of droplet impact dynamics on a dual-scaled superhydrophobic surface and lotus leaf, *Applied Surface Science* 257, 8857– 8863.

Chen Y., Wagner J.L, Farias P.A., DeMauro E.P., Guildenbecher D.R., 2018, Galinstan liquid metal breakup and droplet formation in a shock-induced cross-flow, *International Journal of Multiphase Flow*, 106,147-163

Cheng N, 2008, Formula for the Viscosity of a Glycerol-Water Mixture, *Ind. Eng. Chem. Res* (2008), 47, 3285-3288.

Cheng S., Li T., Chandra S., 2005, Producing molten metal droplets with a pneumatic droplet-on-demand generator, *Journal of Materials Processing Technology*, 159(3), 295-302.

Cimpeanu R., Papageorgiou D., 2018, Three-dimensional high speed drop impact onto solid surfaces at arbitrary angles, *International Journal of Multiphase Flow*, 107, 192–207.

Cite this publication

Cook S C and Murphy B A, 2020, Simulation of melt pool behaviour during additive manufacturing underlying physics and progress, *Additive Manufacturing*, volume 31, 100909

Crawford, R., Koopal L.K. and Ralston J., 1987. Contact angles on particles and plates. *Colloids and Surfaces*, 27(4), 57-64.

Dagdelen J, Montoya J, Maarten De Jong M and Persson K., Computational prediction of new auxetic materials, *Nature Communications* 8, 323, 1-8.

- Dang-Vu T., Hupka J., 2005, Characterization of porous materials by capillary rise method, *Physicochemical Problems of Mineral Processing*, 39, 47-65.
- Darwish S and Aslam M, 2014, Auxetic cellular structures for custom made orthopedic implants using additive manufacturing, *Int. Journal of Engineering and Advanced Technology (IJEAT)*, 4/2, 10-15.
- Davidson M.R. and Cooper-White J.J., 2006. Pendant drop formation of shear-thinning and yield stress fluids. *Applied mathematical modelling*, 30(11), 1392-1405.
- Del Rio O.I., Kwok D.Y., Wu R., Alvarez J.M. and Neumann A.W., 1998, Contact angle measurements by axisymmetric drop shape analysis and an automated polynomial fit program. *Colloids and Surfaces A: Physicochemical and Engineering Aspects*, 143(2-3), 197-210.
- Dingle N.M., Tjiptowidjojo K., Basaran O.A., Harris M., 2005, A finite element based algorithm for determining interfacial tension ( $\gamma$ ) from pendant drop profiles, *Journal of Colloid and Interface Science* 286(2):647-60.
- Drelich J., Fang C., White C.L., 2006, Measurement of interfacial tension in fluid–fluid systems, *Encyclopedia of Surface and Colloid Science*, second ed., CRC Press, Boca Raton.
- Drelich J., Laskowski J.S., Pawlik M. and Veeramasuneni S., 1997, Preparation of a coal surface for contact angle measurements. *Journal of adhesion science and technology*, 11(11), 1399-1431.
- Druzhinin P and Vandepitte D, 2016, A smoothed particle hydrodynamics method for virtual drop tests of polycarbonate suitcases, *Proceedings of ISMA, USA*.
- Duncan O, Shepherd T, Moroney C, Foster L, Venkatraman P, Winwood K, Allen T and Alderson A, 2018, Review of auxetic materials for sports applications: expanding options in comfort and protection, *Appl. Sci.*, 8(6), 941.
- Duncan, O., Foster, L., Senior, T., Alderson, A. and Allen, T., 2016. Quasi-static characterisation and impact testing of auxetic foam for sports safety applications. *Smart Materials and Structures*, 25(5), p.054014.
- Eggers J., 1995, Theory of drop formation, *Physics of Fluids (1994-present)*, 941-953.
- Eggers, J, Fontelos M A, Josserand C and Zaleski S, 2010, Drop dynamics after impact on a solid wall: theory and simulations. *Physics of fluids*, 22(6), 1-12.
- Elger D.F., Williams B.C., Crowe C.T. and Roberson J.A., 2013. *Engineering fluid mechanics*. Energy, 2, 03-01.
- Evans K E and Anderson K L, 2000, Auxetic materials: the positive side of being negative, *Engineering Science and Education Journal*, 9, 4, 148–154.
- Evans K E, 1991, Auxetic polymers: a new range of materials, *Endeavour*, 15, 170–174.
- Evans K. E. and A. Anderson, 2000, Auxetic materials: functional materials and structures from lateral thinking, *Advanced Materials*, 12, 9, 617–628.
- Fathi S., Dickens P., 2013, Challenges in drop-on-drop deposition of reactive molten nylon materials for additive manufacturing, *Journal of Materials Processing Technology*, 213, 1, 84-93
- Fawehinmi O. B., Gaskell P.H., Jimack P.K., Kapur N., and Thompson H.M., 2005, A combined experimental and computational fluid dynamics analysis of the dynamics of drop formation, *Proceedings of the Institution of Mechanical Engineers, Part C: Journal of Mechanical Engineering Science*, 219, 9, 933-947.
- Finotello G., Shauvik D., Vrouwenvelder J.C.R., Padding J.T., Buist K.A., Jongsma A., Innings F., Kuipers J. A. M., 2018, Experimental investigation of non-Newtonian droplet collisions: the role of extensional viscosity, *Experiments in Fluids*, 59, 113.
- Fordham, S., 1948, On the calculation of surface tension from measurements of pendant drops." *Proceedings of the Royal Society of London. Series A. Mathematical and Physical Sciences*, 194.1036, 1-16.
- Gajewski A., 2017, A couple new ways of surface tension determination, *int. J., Heat and mass*

Transfer, 115, 909-917.

Garstecki P., Fuerstman M., Stone H. and Whitesides G.M., 2006, Formation of droplets and bubbles in a microfluidic T-junction—scaling and mechanism of break-up, *Lab Chip*, 6, 437–446

Gaspar N, Ren XJ, Smith CW, Grima JN, Evans KE. 2005. Novel honeycombs with auxetic behavior, *ACTA MATERIALIA*, 53 :2439-2445.

Gatt R, Vella M, Gatt A, 2015, Negative poisson's ratios in tendons: an unexpected mechanical response, *Acta Biomater*, 24, 201-8.

Ghodsi M, Ghodsi M, Hojjat Y, Sadeghian H, Ziaiefar H, Mohammadzaheri M and Al-Yahmedi A, 2017, Investigation of Effective Parameters of Drop-on-Demand Droplet Generator. *The Journal of Engineering Research*, 14(2), 182-190.

Giese R.F., Costanzo P.M. and Van Oss C.J., 1991. The surface free energies of talc and pyrophyllite. *Physics and Chemistry of Minerals*, 17(7), 611-616.

Gingold, R.A. and Monaghan, J.J., 1977. Smoothed particle hydrodynamics: theory and application to non-spherical stars. *Monthly notices of the royal astronomical society*, 181(3), pp.375-389.

Gingold, R.A. and Monaghan, J.J., 1977. Smoothed particle hydrodynamics: theory and application to non-spherical stars. *Monthly notices of the royal astronomical society*, 181(3), 375-389.

Goghari A. A. and Chandra S, 2008, Producing droplets smaller than the nozzle diameter by using a pneumatic drop-on-demand droplet generator, *Experiments in Fluids*, 44(1), .105–114.

Good R.J., 1992, Contact angle, wetting, and adhesion: a critical review, *Journal of adhesion science and technology*, 6(12), 1269-1302.

Grima J, Chetcutie M, Daphne A, et al, 2012, On the auxetic properties of generic rotating rigid triangles, *Proc. R. Soc. A*, 468, 810–830.

Guarino V., Ambrosio L. (ed.), 2018, *Electrofluidodynamic Technologies (EFDTs) for Biomaterials and Medical Devices*, Woodhead Publishing, UK.

Guillot P and Colin A, 2005, Stability of parallel flows in a microchannel after a T junction, *Physical Review E*, 72(6 Pt 2): 066301.

Guo L, Duan Y, Deng W, Guan Y, Huang Y and Yin Z, 2019, Charged satellite drop avoidance in electrohydrodynamic dripping, *Micromachines*, 10(3), 172, 1-13

Hafer S., Poulikakos D., 2002, Transport and solidification phenomena in molten microdroplet pileup, *J. Appl. Phys.*, 92, 1675–1689.

Haidar, J., 2010, The dynamic effects of metal vapour in gas metal arc welding, *Journal of Physics D: Applied Physics*, 43(16), 165204.

Hassoon O H, Tarfaoui M, Moumen A E, Qureshi Y, Benyahia H and Nachtane M, 2019, Mechanical performance evaluation of sandwich panels exposed to slamming impacts Comparison between experimental and SPH results, *Composite Structures* 220 (2019) 776–783.

He B, Yang S., Qin Z., Wen B. and Zhang C. 2017, The roles of wettability and surface tension in droplet formation during inkjet printing, *Scientific Reports*, 7, 11841, 1-7.

Hebbar R.S., Isloor A.M., Ismail A.F., 2017, Contact Angle Measurements, *Membrane Characterization*, 219-255

Heidiger W. J. and Wright, M. W., 1986, Liquid extraction during drop formation: effect of formation time, *AIChEJ*, 32, 1372.

Heidner, M.C. and Adams, D.O., Aga Medical Corporation, 2016. Multi-layered medical device for treating a target site and associated method. U.S. Patent 9,232,992.

Henderson, D. M., Pritchard, W. G., and Smolka, L. B., 1997, On the pinch-off of a pendant drop of viscous liquid. *Phys. Fluids*, 11, 3188 –3200.

Hertel, M., Spille-Kohoff A., Füssel U., and Schnick M., 2013, Numerical simulation of

droplet detachment in pulsed gas–metal arc welding including the influence of metal vapour, *Journal of Physics D: Applied Physics*, 46(22), 224003.

Hieber H., 1989, Method of applying small drop-shaped quantities of melted solder from from a nozzle to surfaces to be wetted and device for carrying out the method, US Patent 4,828,886.

Ho D T, Kwon S., Kim S., 2016, Metal [100] nanowires with negative poisson's ratio, *Scientific Reports*, 1, 1-10.

Hoorfar M. and Neumann A.W., 2006, Recent progress in axisymmetric drop shape analysis (ADSA), *Advances in colloid and interface science*, 121, 1-3, 25-49.

Hu Q., Jiang T., and Jiang H., 2020, Numerical Simulation and Experimental Validation of Liquid Metal Droplet Formation in a Co-Flowing Capillary Microfluidic Device settings, *Micromachines*, 11(2), 169-83

Huh C. and Mason S. G., 1977, Effects of surface roughness on wetting (theoretical), *Journal of Colloid and Interface Science*, 60(1), 11-38.

Huh C., and Reed R.L., 1983, A method for estimating interfacial tensions and contact angles from sessile and pendant drop shapes, *Journal of Colloid and Interface Science*, 91, 2, 472-484.

Idelsohn S R, Del Pin F, Rossi R and Oñate E, 2009, Fluid-structure interaction problems with strong added-mass effect, *Int J Numer Meth Eng*, 80:1261–94.

Ikegawa M. and Azuma H., 2004, Droplet Behaviors on Substrate in Thin-Film Formation Using Ink-Jet Printing, *JSME International Journal Series B*, 47(3), 490-496.

Ionkin N., Harris D.M., 2018, A versatile 3D-printed droplet-on-demand generator, *Review of Scientific Instruments* 89(11):116103.

Jennings J., James W., and Pallas N. R., 1988, An efficient method for the determination of interfacial tensions from drop profiles, *Langmuir*, 4, 959-967.

Jia X., Yang J., Zhang J., Ni M.J., 2019, An experimental investigation on the collision outcomes of binary liquid metal droplets, *International Journal of Multiphase Flow*, 116, 80-90.

Kaid T. 2020, Development of conductive rubber for sensor applications, PhD Thesis, Liverpool John Moores University (In Process)

Kajtaz, M., Karren, J. and Subic, A., 2015. Experimental investigation into suitability of smart polymers as an impact-absorbing material for an improved rugby headgear. *In International Conference on Mechanics, Materials, Mechanical Engineering and Chemical Engineering*, Spain, April 2015, pp. 62-74.

Kang S, Kim J, Kang I, Kwon D, 2009, Effective indenter radius and frame compliance in instrumented indentation testing using a spherical indenter, *J. Mater. Res.*, 24, 9, 2965-2973.

Khojasteha D., Kazeroonib M., Salariana S., Kamalia R., 2016, Droplet impact on superhydrophobic surfaces: A review of recent developments, *Journal of Industrial and Engineering Chemistry*, 42, 1–14

Kim J.H., Jeon T.Y., Choi T.M., Shim T.S., Kim S.H. and Yang S.M., 2013, Droplet microfluidics for producing functional microparticles, *Langmuir*, 30(6), 1473-1488.

Kim U.R., Peterfreund R.A., and Lovich M.A., 2017, Drug Infusion Systems: Technologies, Performance, and Pitfalls; *Anesth Analg*. 124(5), 1493-1505.

Kovacevic, R., and H. Beardsley. "Process Control of 3D Welding as a Droplet-Based Rapid Prototyping Technique." *1998 International Solid Freeform Fabrication Symposium*. 1998.

Kovalchuk N.M., Nowak E., Simmons M., 2017, Kinetics of liquid bridges and formation of satellite droplets: Difference between micellar and bi-layer forming solutions, *Colloids and Surfaces A: Physicochemical and Engineering Aspects*, 521, 20, 193-203

Kumar N, Khaderi S N and Tirumala Rao K, 2020, Elasto-plastic indentation of auxetic and metal foams, *J. Appl. Mech*, 87(1): 011006

Laan N, de Bruin K G, Bartolo D, Josserand C and Bonn D, 2014, Maximum diameter of

- impacting liquid droplets, *Physical Review Applied*, 2(4), 1-7.
- Lake R S, 2017, Negative-poisson's-ratio materials: auxetic solids, *Annual Review of Materials Research*, 47, 63-81.
- Lass N., Riegger L., Zengerle R., Koltay P., 2013, Enhanced Liquid Metal Micro Droplet Generation by Pneumatic Actuation Based on the StarJet Method, *Micromachines* 2013, 4, 49-66.
- Law K, 2014, Definitions for Hydrophilicity, Hydrophobicity, and Superhydrophobicity getting the basic right, *J. Phys. Chem. Lett.* 2014 54686-688.
- Lazarus A and Reis P, 2014, Soft actuation of structured cylinders through auxetic behavior, *Advanced Engineering Materials*, 1-6.
- Li J., Pan L., Fu Q., Zhou Y., Guo N., 2019, Wettability and corrosion behavior of a Ni coating on 304 stainless steel surface *Surface and Coatings Technology*, 357, 740-747.
- Li J., Renardy Y., and Renardy M., 2000, Numerical simulation of breakup of a viscous drop in simple shear flow through a volume-of-fluid method, *Physics of Fluids* 12, 269.
- Li S, 2018, Numerical investigation of deformations of materials with embedded systems and human foot structure under different loading conditions, PhD Thesis, Liverpool John Moores University.
- Li S, Al-Badani K, Gu Y, Lake M, Li L, Rothwell G and Ren J, 2017, The Effects of Poisson's Ratio on the Indentation Behavior of Materials With Embedded System in an Elastic Matrix, *Physica status solidi (b)*, 254(12), 1-8.
- Li W Y, Shuo Y S and Wang X F, 2010, Numerical investigations of the effect of oblique impact on particle deformation in cold spraying by the SPH method, *Applied Surface Science* 256, 3725–3734.
- Libersky, L.D. and Petschek, A.G., 1991. Smooth particle hydrodynamics with strength of materials. In *Advances in the free-Lagrange method including contributions on adaptive gridding and the smooth particle hydrodynamics method* (pp. 248-257). Springer, Berlin, Heidelberg.]
- Lim T. C. 2014, *Auxetic Materials and Structures*, Springer, London 2014.
- Liu J, Tang C, Kaid T, Zhuo Y, Wang L and Ren X, 2019, Preparation and damping properties of simethicone MMT/PU microsphere, 5th International Conference on Green Materials and Environmental Engineering (GMEE2019), December, Guangzhou, China.
- Liu S., Liu F., Zhang H., Shi Y., 2012, Analysis of droplet transfer mode and forming process of weld bead in CO2 laser–MAG hybrid welding process, *Optics & Laser Technology*, 44.4 1019-1025.
- Liu T., Sen P., and Kim C., 2012, Characterization of nontoxic liquid-metal alloy galinstan for applications in microdevices, *Journal of Microelectromechanical Systems*, 21(2), 443-450.
- Liu, B, Feng X and Zhang S M, 2009, The effective Young's modulus of composites beyond the Voigt estimate due to the Poisson effect. *Composites Sci. Tech.* 69, 2198–2204.
- Lu S, Cao G, Zheng H, Li D, Shi M and Qi J, 2018, Simulation and Experiment on Droplet Formation and Separation for Needle-Type Micro-Liquid Jetting Dispenser, *Micromachines* 2018, 9, 330-344.
- Lubarda V.A. and Talke K., 2011, Analysis of the Equilibrium Droplet Shape Based on an Ellipsoidal Droplet Model *Langmuir*, 27, 10705–10713.
- Lucy, L.B., 1977. A numerical approach to the testing of the fission hypothesis. *The astronomical journal*, 82, 1013-1024.]
- Luo J., Qi L., Zhong S., Zhou J., Li H., 2012, Printing solder droplets for micro devices packages using pneumatic drop-on-demand (DOD) technique, *Journal of Materials Processing Technology*, 212 (10), 2066-2073.
- Ma M., Wei X., Shu X., Zhang H., 2019, Producing solder droplets using piezoelectric membrane-piston-based jetting technology, *Journal of Materials Processing Technology*, 263,

233-240.

- Majidi L, Gritsenko D. and Xu J., 2016, Gallium-Based Room-Temperature Liquid Metals: Actuation and Manipulation of Droplets and Flows, *Front. Mech. Eng.*, 1-12.
- Manaf N., Fukuda K., Subhi Z., Radzi M.F., 2019, Influences of surface roughness on the water adsorption on austenitic stainless steel, *Tribology International*, 136, 75-81.
- Mcintosh C, Chapuis J., and Mendez P., Effect of ArCO<sub>2</sub> Gas Blends on Droplet Temperature in GMAW, Effect of ArCO<sub>2</sub> Gas Blends on Droplet Temperature in GMAW, *Welding Journal*, August, 273-279.
- Melo, G.B., Dias C. J., Carvalho M., Cardoso A., Morais F., Figueira A., Filho A., Emerson G.G. and Maia M, 2019, Release of silicone oil droplets from syringes, *International Journal of Retina and Vitreous*, 5, 1-6.
- Michael S, Hana N, Jan K, 2017, The determination of viscosity at liquid mixtures – Comparison of approaches, *AIP Conference Proceedings* 1889, 020035.
- Michel Y, Chevalier J M, Durin C, Espinosa C, Malaise F and Barrau J J, 2006, *Int. J. Impact Eng*, 33, 441–451.
- Milne A.J.B., Amirfazli A., 2012, The Cassie equation: How it is meant to be used, *Advances in Colloid and Interface Science*, 170 (1–2), 48-55.
- Mitra S., Sathe M., Doroodchi E., Utikar R., Shah M., Pareek V., Joshi J., Evans G., 2013, Droplet impact dynamics on a spherical particle, *Chemical Engineering Science*, 100, 105–119.
- Mograne M, Ferrandis J and Laux D, 2019, Instrumented test tube for rapid rheological behaviour of liquids estimation, *Journal of Food Engineering* Volume 247, 126-129.
- Moreira A., Moita A., Pana M., 2010, Advances and challenges in explaining fuel spray impingement: How much of single droplet impact research is useful? *Progress in Energy and Combustion Science*, 36, 554–580.
- Morita A.T., Carastan D.J., Demarquette N.R., 2002, Influence of drop volume on surface tension evaluated using the pendant drop method, *Colloid Polym Sci*, 280, 857–864.
- Moslemi M, Farzin A and Kianoush M R, 2019, Nonlinear sloshing response of liquid-filled rectangular concrete tanks under seismic excitation, *Engineering Structures*, 188, 564–577.
- Mousanezhad D, Babae S, Ebrahimi H and Vaziri A, 2016, Hierarchical honeycomb auxetic Metamaterials, *Nature Scientific Reports*, 5, 28306, 1-8.
- Murr L.E., Johnson W. L., 2017, 3D metal droplet printing development and advanced materials additive manufacturing, *Journal of Materials Research and Technology*, 6(1), 77-89
- Nasser G A, Fath El-Bab M.R., Mohamed H. and Abouelsoud A., 2018, Low Cost Micro-Droplet Formation Chip with a Hand-Operated Suction Syringe, 2018 IEEE 18th International Conference on Bioinformatics and Bioengineering (BIBE), October, Taiwan.
- Needleman, A., Tvergaard, V. and Van der Giessen, E., 2015. Indentation of elastically soft and plastically compressible solids. *Acta Mechanica Sinica*, 31(4), pp.473-480.
- Needleman, A., Tvergaard, V. and Van der Giessen, E., 2015. Indentation of elastically soft and plastically compressible solids. *Acta Mechanica Sinica*, 31(4), pp.473-480.
- Ngo I., Joo S., Byyon C., 2016, Effects of junction angle and viscosity ratio on droplet formation in microfluidic cross-junction, *Journal of Fluids Engineering*, 138, 1-9.
- Niederhauser, W.D. 1950, Process for the preparation of aliphatic nitriles." U.S. Patent No. 2,493,637.
- Norbury A, Al-Badani K, Elmshawet E, Rothwell G and Ren XJ, 2018, Integrated Experimental and Numerical Investigation of Micro-welding process and Applications in Digital Manufacturing, *21st International Conference on Advances in Materials & Processing Technologies*, Dublin, Ireland.
- Norbury A., 2017, Development of an parametric numerical program for temperature sensors, PhD thesis, Liverpool John Moores University.

Offutt S and DeHeer P, 2004, How to address Baxter's Nerve entrapment, *Podiatry Today*, 17, 11, 52-58.

Omocea, I.L., Damian, I.R., Patrascu, C. and Balan, C., 2017, Formation and Break-up of Pendant Drops in a Viscous Liquid. *Energy Procedia*, 112, 204-209.

Oñate E, Idelsohn SR, Celigueta M A, Marti R R J, Carbonell J M and Ryzhakov P, 2011, Advances in the Particle Finite Element Method (PFEM) for solving coupled problems in engineering, *Comput. Methods Appl. Sci*, 25, 1-49.

Oyen, M.L. and Cook, R.F., 2003. Load-displacement behavior during sharp indentation of viscous-elastic-plastic materials. *Journal of Materials Research*, 18(01), 139-150.

Papageorgiou D., 1995, On the breakup of viscous liquid threads, *Physics of Fluids* (1994-present), 1529-1544.

Pardeep B., Srivastava M., Sinha M., 2017, Numerical Simulation of Dynamics of the Drop Formation at a Vertical Capillary Tube, *Applications of Fluid Dynamics*, 371-381.

Patton, D.A. and McIntosh, A.S., 2015. Considerations for the performance requirements and technical specifications of soft-shell padded headgear. *Proceedings of the Institution of Mechanical Engineers*, Part P: Journal of Sports Engineering and Technology, p.1754337115615482.

Patton, D.A. and McIntosh, A.S., 2015. Considerations for the performance requirements and technical specifications of soft-shell padded headgear. *Proceedings of the Institution of Mechanical Engineers*, Part P: Journal of Sports Engineering and Technology, p.1754337115615482.

Photiou D., N. Prastiti, E. Sarris, G. Constantinides, 2016, On the conical indentation response of elastic auxetic materials: effects of Poisson's ratio, contact friction and cone angle *Int. J. Solids Struct.* 2016, 81, 33-42.

Pravinraj T., Patrikar R.M., Design, fabrication, and modeling of a low-cost droplet on demand device for lab-on-chip applications, *Microelectronic Engineering*, 216, 111030

Qin M., Tang C., Tong S., Zhang P., Huang Z., 2019, On the role of liquid viscosity in affecting droplets spreading on a smooth solid surface, *International Journal of Multiphase Flow*, 117, 53-63.

Quinn, T. P., Szanto M., Gilad I., and I. Shai I., 2013, Coupled arc and droplet model of GMAW, *Science and Technology of Welding & Joining*, 10(1):113-119.

Radiom M., Chan W.K. and Yang C., 2009, A study of capillary flow from a pendant droplet, *Microfluidics and Nanofluidics*, 7(5), 697-707.

Rafiee J., Mi X., Gullapalli H., Thomas A.V., Yavari F., Shi Y., Ajayan P.M. and Koratkar N.A., 2012. Wetting transparency of graphene. *Nature materials*, 11(3), 217.

Rayleigh S.J.W., 1878, On the instability of jets, *Proc. London Math. Soc.*, 10. 4.

Rayleigh, L., 1879. On the capillary phenomena of jets. *Proc. R. Soc. London*, 29(196-199), 71-97,

Ren X J, Tang C, Guo J, Li L and Rothwell G, 2019. Data based approach for analysing poisson's ratio of materials and structures at different scales, *The Auxetics Jubilee meeting*, (Sept 2019), Poznan, Poland.

Renardy, Y. and Renardy, M. PROST: a parabolic reconstruction of surface tension for the volume-of- fluid method. *J. Comput. Phys.*, 2002, 183, 400 -421.

Riccardi, B., & Montanari, R., 2004, Indentation of metals by a flat-ended cylindrical punch. *Materials Science and Engineering: A*, 381(1), 281-291.

Richards J.R., Beris A.N. and Lenhoff A.M., 1995, Drop Formation in Liquid-Liquid Systems Before and After Jetting, *Article in Physics of Fluids*, 7(11):2617-2630.

Rotenberg Y., Boruvka L., and Neumann A., 1983, Determination of surface tension and contact angle from the shapes of axisymmetric fluid interfaces, *Journal of colloid and interface science*, 93, 1, 169-183.

Sanamia M, Raviralaa N, Aldersona K and Alderson A, 2014, Auxetic materials for sports applications, *Procedia Engineering*, 453 – 458.

Saqib M., Şahinoğlu O.B. and Erdem E. Y., 2018, Alternating Droplet Formation by using Tapered Channel Geometry, *Scientific Reports*, 8, 1606-1615.

Saxena K, Das R and Calius E P, 2016, Three decades of auxetics research – materials with negative poisson's ratio: a review, *Advanced Engineering Materials*, 18/11, 1847-1870.

Schulkes R.M., 1994, The evolution and bifurcation of a pendant drop. *J. Fluid Mech.*, 278, 83 –100.

Segur J. B.; Oberstar H. E., 1951, Viscosity of Glycerol and Its Aqueous Solutions. *Industrial & Engineering Chemistry*. 43 (9), 2117–2120.

Selvadurai, A.P.S., 2009, Boussinesq indentation of an isotropic elastic halfspace reinforced with an inextensible membrane. *International Journal of Engineering Science*, 47(11), 1339-1345.

Shafrin E.G. and Zisman W.A., 1960, Constitutive relations in the wetting of low energy surfaces and the theory of the retraction method of preparing monolayers<sup>1</sup>. *The Journal of Physical Chemistry*, 64(5), 519-524.

Shankar P N and Kumar M, 1994, Experimental determination of the kinematic viscosity of glycerol-water mixtures, *Proceedings of the Royal Society A*, 444, 573-581.

Shaw M C and DeSalvo G J, 2012, The Role of Elasticity in Hardness Testing, *Metallography, Microstructure, and Analysis*, 1, 310–317.

Shield, T. W., Bogy, D. B., and Talke, F. E., 1987, Drop formation by DOD ink-jet nozzles: a comparison of experiment and numerical simulation, *IBM J. Res. Dev.*, 31(1), 97 –110.

Shimasaki S., Taniguchi S., 2011, Formation of uniformly sized metal droplets from a capillary jet by electromagnetic force; *Applied Mathematical Modelling*, 35, 1571-1580.

Siivola, J.T., Minakuchi, S. and Takeda, N., 2016. Unloading response prediction of indentation loaded foam core sandwich structures using extended foam material model with tensile hardening. *Composites Part B: Engineering*, 84, pp.71-82.

Sneddon I., 1965, The Relation between Load and Penetration in the Axisymmetric Boussinesq Problem for a Punch of Arbitrary Profile,” *International Journal of Engineering Science*, Vol. 3, No. 1, 1965, pp. 47-57.

Solenthaler B, Schläfli J and Pajarola R, 2006, A unified particle model for fluid-solid interactions, *Eurographics/ACM SIGGRAPH Symposium on Computer Animation*, France.

Song B. and J. Springer, 1996, Determination of Interfacial Tension from the Profile of a Pendant Drop Using Computer-Aided Image Processing, *Journal of Colloid and Interface Science*, 184, 64–76

Tang C., Qin M., Weng X., Zhang X., Zhang P., Li J., Huang Z., 2017, Dynamics of droplet impact on solid surface with different roughness, *International Journal of Multiphase Flow*, 96, 56–69.

Tolman, R.C., 1949, The effect of droplet size on surface tension. *The journal of chemical physics*, 17(3), 333-337.

Wang T., Lin J., Lei Y., Fu H., Xiao R., 2019, Research on the droplets formation of gallium based eutectic alloys based on the mode of pulse electromagnetic force, *Vacuum*, 163, 158-163.

Wang T., Lin J., Lei Y., Guo X., Fu H., 2018, Droplets generator: Formation and control of main and satellite droplets, *Colloids and Surfaces A: Physicochemical and Engineering Aspects*, 558, 303-312.

Wang T., Lin J., Lei Y., Guo X., Fu H., Zhang N., 2018, Dominant factors to produce single droplet per cycle using drop-on-demand technology driven by pulse electromagnetic force, 156, 128-134

- Wang Y, Bao W, Wang F, Zhang H, Wang Z and Wang Y, 2020, Generation of micro-droplet on demand with reduced sizes by a hybrid pneumatic electro hydrodynamic method, *Journal of Micromechanics and Microengineering*, 30, 3, 1-6.
- Wang Y, Lai H, and Ren X J, 2019, Enhanced auxetic and viscoelastic properties of filled reentrant honeycomb, *Phys. Status Solidi B*, 1900184, 1-8.
- Ward T., Faivre M., Abkarian M. and Stone H.A., 2005, Microfluidic flow focusing: Drop size and scaling in pressure versus flow-rate-driven pumping. *Electrophoresis*, 26(19), 3716-3724.
- Washburn, E.W., 1921, The dynamics of capillary flow. *Physical review*, 17(3), 273.
- Wilkes E.D., Phillips S. D., and Basaran O.A., 1999, Computational and experimental analysis of dynamics of drop formation. *Physics of Fluids (1994-present)*, 11, 12, 3577-3598.
- Wojciechowski K W and Bilski M, 2016, Tailoring Poisson's ratio by introducing auxetic layers, 253/7, 1318–1323.
- Worthington A.M., 1881, *Proc. R. Soc. Lond.*, 32, 362–377.
- Xu J.H., Tan J., Li S.W. and Luo G.S., 2008. Enhancement of mass transfer performance of liquid–liquid system by droplet flow in microchannels. *Chemical Engineering Journal*, 141(1-3), 242-249.
- Wu, C.E., Lin, K.H. and Juang, J.Y., 2016. Hertzian load-displacement relation holds for spherical indentation on soft elastic solids undergoing large deformations. *Tribology International*, 97, 71–76.
- Xiong W, Qi L, Luo, J, Zhang D, Liang J and Yi H, 2017, Experimental investigation on the height deviation of bumps printed by solder jet technology, *Journal of Materials Processing Technology*, 243, 291-298
- Kei Y., 2010, The measurement of metal droplet temperature in GMA welding by infrared two-colour pyrometry." *Welding International*, 24.2 (2010): 81-87.
- Yan S L and Li L Y, 2003, Finite element analysis of cyclic indentation of an elastic-perfectly plastic half-space by a rigid sphere. *Proceedings of the Institution of Mechanical Engineers, Part C: Journal of Mechanical Engineering Science*, 217(5), 505-514.
- Yeow Y.L., Pepperell C.J., Firdaus M. Sabturani F.M., Leong Y., 2008, Obtaining surface tension from pendant drop volume and radius of curvature at the apex, *Colloids and Surfaces A: Physicochem. Eng. Aspects* 315, 136–146.
- Yonemoto Y. and Kunugi T., 2016, Analytical consideration of liquid droplet impingement on solid surfaces, *Scientific Reports*, 7, 2362, 1-11.
- Yu L, Yan Q and Ruzsinszky A, 2016, Negative Poisson's ratio in 1T-type crystalline two-dimensional transition metal dichalcogenides, *Nature Communications*, 8:15224, 1-8.
- Zahedi S A, Demiral M, Roy A and Silberschmidt V V, 2013, FE SPH modelling of orthogonal micro-machining of f.c.c. single crystal, *Computational Materials Science*, 78 (2013) 104–109.
- Zhang D. F. and Stone H. A. 1997, Drop formation in viscous flows at a vertical capillary tube. *Phys. Fluids*, 9(8), 2234 –2242.
- Zhang X. and Basaran O. A., 1995, An experimental study of the dynamics of drop formation. *Phys. Fluids*, A(7), 1184 –1203.
- Zhang X., 1999, Dynamics of Growth and Breakup of Viscous Pendant Drops into Air, *Journal of Colloid and Interface Science*, 212(1), 107-122.
- Zhang, X., Wang, P., Neo, H., Lim, G., Malcolm, A.A., Yang, E.H. and Yang, J., 2016. Design of glass fiber reinforced plastics modified with CNT and pre-stretching fabric for potential sports instruments. *Materials & Design*, 92, 621-631.
- Zhong Y, Haisheng F, Ma Q and Dong X, 2018, Analysis of droplet stability after ejection from an inkjet nozzle, *Journal of Fluid Mechanics*, 845, 3-12.
- Zhu H X, Fan T X and Zhang D, 2015, Composite materials with enhanced dimensionless Young's modulus and desired Poisson's ratio, *Nature Scientific Reports* 14103, 1-10.
- Zhu J., Tang S.T., Khoshmanesh K. and Ghorbani K., 2016, An Integrated Liquid Cooling

System Based on Galinstan Liquid Metal Droplets, *ACS Appl. Mater. Interfaces*, 8, 2173–2180.  
Zhu M and Scott M H, 2014, Modelling fluid-structure interaction by the particle finite element method in OpenSees. *Comput Struct*, 132, 12–21.

## List of Publications and External Reports

Al-Badani K., Elmshawet E., Tang C., Kaid T., Li L., Liu J., Wang J., and Ren X. J., 2019, Investigating the Effect of TIG Welding on the Surface Roughness of the Welded Closure of Thin Stainless Steel Tubes, *Journal of IOP Conference Series: Materials Science and Engineering (MSE)*. pp1-7.

Al-Badani K., Tang C, Kaid T, Lisa Li, Allanson D and Ren XJ Experimental and Numerical Studies of Droplet Formation of Different Material Systems, 6th International Conference on Nanomanufacturing, *NanoMan2018*, 04-06 July 2018, Brunel University London, UK, pp1-8.

Li S., Al-Badani K., Gu Y., Lake M., Li L., Rothwell G and Ren XJ, 2017, The Effects of Poisson's Ratio on the Indentation Behavior of Materials With Embedded System in an Elastic Matrix, *Physica status solidi (b)* 254(12), pp1-8.

Li. S, Al-Badani K., Gu Y., Lake M., Li L., Rothwell G and Ren XJ, Effect of Auxeticity on the Indentation Resistance of Materials, 7th International Conference "Auxetics and other materials and models with "negative" characteristics" and 12th Workshop "Auxetics and related systems", Szymbark near Gdansk (Poland), September 12-16, 2016.

Al-Badani K, Tang C, Li S, Kaid T, Elmshawet E, Gu Y, Li L, Rothwell G, and Ren XJ, Numerical Modelling of Materials with Embedded System in an Elastic Matrix in Contact with Solid and Liquid Impactors, *9th International Conference and 14th International Workshop on Auxetics and Related Systems with "Negative" characteristics*, Sheffield, UK - 10th to 13th September 2018.

Norbury A, Al-Badani K, Elmshawet E, Rothwell G and Ren XJ, Integrated Experimental and Numerical Investigation of Micro-welding process and Applications in Digital Manufacturing, *21st International Conference on Advances in Materials & Processing Technologies*, Dublin, 2018.

Al-Badani K., 2018-19, Industrial reports (Practical Procedure for Dyne Penetration, X-Ray and Ultrasonic testing of welded carbon steel plates and pipes; (Industrial report).

Al-Badani K., 2017, Comparative Studies of Modelling of Droplet formation with different programs (In preparation). Faculty Research Week.